HYDRATION OF BIO-MACROMOLECULES

by

David Hoffman

B.Pharm., Hebrew University of Jerusalem
M.S., University of California, San Francisco

DISSERTATION

Submitted in partial satisfaction of the requirements for the degree of

DOCTOR OF PHILOSOPHY

in

PHARMACEUTICAL CHEMISTRY

in the

GRADUATE DIVISION

of the

UNIVERSITY OF CALIFORNIA

San Francisco

Date University Librarian

Degree Conferred: JUN 13 1982

To My Mother

ACKNOWLEDGEMENTS

I wish to express my deepest appreciation to Dr. I. D. Kuntz for his guidance, supervision, help, and patience, and to acknowledge Dr. T. L. James, Dr. P. A. Kollman, and Dr. M. D. Shetlar for the stimulating the insightful discussions.

I would also like to thank Dr. G. B. Matson, Dr. V. J. Basus, and Dr. J. A. Murphy for their help in performing the NMR experiments.

I am indebted to Chris Jordan who helped with the typing of my dissertation.

ABSTRACT

The properties of water in the water-macromolecule systems, the properties of water and organic compounds in mixed solvent-macromolecule solutions, and the binding of fluoride ions to a protein were investigated by means of NMR spectroscopy. The macromolecules investigated included poly-L-lysine hydrobromide (PLL) and bovine serum albumin (BSA) in solutions and frozen solutions. The experiments included off-resonance experiments and measurements of spin-lattice, spin-spin, and rotating frame spin-lattice relaxation times of proton, deuteron, and fluorine nuclei.

Study of the water proton spin-lattice and rotating frame spin-lattice relaxation times in frozen PLL and BSA solutions indicates that at least two classes of interactions for water exist at subzero temperatures: one with an apparent correlation time in the nanosecond region and the other with an apparent correlation time in the microsecond region. The results also indicate that at subzero temperatures translational motions may be important. Apparent diffusion-coefficients (D) for the water protons

were calculated at several temperatures. At ∿-20°C the diffusion-coefficients are the same, within the experimental error, in the PLL and BSA samples and $D \approx (1.7 \pm 0.6) \times 10^{-10}$ cm^2/sec.

Study of the spin-spin relaxation times in BSA solutions above 0°C shows the presence of a proton/deuteron fraction that exchanges slowly with the water.

Based on our data, as well as published material, a partial phase diagram was constructed for the water-PLL system.

In BSA solutions that contain an organic solvent the water is affected to a larger degree by the macromolecule than the organic solvent. The water in the three component systems is affected more by the macromolecule than is water in the two component water-macromolecule system.

When BSA is added to a solution of sodium fluoride, the fluorine spin-lattice relaxation time decreases from ∿940 msec to ∿60 msec and the spin-spin relaxation time decreases from ∿100 msec (lower limit) to ∿20 msec. A saturation experiment shows that no dipolar interactions between the macromolecule and the fluoride ions take place. If any fluoride ions bind to the macromolecule, the frequency of such an exchange process is not less than ∿100 MHz. In the

presence of a macromolecule in solution, the fluoride ions relax by the spin rotation mechanism.

In an off-resonance experiment the water protons in frozen and concentrated solutions show a large dependence on the off-resonance field strength. No field dependence is seen in dilute solutions and in solvent deuterons in frozen solutions. The field dependence is not caused by "true" molecular motions, but may arise from the presence of local dipolar fields which do not average out to zero.

TABLE OF CONTENTS

TITLE PAGE i

DEDICATION ii

ACKNOWLEDGEMENTS iii

ABSTRACT iv

TABLE OF CONTENTS vii

LIST OF TABLES xi

LIST OF FIGURES xiv

CHAPTER 1: INTRODUCTION 1

CHAPTER 2: THEORY 15

2.1 Introduction 15

2.1.1 Relaxation in H_2O Molecule 18
2.1.2 Relaxation in D_2O Molecule 19
2.1.3 Relaxation of $^{19}F^-$ Ions 19
2.1.4 Paramagnetics 20
2.1.5 Vibrations 20

2.2 1 Pulse Experiment 20
2.3 Spin-Lattice (T_1) Relaxation 21

2.3.1 Experimental Determination of T_1 . 26

2.4 Spin-Spin (T_2) Relaxation 28

2.4.1 Experimental Determination of T_2 . 31

2.5 Spin-Lattice Relaxation in the Rotating Frame ($T_{1\rho}^{on}$) 32

2.5.1 Experimental Determination of $T_{1\rho}^{on}$. 36

2.6 Rotating Frame Spin-Lattice Relaxation in the Presence of an Off-Resonance rf Field ($T_{1\rho}^{off}$) . . . 37

2.6.1 Experimental Determination of R . . 43

2.7 Cross-Relaxation 44

2.7.1 T_1 in the Presence of Cross-Relaxation 45

2.7.2 T_2 in the Presence of Cross-Relaxation 47

2.7.3 $T_{1\rho}^{on}$ in the Presence of Cross-Relaxation 47

2.7.4 $T_{1\rho}^{off}$ in the Presence of Cross-Relaxation 47

CHAPTER 3: MATERIALS AND PREPARATION OF SAMPLES . 49

CHAPTER 4: EXPERIMENTAL 55

4.1 JEOL 4H-100 Spectrometer 55

4.1.1 T_1 Experiments 56

4.1.2 $T_{1\rho}^{on}$ Experiments 57

4.2 XL-100-15 Spectrometer 58

4.2.1 Proton $T_{1\rho}^{off}$ Experiments 62

4.2.2 Deuterium Experiments at 15.4 MHz . 74

4.2.2.1 Deuterium T_1 Experiments . 75

4.2.2.2 Deuterium $T_{1\rho}^{off}$ Experiments 77

4.2.3 Fluorine Experiments at 94.1 MHz . 77

4.2.3.1 Fluorine Saturation Experiments 78

4.3 Nicolet Superconducting Magnet 78

4.3.1 T_1 and $T_{1\rho}^{on}$ Experiments 79

4.3.2 T_2 Experiments 79

4.4 ESR Experiments 80

CHAPTER 5: DATA PROCESSING 81

5.1 General 81

5.2 T_1 Data 83

5.3 $T_{1\rho}^{on}$ Data 89

5.4 T_2 Data 90
5.5 Linewidth Data 91

5.6 $T_{1\rho}^{off}$ Data 91

CHAPTER 6: RESULTS AND DISCUSSION 94

6.1 Poly-L-Lysine Hydrobromide (PLL) 94

6.1.1 T_1 Data 94

6.1.2 $T_{1\rho}^{on}$ Data 106

6.2 Bovine Serum Albumin (BSA) 144

6.2.1 T_1 Data 144
6.2.2 $LW_{1/2}$ Data at Subzero Temperatures . 171

6.2.3 $T_{1\rho}^{on}$ Data at Subzero Temperatures . 178

6.2.4 T_2 and $T_{1\rho}^{on}$ Data of Solutions . . . 190

6.3 $T_{1\rho}^{off}$ Experiments 208

6.3.1 Introduction 208
6.3.2 Frozen BSA Solutions 212
6.3.3 BSA Solutions 255
6.3.4 BSA in Mixed Aqueous and Organic Solvents 277

6.4 Fluoride Binding to BSA 296
6.5 Summary 305

APPENDIX 309

A. VOFFH Program 309
B. NMRRB Program 314
C. NMRKS4 Program 316

LIST OF ABBREVIATIONS 322

REFERENCES 326

LIST OF TABLES

4.1 Normalized H_1 field strengths at different levels of attenuation. The fields were measured directly on samples of 4.5 M and 2 M LiCl in water at two temperatures. Each sample contained a different amount of ice. 70

4.2 Normalized H_1 field strengths at different levels of attenuation. The fields were measured directly on a sample of 4.5 M LiCl in water and on a sample of glycerine. 71

4.3 Absolute H_1 field strengths at different levels of attenuation. The fields were measured directly on a sample of 4.5 M LiCl in water and on a sample of acetone. 72

5.1 Standard deviation values of the water T_1 relaxation times at 44.4 MHz in PLL samples. The values were calculated by the Nicolet 1180 computer and the associated Nicolet program. Only the largest SD for each sample is shown. 85

5.2 Standard deviation values of the water T_1 relaxation times at 150 MHz in BSA samples. The values were calculated by the Nicolet 1180 computer and the associated Nicolet program. Only the largest SD for each sample is shown. 87

5.3 Standard deviation values of the solvent deuteron T_1 relaxation times at 15.4 MHz in BSA in D_2O samples. The values were calculated by the Nicolet 1180 computer and the associated Nicolet program. Only the largest SD for each sample is shown. . . . 88

6.1 Water Proton T_1, T_2, and T_1/T_2 values at 44.4 MHz in frozen 40% and 70% PLL samples. The values were obtained at the temperature of the T_1 minimum. 102

6.2 Apparent energies of activation for the water proton in 40% and 70% PLL samples. 124

6.3 Diffusion-coefficients of the water proton in 40% and 70% PLL samples. 134

6.4 Percentage deviation of the fitted intercept from the extrapolated $1/T_2$ values in 40% and 70% PLL samples. 137

6.5 Apparent energies of activation for the diffusion of the water protons in 40% and 70% PLL samples. 141

6.6 Differences between $(\frac{2}{5}T_1)$ and $T_{1\rho}^{on}$ values in 40% and 70% PLL samples. 143

6.7 Frequency dependence of the solvent proton and deuteron T_1 relaxation in frozen BSA samples. 158

6.8 Water proton T_1, T_2, and T_1/T_2 values at 150 MHz in frozen BSA samples. The values were obtained at the temperature of the T_1 minimum. . . . 166

6.9 Proton/deuteron T_1 ratios in BSA samples. Proton data obtained at 150 MHz. Deuteron data obtained at 15.4 MHz. 168

6.10 Water proton T_1/T_2 ratios at 150 MHz in frozen BSA samples. 173

6.11 Energies of activation for the water proton in frozen BSA samples. 177

6.12 Percentage deviation of the extrapolated $1/T_2$ values from the $1/T_2$ values derived from $LW_{1/2}$ measurements. 180

6.13 Diffusion-coefficients of the water proton in a frozen 0.154 g/1 ml BSA samples. 184

6.14 Percentage deviation of the fitted intercept from the extrapolated $1/T_2$ values in a frozen 0.154 g/1 ml BSA sample. 188

6.15 $\nu_{1/2}$ and T_2' values for the water proton at 100 MHz in a frozen 0.5 g/1 ml BSA sample. 247

6.16 $\nu_{1/2}$, T_2, and T_2' values at 100 MHz for the water proton in a 70% PLL sample. 249

6.17 $\nu_{1/2}$, T_2, and T_2' values at 100 MHz for the glycerine protons. 251

6.18 $\nu_{1/2}$, T_2, and T_2' values at 100 MHz for the water proton in BSA solutions. 276

6.19 Water proton T_1, organic proton T_1, and organic T_1/water T_1 values at 100 MHz. 287

LIST OF FIGURES

2.1 Free induction decay (FID) in the x-y plane. 22

2.2 Schematic dependence of relaxation times on the correlation time. (A) Rigid lattice limit. (B) Non-rigid solid. (C) Viscous liquid. (D) Nonviscous liquid. 25

2.3 The rotating coordinate system showing the effective rf field in the presence of an off-resonance field. The stationary magnetic field H_0 is aligned along the z axis. 38

2.4 Theoretical dependence of the ratio (R) on the logarithm of $\sin^2\theta$. (o) Correlation time 0.1 nanoseconds; (+) Correlation time 10 nanoseconds; (•) Correlation time 0.3 microseconds. The arrows indicate the H_1 field strength in units of Gauss (g). 41

4.1 A schematic illustration of the experimental set-up for the proton off-resonance experiments. 64

4.2 A schematic illustration of the experimental set-up for the deuterium off-resonance experiments. . . . 76

6.1 Water proton T_1 relaxation times at 44.4 MHz in PLL samples. The high and the low temperature regions are shown. The arrows with the numbers indicate the concentration of the macromolecule in units of percent wt/wt. 97

6.2 Water proton T_1 relaxation times at 44.4 MHz in PLL samples. The low temperature region is shown. The arrows with the numbers indicate the concentration of the macromolecule in units of percent wt/wt. 98

6.3 Water proton T_1 relaxation times at 44.4 MHz in PLL samples. The high temperature region is shown. The arrows with the numbers indicate the concentration of the macromolecule in units of percent wt/wt. 99

6.4 Phase diagram for the system PLL-water. Diagram constructed using our experimental data, the experimental data of Darke and Finer (7) and Woodhouse and Derbyshire (8) and general considerations. 105

6.5 Water proton $T_{1\rho}^{on}$ relaxation times at ν_0 = 44.4 MHz in a 40% PLL sample. (●) +22.7°C; (+) +9.8°C; (o) -0.1°C. The dashed lines show extrapolation to $H_1 \approx 0$. 107

6.6 Water proton $T_{1\rho}^{on}$ relaxation times at ν_0 = 44.4 MHz in a 40% PLL sample. (*) -10.3°C; (●) -20.1°C; (+) -30.2°C; (o) -40.6°C. The dashed lines show extrapolation to $H_1 \approx 0$. Extrapolation at -40.6°C is not shown. 108

6.7 Water proton $T_{1\rho}^{on}$ relaxation times at ν_0 = 44.4 MHz in a 70% PLL sample. (#) +23.7°C; (*) +10.8°C; (●) +0.2°C; (+) -10.4°C; (o) -21.2°C. The dashed lines show extrapolation to $H_1 \approx 0$. Extrapolation at -21.2°C is not shown. 109

6.8 A plot of $\ln(1/T_{1\rho}^{on})$ at $H_1 \approx 0$ vs. the inverse (absolute) temperature. Data are for the water protons in a 40% PLL sample. 111

6.9 A plot of $\ln(1/T_{1\rho}^{on})$ at $H_1 \approx 0$ vs. the inverse (absolute) temperature. Data are for the water protons in a 70% PLL sample. 112

6.10 Water proton $T_{1\rho}^{on}$ relaxation times at ν_0 = 44.4 MHz in 40% and 70% PLL samples. (●) 40% PLL data at +9.8°C; (#) 70% PLL data at +23.7°C; (+) 70% PLL data at +10.8°C; (o) 70% PLL data at +0.2°C. 113

6.11 Water proton $T_{1\rho}^{on}$ relaxation times at ν_0 = 44.4 MHz in 40% and 70% PLL samples. (#) 40% PLL data at -20°C; (+) 70% PLL data at -20°C. 115

6.12 An Arrhenius plot for the water protons in a 70% PLL sample. $T_{1\rho}^{on}$ data at the low H_1 fields were used. 118

6.13 An Arrhenius plot for the water protons in a 70% PLL sample. $T_{1\rho}^{on}$ data at the high H_1 fields were used. 119

6.14 An Arrhenius plot for the water protons in a 40% PLL sample. $T_{1\rho}^{on}$ data at the low H_1 fields were used. Data are for the high temperature region. 120

6.15 An Arrhenius plot for the water protons in a 40% PLL sample. $T_{1\rho}^{on}$ data at the high H_1 fields were used. Data are for the high temperature region. 121

6.16 An Arrhenius plot for the water protons in a 40% PLL sample. $T_{1\rho}^{on}$ data at the low H_1 fields were used. Data are for the low temperature region. 122

6.17 An Arrhenius plot for the water protons in a 40% PLL sample. $T_{1\rho}^{on}$ data at the high H_1 fields were used. Data are for the low temperature region. 123

6.18 A plot of $1/T_{1\rho}^{on}$ vs. $\omega_1^{1/2}$. Data are for the water protons in a 40% PLL sample at -10.3°C. 127

6.19 A plot of $1/T_{1\rho}^{on}$ vs. $\omega_1^{1/2}$. Data are for the water protons in a 40% PLL sample at -20.1°C. 128

6.20 A plot of $1/T_{1\rho}^{on}$ vs. $\omega_1^{1/2}$. Data are for the water protons in a 40% PLL sample at -30.2°C. 129

6.21 A plot of $1/T_{1\rho}^{on}$ vs. $\omega_1^{1/2}$. Data are for the water protons in a 40% PLL sample at -40.6°C. 130

6.22 A plot of $1/T_{1\rho}^{on}$ vs. $\omega_1^{1/2}$. Data are for the water protons in a 70% PLL sample at +0.2°C. 131

6.23 A plot of $1/T_{1\rho}^{on}$ vs. $\omega_1^{1/2}$. Data are for the water protons in a 70% PLL sample at -10.4°C. 132

6.24 A plot of $1/T_{1\rho}^{on}$ vs. $\omega_1^{1/2}$. Data are for the water protons in a 70% PLL sample at -21.2°C. 133

6.25 A plot of ln(1/D) vs. the inverse (absolute) temperature. Data are for the water protons in PLL samples. (#) 40% PLL sample; (+) 70% PLL sample. 140

6.26 Water proton T_1 relaxation times at 150 MHz in BSA samples. The high and low temperature regions are shown. The arrows with the numbers indicate the concentration of the macromolecule in units of gram protein per 1 ml added solvent. 146

6.27 Water proton T_1 relaxation times at 150 MHz in BSA samples. The high temperature region is shown. The arrows with the numbers indicate the concentration of the macromolecule in units of gram protein per 1 ml added solvent. 147

6.28 Water proton T_1 relaxation times at 150 MHz in BSA samples. The low temperature region is shown. The arrows with the numbers indicate the concentration of the macromolecule in units of gram protein per 1 ml added solvent. 148

6.29 Solvent deuteron T_1 relaxation times at 15.4 MHz in BSA samples. The high and low temperature regions are shown. The arrows with the numbers indicate the concentration of the macromolecule in units of gram protein per 1 ml of added solvent. 149

6.30 Solvent deuteron T_1 relaxation times at 15.4 MHz in BSA samples. The high temperature region is shown. The arrows with the numbers indicate the concentration of the macromolecule in units of gram protein per 1 ml of added solvent. 150

6.31 Solvent deuteron T_1 relaxation times at 15.4 MHz in BSA samples. The low temperature region is shown. The arrows with the numbers indicate the concentration of the macromolecule in units of gram protein per 1 ml of added solvent. 151

6.32 Plots of $\ln(1/T_2)$ vs. the inverse (absolute) temperature for the water protons in BSA samples. The high and the low temperature regions are shown. 172

6.33 An Arrhenius plot for the water protons at subzero temperatures in a 0.6 g/1 ml BSA sample. 176

6.34 Water proton $T_{1\rho}^{on}$ relaxation times at ν_0 = 44.4 MHz in a 0.154 g/1 ml BSA sample. (+) -15.0°C; (#) -25.4°C; (o) -33.2°C. The dashed lines show extrapolation to $H_1 \approx 0$. 179

6.35 A plot of $\ln(1/T_{1\rho}^{on})$ at $H_1 \approx 0$ vs. the inverse (absolute) temperature. Data are for the water protons in a frozen 0.154 g/1 ml BSA sample. 182

6.36 Plots of $1/T_{1\rho}^{on}$ vs. $\omega_1^{1/2}$. Data are for the water protons in a 0.154 g/1 ml BSA sample. (#) -15.0°C; (+) -25.4°C; (o) -33.2°C. 183

6.37 A plot of ln(1/D) vs. the inverse (absolute) temperature. Data are for the water protons in a frozen 0.154 g/1 ml BSA sample. 186

6.38 Water proton T_2 relaxation times at 150 MHz vs. the temperature in a 0.4 g/1 ml BSA sample at several pH's. (o) pH = 2.0; (+) pH = 4.45; (#) pH = 7.0; (•) pH = 12.0. 191

6.39 Water proton T_2 relaxation times at 150 MHz vs. the pH in a 0.4 g/1 ml BSA sample at several temperatures. The arrows with the numbers indicate the temperatures at which the data were taken. 193

6.40 Water proton T_1 relaxation times at 150 MHz vs. the temperature in a 0.4 g/1 ml BSA sample at several pH's. The arrows with the numbers indicate the pH's at which data were taken. 194

6.41 Water proton T_2 relaxation times at 55 MHz vs. the temperature in a 0.8 g/1 ml BSA sample. 195

6.42 Solvent deuteron T_2 relaxation times at 23 MHz vs. the temperature in a 0.8 g/1 ml BSA sample. 196

6.43 Water proton $T_{1\rho}^{on}$ relaxation times at ν_0 = 55 MHz in a 0.8 g/1 ml BSA sample. The arrows with the numbers indicate the temperatures at which data were taken. 203

6.44 Theoretical dependence of the ratio (R) on the logarithm of $\sin^2\theta$. (o) Correlation time 0.1 nanoseconds; (+) Correlation time 10 nanoseconds; (•) Correlation time 0.3 microseconds. The arrows with the numbers indicate the H_1 field strength in units of Gauss (g). 210

6.45 Theoretical dependence of the ratio (R) on the logarithm of the correlation time. Values calculated for H_1 = 1.00 g and $\sin^2\theta = 9.977 \times 10^{-4}$ [$\log(\sin^2\theta) \approx -3.001$]. 211

6.46 Water proton off-resonance data in a 0.5 g/1 ml BSA sample at -26.3°C. (+) H_1 field of 0.05 g; (#) H_1 field of 0.08 g; (o) H_1 field of 0.70 g. 213

6.47 Solvent deuteron off-resonance data in a 0.5 g/1 ml BSA in D_2O sample at -25.1°C. (#) H_1 field of 0.62 g; (+) H_1 field of 2.10 g. 214

6.48 Water proton off-resonance data in a 10 mM $FeSO_4$ sample at room temperature. (+) H_1 field of 0.09 g; (#) H_1 field of 0.72 g. 219

6.49 Glycerine proton off-resonance data at three temperatures. (+) -25.8°C; (#) -15.4°C; (o) -5.4°C. The arrows with the numbers indicate the H_1 field strengths in units of Gauss (g). 221

6.50 Glycerine deuteron off-resonance data in a perdeuterated glycerine sample at -16.0°C. (+) H_1 field of 0.42 g; (#) H_1 field of 1.94 g. 222

6.51 Water proton off-resonance data in a SiO_2 powder hydrated with ∿20% wt/wt water. Data obtained at +24.2°C. (+) H_1 field of 0.06 g; (#) H_1 field of 0.09 g; (o) H_1 field of 0.78 g. 225

6.52 Water proton off-resonance data in a 70% PLL sample at +15°C. (+) H_1 field of 0.11 g; (#) H_1 field of 0.29 g; (o) H_1 field of 0.98 g. 228

6.53 Water proton off-resonance data in a 70% PLL sample at -25.3°C. (+) H_1 field of 0.10 g; (#) H_1 field of 0.30 g; (o) H_1 field of 0.98 g. 229

6.54 Three correlation times off-resonance theoretical fit to water proton data in a 0.5 g/1 ml BSA sample at -26.3°C. (•) Experimental data; (+) theoretical fit. The fitted parameters are $\tau_a = 1.0 \times 10^{-11}$ sec, $P_a = 0.694$; $\tau_b = 2.5 \times 10^{-9}$ sec, $P_b = 0.236$; $\tau_c = 1.0 \times 10^{-6}$ sec, $P_c = 0.070$. The arrows with the numbers indicate the H_1 field strengths in units of Gauss (g). 232

6.55 Three correlation times off-resonance theoretical fit to solvent deuteron data in a 0.5 g/1 ml BSA in D_2O sample at -25.1°C. (•) Experimental data; (+) theoretical fit. The parameters used are identical to those used in the three correlation times fit for protons in Figure 6.54. The arrows with the numbers indicate the H_1 field strengths in units of Gauss (g). 235

6.56 Two correlation times off-resonance theoretical fit to solvent deuteron data in a 0.5 g/1 ml BSA in D_2O sample at -25.1°C. (•) Experimental data; (+) theoretical fit. The fitted parameters are $\tau_a = 1.0 \times 10^{-11}$ sec, $P_a = 0.454$; $\tau_b = 3.5 \times 10^{-8}$ sec, $P_b = 0.546$. The arrows with the numbers indicate the H_1 field strengths in units of Gauss (g). 237

6.57 Two correlation times off-resonance theoretical fit to water proton data in a 0.5 g/1 ml BSA sample at -26.3°C. (•) Experimental data; (+) theoretical fit. The parameters used are identical to those used in the two correlation times fit for deuterons in Figure 6.56. The arrows with the numbers indicate the H_1 field strengths in units of Gauss (g). 239

6.58 Two and three correlation times off-resonance theoretical fits to water proton data in a 0.5 g/1 ml BSA sample at -26.3°C. (•) Two correlation times fit; (+) three correlation times fit. Plots are identical with the theoretical plots for protons in Figures 6.54 and 6.57, and they are shown together for clarity. 240

6.59 A plot of 1-R vs. the off-resonance frequency at H_1 = 0.70 g. Data is for the water protons in a 0.5 g/1 ml BSA sample at -26.3°C. The circles represent the experimental points and the solid line represents a Lorentzian fit. Vertical scale is not shown. 242

6.60 A plot of 1-R vs. the off-resonance frequency at H_1 = 0.08 g. Data is for the water protons in a 0.5 g/1 ml BSA sample at -26.3°C. The circles represent the experimental points and the solid line represents a Lorentzian fit. Vertical scale is not shown. 243

6.61 A plot of 1-R vs. the off-resonance frequency at H_1 = 0.05 g. Data is for the water protons in a 0.5 g/1 ml BSA sample at -26.3°C. The circles represent the experimental points and the solid line represents a Lorentzian fit. Vertical scale is not shown. 244

6.62 A plot of 1-R vs. the off-resonance frequency at H_1 = 2.10 g. Data is for the solvent deuterons in a 0.5 g/1 ml BSA in D_2O sample at -25.1°C. The circles represent the experimental points and the solid line represents a Lorentzian fit. Vertical scale is not shown. 245

6.63 Water proton off-resonance data in a 0.05 g/1 ml BSA sample at +25.4°C. (+) H_1 field of 0.12 g; (#) H_1 field of 0.72 g. 257

6.64 Water proton off-resonance data in a 0.1 g/1 ml BSA sample at +25.4°C. (+) H_1 field of 0.12 g; (#) H_1 field of 0.72 g. 258

6.65 Water proton off-resonance data in a 0.3 g/1 ml BSA sample at +25.1°C. The arrows with the numbers indicate the H_1 field strengths in units of Gauss (g). 259

6.66 Water proton off-resonance data in a 0.4 g/1 ml BSA sample at +25.0°C. The arrows with the numbers indicate the H_1 field strengths in units of Gauss (g). 260

6.67 Water proton off-resonance data in a 0.5 g/1 ml BSA sample at +25.0°C. (+) H_1 field of 0.08 g; (#) H_1 field of 0.43 g; (o) H_1 field of 0.71 g. 261

6.68 Water proton off-resonance data in a 0.6 g/1 ml BSA sample at +25.0°C. (+) H_1 field of 0.08 g; (#) H_1 field of 0.43 g; (o) H_1 field of 0.71 g. 262

6.69 Water proton off-resonance data in a 0.7 g/1 ml BSA sample at +25.1°C. (+) H_1 field of 0.09 g; (#) H_1 field of 0.47 g; (o) H_1 field of 0.73 g. 263

6.70 Water proton off-resonance data in a 0.8 g/1 ml BSA sample at +25.1°C. (+) H_1 field of 0.09 g; (#) H_1 field of 0.47 g; (o) H_1 field of 0.73 g. 264

6.71 Water proton off-resonance data in a 0.3 g/1 ml lysozyme sample at +20°C at two pH's. (+) pH = 2.9; (#) pH = 5.4. The arrows with the numbers indicate the H_1 field strengths in units of Gauss (g). . . 267

6.72 Water proton T_1 and T_2 relaxation times at 100 MHz vs. the concentration of the protein in BSA solutions at +25 ± 1°C. Data taken from Table 6.18. 270

6.73 Water proton off-resonance data in a 0.8 g/1 ml BSA sample at +5.0°C. (+) H_1 field of 0.07 g; (#) H_1 field of 0.40 g; (o) H_1 field of 0.68 g. 271

6.74 Water proton off-resonance data in a 0.8 g/1 ml BSA sample at +15.2°C. (+) H_1 field of 0.09 g; (#) H_1 field of 0.49 g; (o) H_1 field of 0.73 g. 272

6.75 Water proton off-resonance data in a 0.8 g/1 ml BSA sample at +25.1°C. (+) H_1 field of 0.09 g; (#) H_1 field of 0.47 g; (o) H_1 field of 0.73 g. 273

6.76 Water proton off-resonance data in a 0.8 g/1 ml BSA sample at +45.0°C. (+) H_1 field of 0.09 g; (#) H_1 field of 0.49 g; (o) H_1 field of 0.73 g. 274

6.77 Water (+) and ethylene glycol (#) off-resonance proton data in a three component system at +24.8°C. The sample contained 0.3 g/1 ml BSA in a mixture of 50% water and 50% ethylene glycol. The arrows with the numbers indicate the H_1 field strengths in units of Gauss (g). 279

6.78 Water (+) and DMSO (#) off-resonance proton data in a three component system at +22.0°C. The sample contained 0.3 g/1 ml BSA in a mixture of 60% water and 40% DMSO. The arrows with the numbers indicate the H_1 field strengths in units of Gauss (g). 280

6.79 Water (+) and 2-chloro ethanol (#) off-resonance proton data in a three component system at +24.8°C. The sample contained 0.3 g/1 ml BSA in a mixture of 70% water and 30% 2-chloro ethanol. The arrows with the numbers indicate the H_1 field strengths in units of Gauss (g). 281

6.80 Water (+) and 2-chloro ethanol (#) off-resonance proton data in a three component system at +24.8°C. The sample contained 0.3 g/1 ml BSA in a mixture of 50% water and 50% 2-chloro ethanol. The arrows with the numbers indicate the H_1 field strengths in units of Gauss (g). . . 282

6.81 Water (+) and dioxane (#) off-resonance proton data in a three component system at -14.0°C. The sample contained 0.25 g/1 ml BSA in a mixture of 50% water and 50% dioxane. The arrows with the numbers indicate the H_1 field strengths in units of Gauss (g). 283

6.82 Water (+) and guanidine-HCl (#) off-resonance proton data in a three component system at +21.2°C. The sample contained 0.3 g/1 ml BSA in a mixture of water and ∿10 M guanidine-HCl. The sample also contained ∿0.2 moles of dithiothreitol to prevent gelling. The arrows with the numbers indicate the H_1 field strengths in units of Gauss (g). 284

6.83 Water proton off-resonance data in a 0.3 g/1 ml BSA sample at +25.1°C. The arrows with the numbers indicate the H_1 field strengths in units of Gauss (g). 285

6.84 Fluoride off-resonance data at ν_0 = 94 MHz at +21.6°C. The sample contained NaF in a 0.5 g/1 ml solution of BSA in D_2O. The arrows with the numbers indicate the H_1 field strengths in units of Gauss (g). 298

6.85 Fluoride T_1 relaxation times at ν_0 = 141 MHz as a function of temperature. The sample contained NaF in a 0.5 g/1 ml solution of BSA in D_2O. 299

6.86 Fluoride T_2 relaxation times at ν_0 = 141 MHz as a function of temperature. The sample contained NaF in a 0.5 g/1 ml solution of BSA in D_2O. 300

CHAPTER 1

INTRODUCTION

> It is water that, on taking different forms constitutes this earth, this atmosphere, this sky, these mountains gods and men, beasts and birds, grass and trees and animals, down to worms, flies and ants. All different forms of water. Meditate on water!
>
> Thales of Milet
> 630(?)-546(?) B.C.

The water constitutes, on the average, about 70% of the living cell (1). On a molecular level, life processes are thought to involve protein chemistry. Because this chemistry takes place in an aqueous environment, it is reasonable to expect that water is essential for life processes to take place. The water may be important in stabilizing the tertiary and quaternary protein structures and in stabilizing the intermediates of enzymatic reactions (1, 2, 3).

Understanding life processes is one of the leading frontiers in science. Detailed knowledge of the water macromolecule interactions is crucial to the understanding of the structure and function of proteins in living systems.

We studied the properties of water in water-macromolecule systems. Such systems should be regarded only as "simple" model systems. Living systems are much more complex. However, an understanding of the simpler systems is needed before a better understanding of the complex living systems is obtained.

We investigated the properties of the water in our system by means of NMR spectroscopy, a technique not likely to have been available to Thales. NMR spectroscopy has the advantages that the water signal can be looked at "directly." The NMR relaxation times and absorption peaks are sensitive to the details of molecular motion, and may provide information on the dynamic properties of the water molecule.

We were interested in studying the properties of water which is most closely associated with, or affected by, the macromolecule. This water constitutes only a small fraction of the total water present. Since conditions of fast exchange with the "bulk" water usually prevail, NMR experiments measure an average property. Because the "bulk" water is in excess, the NMR effects are relatively small. To reduce the interference from the "bulk" water we used concentrated solutions and frozen solutions. Upon freezing, the "bulk" water forms ice and the NMR signal is too

broad to be detected by ordinary NMR methods. We studied the residual unfrozen water at subzero temperatures. Kuntz et al. (4) have presented evidence that this water is closely associated with the macromolecule. Knowledge of the properties of frozen systems is also important in areas such as preservation of foods and preservation of biological tissues.

A few questions may be raised which can be expected to receive at least a partial answer by using NMR methods. These include the question of what kinds of motions are present and what are their correlation times. One can ask whether an exchange process is present. If such a process is present, one would like to know whether the water molecules exchange as a whole, or only the hydrogens are involved in the exchange. One can ask whether a cross-relaxation process between the water and the macromolecule is present. It is important to establish whether a cross-relaxation is present because its presence implies a close distance of approach between the water and the macromolecule and that a slowly exchanging water fraction is present (5). One can also ask whether the water has access into the interior of globular proteins.

We addressed these questions by measuring T_1, T_2, and $T_{1\rho}^{on}$ relaxation times of solvent protons and

deuterons in solutions and frozen solutions of BSA. We also looked at solutions and frozen solutions of poly-L-lysine hydrobromide (PLL). The properties of PLL have been extensively investigated (6, 7, 8, 9), because it may represent a "simple" model system for the proteins. The PLL is composed of only one amino acid, it is highly soluble in water, and it has side chains that may imitate the side chains of proteins. We also applied the recently proposed (10) off-resonance experiment to our systems. We developed a method to measure very low H_1 fields and investigated the effects at these low fields. The off-resonance experiment may be applied to multicomponent systems. We performed off-resonance experiments on systems with an organic component added to BSA solutions. The water and the organic component were monitored simultaneously. Knowledge of the relative interactions of the water and the organic component with the macromolecule may yield information on the role of the solvent in stabilizing the macromolecule structure.

Early proton NMR and electrical dispersion data were interpreted as suggestive of the presence of a water fraction that is "bound" to the macromolecule, or that a "hydration shell," composed of several types of water, surrounds the macromolecule (11, 12).

"Bound" water is difficult to define and more than 10 definitions of such water have been summarized (12). We use the term "bound" water in an intuitive sense, meaning the water which is associated with the macromolecule for a long enough time to alter its properties and/or structure from that of pure liquid water.

Zipp et al. (13) measured the water proton relaxation times in frozen erythrocyte systems and proposed a model with two types of hydration shells. One centered at $\tau_c \approx 10^{-9}$ sec represents a "loose" hydration shell and the other centered at $\tau_c \approx 10^{-6}$ sec represents a "tight" hydration shell.

Oakes (14) measured the water proton relaxation times in solutions of bovine serum albumin (BSA) as a function of the temperature and the concentration. He interpreted his results as suggestive of a bound water fraction with an average mobility lower by a factor of about 100 than that in pure water.

Grösch and Noack (15) studied the frequency dependence of the water proton T_1 and T_2 relaxation times in solutions of BSA at several temperatures, concentrations, and pH's. The data were interpreted in terms of a model that includes three types of water. A bulk water with a correlation time of $\sim 10^{-11}$ sec. A loose hydration shell with a correlation

time of $\sim 10^{-9}$ sec and a tightly bound water fraction with a correlation time of $\sim 10^{-8}$ sec. The tight water fraction is selectively arrayed in the vicinity of ionic protein regions.

More recently, Halle et al. (16) measured the T_1 and T_2 frequency dependence of ^{17}O in solutions of seven proteins at several temperatures, concentrations, and pH's. A two-state model was proposed with one class water of hydration. This hydration water is composed of approximately two water layers and is hindered in its mobility by a factor of ~ 8 as compared to liquid water. The hydration water has a small anisotropic component which is averaged out by protein reorientation. Charged residues, particularly carboxylate, are hydrated to a greater extent than other residues. This fact accounts for the variation in the extent of hydration of different proteins.

The work of Halle et al. (16), and the papers of Koenig et al. (17) and Hallenga and Koenig (18), who examined the T_1 dispersion of the solvent proton, deuteron, and ^{17}O in protein solutions, are inconsistent with the early models that proposed the existence of a tightly bound water of hydration. The hydration model leads to inconsistencies when the data of the three nuclei are considered collectively, even if only a

few long lived irrotationally bound water molecules are assumed (12).

To explain their data, Koenig et al. (17) proposed a model in which the macromolecule affects the water motions through a hydrodynamic effect, rather than through a tightly bound water. The macromolecule imparts a small anisotropic component to a large number of water molecules. The anisotropic component is averaged on a time scale comparable to the reorientational relaxation time of the macromolecule and is transferred among the water molecules by fast exchange. Although no theoretical calculations were presented, such an effect may be expected to be amplified when NMR methods are used. For lysozyme, X-ray data indicate a monolayer of water in well defined positions. The positions of the oxygen atoms correspond to well defined locations on the protein surface such that hydrogen bonds with the protein can be formed. Because the hydrogen bond is relatively weak, it takes less than $\sim 10^{-11}$ sec to break and reform two hydrogen bonds. The authors explain that this water will be contributing to the hydrodynamic size of the protein but may be exchanging too fast to contribute to the NMR relaxation of solvent protons, deuterons, and ^{17}O.

Edzes and Samulski (5) presented experimental evidence that cross-relaxation may take place between the water and the macromolecule in hydrated collagen fibers. Hilton et al. (19) presented evidence for cross-relaxation in a system of water adsorbed on lysozyme powder. Hsi and Bryant (20) suggested that cross-relaxation may exist in frozen protein solutions. Eisenstadt and Fabry (21) showed that cross-relaxation may exist between water and hemoglobin in suspensions of red blood cells, and Koenig et al. (22) presented evidence for cross-relaxation in dilute protein solutions.

The brief summary of the various works indicates that different interpretations and models are offered when the water-macromolecule interactions are studied by the NMR methods. Different interpretations also result when non-NMR methods are used. The non-NMR methods include, among others, electrical dispersion, infrared spectroscopy, X-ray diffraction, neutron diffraction, and different thermodynamic measurements, such as equilibrium water pressure, calorimetry, etc. (11).

One may wonder why experiments performed on similar systems give rise to different interpretations and to models that appear to be mutually exclusive. One reason is that usually only a limited set of

experimental parameters is measured, even within a given experimental technique. For example, in NMR one can look at the solvent proton, deuteron, and oxygen nuclei. Some of the parameters that can be measured include T_1, T_2, $T_{1\rho}^{on}$, and $T_{1\rho}^{off}$ relaxation times, as well as frequency dependence, etc. Only a few of these parameters are usually measured in a given system. The choice of the parameters to measure is usually determined by a combination of practical and conceptual considerations. A second reason is that different experiments may be intrinsically more sensitive to different variables. A third reason is the dynamic nature of the water-macromolecule interaction. Different techniques measure phenomena on a different time scale. For example, NMR experiments are sensitive to molecular motions in the approximate range of 10^{-9}-10^{-4} sec. Motions with correlation times much longer or much shorter than these limits will not affect the NMR data. X-ray experiments will be sensitive to motions shorter than $\sim 10^{-11}$ sec. Thermodynamic experiments measure phenomena on a relatively long time scale of seconds or minutes (23). The details of an interpretation and of a model may depend on the experimental technique used and on the effective time scale of that technique.

In some works, previously published data are reexamined and fitted with a new model equation (24). If a better fit is obtained with the new equation, it is taken as an evidence that the new model represents better the phenomena. In most cases, the new equation is more complicated and has more terms and/or more parameters than the old equation. There is little doubt that if an equation represents better a physical phenomena, it will result in a better fit to the experimental points. However, one should bear in mind that such a "better" fit may only reflect the more complicated mathematical nature of the new equation, rather than any physical "reality."

Heuristic equations have been used to describe data and to derive conclusions. It has been common, for instance, to use the dielectric (Cole & Cole) dispersion equation to describe NMR data (22), because this equation gives a Lorentzian lineshape for certain parameter values. Although good fits are often obtained using heuristic equations, one would like to use equations that are derived from basic physical principles and considerations. Such equations are expected to contain adjustable parameters that may have a "physical" interpretation.

As our understanding of the water-macromolecule interactions advances, a picture should emerge which

will be consistent with most of the NMR data as well as with data derived from other types of experiments.

To illustrate some of the more general points in this chapter, the following passage from the modern-age Galilean dialogue by J. M. Jauch (25) is cited:

Salviati — Suppose I give you two sequences of numbers, such as

7 8 5 3 9 8 1 6 3 3 9 7 4 4 8 3 0
9 6 1 5 6 6 0 8 4 . . .

and

1, -1/3, +1/5, -1/7, +1/9, -1/11, +1/13, -1/15, . . .

If I asked you, Simplicio, what the next number of the first sequence is, what would you say?

Simplicio — I could not tell you. I think it is a random sequence and that there is no law in it.

Salviati — And for the second sequence?

Simplicio — That would be easy. It must be +1/17.

Salviati — Right. But what would you say if I told you that the first sequence is also constructed by a law and this law is in fact identical with the one you have just discovered for the second sequence?

Simplicio — This does not seem probable to me.

Salviati — But it is indeed so, since the first sequence is simply the beginning of the decimal fraction [expansion] of the sum of the second. Its value is $\pi/4$.

Simplicio You are full of such mathematical tricks, but I do not see what this has to do with abstraction and reality.

Salviati The relationship with abstraction is easy to see. The first sequence looks random unless one has developed through a process of abstraction a kind of filter which sees a simple structure behind the apparent randomness.

It is exactly in this manner that laws of nature are discovered. Nature presents us with a host of phenomena which appear mostly as chaotic randomness unless we select some significant events, and abstract from their particular, irrelevant circumstances so that they become idealized. Only then can they exhibit their true structure in full splendor.

Sagredo This is a marvelous idea! It suggests that when we try to understand nature, we should look at the phenomena as if they were <u>messages</u> to be understood. Except that each message appears to be random until we establish a code to read it. This code takes the form of an abstraction, that is, we choose to ignore certain things as irrelevant and we thus partially select the content of the message by a free choice. These irrelevant signals form the "background noise," which will limit the accuracy of our message.

But since the code is not absolute there may be several messages in the same raw material of the data, so changing the code will result in a message of equally deep significance in something that was merely noise before, and <u>conversely</u>: In a new code a former message may be devoid of meaning.

> Thus a code presupposes a free choice among different, complementary aspects, each of which has equal claim to reality, if I may use this dubious word.
>
> Some of these aspects may be completely unknown to us now but they may reveal themselves to an observer with a different system of abstractions.
>
> But tell me, Salviati, how can we then still claim that we discover something out there in the objective real world? Does this not mean that we are merely creating things according to our own images and that reality is only within ourselves?

Salviati I don't think that this is necessarily so, but it is a question which requires deeper reflection.

Our experimental results are presented in Chapter 6. We did not attempt to present a model that will be consistent with all the experimental data. Instead, each set of data is discussed after the results are presented. Conclusions derived from each set of data are compared to conclusions derived from our other sets of data and to data obtained by others. Trends that emerge among the various data sets are pointed out, as well as any inconsistencies. Whenever possible, explanations are offered why such inconsistencies may exist.

Chapter 2 presents a theoretical background. Only the theory relevant to our experiments is presented.

Chapter 3 describes the materials and the methods we used to prepare the samples.

Chapter 4 describes the instruments and the experimental set-ups.

Chapter 5 describbes the methods used to process the raw experimental data and to plot the results.

The Appendix lists the self-written computer programs that were used to process the data.

CHAPTER 2

THEORY

2.1 Introduction

Quantum mechanics predicts that nuclei with a spin number $I = \frac{1}{2}n$, where n is an integer, have degenerate energy levels. When such nuclei are placed in an external magnetic field H_0 "nuclear Zeeman splitting" takes place and the energy levels are separated. The number of energy levels depends on the quantum number m, which may take the values

$$m_I = I,(I - 1),(I - 2), \ldots ,-(I - 2),-(I - 1),-I.$$

In nuclei with $I = \frac{1}{2}$ the electrical charge is spherically distributed. In nuclei with $I > \frac{1}{2}$ charge distribution is not spherical and these nuclei possess quadrupole and higher electrical moments.

For a given nucleus the energy levels are equally spaced. The energy separation between adjacent levels in units of Hz is given by

$$\nu_0 = \frac{\gamma H_0}{2\pi},$$

where ν_0 is the resonance frequency and γ is the gyromagnetic ratio. Nuclear Magnetic Resonance (NMR) involves the detection of transitions between these nuclear levels. For proton nuclei in an external field of 23.5 kilo-Gauss $\nu_0 \approx 100$ MHz, i.e., the nuclear transition falls in the radio frequency (rf) portion of the electromagnetic spectrum (26).

Rf spectroscopy has a few important characteristics. Frequencies can be generated with great precision, so that the uncertainty $\Delta\nu$ in frequency is smaller than the energy separation between nuclear levels. Because of the low energy of each photon in the rf region and small $\Delta\nu$, a large number of photons ($\sim 10^{17}$) can be generated per unit frequency range with very low power.

Quantum theory of radiation shows that because of the large number of photons present, rf spectroscopy is governed by induced emission and absorption processes, rather than by spontaneous emission, as is the case in higher frequency spectroscopies. This fact has two important consequences in NMR (27):

1. For most purposes NMR experiments may be described in classical rather than quantum mechanical terms.

2. Relaxation processes in NMR are radiationless, i.e., they are coupled directly to rotational and translational motions.

Therefore, in principle information on rotational and translational motions as well as internuclear distances can be derived from NMR relaxation studies.

Following absorption of rf energy at the resonance frequency, nuclei will be excited to the higher energy state. The probability of a spontaneous transition to a lower level is 10^{-22} sec^{-1} and a calculation shows that it will take about 30 million years for 63% of the nuclei to go back to the lower state (28).

In real systems nearby nuclei which have magnetic moments are present. These nuclei undergo random Brownian motion. The randomly oscillating magnetic moments will have Fourier components at the resonance frequency. These will induce transitions between nuclear states and cause relaxation. The relaxation rates can under simplifying assumptions be expressed as analytic functions of the correlation time τ_r and the internuclear distances.

The correlation time can be roughly defined as the time required for rotation of the nuclear magnetic moment through an angle of 33° for rotational motion and as the time required for the diffusion through a

distance equal to the length of the molecule for translational motion (26, 28).

2.1.1 Relaxation in H_2O Molecule

For a molecule of H_2O, two modes of relaxation are available (28):

1. Dipole-dipole interaction of a proton with a nearby proton on the same molecule. This relaxation is modulated by the rotational motion of the molecule.
2. Dipole-dipole interaction with protons on neighboring molecules. This relaxation is modulated by the translational motion of the nearby molecules. The contribution from the rotational motion of nearby molecules is negligible.

Theoretical considerations (28), as well as experimental results (29), suggest that in liquid water and in water adsorbed on surfaces the rotational and translational motions are strongly coupled and both motions have about equal contribution to the overall observed relaxation. In complicated systems, such as protein in water, where the structure of liquid water may be modified, this is not necessarily the case (13).

2.1.2 Relaxation in D_2O Molecule

The deuterium nucleus has I = 1 and it possesses a quadrupole moment. The quadrupole moment will produce a field gradient at the same nucleus. The field gradient at the nucleus will be oscillating because of rotational motion and will induce relaxation. Because deuterium possesses quadrupole moment and because its gyromagnetic ratio is relatively low, dipole-dipole interactions with nearby nuclei will be negligible. The dominant mode of relaxation in D_2O molecule is expected to be rotation of the molecule (26).

2.1.3 Relaxation of $^{19}F^-$ Ions

The ^{19}F nucleus has $I = \frac{1}{2}$. Unlike the situation in the water molecule, there are no nearby nuclei on the same molecule and relaxation may be brought about by dipole-dipole interactions with solvent protons or protein protons, if the distance of approach is small.

If dipole-dipole interactions are not efficient other relaxation mechanisms, such as spin-rotation and anisotropic electronic shielding, may become important.

The anisotropic electronic shielding mechanism may be distinguished from other relaxation processes, because the relaxation rate in this case is

proportional to the square of the external magnetic field strength (26).

2.1.4 Paramagnetics

The magnetic moment of an unpaired electron is 657 times greater than the magnetic moment of a proton. Therefore, the unpaired electron is about 500,000 times more efficient in inducing nuclear relaxation (26).

If paramagnetic impurities are present, these may be the dominant cause of the observed relaxation rates. Care was taken to prevent contamination of samples with paramagnetic impurities.

ESR experiments were performed to detect the possible presence of paramagnetic ions. Experiments were performed on solutions of paramagnetic ions to establish their possible influence on the interpretation of relaxation data.

2.1.5 Vibrations

In general, vibrational motions do not contribute to nuclear relaxation, because of their high frequency and small amplitude (28).

2.2 1 Pulse Experiment

It is convenient to describe NMR experiments in a frame of reference rotating at an angular frequency $\omega = -\gamma H_1$, where H_1 is the applied rf field (27).

When an external field H_0 is applied along the z' direction to a sample containing a collection of nuclei, a net magnetic moment of magnitude M_0 will result along the z' axis. The magnetization can be nutated away from the z' axis through an angle θ by application of an rf pulse along the x' axis. The nutation angle is given by (26)

$$\theta = \gamma H_1 t,$$

where t is the length of time the H_1 field is on.

After a 90° pulse is applied, M_0 will be nutated into the x'-y' plane and begin to decay because of relaxation processes. A detector placed in the x'-y' plane will sample the magnetization as a function of time and a free induction decay (FID) signal will result. This is shown in Figure 2.1.

The FID can be Fourier transformed using a digital computer. The result is a display of the magnetization as a function of the frequency (30). This is a more convenient and more efficient way of observing NMR signals and is referred to as the NMR absorption signal.

2.3 Spin-Lattice (T_1) Relaxation

Following absorption of rf energy nuclei will be excited to higher energy levels. Because of

Fig. 2.1. Free induction decay (FID) in the x-y plane.

relaxation processes, energy will be lost to the surrounding (lattice) and thermal equilibrium will be reestablished. T_1 is the time constant for this process.

In the classical description T_1 is the time constant for the equilibrium magnetization M_0 to be reestablished along the z' axis after is was nutated away.

If relaxation is assumed to be caused solely by isotropic rotation, T_1 is given by (26)

$$\frac{1}{T_1} = 2\sigma_0^2 \left[\frac{\tau_r}{1 + \omega_0^2 \tau_r^2} + \frac{4\tau_r}{1 + 4\omega_0^2 \tau_r^2} \right], \qquad [2.1]$$

where τ_r is the rotational correlation time and ω_0 is the spectrometer frequency in units of radians/second. σ_0^2 is the rigid lattice second moment. For protons,

$$\sigma_{0p}^2 = \frac{2}{5}\gamma^4 h^2 I(I + 1) \sum_j r_{ij}^{-6}$$

where r_{ij} is the internuclear distance. For deuterons,

$$\sigma_{0d}^2 = (QCC)^2 \left(1 + \frac{\eta^2}{3}\right) \frac{6\pi^2}{80},$$

where QCC is the quadrupole coupling constant and η is the asymmetry parameter (26, 29). Experimental results show that (29)

$$\frac{\sigma^2_{0d}}{\sigma^2_{0p}} \approx 10,$$

i.e., the effective second moment for deuterons is about ten times that for protons.

Figure 2.2 shows a plot of log T_1 as a function of log τ_r. The graph goes through a minimum at

$$\tau_r = \frac{1}{\sqrt{2}\omega_0} \approx \frac{1}{\omega_0} \qquad [2.2]$$

and at that point (28)

$$T_{1(\min)} = \frac{3\omega_0}{2^{1.5}\sigma_0^2}. \qquad [2.3]$$

T_1 relaxation rates will be most sensitive to motions with correlation times about equal to the inverse of the spectrometer frequency.

In this study T_1 data at the lowest frequency was acquired at 15.4 MHz for deuterons and T_1 data at the highest frequency was acquired at 150 MHz for protons. This covers correlation times in the approximate range of

$$\tau_r \approx 1.0 \times 10^{-9} - 1.0 \times 10^{-8} \text{ sec.}$$

A plot of $1/T_1$ as a function of the spectrometer frequency (disperson curve) has an inflection point at (18)

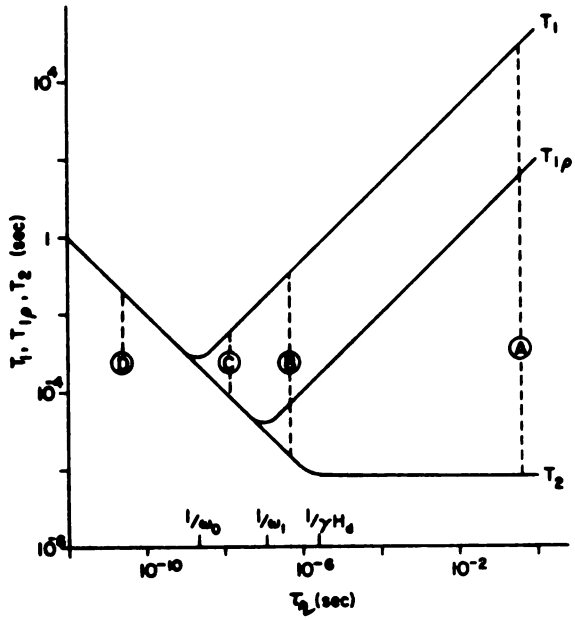

Fig. 2.2. Schematic dependence of relaxation times on the correlation time. (A) Rigid lattice limit. (B) Nonrigid solid. (C) Viscous liquid. (D) Nonviscous liquid.

$$\tau_r \approx \frac{\sqrt{3}}{\omega}.$$

Studying relaxation times by the frequency dependence method has the advantage that all the experiments can be done at the same temperature. The temperature dependence of the correlation times need not be known. The drawback is the technical difficulty in changing the external magnetic field.

2.3.1 Experimental Determination of T_1

Usually, a given relaxation time can be measured by a variety of pulse sequences. Only the pulse sequences used in this study will be described.

All the T_1 relaxation times were measured by the standard inversion recovery technique (31). The pulse sequence was: 180° - τ - 90°. Following the application of a 180° pulse the magnetization M_0 is aligned along the negative z' axis. Because of T_1 relaxation, the magnetization returns to its equilibrium value. The value of the magnetization along the z' axis as a function of time (τ) is given by (26)

$$M_z(\tau) = M_0 \left[1 - 2 \exp\left(-\frac{\tau}{T_1}\right)\right]. \qquad [2.4]$$

After the application of a 180° pulse and a waiting time τ, a 90° observing pulse is applied and the magnitude of the magnetization is detected. This

sequence is repeated for different values of τ and values of the magnetization as a function of time are obtained.

The 180° pulse (t_π) was determined by finding the pulse length where the signal amplitude was zero or went through a minimum. The 90° pulse length ($t_{\pi/2}$) was then set to be

$$t_{\pi/2} = \frac{t_\pi}{2}.$$

It is desirable that the length of the pulses is very short compared to T_1 and T_2, so that no appreciable relaxation occurs during the application of the pulses (26). In all the experiments $t_\pi < 40$ μsec and this condition was satisfied.

Because of field inhomogeneities, the 180° pulse width cannot be set precisely (26, 32). To correct for this and other possible experimental errors, T_1 values were obtained using the three parameter function, rather than Equation 2.4 (see Chapter 5, Section 5.2).

To avoid saturation the delay time (DT) after the 90° pulse was set so that

$$DT \geqslant 5T_1.$$

To set the value of DT, T_1 was estimated at the beginning of each experiment by finding the value of τ, (τ_0),

at which the amplitude of the magnetization is equal to zero,(the zero-point method). The value of T_1 is given then by (26)

$$T_1 \approx \frac{\tau_0}{0.7}.$$

2.4 Spin-Spin (T_2) Relaxation

Following absorption of rf energy, dipole-dipole interactions among nuclei will induce mutual spin flips. Transitions such that $\Delta m_i = +1$ and $\Delta m_j = -1$ (and vice versa) will occur simultaneously. This process does not change the total energy of the system, but it distributes the absorbed energy equally among the spins (28). The time constant for this process is referred to as spin-spin or T_2 relaxation time.

In classical terms, following the nutation of the magnetization into the x'-y' plane the magnetization will begin to decay because of relaxation processes. The time constant for the relaxation in the x'-y' plane is T_2.

Because of inhomogeneities in the H_0 field, spins in different parts of the sample will experience slightly different fields. This will cause the spins to dephase and consequently the measured relaxation time will be shorter than the true T_2. Transverse

relaxation time that contains contributions from inhomogeneities is designated T_2^*. The following two relations hold:

$$\frac{1}{T_{2\,true}} = \frac{1}{T_{2\,obs}} - \frac{1}{T_{2\,inh}}$$

$$T_2^* \leqslant T_{2\,true}.$$

$T_{2\,true}$ is the true value of T_2, $T_{2\,obs}$ is the measured value, and $T_{2\,inh}$ is the contribution from inhomogeneities (26).

Spin-spin relaxation processes are most efficient when no motions are present. When

$$\tau_r \geqslant \frac{1}{\gamma H_L},$$

where H_L is the local dipolar field, T_2 reaches its shortest value. This region is referred to as the rigid lattice limit. The limiting value of T_2 is given by (28)

$$T_2 = \left(\frac{1}{3\sigma_0^2}\right)^{\frac{1}{2}}.$$

For an isotropic rotational motion T_2 is given by (26, 29)

$$\frac{1}{T_2} = \sigma_0^2 \left[3\tau_r + \frac{5\tau_r}{1 + \omega_0^2 \tau_r^2} + \frac{2\tau_r}{1 + 4\omega_0^2 \tau_r^2} \right]. \quad [2.5]$$

If T_2 is governed by isotropic rotational motions, the absorption lineshape will be Lorentzian and T_2 will be related to the linewidth at half maximum amplitude ($LW_{1/2}$) by (26)

$$T_2^* = \frac{1}{\pi LW_{1/2}}.$$

For broad lines and Lorentzian lineshape $T_{2_{inh}} >> T_{2_{true}}$ and

$$T_2 \approx \frac{1}{\pi LW_{1/2}}. \quad [2.6]$$

Figure 2.2 shows T_2 as a function of τ_r. Both the isotropic rotation region and the rigid lattice limit are shown. T_2 is sensitive to very slow motions ($\tau_r > 10^{-7}$ sec). Slow motions do not contribute significantly to T_1 relaxation. However, processes that contribute to T_1 relaxation also contribute to T_2 relaxation. Therefore, $T_2 \leqslant T_1$. If slow motions, such as exchange, exist together with fast motions a large T_1/T_2 ratio may result.

2.4.1 Experimental Determination of T_2

T_2 relaxation times were measured by the Hahn spin-echo method (33). This method is based on the fact that spin dephasing due to inhomogeneity effects is reversible, while spin dephasing due to true spin-spin relaxation effects is irreversible. The pulse sequence is: 90° - τ - 180° - τ - spin-echo detection.

A 90° pulse is applied at time $\tau = 0$ and the magnetization M_0 is nutated into the x'-y' plane. The magnetization precesses in the x'-y' plane. Because of T_2 relaxation processes the magnetization begins to decay. Since H_0 is not perfectly homogeneous, spins in different parts of the sample experience slightly different fields. This results in loss of phase coherence and the spins fan out in the x'-y' plane. After a time τ, a 180° pulse is applied and each spin is flipped in the opposite direction. At time 2τ the spins are in phase again, but along the negative y' axis. This results in a spin-echo the magnitude of which is detected. To allow enough time for the magnetization to return to its equilibrium value there is a delay time of $5T_1$ before the sequence is repeated.

The echo amplitude is measured for different values of the delay time τ. The amplitude of the echo as a function of 2τ is given by (26)

$$M(2\tau) = M_0 \exp\left[\left[-\frac{2\tau}{T_2}\right] - \frac{2}{3}\gamma^2 G^2 D\tau^3\right],$$

where G is the magnetic field gradient across the sample and D is the self-diffusion coefficient.

If the diffusion terms on the right side of the equation are not negligible the decay will not be exponential. Since only the G term is not an intrinsic property of the sample, field homogeneity was carefully adjusted before each experiment to reduce the field gradients. Data were fitted using the equation

$$M(2\tau) = M_0 \exp\left(-\frac{2\tau}{T_2}\right).$$

All T_2 relaxation decays were strictly exponential, thereby showing that the assumption that the contribution from the diffusion term was negligible was correct.

2.5 Spin-Lattice Relaxation in the Rotating Frame ($T_{1\rho}^{on}$)

In this experiment the spin system is "locked" along the H_1 field. Relaxation processes similar to those described for T_1 relaxation will take place and the magnetization along the H_1 field will decay with time. The relaxation time for this decay is $T_{1\rho}^{on}$.

If isotropic rotational motion is assumed and $H_1 \ll H_0$, $T_{1\rho}^{on}$ for protons is given by (34)

$$\frac{1}{T_{1\rho}^{on}} = \sigma_0^2 \left[\frac{3}{2} \frac{\tau_r}{1 + 4\omega_1^2 \tau_r^2} + \frac{5}{2} \frac{\tau_r}{1 + \omega_0^2 \tau_r^2} + \frac{\tau_r}{1 + 4\omega_0^2 \tau_r^2} \right],$$

where $\omega_1 = \gamma H_1$. If $T_{1\rho}^{on}$ is plotted as a function of τ_r, a minimum will occur at $\tau_r \approx 1/\omega_1$ (Figure 2.2). If $1/T_{1\rho}^{on}$ is plotted as a function of ω_1 (dispersion curve), an inflection point will occur at $1/T_{1\rho}^{on} \approx 1/\omega_1$.

Unlike changing the H_0 field, it is relatively easy to change the strength of the H_1 field. Therefore, all $T_{1\rho}^{on}$ relaxation times were measured as a function of H_1.

In a typical $T_{1\rho}^{on}$ experiment, H_1 was changed from ∿15 Gauss (g) to ∿0.2 g. This covers correlation times in the range $\tau_r \approx 1.0 \times 10^{-6} - 1.0 \times 10^{-4}$ sec, i.e., $T_{1\rho}^{on}$ relaxation is dominated by very slow motions.

H_1 fields higher than ∿15 g are difficult to achieve because of the requirement for a very powerful amplifier. Problems arise because of the need to protect the receiver from the amplifier and because of heating effects.

Attempts to obtain $T_{1\rho}^{on}$ relaxation times of deuterons were unsuccessful. Because of the lower

gyromagnetic ratio of deuterons, amplifications higher by a factor of about 7 as compared to protons are needed. Although a lower observing frequency was used, the heating effects were significant and heating of the coil caused severe distortion of the peaks.

H_1 fields lower than $\sim$0.2 g are difficult to measure accurately. (See Chapter 4, Section 4.2.1.1.) Problems arise because of phase-shifting effects. At very low H_1 fields the magnetization will be aligned along an effective field rather than along the H_1 field (35).

Theoretical considerations show that if in a given system the relaxation is dominated by translational motions and $\langle r^2 \rangle \gg d^2$, where $\langle r^2 \rangle$ is the mean square jumping distance and d is the distance of closest approach between spins, the relaxation is described by (36, 37)

$$\frac{1}{T_{1\rho}^{on}} = C\omega_1^{1/2} + \frac{1}{T_2}.$$

It follows that a plot of $1/T_{1\rho}^{on}$ versus $\omega_1^{1/2}$ will result in a straight line. The intercept will be equal to $1/T_2$ and the slope will be equal to C. The value of C is given by

$$C = \frac{-\sqrt{2}\gamma^4 h^2 N}{80\pi D^{3/2}} \qquad [2.7]$$

where h is Planck's constant, N is the density of the spins that contribute to translational relaxation, and D is the diffusion-coefficient. The diffusion-coefficient can be calculated from the slope, if a value of N can be estimated. In such a plot, only ω_1 values in the dispersion region should be used. Very low ω_1 values or ω_1 values in the region where the dispersion is absent should not be used. If other modes of relaxation contribute as well, the plot may not result in a straight line and/or the intercept may be not equal to $1/T_2$.

If $\langle r^2 \rangle \ll d^2$ the relaxation rates are given by a complicated mathematical equation (24).

Two important limiting cases should be considered:

1. H_1 is very large and $\omega_1 \rightarrow \omega_0$.
   As H_1 becomes larger the value of $T_{1\rho}^{on}$ gets longer. In the limit of $\omega_1 = \omega_0$, $T_{1\rho}^{on} = \frac{2}{5}T_1$.
2. H_1 is very small and $\omega_1 \rightarrow 0$.
   As H_1 becomes smaller the value of $T_{1\rho}^{on}$ gets shorter and in the limit of $H_1 = 0$, $T_{1\rho}^{on} = T_2$.

2.5.1 Experimental Determination of $T_{1\rho}^{on}$

$T_{1\rho}^{on}$ relaxation times were determined by the Solomon spin-locking method (38). First, a 90° pulse is applied along the x' axis. This nutates the magnetization M_0 to the y' axis. Immediately after, the phase of the rf is changed by 90° and H_1 is applied for a time τ. Because of the 90° phase change, H_1 now lies along the y' axis. Since H_1 and M_0 are now aligned, no torque is exerted on M_0 and it remains along y'. Because of relaxation processes M_0 begins to decay. After H_1 is on for a time τ it is switched off and the magnitude of the remaining magnetization is detected. To allow enough time for the magnetization to recover to its equilibrium value, there is a delay time of $5T_1$ before the sequence is repeated. By changing the value of τ, the magnitude of the magnetization is obtained as a function of the time H_1 is on. The magnitude of the magnetization as a function of τ is given by (26)

$$M(\tau) = M_0 \exp\left(-\frac{\tau}{T_{1\rho}^{on}}\right).$$

If very slow motions ($\tau_r > 1.0 \times 10^{-4}$ sec) are present, the local dipolar fields are not completely averaged out. In such cases the relation $H_1 >> H_L$, where H_L is the local dipolar field, is not satisfied.

Theoretical considerations (39), as well as experimental results (40), show that in such cases $T_{1\rho}^{on}$ will decay with damped oscillations. The oscillations persist for a time of the order of T_2 and the oscillation frequency is $\sim 2\omega_1$. When oscillatory decay is seen, $T_{1\rho}^{on}$ values still can be measured accurately only if long τ values ($\tau > T_2$) are used (40).

In the present study oscillatory behavior was observed in a 70% PLL sample below 0°C. The interference became more pronounced as the temperature was lowered and it prevented obtaining data below -20°C. Oscillatory behavior was also observed in a BSA sample of 0.154 g/1 ml at -25°C at low H_1 fields.

2.6 Rotating Frame Spin-Lattice Relaxation in the Presence of an Off-Resonance rf Field ($T_{1\rho}^{off}$)

In this experiment an H_1 field which is off-resonance by ν_{off} is applied along the x' axis. As a result the magnetization will be aligned along an effective field H_e which forms an angle θ with the z axis. This is shown in Figure 2.3. The effective field is given by (10)

$$H_e = \frac{\omega_e}{\gamma} = \left[H_0 - \frac{\omega}{\gamma}\right]\vec{k} + H_1\vec{i},$$

where ω is the frequency of the rotating frame in

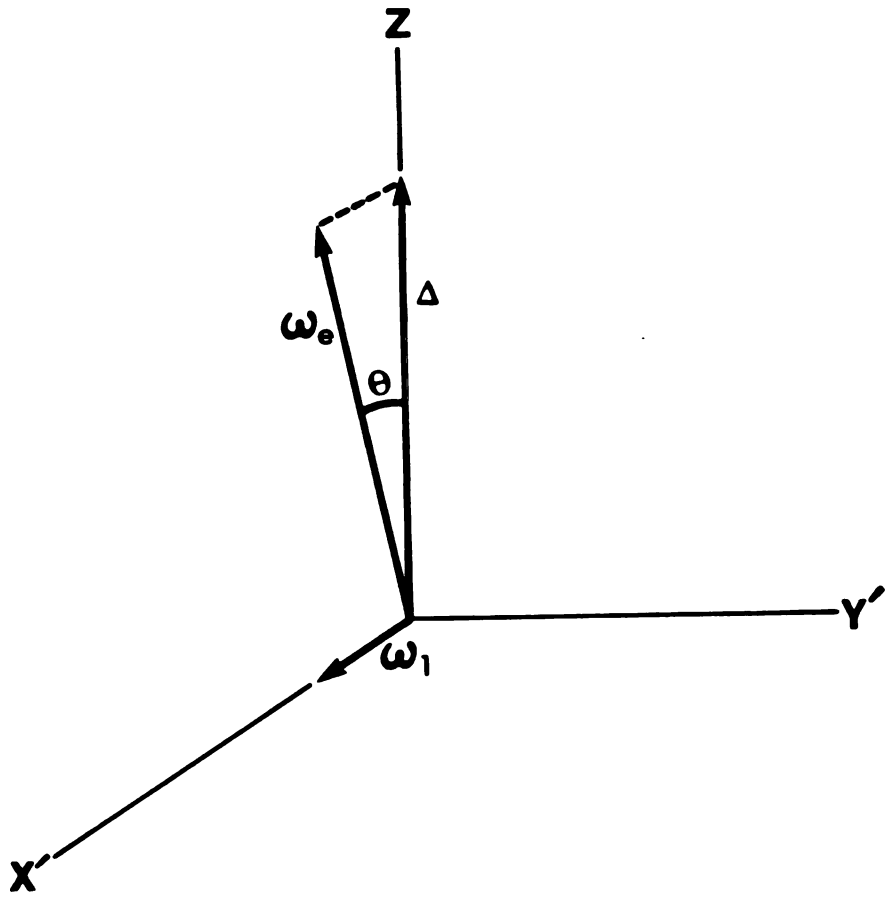

Fig. 2.3. The rotating co-ordinate system showing the effective rf field in the presence of an off-resonance field. The stationary magnetic field H_0 is aligned along the z axis.

units of radians/second. The distance from resonance in units of Hz is given by

$$\nu_{off} = \frac{\Delta}{2\pi} = \frac{\gamma H_0 - \omega}{2\pi}.$$

The angle θ is given by

$$\theta = \text{Arctan}\left(\frac{\omega_1}{\Delta}\right).$$

If the off-resonance H_1 field is on for a long enough time ($\sim 5T_1$), the magnetization along the effective field will reach a steady-state value, M_e. The steady-state value is a combination of spin-lattice relaxation processes which tend to restore it to M_0 and the effect of the H_1 field which tends to reduce it to zero. $T_{1\rho}^{off}$ can be described as the time constant for the steady-state value to be reestablished along the effective field.

If the rf field is applied far off-resonance such that

$$\frac{\omega_1}{\Delta} < 0.2 \qquad [2.8]$$

and $H_e \ll H_0$ and if an isotropic rotational motion is assumed, $T_{1\rho}^{off}$ is given by (10)

$$\frac{1}{T_{1\rho}^{off}} = 2\sigma_0^2 \left[\left(\frac{3}{2}\right)\sin^2\theta \frac{\tau_r}{1 + \omega_e^2 \tau_r^2}\right] + \frac{1}{T_1},$$

where $1/T_1$ is the same as in Equation 2.1.

In practice, $T_{1\rho}^{off}$ is difficult to measure directly. James et al. (10) suggested that the intensity ratio R can be measured instead. R is defined as

$$R = \frac{M_e}{M_0}$$

and is given by

$$R = \frac{T_{1\rho}^{off}}{T_1}.$$

The original data representation of James et al. (10) was modified and R was plotted as a function of $\sin^2\theta$. When plotted this way R becomes H_1 field dependent for $\tau_r > 10^{-7}$ sec. This enables one to detect the presence of slow motions by simply inspecting the data plots. When 10^{-7} sec $> \tau_r > 10^{-9}$ sec no H_1 field dependence is seen. However, the ratio values are highly dependent on the values of $\sin^2\theta$. When $\tau_r < 10^{-9}$ sec the dependence of the ratio on $\sin^2\theta$ is negligible. This is illustrated in Figure 2.4. The arrows in the figure indicate the H_1 field strength in units of Gauss (g).

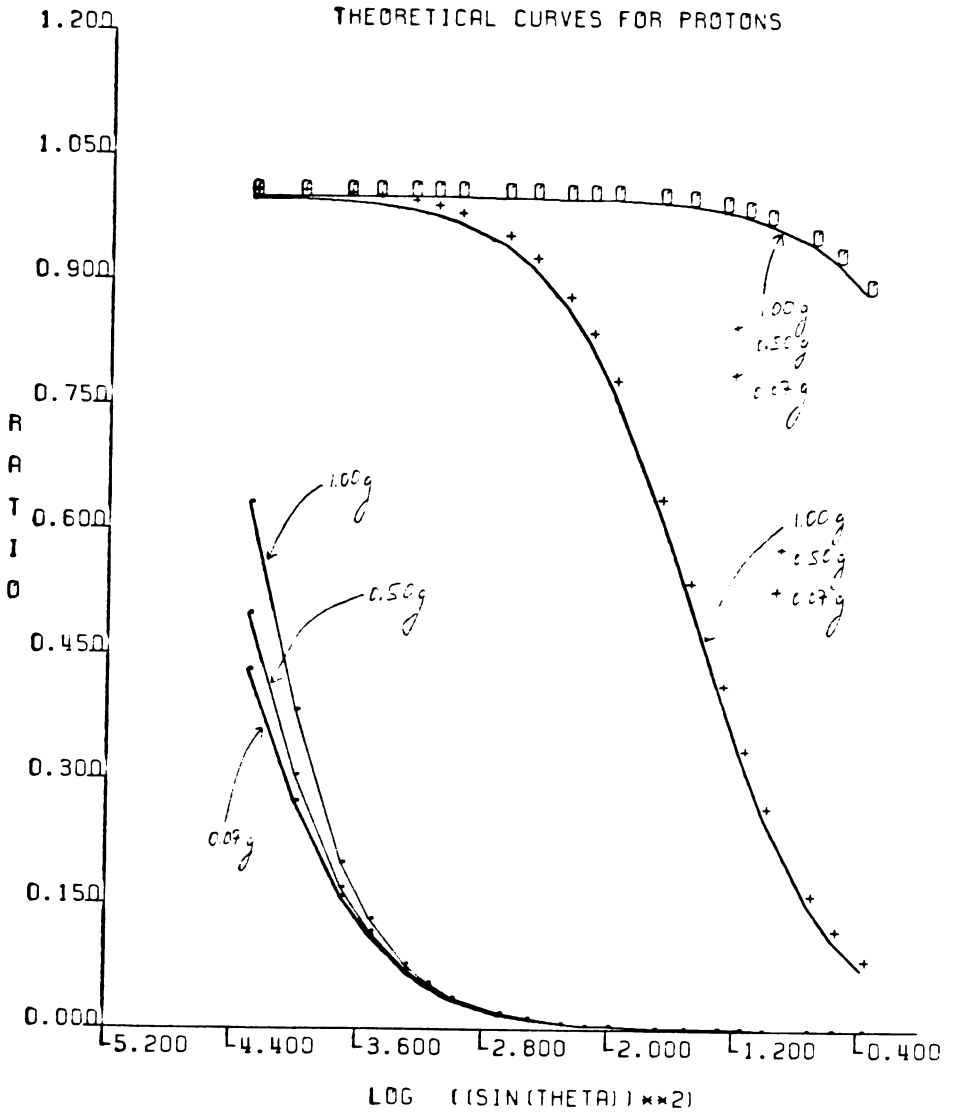

Fig. 2.4. Theoretical dependence of the ratio (R) on the logarithm of $\sin^2\vartheta$. (0) Correlation time 0.1 nanoseconds; (+) Correlation time 10 nanoseconds; (•) Correlation time 0.3 microseconds. The arrows indicate the H_1 field strength in units of Gauss (g).

The gyromagnetic ratio of deuterons is about 6.5 times less than that of protons. Therefore, the above effects will occur in deuterium spectra for values of τ_r longer by a factor of $\sim$7 as compared to protons. When $\tau_r < 10^{-8}$ sec, the dependence of R on $\sin^2\theta$ is very small. Unless H_1 fields of the order of 6-7 Gauss are achieved, only deuterium motions with $\tau_r > 10^{-7}$ sec can be studied. The highest H_1 field achieved was determined by the off-resonance amplifier output and was $\sim$2 g for deuterons.

As the values of $\sin^2\theta$ become very small (far off-resonance), R reaches its limiting value of 1.0. The upper values of $\sin^2\theta$ are limited by Equation 2.8 and the highest H_1 field. The highest H_1 field was determined by the off-resonance amplifier output and was $\sim$0.8 g for protons. This gives an upper limit of $\sim 5.7 \times 10^{-2}$ for $\sin^2\theta$ (log $\sin^2\theta$ = -1.25) and a lower limit of $\sim$17 KHz for ν_{off}.

It is possible to use the complete equation of Jones (34) to eliminate the restriction set by Equation 2.8 (41). Since for most samples examined in this study R reached a value of $\sim$0.2 within $\sin^2\theta$ value limits set by Equation 2.8, this was not done.

The main advantage of the $T_{1\rho}^{off}$ method is the possibility of examining multiline spectra. With the exception of T_2 data obtained from linewidth

measurements, T_2 and $T_{1\rho}^{on}$ experiments are difficult to perform and to interpret when more than one line is present (10). Examining multiline spectra is important in systems like protein + water + organic solvent where it is desirable to obtain information on the motions present in the water and in the organic solvent, both in the same system.

$T_{1\rho}^{off}$ measurements are sensitive to intermediate and slow motions. While information on both types of motions is contained in one experiment, it also complicates interpretation of data, since more parameters are needed to explain the results.

Since R is the ratio of two relaxation times, the rigid-lattice second moment cancels out. This eliminates one parameter when attempts are made to fit theoretical calculations to experimental results. However, information on internuclear distances is lost.

Since R is the ratio of two relaxation times, it will be relatively insensitive if $T_{1\rho}^{off}$ and T_1 happen to change in the same direction and at a similar rate. Such a situation may occur, for example, if R is studied as a function of temperature and concentration.

2.6.1 Experimental Determination of R

An off-resonance H_1 field is applied to the sample. H_1 is on for a time of $\sim 5\ T_1$ to allow the

magnetization to reach its steady-state value along the effective field. Immediately after the H_1 field is switched off, a 2 msec homospoil pulse is applied in the x'-y' plane to destroy any magnetization that may arise from the sudden switching off of the H_1 field. Next, a 90° observation pulse is applied at the resonance frequency and the resulting FID is Fourier transformed. The height of the resulting absorption peak is proportional to the magnetization M_e along the effective field. This sequence is repeated for different values of ν_{off} and a given H_1 field strength. Then, the H_1 field strength is changed and the magnitude of M_e is monitored for a different set of ν_{off} values.

The equilibrium magnetization M_0 along the H_0 field is monitored at each H_1 field strength by applying the H_1 field far enough off-resonance so that $M_e \approx M_0$. The ratio R and $\sin^2\theta$ values are then calculated for each ν_{off} value at each field and R is plotted as a function of $\sin^2\theta$.

2.7 Cross-Relaxation

A sample of protein in water can be regarded as a two "phase" system. The protein protons may be regarded as belonging to one "phase" and the protons

(or deuterons) of the water as belonging to the second "phase."

If a proton of one "phase" gets close to a proton of the other "phase" a dipolar interaction may take place. Simultaneous spin flip may occur and Zeeman energy will be exchanged between the two "phases" (5). This is referred to as a cross-relaxation process.

The dipolar coupling is essential for the spin flip to occur. Thus, the dipolar interaction between protons is 16 times more effective than the dipolar interaction between a proton and a deuteron. Only negligible cross-relaxation effects are expected to occur between the protein protons and the deuterons of D_2O (42).

2.7.1 T_1 in the Presence of Cross-Relaxation

In the presence of cross-relaxation, spin-lattice relaxation is described by a set of coupled differential equations. The solution shows that the magnetization in either phase will in general be described by two apparent exponential relaxation times which are the same for both phases (5).

The presence of a two-phase exponential decay is not by itself an evidence that cross-relaxation is present. Two component decay will be observed if two

slowly exchanging environments exist and $\tau_{res} > T_1$, where τ_{res} is the shortest residence time. Since in real systems $T_2 < T_1$, $\tau_{res} > T_2$, and the transverse relaxation should also show a two component decay. However, if the T_2 values in the two environments are similar, the two components may not be resolved. Thus, a situation may arise where T_1 shows a two component decay because of two slowly exchanging environments, while only one component is seen in the transverse relaxation (19).

On the other hand, the presence of only one component exponential decay should not be taken as an evidence that cross-relaxation is not present. If one of the components is very short and its relative contribution is small, it may not be detected.

In general, the cross-relaxation is expected to become more important at higher spectrometer frequencies (43). The precise frequency dependence of the cross-relaxation depends on the model being used to describe the interaction between the two "phases." Koenig et al. (22) investigated the solvent proton and deuteron T_1 frequency dependence of a number of dilute protein solutions. They concluded that the frequency dependence of the cross-relaxation term is the same as that of the solvent in the absence of cross-relaxation.

2.7.2 T_2 in the Presence of Cross-Relaxation

In general, cross-relaxation will contribute to the observed value of T_2, but the decay is expected to be single exponential (43). Usually, a model of unlike interacting spins is used, but the precise contribution to T_2 depends on the mechanism that is assumed to govern the cross-relaxation.

2.7.3 $T_{1\rho}^{on}$ in the Presence of Cross-Relaxation

No explicit theory exists to take into account the contribution of cross-relaxation to $T_{1\rho}^{on}$ relaxation. $T_{1\rho}^{on}$ can be regarded as being roughly analogous to measuring T_1 relaxation at very low fields. Since cross-relaxation is important only at high fields, its contribution to $T_{1\rho}^{on}$ is expected to be small. However, since cross-relaxation does contribute to T_2 values, some contribution to $T_{1\rho}^{on}$ values is expected.

There exists the possibility that $T_{1\rho}^{on}$ measurements may detect the transfer of magnetization, due to cross-relaxation processes, between the two "phases." This may be interpreted as the presence of some kind of "slow motion."

2.7.4 $T_{1\rho}^{off}$ in the Presence of Cross-Relaxation

No theory exists to predict the contribution of cross-relaxation to $T_{1\rho}^{off}$ relaxation. The low range of the effective field H_e in this experiment

is similar to the low range of the H_1 field in the $T_{1\rho}^{on}$ experiment. The high range of $H_e \sim 20$ g and the high range of $H_1 \sim 15$ g. Although H_e covers a somewhat wider range than H_1, considerations similar to those described for the $T_{1\rho}^{on}$ experiment may hold.

CHAPTER 3

MATERIALS AND PREPARATION OF SAMPLES

POLY-L-LYSINE HYDROBROMIDE (PLL) type V was purchased from Sigma. Reported molecular weight (M.W.) = 15,000 and degree of polimerization = 70. Type V PLL is prepared without chemical initiator.

The PLL was dialyzed against distilled water and recovered by lyophilization at $\sim$5 μ pressure. Preliminary experiments showed that a large amount of PLL was lost, because of leakage through the membrane. To minimize the leakage Spectrapor membrane tubing (Spectrum Medical Industries No. 132650) with a reported M.W. cutoff of 6,000-8,000 was used. Prior to dialysis the membrane was treated to remove glycerol and sulfides according to the manufacturer's instructions. The treatment procedure consisted of 4 steps:

1. Tubing was treated with 0.3% sodium sulfite solution at 80°C for 1 minute.
2. Washed with distilled water at 60°C for 2 minutes.
3. Treated with 0.2% sulfuric acid solution.
4. Washed with distilled water.

Treated tubing was stored in distilled water under refrigeration.

The lyophilized material had a very low density and was difficult to transfer into NMR tubes. To circumvent this problem, a small amount of water was added to the lyophilized material and then it was lyophilized again. A high density "cake" which was easy to handle formed. This "cake" was stored frozen at $\sim$ -20°C.

Samples were prepared by weighing the PLL directly into 5 mm NMR teflon sleeves (Wilmad WG-1262). Teflon tubes were used to prevent cracking at subzero temperatures. The teflon tubes with the PLL powder were kept at $\sim$5 μ pressure until constant weight was achieved. The desired amount of distilled water was added using microsyringes and the tubes were immediately sealed with epoxy. To assure mixing the samples were centrifuged repeatedly back and forth along the tubes. The most concentrated sample was too viscous to centrifuge. Mixing of this sample was achieved by heating the bottom of the tube at $\sim$ +60°C while cooling the top with a stream of cold air. The resulting condensate was forced back into the mixture by centrifugation. This procedure was repeated until the sample appeared to be homogeneous. The procedure was repeated further to assure good

mixing. The concentrations of the PLL samples are reported in units of wt/wt.

BOVINE SERUM ALBUMIN (BSA) was purchased from Sigma and was No. A-7638. This BSA is prepared from bovine serum by crystallization and lyophilization and is reported to contain less than 0.1% globulins.

Samples were prepared by weighing the BSA powder into a test tube and adding doubly distilled water by pipetation. After dissolution, samples were transferred either into NMR teflon sleeves or into 5 mm NMR glass tubes (Wilmad 503-PS). The teflon sleeves were immediately sealed with epoxy. The glass tubes were immediately capped and wrapped with parafilm.

BSA IN D_2O samples were prepared in a similar way, except that D_2O was added instead of distilled water. Whenever D_2O was added directly into samples, D_2O low in paramagnetic impurities (Aldrich 19,234-1) was used. All samples were handled with teflon coated spatulas to prevent contamination with paramagnetic impurities. The concentrations of the BSA samples are reported in units of weight of protein per 1 ml of added solvent.

LYSOZYME was purchased from Sigma and was Grade 1, No. L-6876. It was a three times crystallized, dialyzed, and lyophilized powder.

Experiments at subzero temperatures were performed by first cooling the NMR probe to the desired temperature. The 12 mm tube with the deuterated locking solvent was precooled in dry ice. The teflon tube with the sample was immersed quickly into liquid nitrogen in a dewar flask and it was held there for a few minutes. Then it was transferred into the 12 mm tube and the tube with the sample was quickly transferred into the probe. Samples were allowed to equilibrate in the probe for about an hour. The linewidth was checked occasionally to assure that a constant temperature was achieved.

pH was measured with Corning model 10 pH meter and Sargent-Welch model S-30070-10 combination electrode. The instrument was standardized with buffers supplied by Mallinckrodt.

Buffers were not used to prepare the samples in order to avoid complications in interpretation that may arise from the presence of salts. Because of the high concentrations of the BSA solutions which we used, it was impossible to measure the pH directly. The BSA coagulated around the electrode and formed a solid film that prevented reliable pH readings. In the pH dependence study of the BSA solutions, the pH is reported as the pH of the added water. The pH of

the water was adjusted with ∿1 M solution of NaOH or ∿1 M solution of HCl.

BSA + NaF samples were prepared by adding NaF to a solution of 0.5 g/1 ml BSA in D_2O or H_2O. Enough NaF was added to make a final concentration of ∿1 M NaF. To allow time for equilibration, the solutions were kept in the refrigerator for one week and shaked occasionally. To remove undissolved NaF, samples were centrifuged and the clear upper solution was transferred into NMR glass tubes.

SODIUM FLUORIDE (NaF) crystalline was purchased from Sigma and was No. S-1504. Approximate purity was 99%.

POTASSIUM FLUORIDE (KF) anhydrous, granular was obtained from Allied Chemical and was of analytical grade.

GLYCERINE sample was prepared by first drying a small amount of glycerine in the lyophilizer at ∿5 μ pressure. Part of the sample was transferred to a teflon tube immediately after the lyophilizer was shut off and the tube was sealed.

PERDEUTERATED GLYCERINE was supplied by Merck Sharp & Dohme, Canada. Its isotopic purity was reported to be 98% atom D.

HYDROCHLORIC ACID (HCl) was purchased from Alfa Products and was of ultrapure grade.

SODIUM HYDROXIDE (NaOH) pellets were obtained from Mallinckrodt and were of analytical grade.

CHAPTER 4

EXPERIMENTAL

4.1 JEOL 4H-100 Spectrometer

Poly-l-lysine (PLL) proton T_1 and $T_{1\rho}^{on}$ relaxation times were measured at 44.4 MHz using a JEOL model 4H-100 electromagnet and power supply. The 44.4 MHz frequency was generated by a phase coherent model CPS-2 NMR spectrometer in conjunction with a PGS-2 pulse programmer, both manufactured by Spin-Lock Electronics Ltd. of Canada. Home-built single coil probe with thermal teflon insulation was used.

Temperature was controlled by JEOL temperature control assembly. This consisted of a heating element inserted into liquid nitrogen container, a heater, and a model JES-VT-3 temperature controller. Temperature was measured with copper/constantan thermocouple inserted into the probe at the coil level and connected to a digital thermometer (Fluke model 2100A). Samples were equilibrated at a given temperature for about an hour and the temperature was rechecked after the experiment was completed. Temperature remained constant within ±1.0°C for temperatures above 0°C and within ±2.0°C for temperatures below 0°C.

Homogeneity was adjusted by using fine screws that made it possible to move the probe with the sample in either the horizontal or the vertical directions. While this was done, the FID was observed under off-resonance conditions. Homogeneity was judged to be best when the beat pattern persisted for the longest time and the decay envelope seemed to consist of only one component.

Field stability was achieved by establishing the direction of the field drift first. Then, the fine field stabilizer was turned in the appropriate direction and its value adjusted until no further drift occurred within the estimated duration time of the experiment.

Relaxation times were measured by monitoring the heights of the free induction decay (FID) with a boxcar integrator (Princeton Applied Research model CW-1) combined with a digital display voltmeter (Keithley model 171).

4.1.1 T_1 Experiments

T_1's were estimated at the beginning of each experiment by the zero-point method. In experiments, the delay time (DT) was set so that

$$DT \geqslant 5T_1. \qquad [4.1]$$

The time needed to integrate the signal (IT) is given by

$$IT \geq \frac{5 \times \text{Time Constant}}{\text{Total Time Gate Is Open}}, \qquad [4.2]$$

where Time Constant is the time constant of the integration box. To reduce noise, it is desirable that

$$\text{Gate Width} < (\text{Time Constant}) \times (DT). \qquad [4.3]$$

The gate width and the time constant were adjusted to satisfy Equations [4.1], [4.2], and [4.3].

Preliminary experiments showed the dead time (DE) of the probe to be ∿10 μsec. The gate was placed at 100 μsec from the last pulse for samples with long FID's. This value was decreased for shorter FID's, but never below 10 μsec.

4.1.2 $\underline{T_{1\rho}^{on}}$ Experiments

$T_{1\rho}^{on}$ experiments were performed at 44.4 MHz using the same instrumentation as for the T_1 experiments. The spin-locking field strength was determined by measuring the pulse length (t_π) required to rotate the magnetization vector through (n x 180)°, n=1,2,3.... t_π was measured for up to n = 7 and its average value was used. The field strength (ν_1) in units of KHz is given by (26)

$$\nu_1 = \frac{1}{2t_\pi},$$

if t_π is given in milliseconds (msec).

4.2 XL-100-15 Spectrometer

Proton data at 100 MHz, deuterium data at 15.4 MHz, and fluorine data at 94.1 MHz were acquired on a Varian XL-100-15 spectrometer. This spectrometer consists of a 100 MHz model V-7405 electromagnet and Nicolet TT-100 Fourier transform (FT) data processor.

Temperature in the probe was controlled by passing air or dry nitrogen through a coil inserted in a dewar flask. The dewar flask contained ethanol, or ethanol/dry ice mixture, and its temperature was regulated with FTS systems model FC-20-84-P4-SV temperature regulator. The cold gas passed through a heating element and a temperature sensor located under the coil and connected to Varian model 906790-I0 variable temperature controller. Temperature was stable within ±0.5°C above 0°C and within ±1.0°C below 0°C.

Homogeneity was adjusted by maximizing the FID of the deuterium signal which was used as the lock reference. Shim coils built in by the manufacturer were used.

All the data on the XL-100-15 spectrometer were acquired using quadrature detection (QPD). In

the QPD detection mode the signal passes through two parallel detection channels which are out of phase by 90° with respect to each other. This is equivalent to sampling the signal along the x and y axes simultaneously. As a result, one can distinguish signal frequencies which are higher than the spectrometer frequency, from those which are lower than the spectrometer frequency. In practice, one changes the spectrometer offset frequency until resonance condition is achieved and the FT of the FID is positioned in the middle of the screen. QPD detection allows to view the complete absorption peak of a signal which is on resonance. This is advantageous in relaxation experiments where peak heights need to be measured. In the QPD detection mode the observing frequency is positioned in the middle of the spectral region of interest. This cuts the effective bandwidth in half and increases the signal to noise ratio (S/N) by a factor of $\sqrt{2}$, as compared to a single phase detection. Narrowing the spectral region allows for shorter observing pulses and longer dwelling times (26).

If the spectra contains peaks outside the effective QPD spectral bandwidth, these peaks will "fold-in" and appear on the screen, but their intensity and/or

phase might be distorted. To ascertain that no "folding-in" occurred, two experiments were performed:

1. The spectrometer offset frequency was changed by a certain amount. If no "folding-in" occurred, the peak would be expected to "move" a proportional distance on the screen and in the appropriate direction.
2. The filter was increased to a value of at least twice the sweepwidth. If no "folding-in" occurred, peak height would be expected to remain unchanged.

It was found that method 1. alone was not sufficient to detect "folding-in" and consequently both methods were always used.

The two channels employed in the QPD detection mode cannot be perfectly matched. To equalize the channels a two-part four-phase cycle is used. Each part consists of two pulses. One part involves a 90° phase shift, in respect to each channel, of the pulse which initiates the data acquisition. This amounts to using both channels to detect the x and the y components and equalizes any differences in phase and gain. The second part involves a 180° phase shift, with respect to each channel, of the pulse which initiates the data acquisition. This part eliminates

DC offset differences and any coherent noise whose sign is not changed by the 180° shifts. In all the experiments the number of acquisitions was always a multiple of four.

Varian XL-100-15 spectrometer is equipped with both internal and external locking capabilities. The internal lock operates in the pulse mode and uses deuterium signal at 15.4 MHz as its reference. The external lock operates in the continuous sweep mode. It uses fluorine signal at 94.1 MHz as its reference and is modulated at an audio-frequency of 40.96 KHz.

The deuterium signal in the concentrated and the frozen samples is too broad to be used as a lock reference. Preliminary experiments showed that, in the off-resonance experiments the external lock cannot be used either. The audio modulation frequency interferes with the experiment when its value is close to a multiple of the off-resonance frequency and causes reduction in peak heights. Consequently, the off-resonance experiments on the frozen samples were carried out with the teflon tube inside a 12 mm coaxial inner cell (Wilmad WGS-12BL). The coaxial tube with the sample was inserted into a 12 mm NMR tube (Wilmad 514A-1PP) that contained per-deuterated chloroform (Aldrich 15,185-8, 100% D) or per-deuterated acetone (Aldrich 15,179-3, 99.5% D) and the spectrometer

was locked on the deuterated solvent. The connection between the inner and the outer tubes was sealed at the top to prevent absorption of moisture by the deuterated solvent.

Experiments above freezing temperatures were carried out on samples that contained 30% v/v D_2O. The deuterium signal from the 0.8 g/1 ml BSA sample was too broad to be used as a lock. Locking on this sample was achieved by placing a glass capillary, sealed at both ends and filled with D_2O (Aldrich 15,189-0 100.0% D), inside the sample tube.

4.2.1 Proton $T_{1\rho}^{off}$ Experiments

Proton data at 100 MHz were obtained using Varian model 934701-03 cross-coil probe. The additional off-resonance frequency needed for the off-resonance experiment was generated by Fluke model 3400A frequency synthesizer. Its reference frequency was locked to the master oscillator of the XL-100-15, but was phase incoherent. To allow control of the off-resonance H_1 field strengths, the generated frequencies passed through an rf multiple switch attenuator (Pine Brook model 32-0) and through an rf amplifier (Amplifier Research model 30LA). The off-resonance frequencies and the observing on-resonance frequencies were introduced into the transmitter coils of the probe

through a pulse divider (EIN model PM 40-2). Variability in the duration of the off-resonance H_1 field was made possible by an rf switch. The rf switch and the off-resonance frequency were controlled by the computer.

To protect the receiver from overload, probes' paddles were carefully adjusted before each experiment to maximize the orthogonality between the transmitter and the receiver coils. It was found that a "glitch" originating at the off-resonance amplifier was present. To protect the preamplifier and the receiver coils, a home-built pair of cross-diodes was added at the amplifier output and a x5 attenuator (Tektronix 011-0060-02) was added at the output of the synthesizer. The amplifier gain was set to maximum and its output was set to ~ 20 watts by adjusting the output gain knob of the Synthesizer. Preliminary experiments showed that this set-up was the most efficient in reducing the pulse breakthrough. A schematic illustration of the experimental set-up is shown in Figure 4.1.

At the beginning of an experiment, the signal was brought to resonance by changing the spectrometer offset frequency. T_1 was estimated from the zero-point. The basic frequency of the off-resonance frequency synthesizer was set to the spectrometer frequency by inspecting its beat pattern against the spectrometer

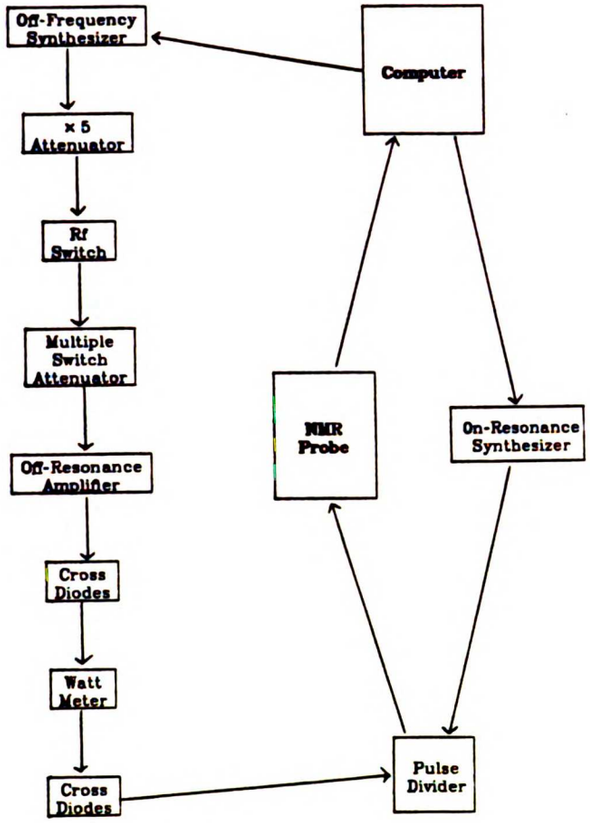

Fig. 4.1. A schematic illustration of the experimental set-up for the proton off-resonance experiments.

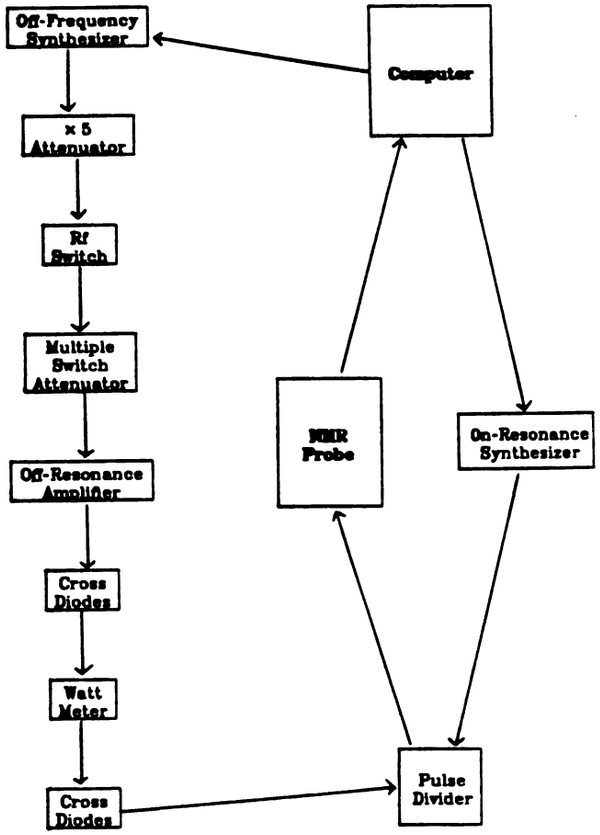

Fig. 4.1. A schematic illustration of the experimental set-up for the proton off-resonance experiments.

frequency. The frequency of the synthesizer was changed until a minimum in the beat frequency was achieved. The two frequencies did not differ by more than ±2 Hz. All the off-resonance frequencies were generated relative to this basic frequency.

The off-resonance H_1 field was applied for at least $5T_1$. Then it was switched off and a 2 msec homospoil pulse was applied in the x-y plane. Immediately after, the sample was subjected to a 90° on-resonance observation pulse and the FID stored on a magnetic disc (Nashua Cartridge DD15-8).

The efficiency of the homospoil pulse was checked at the highest and the lowest H_1 fields used for each sample, at a value of the off-resonance frequency closest to resonance. The checking experiment was performed in a similar way to the actual experiment, except that the observation pulse was set to 0°. In all the cases the residual signal was insignificant (less than 1%) as compared to the peak seen with the 90° observation pulse.

For the purpose of the off-resonance experiment, the equilibrium peak intensity of the stationary H_0 magnetic field must be known. Preliminary experiments showed that at 500 KHz off-resonance the peak intensity is equal to the peak intensity if measured by a 90° one pulse experiment. To keep all measurements under

similar conditions, equilibrium peak intensities were measured at ν_{off} = 500 KHz.

When applying rf fields for relatively long times, one should worry about the possibility of raising the temperature of the sample. The heating effect may be significant, if the sample contains small ions. In order to check for heating effects, a "simulation" experiment was performed on a sample of 4.5 M LiCl in water at +25°C. The rf amplifier output was ∿20 watts, which was the highest output used in the experiments. It was applied at off-resonance frequencies and for a total time of a typical off-resonance experiment. At the end of the "simulation" experiment, the temperature had increased by ∿4°C.

To average the heating effect and other drifts, all the off-resonance frequencies were applied in a random fashion, i.e., never in an ascending or a descending order. At least two equilibrium peak intensities were measured, one at the beginning of an experiment and one at the end of an experiment and their average value was used. The two peak intensities did not differ by more than ±3%.

Since in the off-resonance experiment frequencies are applied which are off-resonance by many KHz, there is a possibility of probe detuning at high off-resonance values. Consequently, the H_1 field strength

at the sample at high off-resonance values might be smaller than the H_1 field strength measured on-resonance. The rf power introduced into the probe and the reflected power were measured on a wattmeter (Sola Basic model 1000) at different off-resonance frequency values. The difference between the rf introduced into the probe and the reflected power was taken as a relative measure of the H_1 field strengths. It was found that up to ν_{off} = 500 KHz there was no measurable loss of power. At ν_{off} = 1 MHz there was $\sim$5% reduction in field strength.

In attempting to measure the H_1 field strengths, three major problems were encountered:

1. The off-resonance frequency synthesizer was phase incoherent, and therefore H_1 had to be measured with one accumulation only. This eliminated the possibility of measuring H_1 directly on the frozen and the broad line samples.
2. The low H_1 fields employed in this experiment were too low to be accurately measured directly. To be accurately measured the following relation should hold:

$$\gamma H_1 >> LW_{1/2}.$$

For protons γ = 4.26 KHz/Gauss (22). For

a field of H_1 = 0.1 Gauss (g), γH_1 = 426 Hz. The requirement that $\gamma H_1 >> LW_{1/2}$ was not satisfied for the frozen samples which had $LW_{1/2} \approx 500$ Hz. For the low H_1 fields a plot of the FID height as a function of the pulse length goes through a broad minimum at $t_\pi = 180°$. The minimum gets broader as the H_1 field becomes smaller and the 180° pulse length cannot be located precisely. Consequently, even when samples had relatively narrow linewidths, low H_1 fields could not be determined directly on the samples.

3. The frozen samples were in a different physical state. This could have changed the dielectric constant of the sample and the actual H_1 field at the sample, as compared to the same sample in the liquid state, could have been different.

A series of preliminary experiments were performed to check if the H_1 field strengths could be measured on a water sample containing LiCl. Using water had the advantage of a strong signal and narrow linewidths. LiCl was added to prevent freezing at the low temperatures.

The H_1 field strengths were measured by finding the pulse length at which the FID height was zero (180° pulse). H_1 in units of Gauss is given then by (22, 26)

$$H_1 = \frac{1000}{2 \times 4.26 \times t_\pi},$$

where t_π is in microseconds (μsec).

The H_1 fields were changed by activating different combinations of switches on the rf attenuator. For each H_1 strength, the voltage introduced into the probe was measured between the NMR probe and the pulse-divider (see Figure 4.1). The voltage was measured on Tektronix model 475 oscilloscope in conjunction with a 50 Ω resistor (Sola Basic model 4025).

Table 4.1 compares the H_1 field strengths at different attenuations, as measured directly on the LiCl samples and as measured from the voltage readings. Each column was normalized relative to the highest H_1.

LiCl in water forms an eutectic mixture at -40°C and the eutectic composition is ∿4.5 M (44). LiCl 2 M at -30°C forms ice, but enough liquid water exists in equilibrium with the solid to give an appreciable signal. At -25°C only little ice is formed.

Table 4.2 compares the normalized H_1 fields as measured directly on the LiCl 4.5 M sample and on a glycerine sample, both at -25.0°C. Table 4.3 compares

Table 4.1. Normalized H_1 field strengths at different levels of attenuation. The fields were measured directly on samples of 4.5M and 2M LiCl in water at two temperatures. Each sample contained a different amount of ice.

Attenuation Decibels (db)	Volts	H_1 (Normalized) LiCl 4.5M −25.0°C No Ice	H_1 (Normalized) LiCl 2M −25.0°C Little Ice	H_1 (Normalized) LiCl 2M −30.0°C "Solid"
13	1.000	1.000	1.000	1.000
14	0.913	0.932	----------	0.920
19	0.522	0.527	0.523	0.531
24	0.261	0.269	----------	0.265
29	0.141	0.150	0.147	0.147

Table 4.2. Normalized H_1 field strengths at different levels of attenuation. The fields were measured directly on a sample of 4.5M LiCl in water and on a sample of glycerine.

Attenuation (db)	H_1 (Normalized) LiCl 4.5M −25.0°C	H_1 (Normalized) Glycerine −25.0°C
14	1.000	1.000
24	0.276	0.247
29	0.145	0.084

Table 4.3. Absolute H_1 field strengths at different levels of attenuation. The fields were measured directly on a sample of 4.5M LiCl in water and on a sample of acetone.

Attenuation (db)	H_1 (g) LiCl 4.5M −25.0°C	H_1 (g) Acetone −25.0°C
14	0.838	0.851
24	0.235	0.210
29	0.132	0.074

the absolute H_1 field strengths that were measured directly on the LiCl 4.5 M sample and on a sample of acetone, both at -25.0°C.

Inspection of the data in Table 4.1 shows that ice formation does not interfere with the H_1 measurements. Inspection of Tables 4.2 and 4.3 shows that discrepancies of up to ∿50% exist between measurements of the very low H_1 fields on different samples. For the acetone and the LiCl 4.5 M samples, the discrepancy is ∿11% at the intermediate H_1 fields and only ∿2% at the high fields.

We measured the voltage introduced into the probe at a point between the probe and the pulse-divider, after the cross-diodes. Therefore, the H_1 field at the sample should be proportional to the voltage introduced into the probe. In all the following experiments, H_1 field strengths were determined by first measuring the high H_1 field on the LiCl 4.5 M sample. Then, the voltage introduced into the probe was measured for the same field and for the lower H_1 fields used. The lower H_1 field strengths were calculated in proportion to their measured voltages. To eliminate errors as much as possible, all H_1's were measured at the same temperatures as the samples. LiCl sample in a teflon tube was used for the frozen samples. LiCl sample in a glass tube was used for the liquid

samples. To eliminate effects arising from different geometrical shapes, LiCl samples were placed in the probe using exactly the same arrangement as for the samples.

All peak ratios were determined by measuring the heights of the absorption peaks. A large exponential line broadening (45) was applied to the FID's before FT to smooth the peaks and to reduce noise. Peak heights were measured by zooming on the upper part of the absorption peaks and using the computer to read out the heights (45).

4.2.2 Deuterium Experiments at 15.4 MHz

Deuterium data at 15.4 MHz were acquired on the XL-100-15 electromagnet using variable frequency single coil probe (Nicolet model NT 74012). Observing frequency was generated by Nicolet model NT 440 Multi Observe Nuclei Accessory (MONA). All the deuterium data at 15.4 MHz were acquired using the QPD detection mode and the external lock.

Preliminary experiments showed that a large pulse breakthrough interfered with measurements on frozen samples. To protect the receiver from the transmitter, the original cable arrangement was modified to include a pair of cross-diodes and a cable that had a length (l) such that $l \approx \frac{\lambda}{4}$, where λ is the

deuterium wavelength in the cable. A schematic illustration of this arrangement is shown in Figure 4.2. To keep conditions uniform, all the deuterium data at 15.4 MHz were acquired using this arrangement.

Despite this arrangement, a residual pulse-breakthrough caused some distortion of the base line of frozen samples. Base line distortion was more pronounced with the off-resonance data. Consequently, the off-resonance data on frozen samples was processed by first plotting the absorption peaks. Then, an "average" base line was drawn for each peak. Peak heights were measured relative to the "average" base line.

4.2.2.1 Deuterium T_1 Experiments

Deuterium T_1 relaxation times at 15.4 MHz were measured by monitoring the heights of the absorption peaks. The 180° pulse needed for the T_1 experiment cannot be set precisely and a small residual component remains in the x-y plane. This component decays with a time constant of T_2^* and might interfere with the measurements if the delay time (τ) between the 180° and 90° pulses is short. To avoid this problem, T_2^* was estimated first from the absorption peak linewidth using the relation (26)

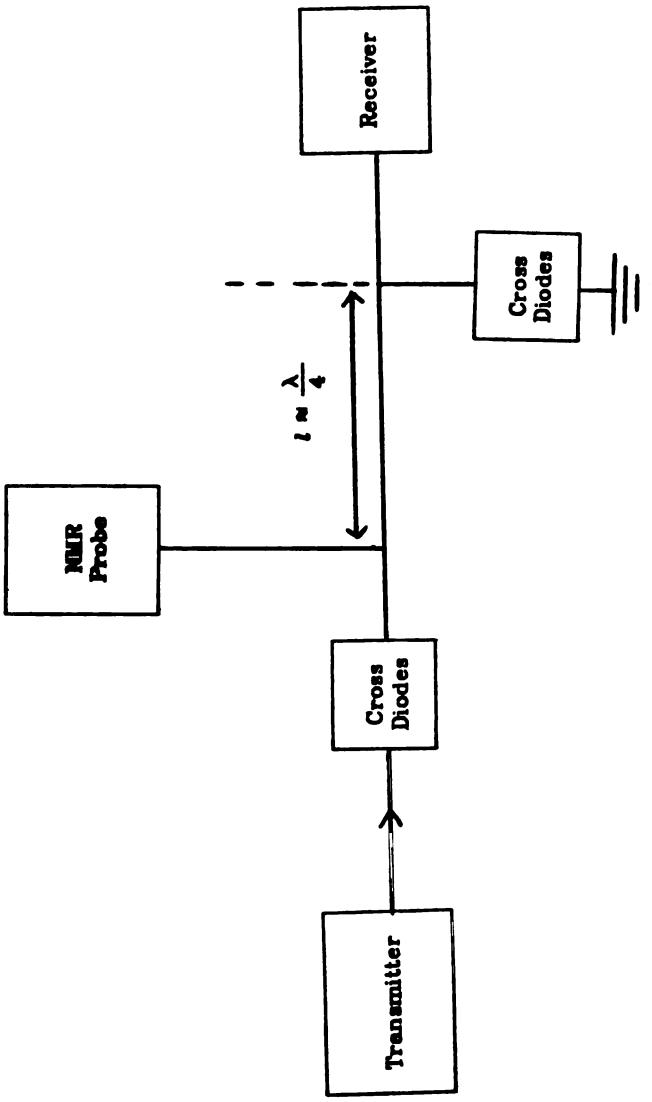

Fig. 4.2. A schematic illustration of the experimental set-up for the deuterium off-resonance experiments.

$$T_2^* = \frac{1}{\pi LW_{1/2}}.$$

$LW_{1/2}$ was calculated using the Lorentzian fit program supplied by Nicolet. The shortest delay time (τ_{min}) was then set so that

$$\tau_{min} \geq 4T_2^* .$$

4.2.2.2 Deuterium $T_{1\rho}^{off}$ Experiments

Deuterium $T_{1\rho}^{off}$ experiments at 15.4 MHz were performed as described for protons at 100 MHz. The H_1 field strengths needed for the off-resonance experiment were measured as described for protons at 100 MHz, except that the highest H_1 field was measured on a sample of 4.5 M LiCl in D_2O. For deuterons γ = 0.654 KHz/Gauss (22) and the equilibrium peak intensities were measured at ν_{off} = 100 KHz. The H_1 field strengths as a function of the off-resonance frequency were measured as described for protons at 100 MHz. At ν_{off} = 100 KHz there was ∿1.5% reduction in the field strength. At ν_{off} = 200 KHz there was ∿11% reduction in the field strength.

4.2.3 Fluorine Experiments at 94.1 MHz

Fluorine experiments at 94.1 MHz were carried out on the XL-100-15 spectrometer using same techniques and accessories as described for protons at 100 MHz.

4.2.3.1 Fluorine Saturation Experiments

Fluorine saturation studies were performed at +20°C. The fluorine signal was sampled at 94.1 MHz while the proton signal was irradiated with a broadband Nicolet TT760 decoupler whose frequency was centered at 100.05 MHz. To assure that steady-state was established, the first eight accumulations were ignored.

A saturated solution of KF in water was used as a reference. This sample had $T_1 \approx 0.94$ sec and $LW_{1/2} \approx 3$ Hz. When the decoupler was off the fluorine signal had an amplitude of 650.2 (arbitrary units). When the fluorine was irradiated with a power of ∿5 watts for 5 seconds, just prior to acquisition, complete saturation took place and no signal could be detected.

4.3 Nicolet Superconducting Magnet

Proton data at 55 MHz and 100 MHz, deuterium data at 22 MHz and fluorine data at 141 MHz, were acquired on a superconducting variable field magnet (Nicolet Corporation). Home-built probe and circuitry were used. The observing frequency was generated by Programmed Test Sources, Inc., model PTS 160 frequency synthesizer. Nicolet model 1180 computer was used for data acquisition and processing.

Temperature was controlled as described for protons at 100 MHz, except that the temperature in the dewar flask was not regulated. Fisher Scientific model 22 proportional temperature controller was used. All temperatures were stable within ±0.5°C.

The field was stable within ±2 Hz and no lock was used. Homogeneity was adjusted using home-built shim coils, while the signal was observed under off-resonance conditions as described in Section 4.1. All data were acquired using the QPD detection mode.

4.3.1 T_1 and $T_{1\rho}^{on}$ Experiments

T_1 and $T_{1\rho}^{on}$ relaxation times were measured by monitoring the heights of the absorption peaks.

4.3.2 T_2 Experiments

T_2 relaxation times were measured using the Hahn spin-echo method (33). The FID of each echo was Fourier transformed and the heights of the resulting peaks were measured. Preliminary experiments showed that the values of T_2 did not depend on the DE. However, to optimize the S/N ratio and to keep uniform conditions all the DE's were set to have values so that

$$t_\pi < DE \leqslant 1.5t_\pi.$$

4.4 ESR Experiments

Electron spin resonance (ESR) experiments were carried out on Varian E3 EPR spectrometer. The Mn^{++} ion spectra were obtained at room temperature at 9.525 Gigahertz.

CHAPTER 5

DATA PROCESSING

5.1 General

PLL relaxation data were fitted using the PROPHET computer system and the associated FITFUN program. All the other T_1, $T_{1\rho}^{on}$, and T_2 data were fitted using either the Nicolet 1180 computer and the associated Nicolet programs, or the Nicolet TT-100 data processor and the associated Nicolet programs. All fitting programs employed nonlinear least square procedures. In a few cases the same data were fitted using the two computer systems. In all such cases, similar results were obtained for the fitted parameters.

Off-resonance data were processed using the UNIX computer system and the self-written VOFFH, NMRRB, and NMRKS4 Fortran programs (see Appendix for a listing of these programs).

Plots were obtained using either the VERSATEC plotter and the SCAT plotting program, or the Houston Instrument model DP2-5H plotter and the associated Nicolet program.

Occasionally, a local minimum was encountered during a fitting procedure. In such cases the standard

deviation (SD), as calculated by the computer, would indicate a "good" fit, while visual inspection of the calculated "best" fit would show a curve that did not match the experimental points. To avoid the local minimum, different combinations of the initial parameter values were tried until the fitted curve matched the experimental points. To assure that the fitted parameters did not correspond to a local minimum, all fitted curves were visually inspected.

Experimental errors are difficult to evaluate precisely, because the "true" value of the measured parameters is usually not known. SD is a measure of the "goodness" of fit, rather than of the "true" experimental error. A fit can be good and have a small SD value, even when systematic errors are present. It is unlikely that systematic errors will remain undetected, if data on many samples are taken over a long period of time using the same instrumentation, as is the case in our study. However, the SD values should only be regarded as a lower limit on the experimental error which can be objectively calculated.

Whenever it is judged that the "true" experimental errors are larger than the SD values, the estimated experimental errors, either alone or together with the SD values, are given.

5.2 T_1 Data

T_1 data were fitted to a three parameter function, which had the form

$$y = A - B \exp\left(-\frac{\tau}{T_1}\right).$$

A, B, and T_1 are the parameters to be fitted and y and τ are the experimental amplitudes and delay times, respectively. T_1 is the relaxation time.

Some of the PLL samples showed a biphasic T_1 decay. This data were fitted to a five parameter function, which had the form

$$y = A - B \exp\left(-\frac{\tau}{T_1}\right) - C \exp\left(-\frac{\tau}{T_{1,2}}\right).$$

C and $T_{1,2}$ are the additional parameters to be fitted. $T_{1,2}$ is the second relaxation time. Only the longer relaxation times corresponding to the water signal are reported.

The three parameter fit was chosen, rather than the more conventional two parameter fit, because the three parameter fit is capable of producing reliable data in cases of misadjusted pulse widths, large frequency offsets, and partial saturation of the signal if $DT < 5T_1$ (46).

In experiments, DT was set by using the T_1 value estimated from the zero-point method. This

method gives inaccurate values (26) and frequently the "true" T_1 value (as judged from a three parameter fit) was longer. In such cases partial saturation might occur.

Preliminary experiments in which the 180° pulse length was intentionally misadjusted, showed that the T_1 values varied with the pulse width, when the two parameter fit was used. Some of the data looked like a biphasic decay. When the three parameter fit was used for the same data, all gave similar T_1 values and none looked like a biphasic decay.

Three parameter fits perform best when the "infinity" plateau (very long τ values) is well defined. Most T_1 data contained at least 3-4 points in the "infinity" plateau region.

Table 5.1 shows the SD's as calculated by the computer, for T_1 data of PLL samples. Only the largest SD for each sample is shown. As can be seen from the table, the SD's are the largest for the two samples that showed a two component T_1 decay. The SD is bigger for the more concentrated sample. Within each sample, the SD is largest at the lowest temperature where a two component decay is still observed.

Exponential least squares fitting programs are known to perform poorly when more than one component

Table 5.1. Standard deviation values of the water T_1 relaxation times at 44.4 MHz in PLL samples. The values were calculated by the Nicolet 1180 computer and the associated Nicolet program. Only the largest SD for each sample is shown.

Sample	Number Of Components In T_1 Decay	SD (± %)	Remarks
PLL 40%	2	3.7	One Component T_1 Decay Below −0.2°C
	1	1.7	
PLL 50%	2	19.9	One Component T_1 Decay Below −0.3°C
	1	1.5	
PLL 60%	1	2.1	One Component T_1 Decay Throughout
PLL 70%	1	0.86	One Component T_1 Decay Throughout

is present. The performance is worse when the two components contribute equally to the decay. In the case of PLL, the observed relative contribution of each component depends on the position of the gate. After the fits were performed, it turned out that the relative contribution of each component was ∿50%.

The big SD's of PLL samples that showed biphasic decays do not affect the conclusions of the study. The conclusions are based on results at freezing temperatures, where the SD's were small (within ±2%). T_1 values of PLL samples that showed biphasic decay decrease with decreasing temperature and increasing concentration. Thus, the expected trends are observed.

Table 5.2 shows the SD's of BSA samples above 0.0°C (L) and below 0.0°F (F). Data is for T_1 values at 150 MHz. Only the largest SD's are shown. All the SD's are less than ±1%.

In general, signals obtained on the Nicolet superconducting magnet had the highest sensitivity and the highest S/N ratios. Data obtained using this spectrometer had small SD's.

Table 5.3 shows the SD's of BSA in D_2O samples. Data is for deuterium T_1's at 15.4 MHz. For liquid samples the SD is within ±1%. The largest SD for the frozen samples is ±8% for BSA 0.8 g/1 ml at -25.5°C.

Table 5.2. Standarad deviation values of the water T_1 relaxation times at 150 MHz in BSA samples. The values were calculated by the Nicolet 1180 computer and the associated Nicolet program. Only the largest SD for each sample is shown.

Sample	Liquid (L) Or Frozen (F)	SD (±%)
BSA 0.2 g/ml	L	0.53
	F	0.92
BSA 0.4 g/ml	L	0.41
	F	0.73
BSA 0.6 g/ml	L	0.27
	F	0.68
BSA 0.8 g/ml	L	0.10
	F	0.94

Table 5.3. Standarad deviation values of the solvent deuteron T_1 relaxation times at 15.4 MHz in BSA in D_2O samples. The values were calculated by the Nicolet 1180 computer and the associated Nicolet program. Only the largest SD for each sample is shown.

Sample	Liquid (L) Or Frozen (F)	SD (±%)
BSA 0.2 g/1ml	L	0.45
	F	4.4
BSA 0.4 g/1ml	L	0.50
	F	2.9
BSA 0.6 g/1ml	L	0.48
	F	3.1
BSA 0.8 g/1ml	L	1.2
	F	8.1

In general, deuterium signals at 15.4 MHz had lower sensitivity and smaller S/N ratios, as compared to proton signals at 100 MHz. The experimental error in T_1 measurements is estimated to be within ±15% for PLL samples that showed only one component decay. T_1 data of BSA samples taken on the superconducting Nicolet magnet is estimated to be within ±5% for the liquid samples and within ±10% for the frozen samples. The accuracy of the T_1 data of deuterium at 15.4 MHz is estimated to be within ±10% for the liquid samples and within ±20% for the frozen samples.

5.3 $T_{1\rho}^{on}$ Data

$T_{1\rho}^{on}$ data were fitted to an exponential function of the form

$$y = A \exp\left(-\frac{\tau}{T_{1\rho}^{on}}\right).$$

A and $T_{1\rho}^{on}$ are the parameters to be fitted and y and τ are the experimental amplitudes and times H_1 field was on, respectively. $T_{1\rho}^{on}$ is the relaxation time.

Some of the PLL data showed a biphasic decay. This data were fitted to a double exponential function which had the form

$$y = A \exp\left(-\frac{\tau}{T_{1\rho}^{on}}\right) + B \exp\left(-\frac{\tau}{T_{1\rho,2}^{on}}\right).$$

B and $T^{on}_{1\rho,2}$ are the additional parameters to be fitted. $T^{on}_{1\rho,2}$ is the second relaxation time. Only the longer relaxation times, corresponding to the water signal are reported.

In $T^{on}_{1\rho}$ measurements, the greatest source of experimental error is introduced when the H_1 field strength is measured. The error is largest for the smallest H_1 values (13), for reasons discussed in the experimental chapter. For data taken on the JEOL 4H-100 spectrometer, the error is estimated to be within ±10% for the liquid samples and within ±20% for the frozen samples. Accuracy of data taken on the Nicolet superconducting magnet is estimated to be within ±10%.

5.4 T_2 Data

T_2 data were fitted to a single exponential function, which had the form

$$y = A \exp\left(-\frac{\tau}{T_2}\right).$$

A and T_2 are the parameters to be fitted. T_2 is the relaxation time. y is the observed spin-echo height and τ is the time interval from the 90° pulse to the appearance of the echo.

All T_2's showed a strictly exponential decay. The largest SD was ±1.5% for a deuterium sample, but most data had SD's smaller than ±1%. The experimental

error is estimated to be within ±5% for proton data and within ±10% for deuterium data.

5.5 Linewidth Data

Linewidths at half peak heights ($LW_{1/2}$) were calculated by fitting the absorption peaks to a Lorentzian line shape (26). The function had the form

$$y = \frac{A}{\left\{1 - \left[\frac{2(x - T)}{w}\right]^2\right\}}.$$

A is the amplitude at the center frequency, T is the center frequency, x is the frequency, and w is $LW_{1/2}$. Before the FID's were Fourier transformed, either very small or no line broadening was applied. This assured that the linewidths were not artificially broadened. $LW_{1/2}$'s are estimated to have errors of ±10% in the liquid samples and ±25% in the frozen samples.

5.6 $T_{1\rho}^{off}$ Data

To extract information on correlation times (τ_r), Fortran NMRRB computer program was written (see Appendix). The program calculated the theoretical ratios and $\sin^2\theta$ values, as well as the theoretical T_1 and T_2 values. Up to three different correlation times with corresponding fractions could be used to

calculate the theoretical values. Values were printed out for three different H_1 fields.

To calculate T_1 and T_2, an explicit value for the rigid lattice second moment must be known. Experimental estimates of the rigid lattice second moment cover a wide range of values (13). It was decided to use values for the rigid lattice second moment that reproduce the T_1 values of liquid water at room temperature. For protons, the rigid lattice second moment was set to give T_1 = 3.5 sec when $\tau_r = 3.0 \times 10^{-12}$ sec. For deuterons, the rigid lattice second moment was set to give T_1 = 0.37 sec when $\tau_r = 3.0 \times 10^{-12}$ sec. The T_2 relaxation rate in the rigid lattice limit was set to 3.0×10^5 sec^{-1}.

Agreement between theory and experimental results was judged by comparing visually theoretical and experimental plots. The greatest source of experimental error was introduced when H_1 field strengths were measured. Signals on the XL-100-15 spectrometer had better sensitivity and higher S/N ratios as compared to signals on the JEOL 4H-100 spectrometer. Consequently, H_1 field strengths could be measured more accurately for the off-resonance experiments on the XL-100-15 than for the $T_{1\rho}^{on}$ experiments with the 4H-100 instrument. Only the highest H_1 fields were measured directly and a strong water sample was used.

The experimental error in measuring H_1's is estimated to be within ±5% for protons in liquid samples, within ±10% for protons in frozen samples, and within ±15% for deuterium in frozen samples.

CHAPTER 6

RESULTS AND DISCUSSION

6.1 Poly-L-Lysine Hydrobromide (PLL)

6.1.1 T_1 Data

PLL was chosen as a model system to investigate the properties of water in protein solutions for the following reasons:

1. PLL is composed of only one amino acid. This makes it a relatively "simple" system.
2. PLL is very soluble in water. Highly concentrated solutions and gels can be prepared.
3. PLL has long side chains that may imitate the side chains of "real" proteins.
4. It is commercially available (6, 7, 8, 47, 48).

In investigating the properties of water in protein solutions it is of most interest to learn about the properties of water which is closely associated with the protein. This water constitutes only a small fraction of the total water present. Because conditions of fast exchange usually prevail, NMR

experiments measure an average property between the closely associated water and the "bulk" water. Since the "bulk" water is in excess, the NMR effects are relatively small. To reduce the interference from the "bulk" water, one can use very concentrated solutions (14, 19, 49), or quickly freeze the dilute protein solutions (4). Upon freezing, the "bulk" water forms ice and the NMR signal is too broad to be detected by ordinary NMR methods. The properties of the residual water which does not freeze are then studied at subzero temperatures. This water has relatively narrow linewidth: $LW_{1/2} \sim 500$ Hz at -25°C and $\nu_0 = 100$ MHz. Evidence has been presented by Kuntz et al. (4) that this water is closely associated with the macromolecule present. The solution has to be frozen quickly to avoid separation of macromolecule and water and to trap, as much as possible, the original conformation.

A question arises naturally as to whether the two modifications form similar systems and whether the properties of the water in either modification are similar to the properties of "water of hydration" in dilute protein solutions. To answer this question the T_1 relaxation times at $\nu_0 = 44.4$ MHz of water in 40% wt/wt (0.67 g/1 ml), 50% wt/wt (1.0 g/1 ml), 60% wt/wt (1.5 g/1 ml), and 70% wt/wt (2.3 g/1 ml)

solutions of PLL in water were measured in the temperature range +25°C to -50°C. The results are illustrated in Figure 6.1. Figure 6.2 shows the low temperature region and Figure 6.3 shows the high temperature region of the same data.

The most interesting result of Figure 6.1 is that at ∿-20°C the T_1's of the 40%, 50%, and 60% samples go through a common minimum, within the experimental error. This equality continues at temperatures below the temperature of the minimum. The variations at -50°C are probably caused by the low signal/noise ratio at this temperature. The 70% sample appears to have a broader minimum which is shifted to ∿-25°C (Figure 6.2). It has the shortest T_1 value at -40°C, but at -50°C its T_1 value approaches the T_1 values of the less concentrated samples. Because of the low signal/noise ratio, T_1 data could not be obtained at temperatures below -50°C.

Kuntz et al. (4) have shown that when protein solutions are quickly frozen the amount of unfrozen residual water (the "bound" water) is about 0.4 g water/1 g protein (∿70% protein). When the temperature is lowered the linewidth increases but the total amount of water remains constant. This observation and our observation that the T_1's become equal at low temperatures indicate that a common "phase" may exist

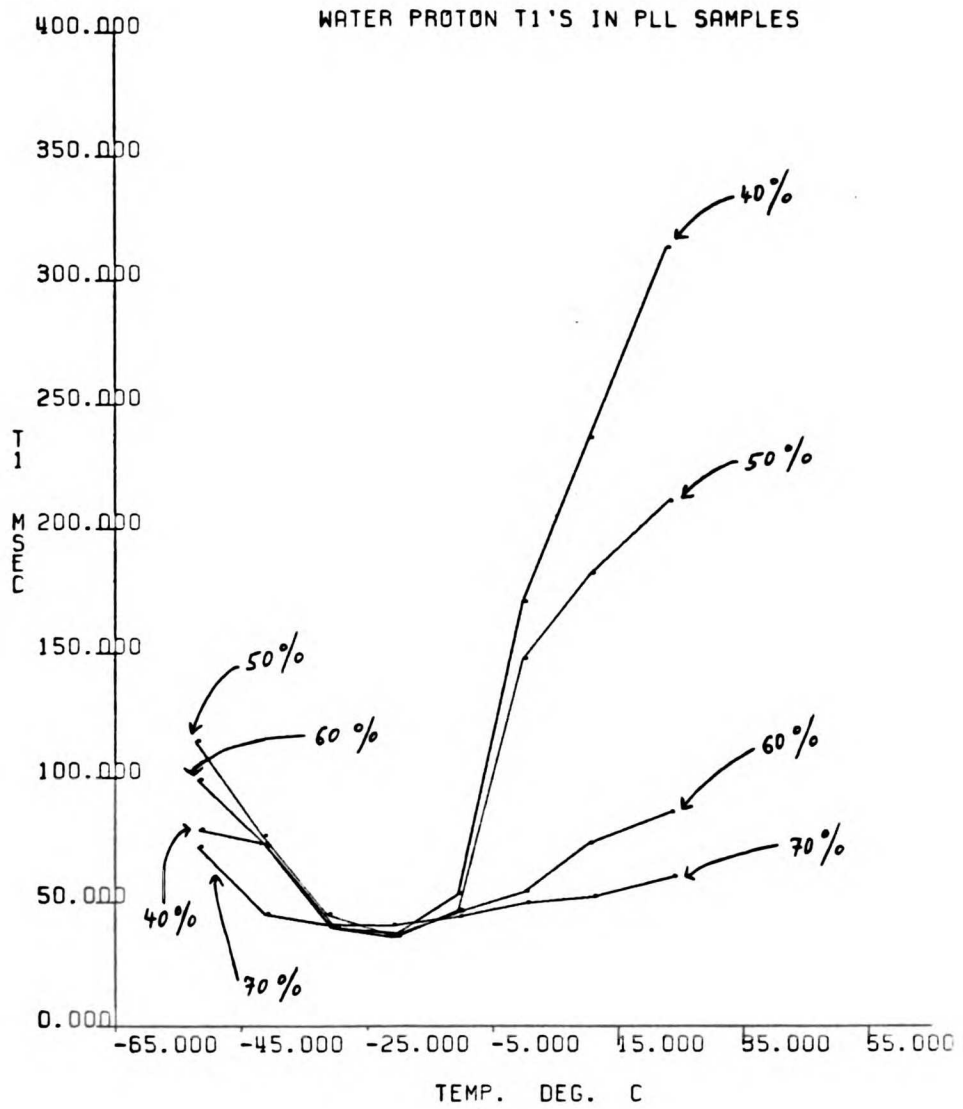

Fig. 6.1. Water proton T_1 relaxation times at 44.4 MHz in PLL samples. The high and the low temperature regions are shown. The arrows with the numbers indicate the concentration of the macromolecule in units of percent wt/wt.

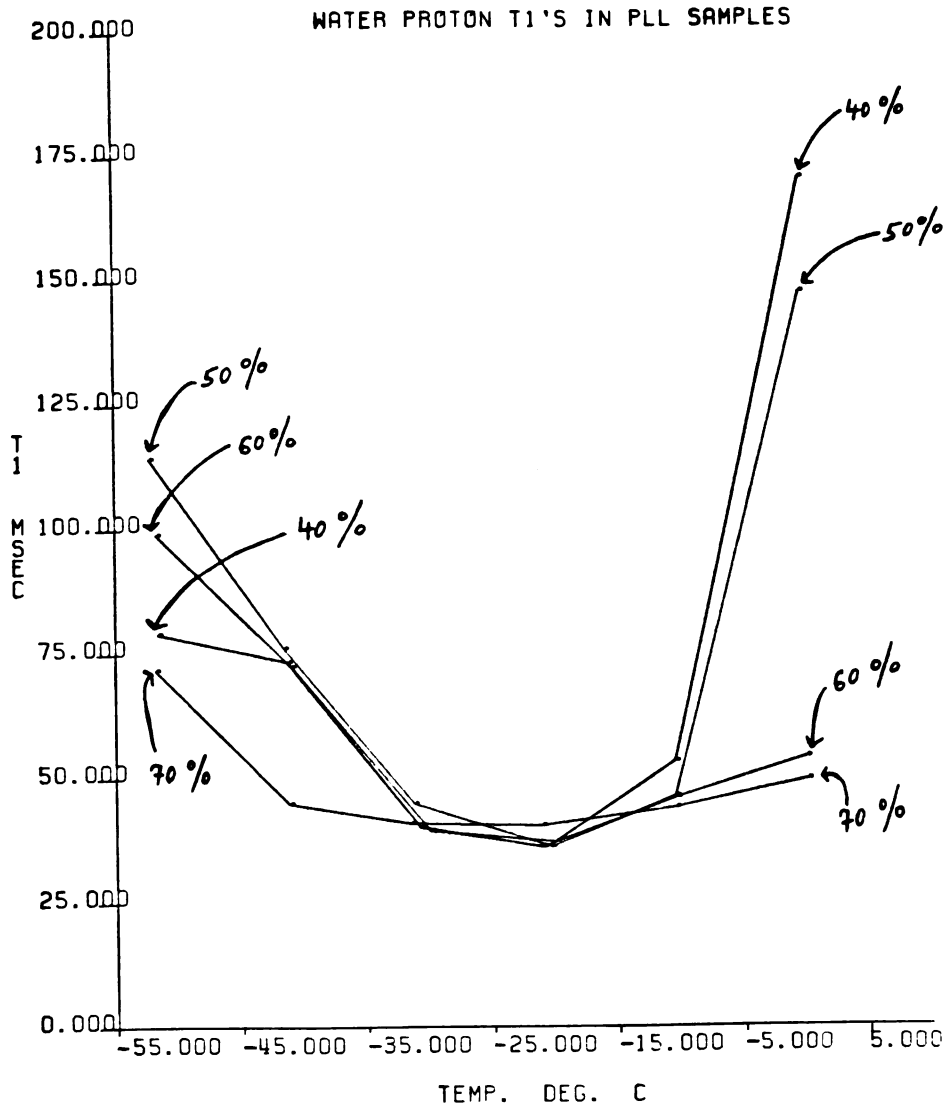

Fig. 6.2. Water proton T_1 relaxation times at 44.4 MHz in PLL samples. The low temperature region is shown. The arrows with the numbers indicate the concentration of the macromolecule in units of percent wt/wt.

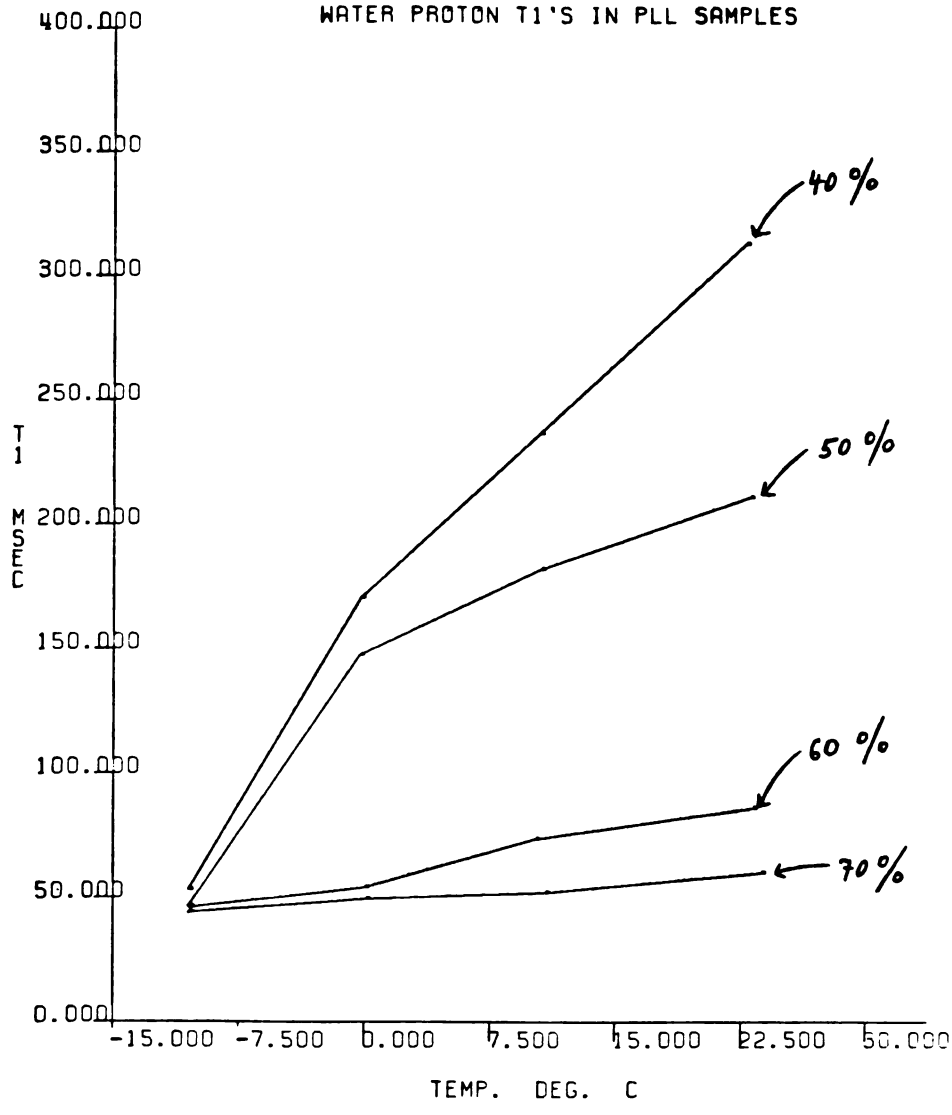

Fig. 6.3. Water proton T_1 relaxation times at 44.4 MHz in PLL samples. The high temperature region is shown. The arrows with the numbers indicate the concentration of the macromolecule in units of percent wt/wt.

in the frozen systems. As long as the initial concentration of the macromolecule in solution (above freezing) is less than ∿70%, quickly freezing the solution produces the same "phase," independent of the initial concentration. If the initial concentration of the water in solution is smaller than the amount of "bound" water (macromolecule concentration $\geqslant$ 70%), a different "phase" may be generated upon freezing. This "phase" may convert to the other "phase" at Temperature $\leqslant$ -50°C. It is not known whether such "phases" are true equilibrium thermodynamic phases. For a more detailed discussion of metastable "phases" see Section 6.2.1.

The water proton T_1's were measured by directly sampling the FID's. A possibility exists that the FID's contained some residual signal from the macromolecule protons. The relative contribution of these protons will increase with increasing macromolecule concentration. This may cause a broadening of the T_1 minimum and make the T_1 values longer. On a molecular level, a broad distribution of correlation times and/or the presence of cross-relaxation will produce similar effects. The broadening of the T_1 minimum in the 70% sample could have been caused by the experimental artifact, by a distribution of correlation times and/or the presence of cross-relaxation, or by any combination of these factors (13, 50).

Distribution of correlation times and cross-relaxation effects are discussed in more detail in Section 6.2.1.

If the relaxation is dominated by only one isotropic motion, the expected values of T_1 and T_2 at the minimum at ν_0 = 44.4 MHz can be calculated to be 9.55 msec and 6.31 msec, respectively (see Chapter 2, Sections 2.3 and 2.4). The ratio $T_1/T_2 \approx 1.5$. Table 6.1 summarizes the experimental values of T_1, T_2, and the T_1/T_2 ratios at the minima for the 40% and the 70% samples. T_2 values were obtained by extrapolating $T_{1\rho}^{on}$ relaxation rates to $H \approx 0$ (see Section 6.1.2 and Table 6.4). The experimental T_1/T_2 ratios are much greater than the theoretical ratio of 1.5. The experimental ratios are larger because the experimental T_1 values are longer and the experimental T_2 values are shorter than the values expected from the simple theory. By comparing T_1 and T_2 to the theoretical values we see that most of the effect is caused by the very small values of T_2. The short values of T_2 indicate that either slow processes, such as slow rotation, exchange, or translational motions are present, or that a motional anisotropy is present (8). All the effects may, of course, take place simultaneously.

The occurrence of the minimum at -20°C implies that at this temperature a significant fraction of the

Table 6.1. Water proton T_1, T_2 and T_1/T_2 values at 44.4 MHz in frozen 40% and 70% PLL samples. The values were obtained at the temperature of the T_1 minimum.

PLL Sample	T_1 (msec)	T_2 (msec)	$\frac{T_1}{T_2}$
40%	36.3	0.35	104.
70%	40.2	0.45	89.

water molecules has a correlation time in the nanosecond region. This should be regarded only as an apparent correlation time. Our results indicate that more than one motion and/or process may take place.

On the "high" temperature side (Figure 6.3), a breaking point is seen in the 40% and the 50% samples between 0°C and -10°C. No breaking point is seen in the 60% and the 70% samples. The occurrence of the breaking point is evidence that at least two different water fractions are present in the 40% and 50% PLL solutions. If the amount of water in solution before freezing is higher than the amount of "bound" water, the excess water freezes at subzero temperatures and forms ice. If the amount of water in solution before freezing is less than the amount of "bound" water, no ice will be formed at subzero temperatures. Ice formation by itself cannot account for the sharp decrease in T_1 values. The T_1 value of water in a water-ice mixture is not much different from the T_1 value of pure water. If the "bound" water is in fast exchange with the "bulk" water, an average T_1 is measured. After freezing, only the shorter T_1 of the "bound" fraction is detected. If the amount of water in solution before freezing is less than the amount of "bound" water, only the shorter T_1 is measured throughout. Elimination of fast averaging

with the "bulk" water is responsible for the breaking-points in relaxation times observed upon freezing (8).

The freezing event in the water-PLL system disappears at a concentration of about 60% (Figure 6.3) and the water of hydration is calculated to be approximately 0.5 g/1 g macromolecule. This is equivalent to ∿6 moles water/mole of amino acid. This result compares favorably with the hydration number of 5.0 moles water/mole of amino acid at -25°C reported by Kuntz (51). Kuntz found that the hydration of PLL decreases as the temperature is lowered below -25°C. The slightly higher hydration number of 6 found in this study should be regarded as the high temperature "limit" of the hydration number reported by Kuntz.

Using our data and the gel to liquid transition temperatures reported by Darke and Finer (7) and Woodhouse and Derbyshire (8), an approximate phase diagram was constructed for the water-PLL system. It is illustrated in Figure 6.4. The dotted line separates the left region of the graph, where freezing occurs from the right region of the graph, where freezing does not occur. The square area at the bottom delimits the region where a common phase, as judged by the equality of T_1 values, exists. In this region the T_1's are concentration independent, but they change with the temperature. The solution-"solid"

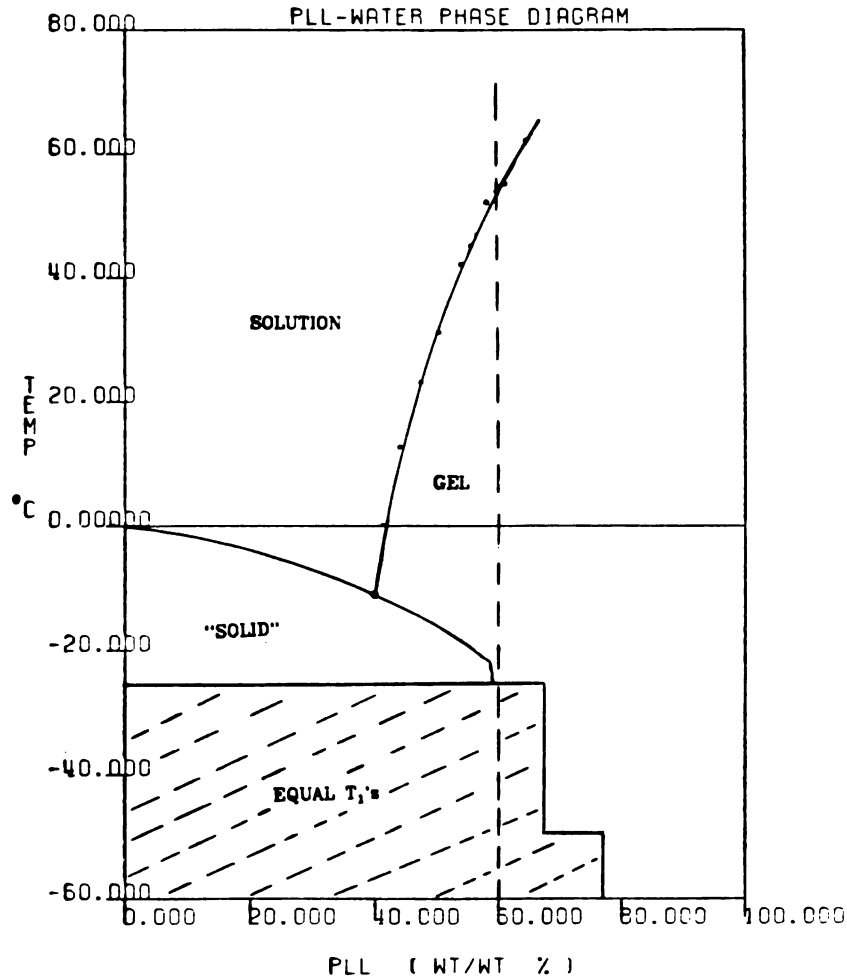

Fig. 6.4. Phase diagram for the system PLL-water. Diagram constructed using our experimental data, the experimental data of Darke and Finer (7) and Woodhouse and Derbyshire (8) and general considerations.

curve was drawn approximately, using data from Figure 6.8 and general considerations. From Figure 6.8 the freezing event for the 40% sample occurs at ∿-10°C. This curve is also expected to pass through the 0°C point, where pure water freezes and its slope is expected to become negative and very large in the vicinity of the dotted line. In the region to the right of the solution-gel curve, the T_1 values vary with both the temperature and the concentration, as expected for a gel or solution.

6.1.2 $T_{1\rho}^{on}$ Data

To investigate the slow motions in the model system, $T_{1\rho}^{on}$ relaxation times at ν_0 = 44.4 MHz were measured in the most dilute (40%) and the most concentrated (70%) samples. Figure 6.5 shows the data obtained from the 40% sample at high temperatures and Figure 6.6 shows the data obtained from the same sample at subzero temperatures. Figure 6.7 shows the data obtained from the 70% sample.

No dispersion is seen in the 40% sample at room temperature. Some dispersion appears at +9.8°C but it becomes significant only at subzero temperatures. If the $T_{1\rho}^{on}$ relaxation rates are extrapolated to $H_1 \approx 0$ and the natural logarithms (ln) of the resulting values are plotted as a function of the inverse temperature,

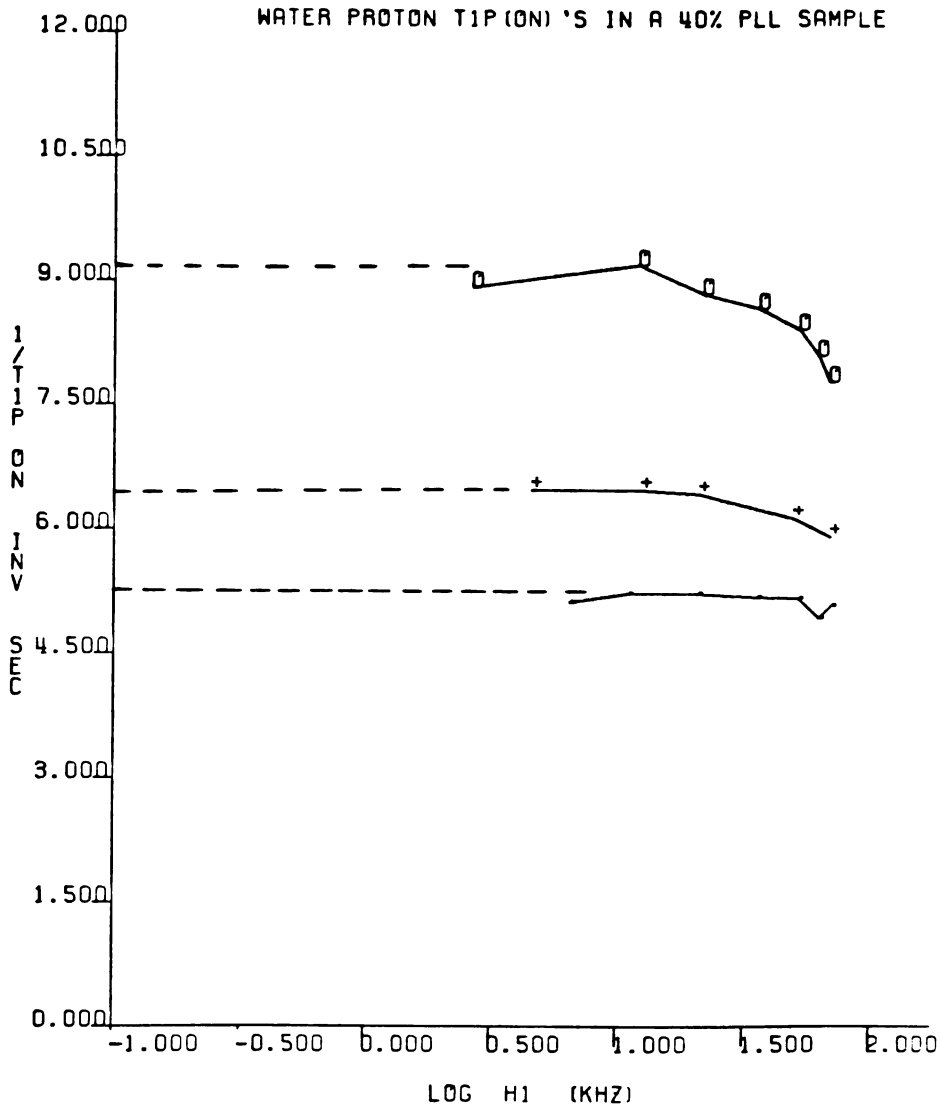

Fig. 6.5. Water proton $T_{1\rho}^{on}$ relaxation times at ν_0 = 44.4 MHz in a 40% PLL sample. (•) +22.7°C; (+) +9.8°C; (0) −0.1°C. The dashed lines show extrapolation to $H_1 \approx 0$.

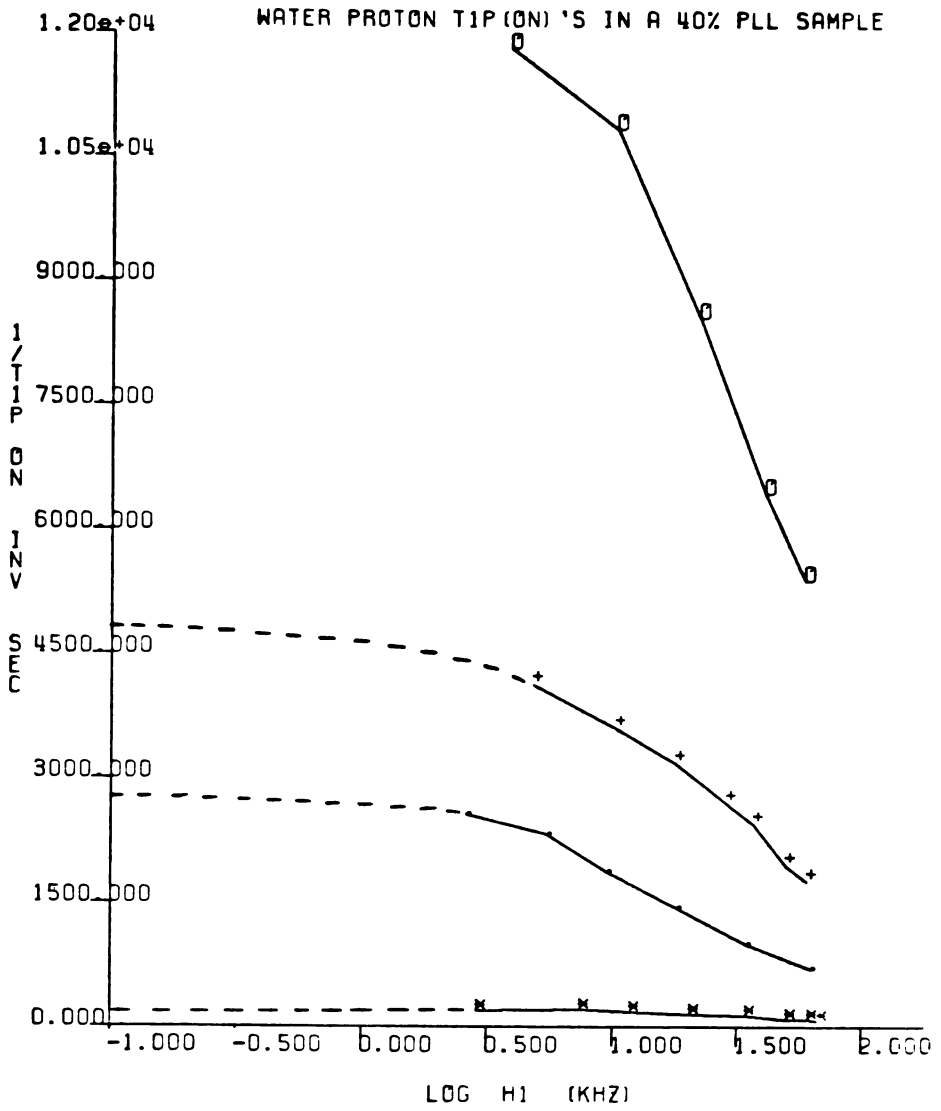

Fig. 6.6. Water proton $T_{1\rho}^{on}$ relaxation times at ν_0 = 44.4 MHz in a 40% PLL sample. (*) −10.3°C; (•) −20.1°C; (+) −30.2°C; (0) −40.6°C. The dashed lines show extrapolation to $H_1 \approx 0$. Extrapolation at −40.6°C is not shown.

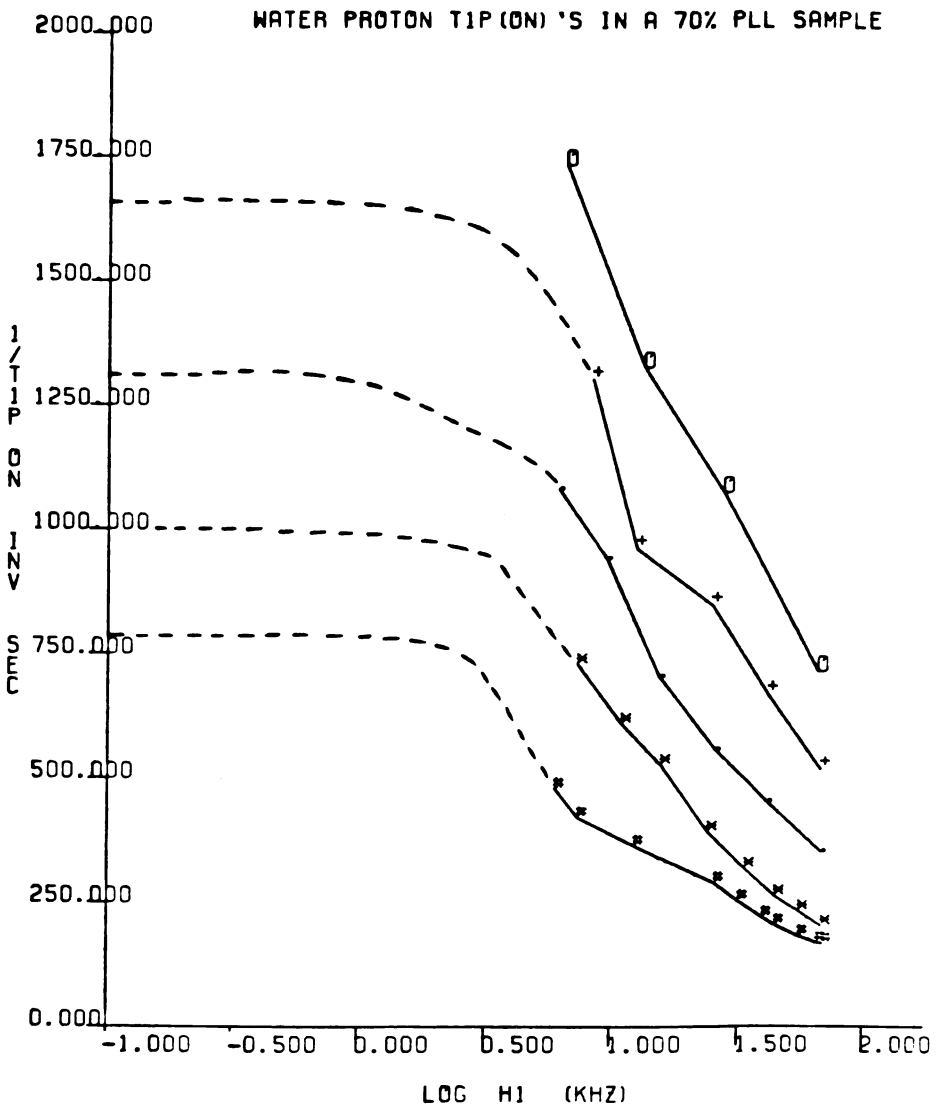

Fig. 6.7. Water proton $T_{1\rho}^{on}$ relaxation times at ν_0 = 44.4 MHz in a 70% PLL sample. (#) +23.7°C; (*) +10.8°C; (•) +0.2°C; (+) −10.4°C; (O) −21.2°C. The dashed lines show extrapolation to $H_1 \approx 0$. Extrapolation at −21.2°C is not shown.

a breaking point is seen between -0.1°C and -20.1°C (Figure 6.8). This is the same temperature region where a breaking point in the T_1 values is observed in the 40% and 50% samples (Figure 6.3). Reliable $T_{1\rho}^{on}$ relaxation data could not be obtained below -40°C for the 40% sample, because the relaxation times became very short.

A dispersion is observed in the 70% sample in both the high and the low temperature regions. If the $T_{1\rho}^{on}$ relaxation rates are extrapolated to $H_1 \approx 0$ no breaking point is observed (Figure 6.9). No data could be obtained for the 70% sample below -20°C, because of the interference of oscillations (see Chapter 2, Section 2.5.1).

Within each sample the $T_{1\rho}^{on}$ relaxation rates become larger as the temperature is lowered. At temperatures above 0°C the 70% sample has larger relaxation rates than the 40% sample (Figure 6.10). At the high H_1 fields the ratio of the relaxation rates of the 70% sample to those of the 40% sample is $\sim$30. At the low H_1 fields the ratio of the relaxation rates is $\sim$100. At -20°C and high H_1 fields the two samples have the same relaxation rates, within the experimental error. At the low H_1 fields the 70% sample has somewhat shorter relaxation rates than the 40% sample. At

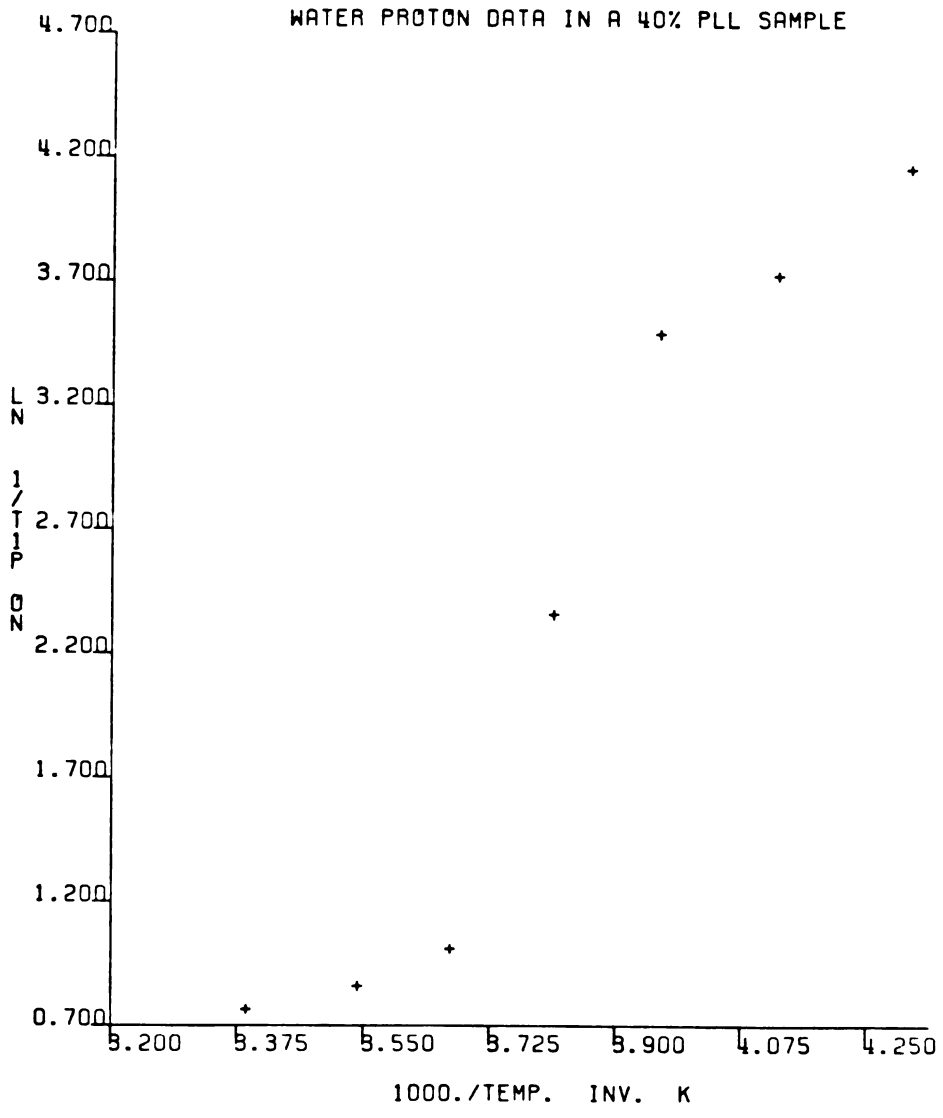

Fig. 6.8. A plot of ln $(1/T_{1\rho}^{on})$ at $H_1 \approx 0$ vs. the inverse (absolute) temperature. Data are for the water protons in a 40% PLL sample.

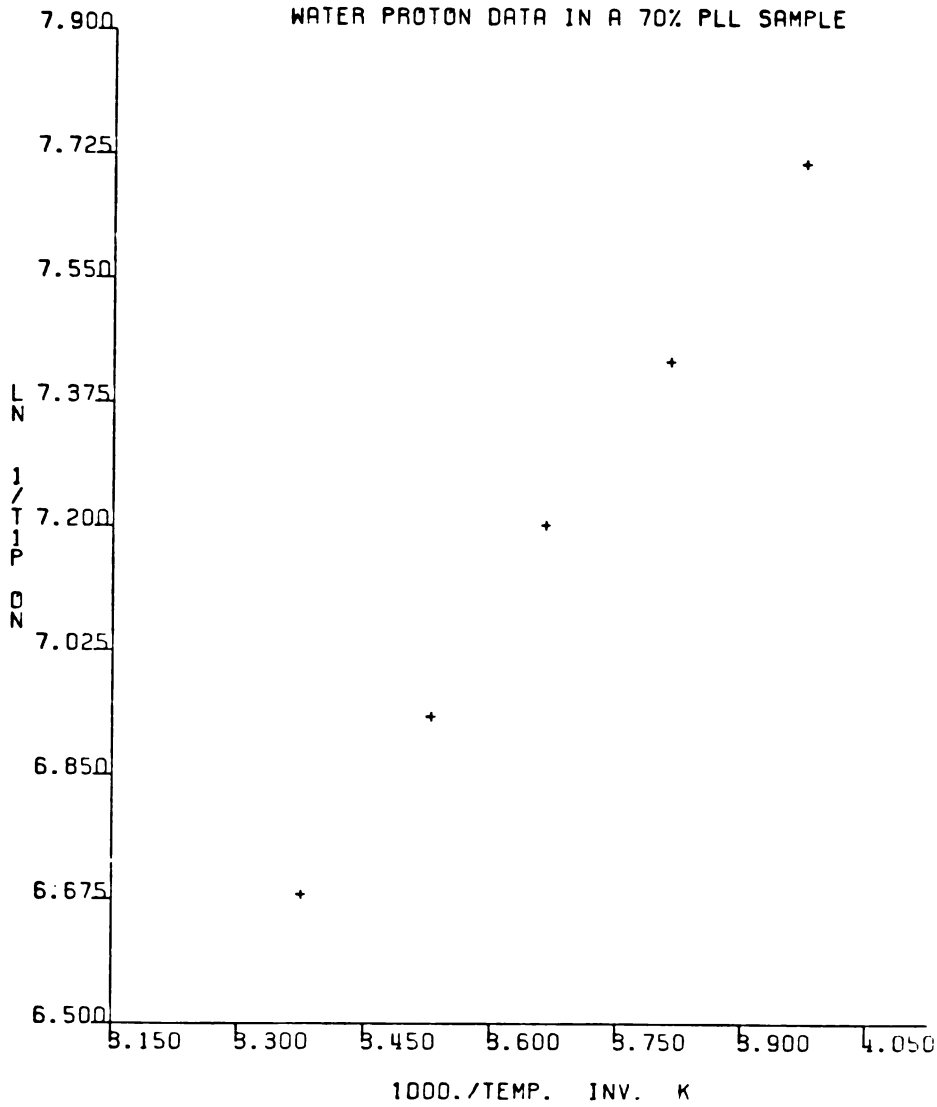

Fig. 6.9. A plot of ln $(1/T_{1\rho}^{on})$ at $H_1 \approx 0$ vs. the inverse (absolute) temperature. Data are for the water protons in a 70% PLL sample.

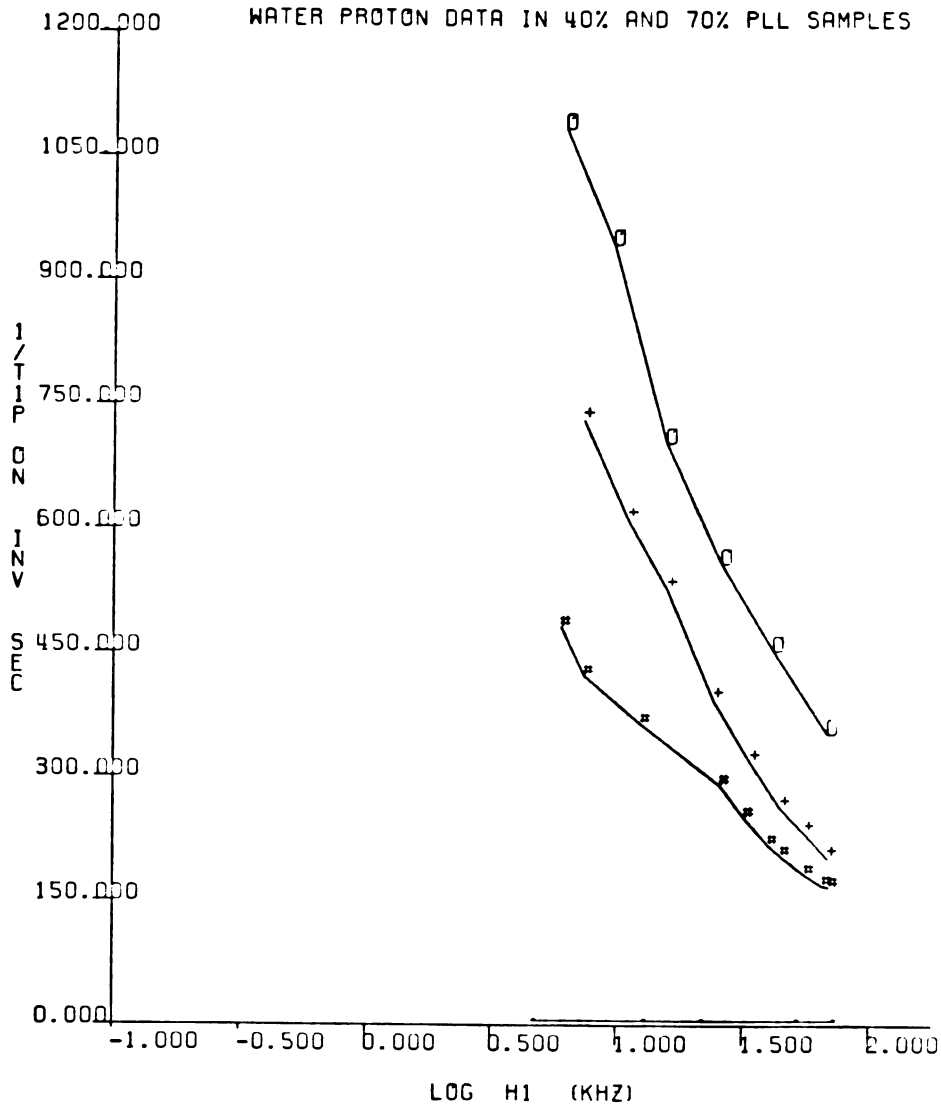

Fig. 6.10. Water proton $T_{1\rho}^{m}$ relaxation times at ν_0 = 44.4 MHz in 40% and 70% PLL samples. (•) 40% PLL data at +9.8°C; (#) 70% PLL data at +23.7°C; (+) 70% PLL data at +10.8°C; (0) 70% PLL data at +0.2°C.

the lowest H_1 fields the ratio of the relaxation rates is ∿1.1-1.2 (Figure 6.11).

The occurrence of a breaking point in the 40% sample upon freezing, the absence of a breaking point in the 70% sample upon freezing, and the fact that the relaxation rates of the 70% sample at temperatures above 0°C are much longer than those of the 40% sample at the same temperatures, are consistent with the interpretation that at least two different populations of water exist in PLL solutions above 0°C, when the macromolecule concentration is less than ∿60%. One fraction constitutes the "bulk" of the water and has a short correlation time. The second fraction is associated more closely with the macromolecule, has a longer correlation time, and does not form ice at subzero temperatures.

$T_{1\rho}^{on}$ and T_2 relaxations are more sensitive to slow motions than the T_1 relaxation. Therefore, a larger change in the $T_{1\rho}^{on}$ values than in the T_1 values is expected when the contribution from the "bulk" water is eliminated upon freezing. This is indeed the case: the ratio of the T_1 values of the 40% sample between -0.2°C and -20.1°C is ∿4.6. The ratio of the $T_{1\rho}^{on}$ values at the lowest H_1 fields for the same sample between the same temperatures is ∿287. At room temperature (∿+23°C), the T_1 ratio

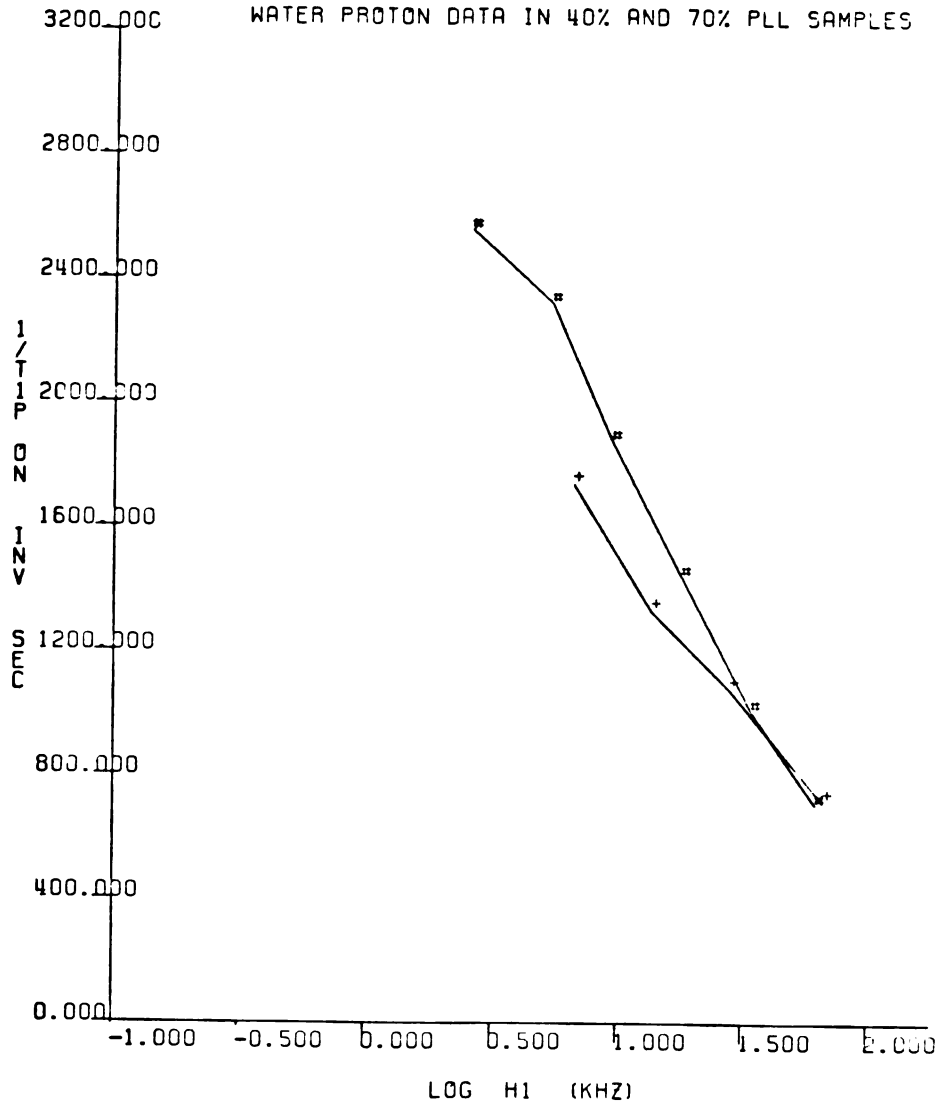

Fig. 6.11. Water proton $T_{1\rho}^{m}$ relaxation times at ν_0 = 44.4 MHz in 40% and 70% PLL samples. (#) 40% PLL data at −20°C; (+) 70% PLL data at −20°C.

between the 40% and the 70% samples is ∿5.2. Under similar conditions, the ratio of the $T_{1\rho}^{on}$ values at the low H_1 fields is ∿85.

The fact that the $T_{1\rho}^{on}$ relaxation rates of the 70% sample at the low H_1 fields at -20°C are somewhat shorter than the relaxation rates of the 40% sample under similar conditions is consistent with the interpretation that a broader distribution of correlation times may exist in the more concentrated sample. Cross-relaxation may contribute to the dispersion curve shape and relaxation values, but an appropriate theory is lacking (see Chapter 2, Section 2.7.3). For a more detailed discussion of the cross-relaxation effects in frozen systems, see next section. Because data could not be obtained below -20°C, it is not known whether the $T_{1\rho}^{on}$ relaxation parallels the T_1 relaxation and the $T_{1\rho}^{on}$ relaxation rates of the two samples become equal at low enough temperatures.

The 70% sample dispersion curves have an interesting feature: while the relaxation rates become longer at lower temperatures the inflection points are temperature independent, within the experimental error. For all curves the inflection points occur at $H_1 \sim 25$ KHz (log 25 ∿ 1.4). This observation indicates that within the investigated temperature range, temperature changes affect mostly the amplitude

of the motions and have a smaller effect on the correlation times.

To obtain the apparent energies of activation, $\ln(1/T_{1\rho}^{on})$ at $H_1 \approx 0$ were plotted versus the reciprocal temperatures (13). If the relaxation is dominated by a single motion, the Arrhenius plot is expected to result in a straight line with the slope proportional to the apparent energy of activation (52, 53, 54). An Arrhenius plot for the 70% sample using the low H_1 fields is shown in Figure 6.12. An Arrhenius plot using the high H_1 fields is shown in Figure 6.13. The plots include both the high and the low temperatures regions. Figures 6.14 and 6.15 show the Arrhenius plots for the 40% sample at the high temperatures at the low H_1's and the high H_1's, respectively. Figures 6.16 and 6.17 show the Arrhenius plots for the 40% sample at the low temperatures at the low H_1's and the high H_1's, respectively. The point at -10.3°C for the 40% sample was ignored because it falls in the phase transition region (Figure 6.8).

The apparent energies of activation derived from the slopes are summarized in Table 6.2. The slopes were calculated by the Nicolet 1180 computer using the associated Nicolet program. The reported errors for the apparent energies of activation were

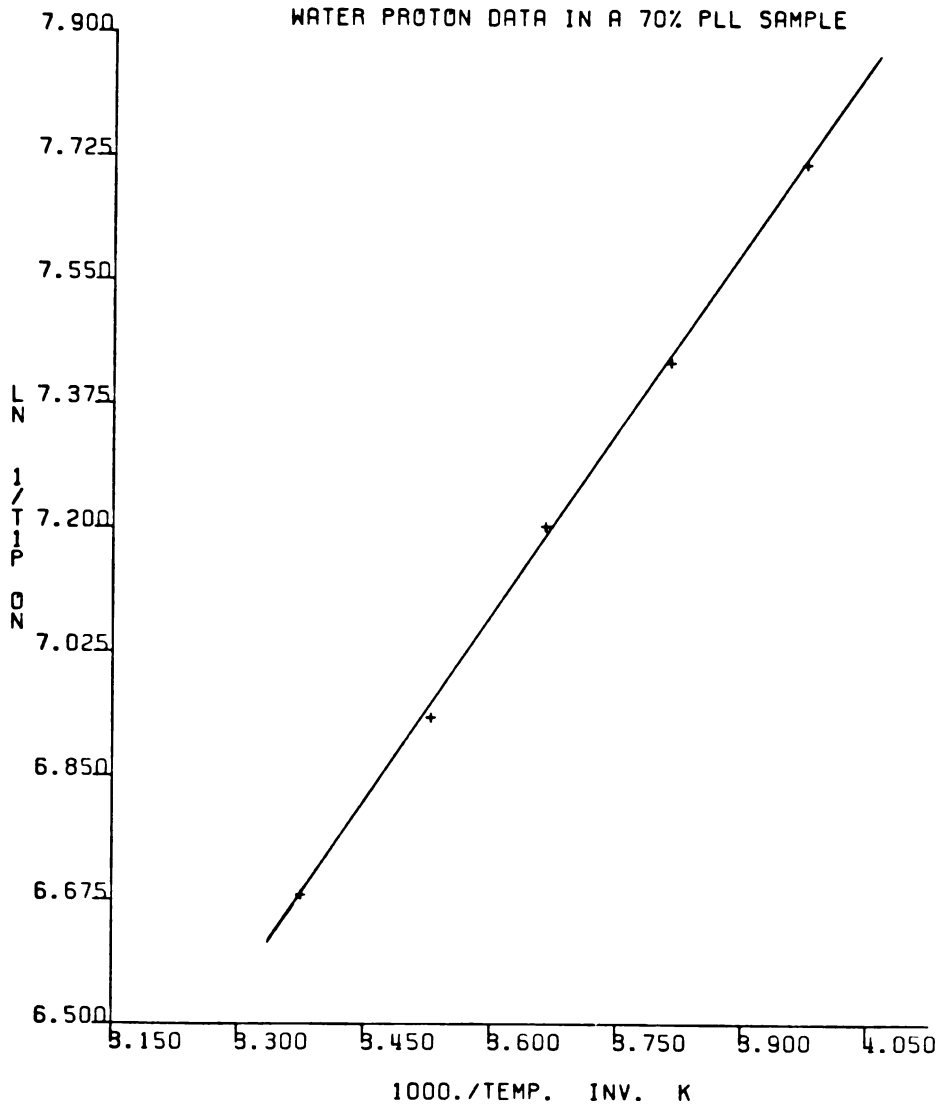

Fig. 6.12. An Arrhenius plot for the water protons in a 70% PLL sample. $T_{1\rho}^{on}$ data at the low H_1 fields were used.

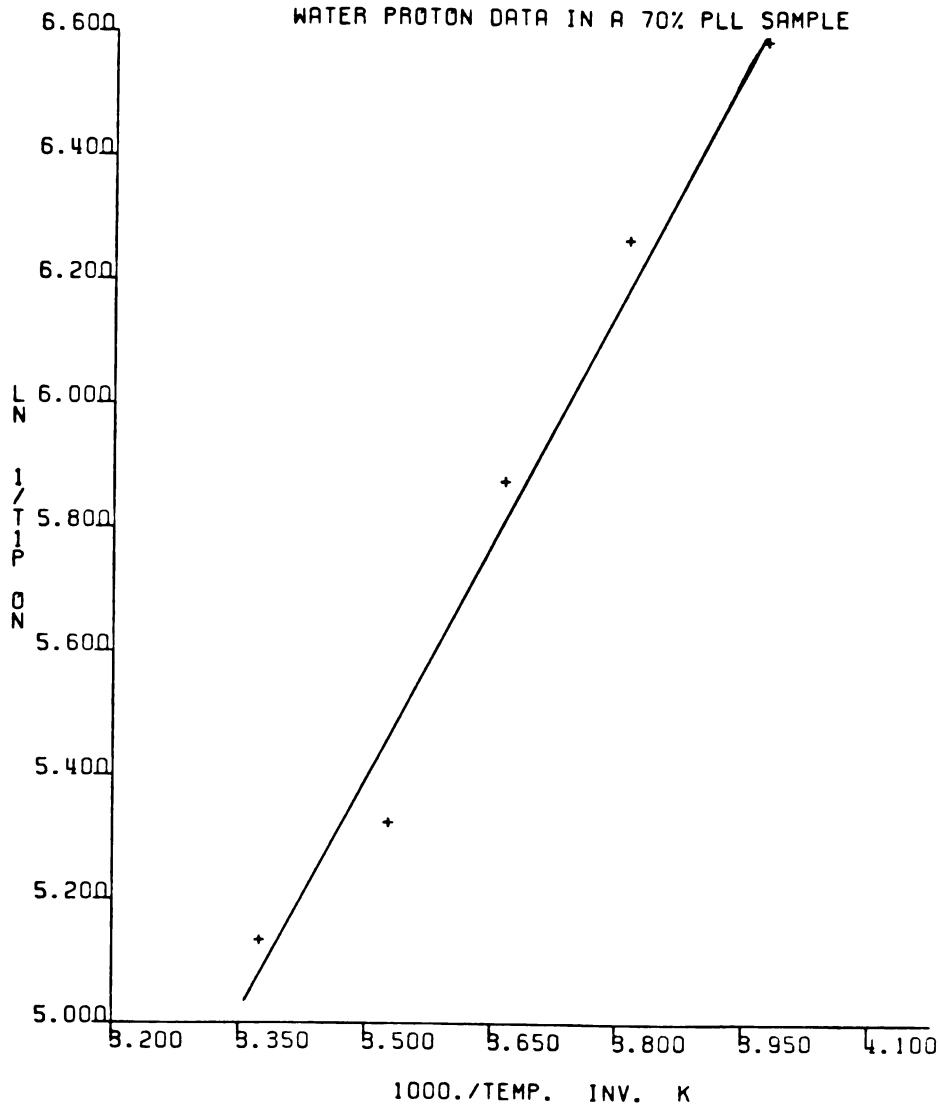

Fig. 6.13. An Arrhenius plot for the water protons in a 70% PLL sample. $T_{1\rho}^{on}$ data at the high H_1 fields were used.

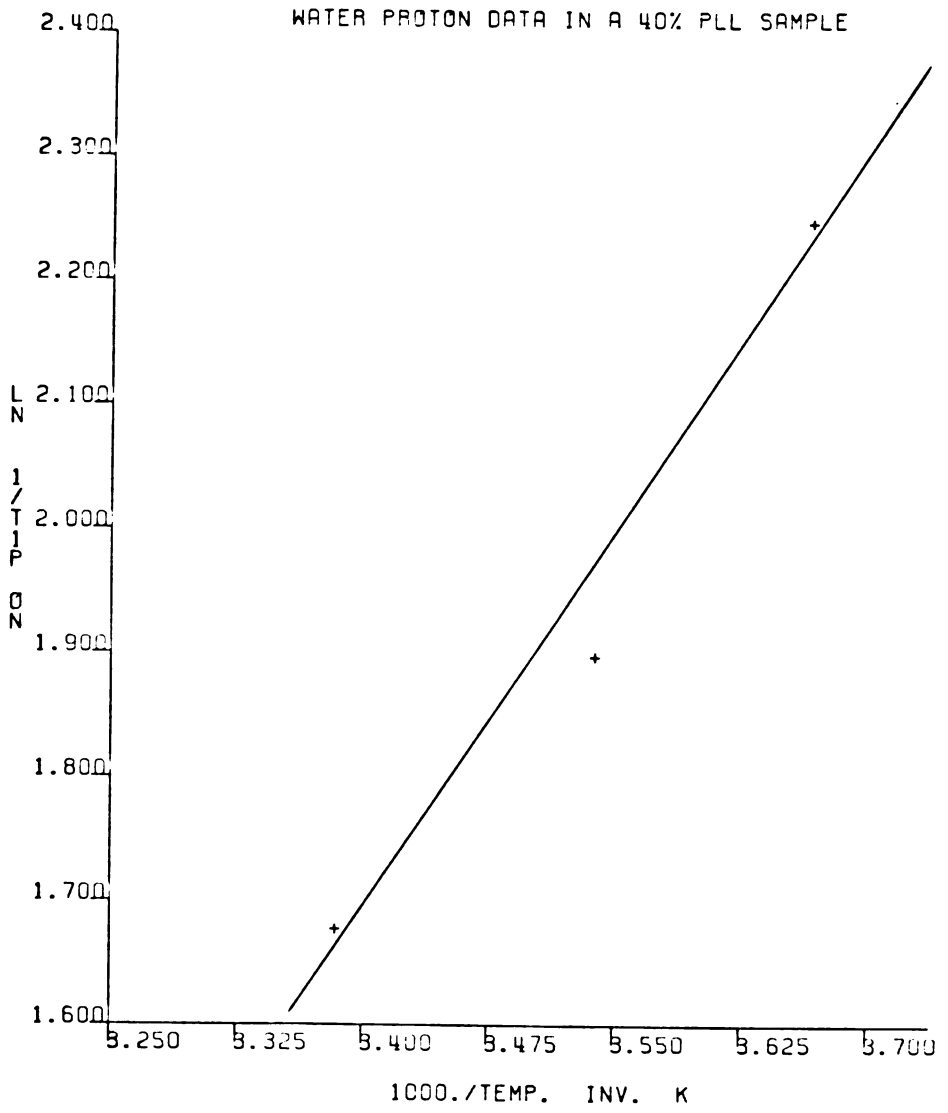

Fig. 6.14. An Arrhenius plot for the water protons in a 40% PLL sample. $T_{1\rho}^{on}$ data at the low H_1 fields were used. Data are for the high temperature region.

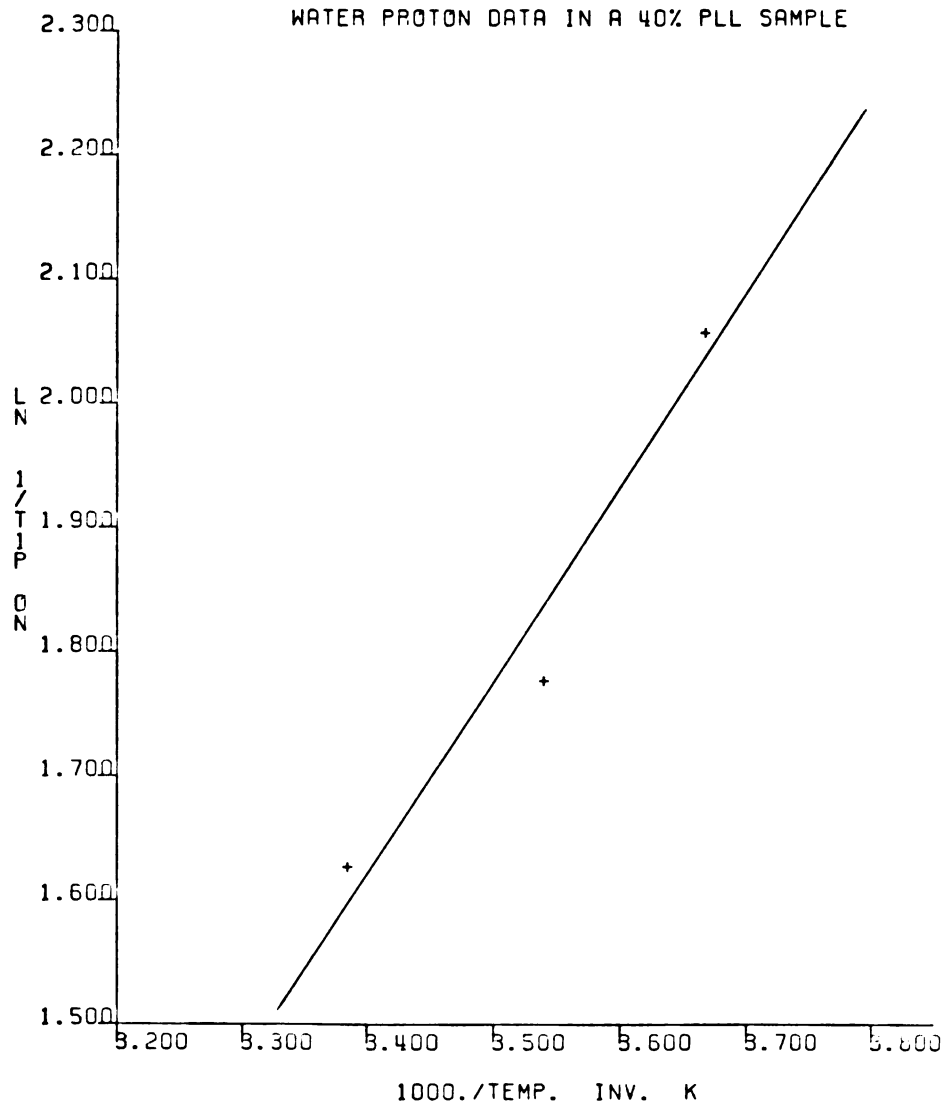

Fig. 6.15. An Arrhenius plot for the water protons in a 40% PLL sample. $T_{1\rho}^{on}$ data at the high H_1 fields were used. Data are for the high temperature region.

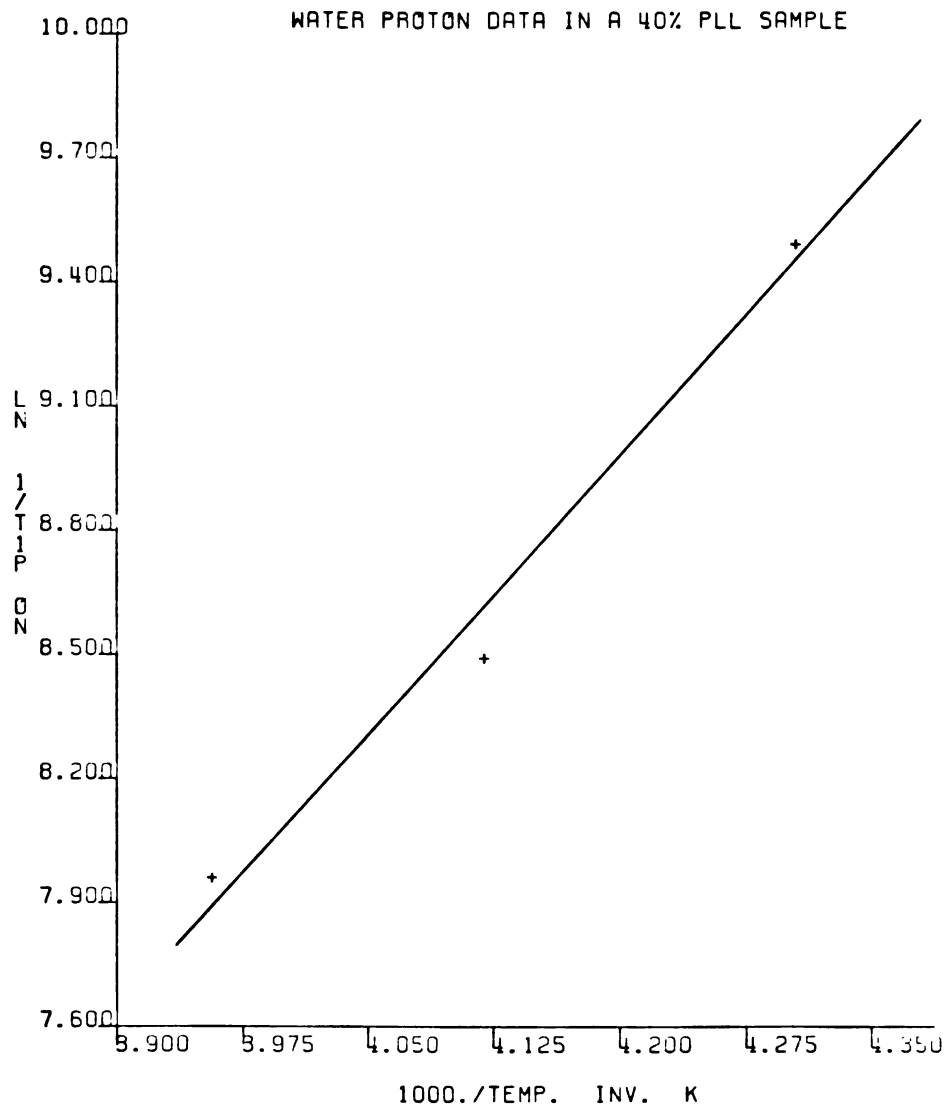

Fig. 6.16. An Arrhenius plot for the water protons in a 40% PLL sample. $T_{1\rho}^{m}$ data at the low H_1 fields were used. Data are for the low temperature region.

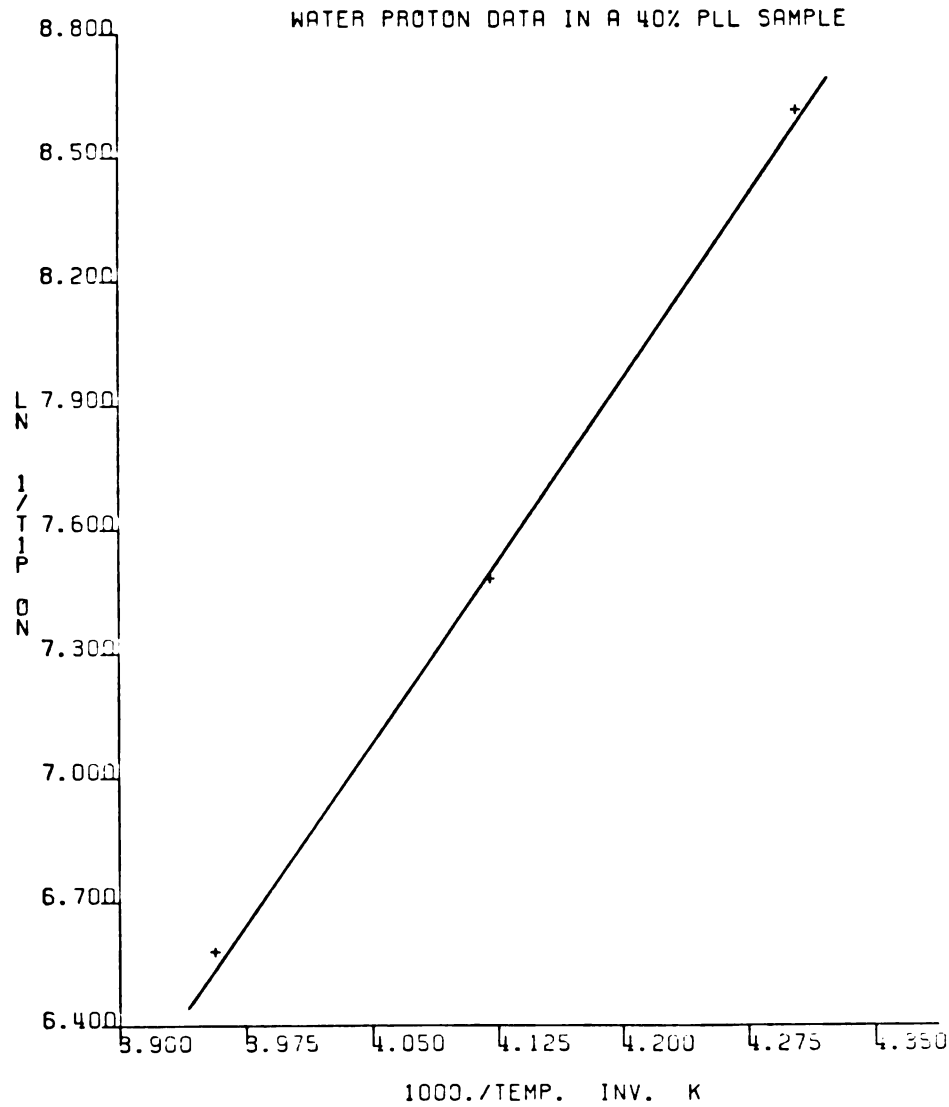

Fig. 6.17. An Arrhenius plot for the water protons in a 40% PLL sample. $T_{1\rho}^{m}$ data at the high H_1 fields were used. Data are for the low temperature region.

Table 6.2. Apparent energies of activation for the water proton in 40% and 70% PLL samples.

PLL Concentration	Temperature Range Of Data	Slope[3] (°K)	E_a[4] (Kcal/mole)
40%	High[1]	1990 ± 200	4.0 ± 0.8
40%	High[2]	1500 ± 150	3.0 ± 0.6
40%	Low[1]	4420 ± 885	8.8 ± 2.6
40%	Low[2]	5820 ± 1160	11.6 ± 3.5
70%	High + Low[1]	1730 ± 345	3.5 ± 1.1
70%	High + Low[2]	2570 ± 515	5.1 ± 1.5

[1]Relaxation data taken at the low H_1 fields.

[2]Relaxation data taken at the high H_1 fields.

[3]Slopes calculated by the Nicolet 1180 computer using the associated Nicolet program.

[4]Reported errors are estimates (see text).

estimated assuming ∿10% error in measuring $T_{1\rho}^{on}$ relaxation rates in the 40% sample above 0°C and ∿20% error in measuring $T_{1\rho}^{on}$ values below 0°C and in the 70% sample (see Chapter 5, Section 5.3). All the other errors were assumed to be additive. A total of ∿10% error was assumed to be introduced by the extrapolation method and by any other sources to the calculated values of the E_a's.

The Arrhenius plot for the 70% sample using data at the low H_1 fields gives a good fit to a straight line. The apparent E_a ∿ 3.5 ± 1.1 Kcal/mole, i.e., the energy of activation needed to break one hydrogen bond (23, 55). When relaxation data at the high H_1 fields is used, the data are noisier and the derived E_a has a higher value. Data derived from plots for the 40% sample were included in Table 6.2, but it should be noted that only three points were used in each plot and each plot covers a small temperature range. If nonlinearity exists in these plots, it may not be detected. In solution the 40% sample has an apparent E_a ∿ 3.0 ± 0.6-4.0 ± 0.8 Kcal/mole. At subzero temperatures the apparent E_a ∿ 8.8 ± 2.6-11.6 ± 3.5 Kcal/mole, i.e., ∿2 times larger than the energy of activation in solution.

If translational motions are important and if $\langle r^2 \rangle \gg d^2$, where $\langle r^2 \rangle$ is the mean square jumping

distance and d is the distance of closest approach between spins, a plot of $1/T_{1\rho}^{on}$ versus $\omega_1^{1/2}$ is expected to give a straight line (see Chapter 2, Section 2.5). Such plots were done for the 40% and 70% samples. For the 40% sample straight lines were obtained only below -10°C. The plots at -10.3°C, -20.1°C, -30.2°C, and -40.6°C are shown in Figures 6.18-6.21, respectively. At temperatures above -10°C the data points did not fall on straight lines. For the 70% sample straight lines were obtained only at 0°C and below. The plots at +0.2°C, -10.4°C, and -21.2°C are illustrated in Figures 6.22-6.24, respectively. At temperatures above 0°C the data points did not fall on straight lines. For both samples only relaxation rates at $H_1 > 10$ KHz were used.

The apparent diffusion coefficients (D) were calculated from the slopes of the fitted straight lines using Equation 2.7. The only unknown parameter in Equation 2.7 is the density of the spins (N). N was calculated assuming equal contribution from the PLL and the water protons and assuming that both samples had a density of 1 g/ml.

The values of D are summarized in Table 6.3. The slopes and their standard deviations were calculated using the Nicolet program. The errors in the calculated D values were estimated assuming a

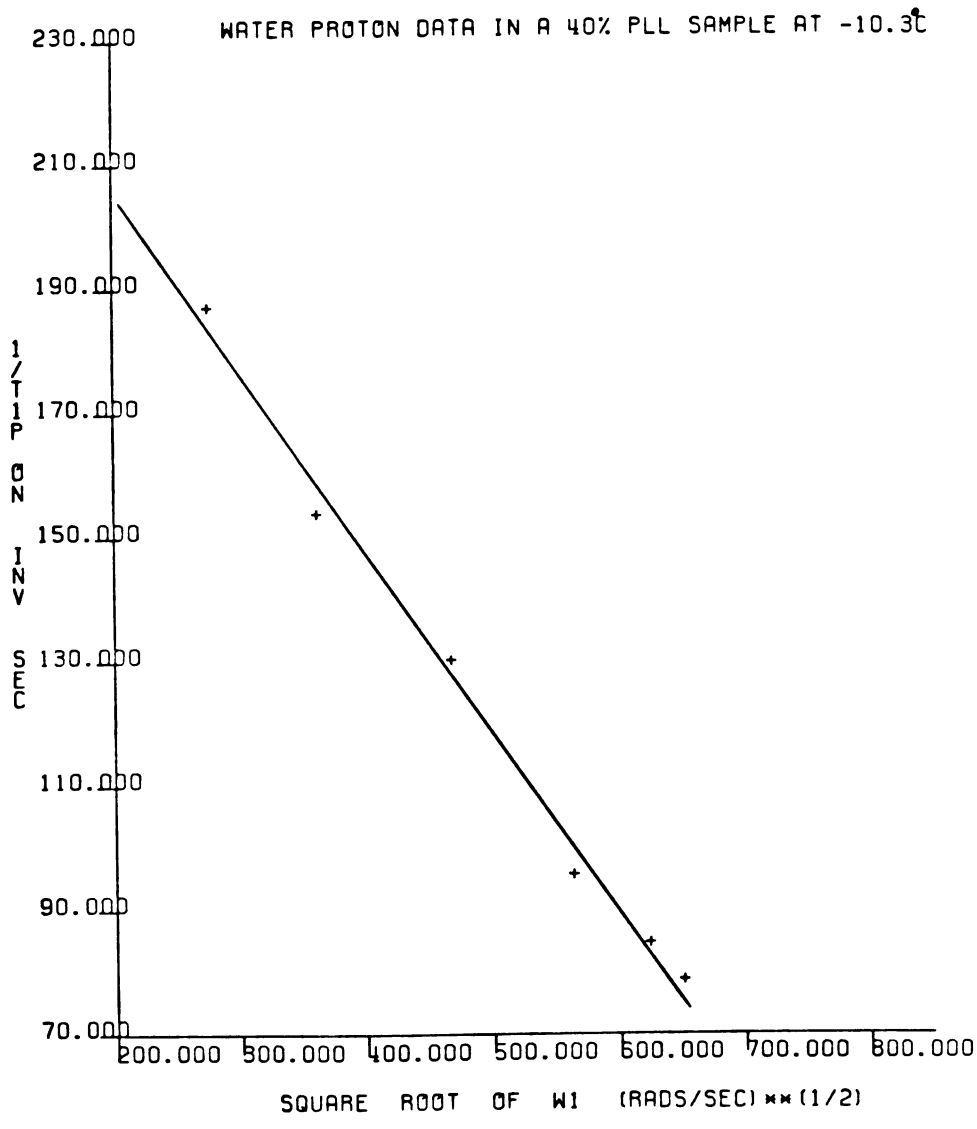

Fig. 6.18. A plot of $1/T_{1\rho}^{m}$ vs. $\omega_1^{1/2}$. Data are for the water protons in a 40% PLL sample at −10.3°C.

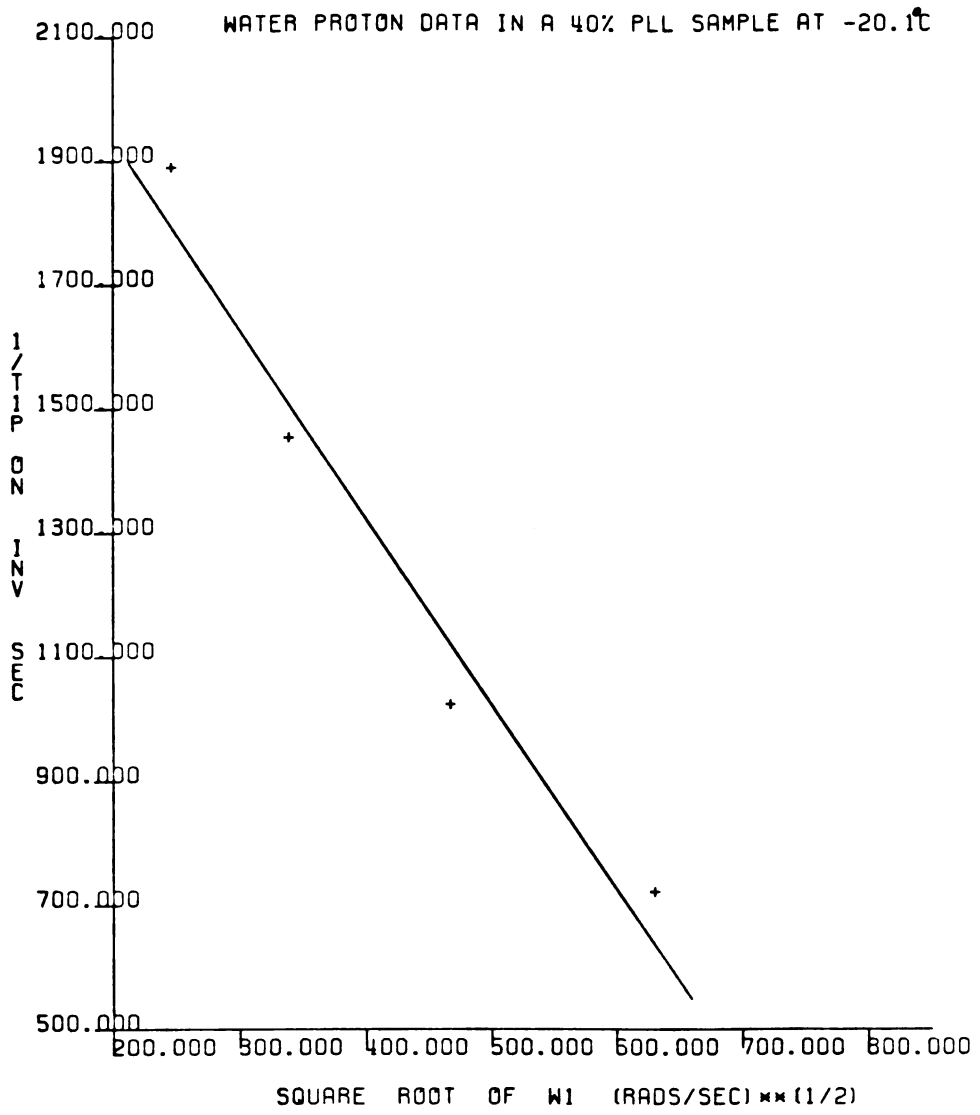

Fig. 6.19. A plot of $1/T_{1\rho}^{on}$ vs. $\omega_1^{1/2}$. Data are for the water protons in a 40% PLL sample at −20.1°C.

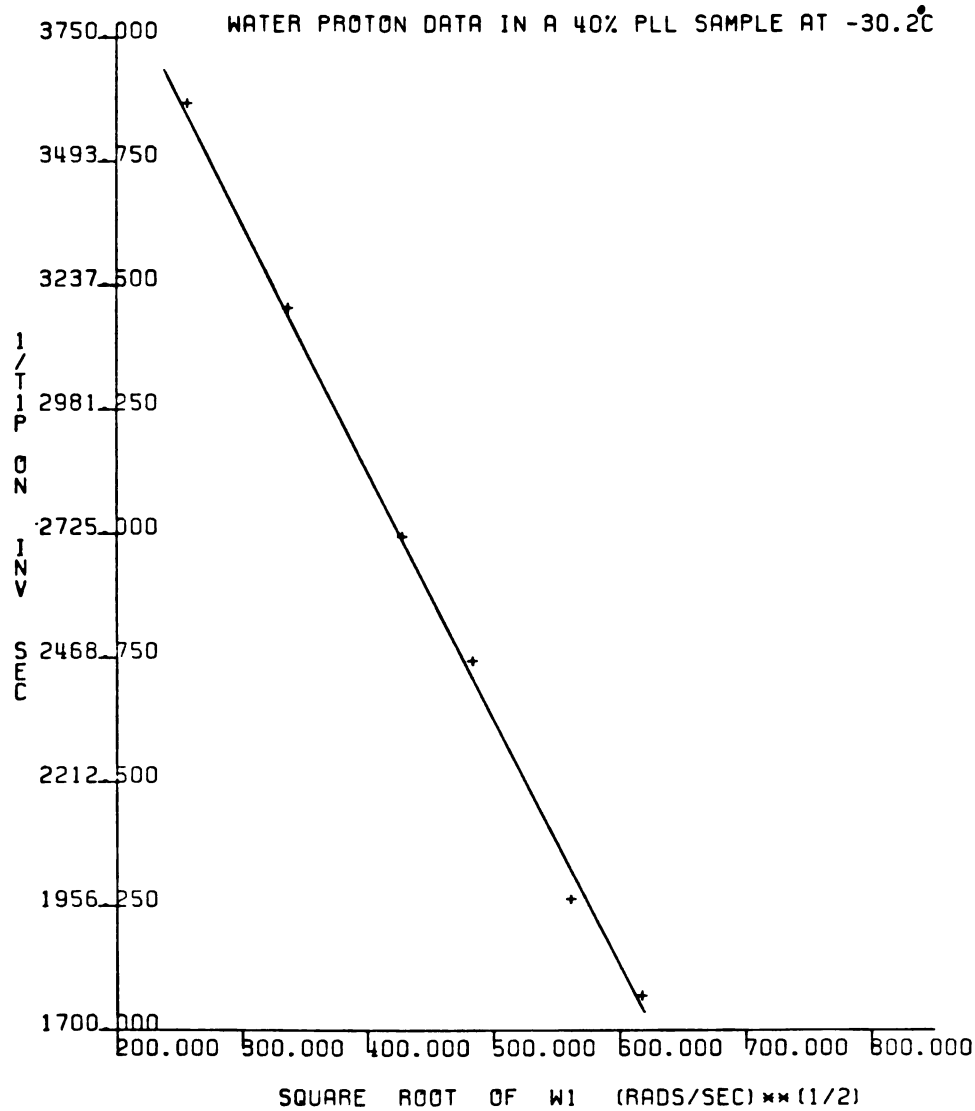

Fig. 6.20. A plot of $1/T_{1\rho}^{on}$ vs. $\omega_1^{1/2}$. Data are for the water protons in a 40% PLL sample at −30.2°C.

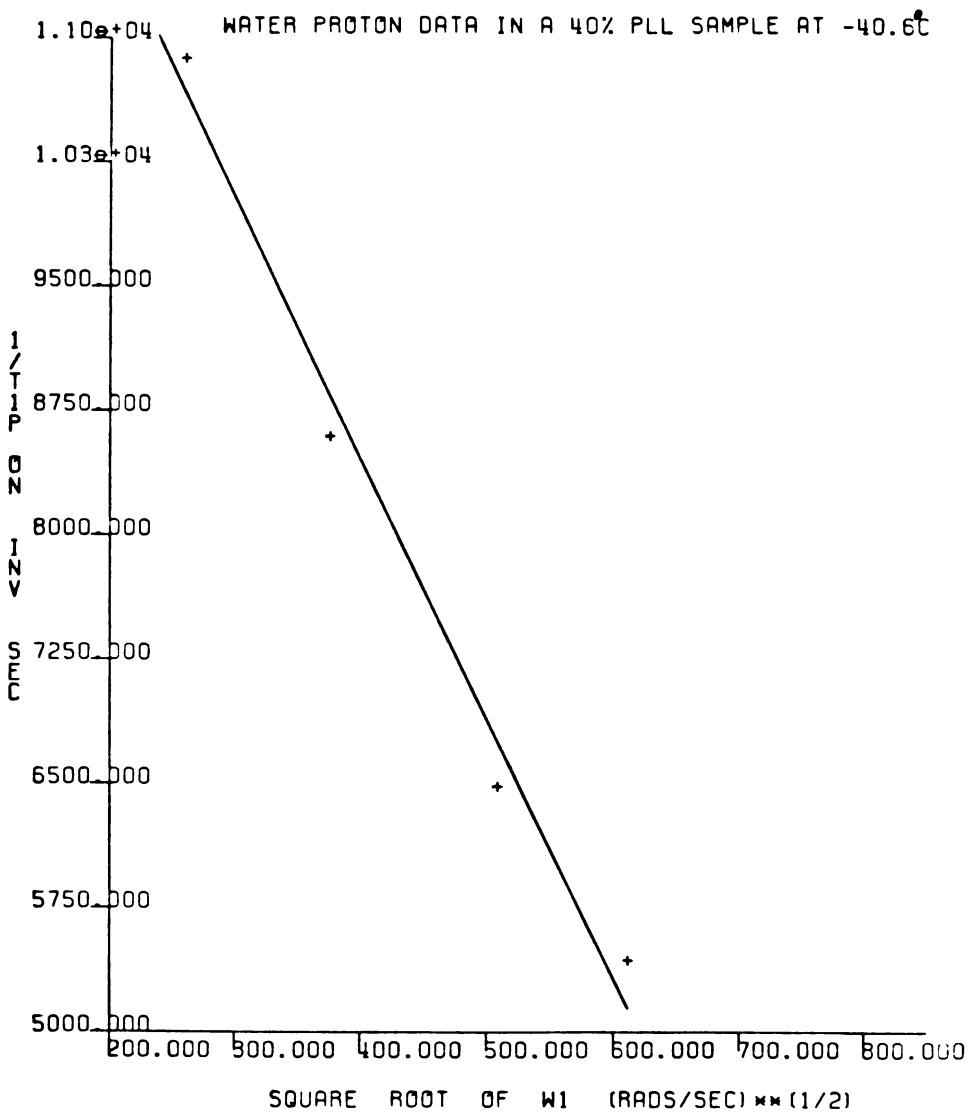

Fig. 6.21. A plot of $1/T_{1\rho}^{on}$ vs. $\omega_1^{1/2}$. Data are for the water protons in a 40% PLL sample at −40.6°C.

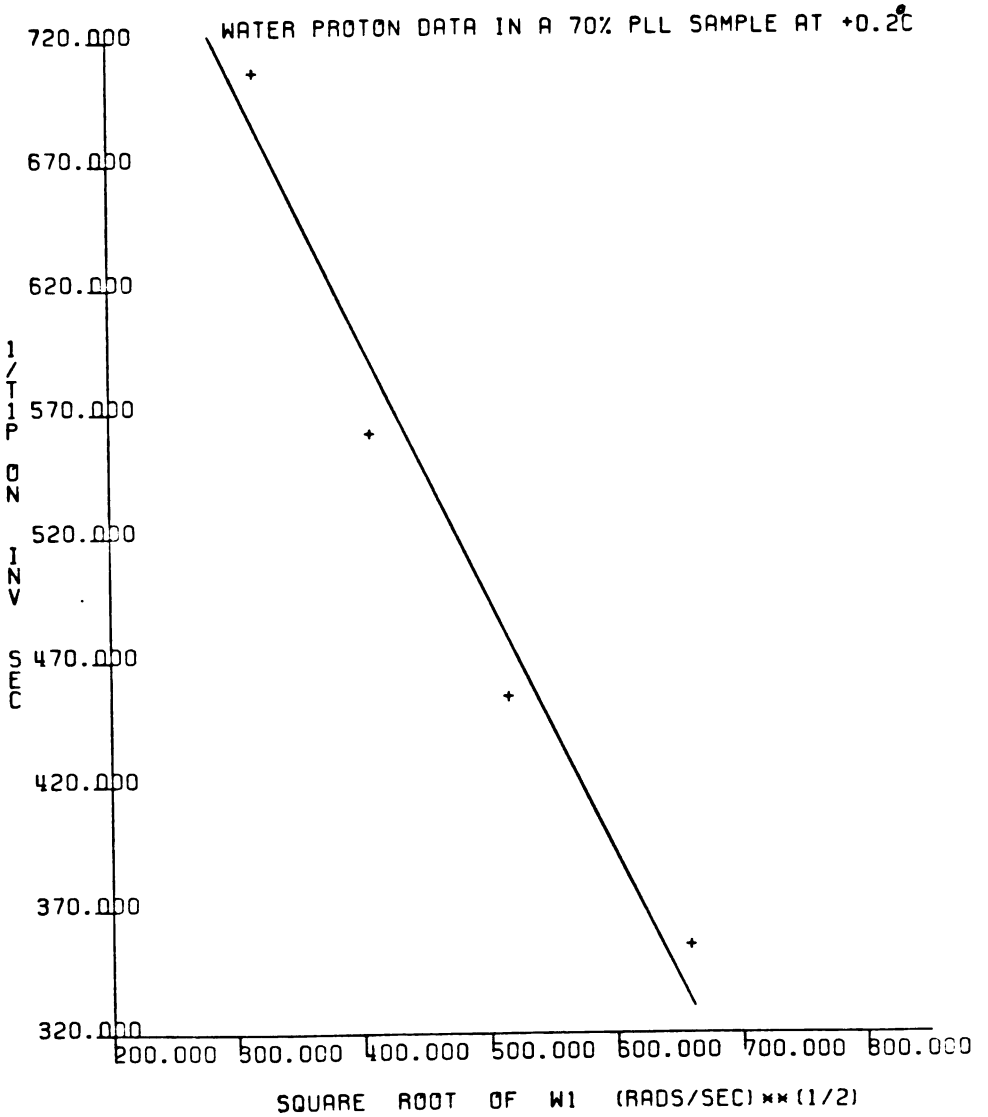

Fig. 6.22. A plot of $1/T_{1\rho}^{on}$ vs. $\omega_1^{1/2}$. Data are for the water protons in a 70% PLL sample at +0.2°C.

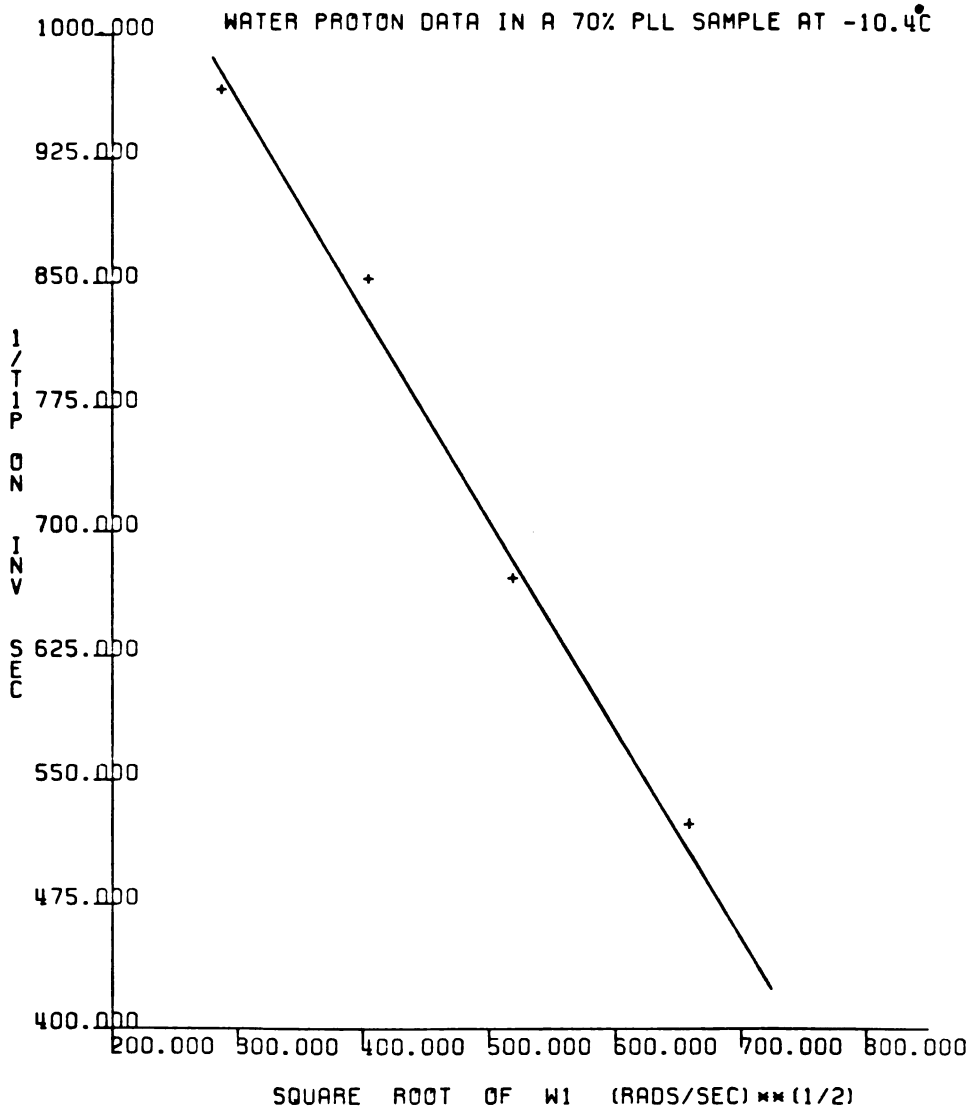

Fig. 6.23. A plot of $1/T_{1\rho}^{on}$ vs. $\omega_1^{1/2}$. Data are for the water protons in a 70% PLL sample at −10.4°C.

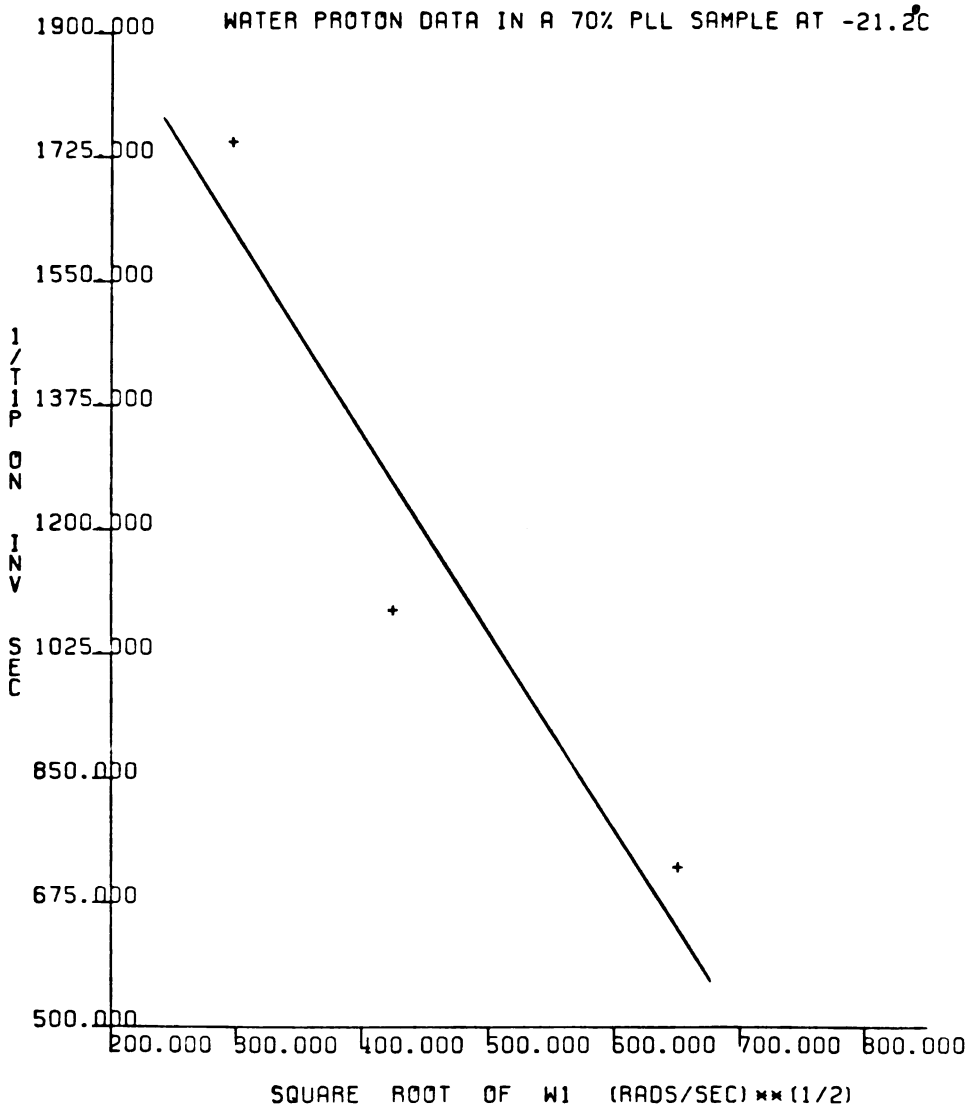

Fig. 6.24. A plot of $1/T_{1\rho}^{on}$ vs. $\omega_1^{1/2}$. Data are for the water protons in a 70% PLL sample at −21.2°C.

Table 6.3. Diffusion-coefficients of the water proton in 40% and 70% PLL samples.

Temp. (°C)	Slope[1] (sec × rads)$^{-1/2}$	Diffusion-Coefficient (D)[2] (cm^2/sec) × 10^{10}
40% Sample		
−10.3	−0.29 ± 0.01	8.4 ± 2.9
−20.1	−3.00 ± 0.14	1.8 ± 0.6
−30.2	−5.19 ± 0.03	1.2 ± 0.4
−40.6	−15.58 ± 0.40	0.6 ± 0.2
70% Sample		
+0.2	−1.01 ± 0.36	3.2 ± 1.1
−10.4	−1.23 ± 0.02	2.8 ± 1.0
−21.2	−2.73 ± 0.29	1.7 ± 0.6

[1]Slopes and standard deviations calculated by the Nicolet program.

[2]Reported errors are estimates (see text).

contribution of ∿15% error from sources other than relaxation times measurements.

It should be noted that Equation 2.7 assumes an isotropic translational motion. In real systems the water molecules diffuse along the macromolecule surface and their motion may be restricted. The "true" values of the diffusion-coefficients may therefore be expected to have smaller values than their apparent values. Fisher and James (37) have used a minor modification of Equation 2.7 to calculate D in phospholipid bilayers, where the translational motion takes place in two dimensions only. This modification reduces the calculated values of D by ∿35%. Because of the small dimensions of the water molecule (diameter ∿1 Å) and its almost spherical shape (23, 55), it is unlikely that its translational motion will be restricted enough to reduce the values of the diffusion-coefficient by as much as 35%. A correction of ∿10%-20% may be more realistic for the water molecule, but because this value is uncertain and because it falls within the experimental error range for the diffusion-coefficient measurements, no corrections were applied to Equation 2.7.

Within each sample the diffusion-coefficient becomes smaller as the temperature is lowered. In the 40% sample D changes by a factor of ∿5 when the

temperature is changed from -10.3°C to -20.1°C. This change corresponds to the freezing event observed in this sample between 0°C and -20°C. No big changes in D are observed in the 70% sample. At ∿-20°C the diffusion-coefficients in both samples are equal. Since data below -20°C is lacking for the 70% sample it is not known whether this equality continues at temperatures below -20°C.

The order of magnitude of the values of D (Table 6.3) is smaller by a factor of $\sim 10^5$ as compared to the values measured in liquid water at 0°C (55). It is smaller by a factor of ∿10 as compared to the value of D found in water bound to red cell membrane (56) and the value reported for glycerine at -2.3°C (36). The small values of D indicate that in the water-PLL system at low temperatures and/or high macromolecule concentration, a fraction of the water molecules is highly restricted in its translational mobility.

If translational motions dominate the relaxation, the intercept in a $1/T_{1\rho}^{on}$ versus $\omega_1^{1/2}$ plot is expected to be equal to $1/T_2$. Table 6.4 lists the fitted intercepts, the extrapolated $1/T_2$ values, and the percent (%) deviation of the fitted intercepts from the extrapolated values of $1/T_2$. $1/T_2$ values were found by extrapolating $1/T_{1\rho}^{on}$ relaxation rates to $H_1 \approx 0$.

Table 6.4. Percentage deviation of the fitted intercept from the extrapolated $1/T_2$ values in 40% and 70% PLL samples.

Temp. (°C)	Intercept[1] (sec)$^{-1}$	$1/T_2$ Extrapolated (sec)$^{-1}$	Deviation (%)
40% Sample			
−10.3	260 ± 52	209.	24.
−20.1	2510 ± 500	2820.	11.
−30.2	4910 ± 980	4860.	1.
−40.6	14600 ± 2900	13100.	11.
70% Sample			
+0.2	991 ± 200	1330.	25.
−10.4	1320 ± 265	1680.	21.
−21.2	2410 ± 480	2230.	8.

[1]Intercepts calculated be the Nicolet program.

Within each sample the deviation of $1/T_2$ from the fitted intercept becomes smaller as the temperature is lowered. In the 40% sample, the deviation becomes bigger on going from -30.2°C to -40.6°C. This is probably caused by the larger experimental error at the low temperature. Beginning at a temperature of ∿-15°C and down, the intercepts of both samples are equal to their extrapolated $1/T_2$ values, within the experimental error. This result strongly indicates (36) that below ∿-15°C, the frequency dependence of the relaxation processes in both PLL samples arises mostly from the translational motions. The greater deviations at temperatures above ∿-15°C indicate that at those temperatures other frequency dependent relaxation processes contribute. At temperatures above ∿-10°C for the 40% sample and above ∿ 0°C for the 70% sample, where data points do not fall on straight lines in a $1/T_{1\rho}^{on}$ versus $\omega_1^{1/2}$ plots, the relaxation is dominated by motions other than translation. Based on indirect evidence, it has been previously suggested that in heterogeneous systems the relaxation of water protons is dominated by translational motions (57, 58). This study provides a direct evidence that in the water-PLL system at temperatures below ∿-15°C the relaxation may be dominated by translational motions.

It is possible to perform deuterium dilution experiments to check whether protons and adjacent water molecules relax one another. As the fraction of the solvent deuterons increases, one would expect this mechanism to become less important.

To obtain the apparent energies of activation for the diffusion processes, ln(1/D) were plotted versus the reciprocal temperature. The plots for both samples are illustrated in Figure 6.25. Table 6.5 summarizes the fitted values obtained for the slopes and the apparent energies of activation. The slopes were calculated by the Nicolet program. A total error of ∿40% was estimated for the calculated values of E_a.

The 40% sample has a higher energy of activation than the 70% sample. This is similar to the result obtained when the extrapolated $1/T_2$ values were plotted versus the inverse temperature (Table 6.2).

Theory predicts that in the high H_1 field limit $T_{1\rho}^{on} = \frac{2}{5}T_1$ (see Chapter 2, Section 2.5). This fact may be used to establish indirectly the presence of a dispersion: if at the highest H_1 fields where data were obtained $T_{1\rho}^{on} < \frac{2}{5}T_1$, an additional dispersion in $T_{1\rho}^{on}$ values should be present at still higher fields. In addition, this theoretical prediction may be used to check the reliability of the $T_{1\rho}^{on}$ and T_1 relaxation

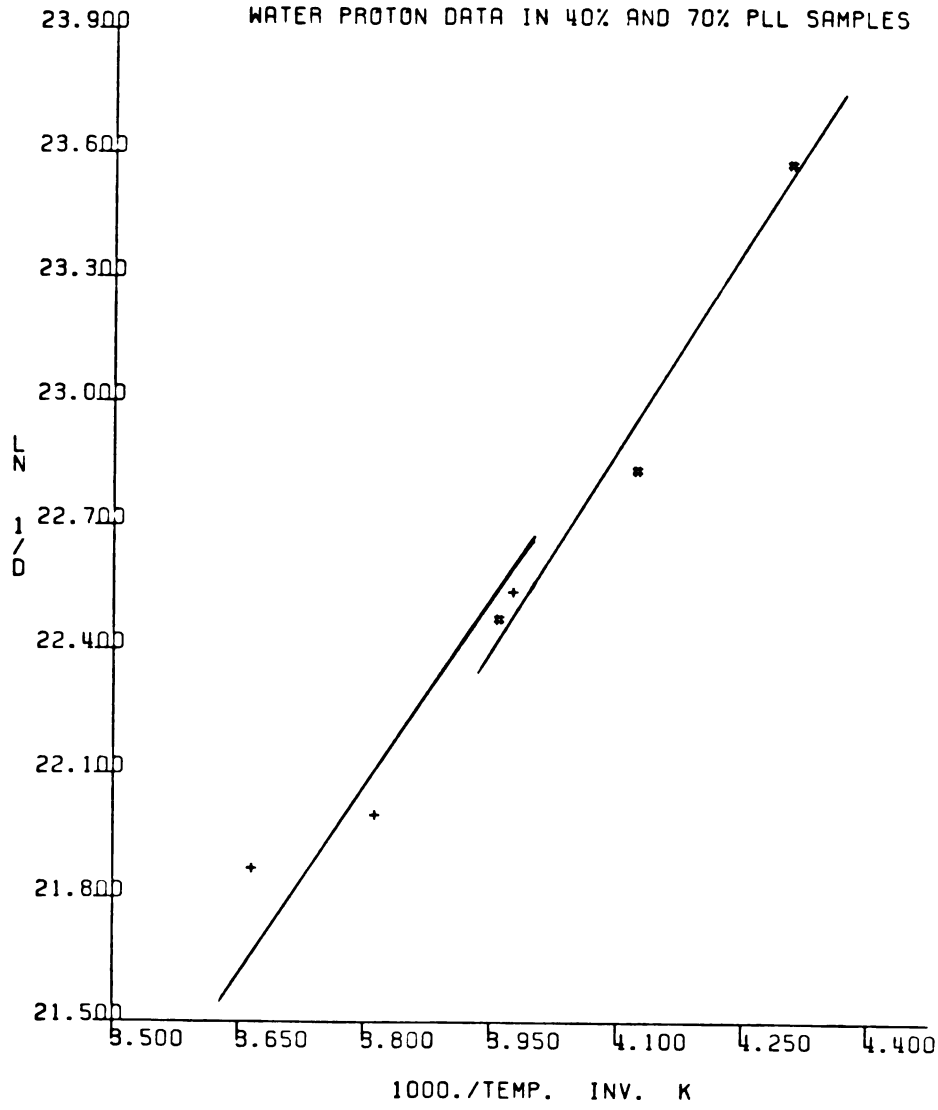

Fig. 6.25. A plot of ln (1/D) vs. the inverse (absolute) temperature. Data are for the water protons in PLL samples. (#) 40% PLL sample; (+) 70% PLL sample.

Table 6.5. Apparent energies of activation for the diffusion of the water protons in 40% and 70% PLL samples.

Sample	Slope[1] (°K)	E_a[2] (Kcal/mole)
40%	3160 ± 1100	6.3 ± 2.5
70%	2260 ± 790	4.5 ± 1.8

[1]Slopes calculated by the Nicolet program.

[2]Reported errors are estimates (see text).

data. Table 6.6 summarizes the $\frac{2}{5}T_1$ and $T_{1\rho}^{on}$ data for 40% and 70% PLL samples. The differences between the $\frac{2}{5}T_1$ and $T_{1\rho}^{on}$ are also given.

The differences are negative for the 40% sample at high temperatures. This is most likely caused by the experimental error. At the high temperatures, both the T_1 and the $T_{1\rho}^{on}$ relaxations showed biphasic decays, some of them with $\sim$50% contribution from each component. Biphasic decays are difficult to resolve, especially when the relative contribution of each component is about equal (see Chapter 5, Sections 5.2 and 53.). If the difference between the T_1 and the $T_{1\rho}^{on}$ relaxation times is not big and the experimental error tends to make the apparent T_1 values shorter than their "true" values and the apparent $T_{1\rho}^{on}$ values longer than their "true" values, a negative difference may result. At the low temperatures, where all decays were single exponential, all the differences are positive.

For the 40% sample below 0°C the differences increase quickly as the temperature is lowered. For the 70% sample, the differences remain constant within the experimental error throughout the investigated temperature range. These facts indicate that the slow motions governing the $T_{1\rho}^{on}$ relaxation in the 40% sample have a higher energy of activation than the

Table 6.6. Differences between $(\frac{2}{5}T_1)$ and $T_{1\rho}^{on}$ values in 40% and 70% PLL samples.

Temp. (°C)	$\frac{2}{5}T_1$ (msec)	$T_{1\rho}^{on}$ (msec)	$\left(\frac{2}{5}T_1 - T_{1\rho}^{on}\right)$ (msec)
40% Sample			
+22.7	125.15	197.44	−72.
+9.8	94.00	169.60	−76.
−0.1	68.20	128.69	−60.
−10.3	21.28	12.92	8.
−20.1	14.95	1.41	14.
−30.2	15.78	0.57	15.
−40.6	28.80	0.19	29.
70% Sample			
+23.7	24.04	5.94	18.
+10.8	20.83	4.94	16.
+0.2	19.75	2.84	17.
−10.4	17.64	1.93	16.
−21.2	16.19	1.40	15.

slow motions governing the $T_{1\rho}^{on}$ relaxation in the 70% sample. This is consistent with the measured values of E_a listed in Tables 6.2 and 6.5.

Our study indicates that at least two populations of water exist in the water-PLL system at subzero temperatures:

1. A population with an apparent correlation time in the nanosecond region. This population dominates the T_1 relaxation and is responsible for the minimum in the T_1 values at $\sim$-20°C.
2. A population with an apparent correlation time in the microsecond region. This population is responsible for the dispersion observed in the $T_{1\rho}^{on}$ values. We have presented evidence that at temperatures below $\sim$-15°C the $T_{1\rho}^{on}$ relaxation rates have an important contribution from translational motions.

6.2 Bovine Serum Albumin (BSA)

6.2.1 T_1 Data

It is of interest to establish to what extent the properties of the model PLL system are common to "real" proteins. BSA has been chosen for this purpose

because it is a cheap and commercially available globular protein.

Figure 6.26 shows the water proton T_1 relaxation times at 150 MHz of BSA solutions of four different concentrations: 0.2 g protein/1 ml water (16.7% wt/wt), 0.4 g protein/1 ml water (28.6% wt/wt), 0.6 g protein/1 ml water (37.5% wt/wt), and 0.8 g protein/1 ml water (44.4% wt/wt). The data cover a temperature range from +45°C to -65°C. Figure 6.27 shows the high temperature portion of the data and Figure 6.28 shows the subzero temperature portion of the data. Figure 6.29 shows the deuterium T_1 relaxation times of BSA in D_2O solutions of similar concentrations. The deuterium data were taken at 15.4 MHz and cover a temperature range from +45°C to -25°C. Figure 6.30 shows the high temperature region of the deuterium data and Figure 6.31 shows the subzero region of the data. Deuterium data below -25°C could not be obtained because the lines became very broad.

The general behavior of the T_1 relaxation curves is similar to that found in the water-PLL system. On the "low" temperature side of the T_1 plot a discontinuity occurs between +5°C and -5°C in both the proton and the deuterium data. All the proton T_1 values go through a minimum at about -25°C. Within the experimental error, all the deuterium T_1 values

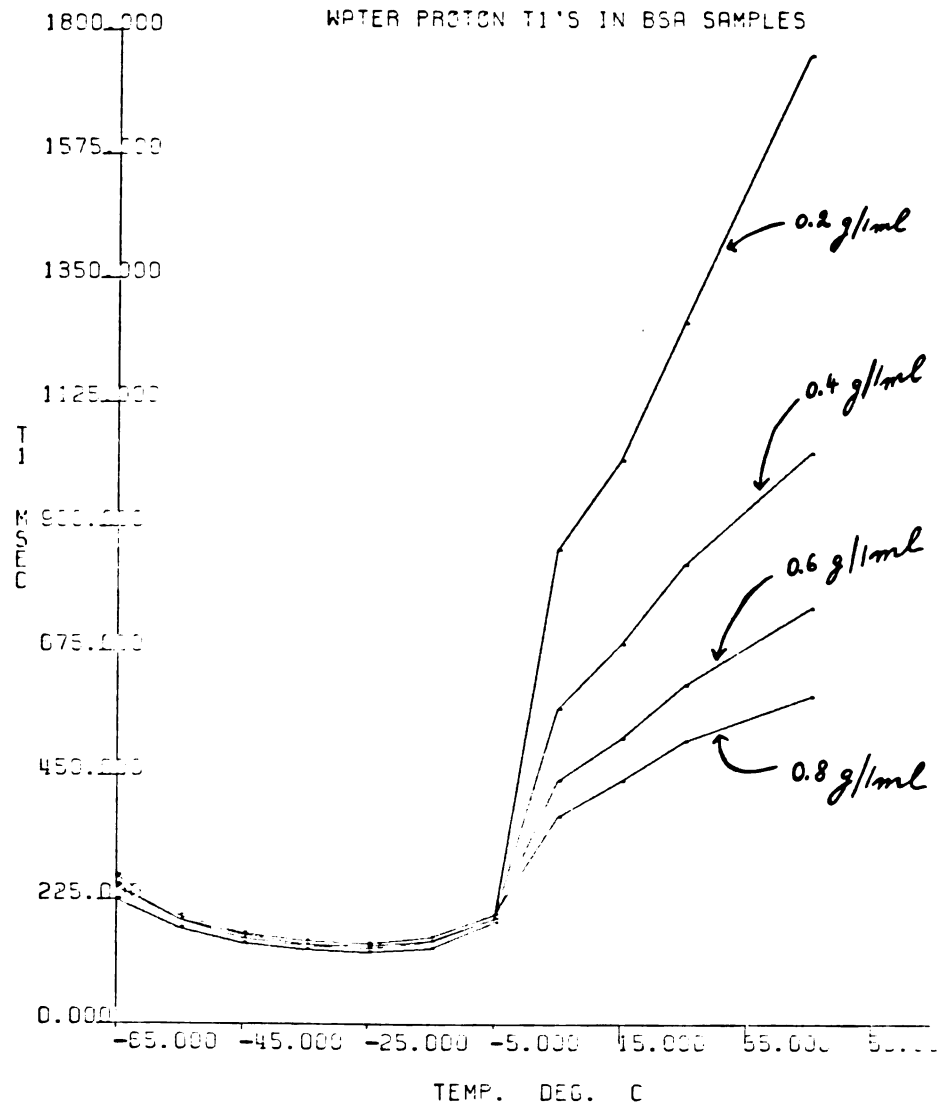

Fig. 6.26. Water proton T_1 relaxation times at 150 MHz in BSA samples. The high and the low temperature regions are shown. The arrows with the numbers indicate the concentration of the macromolecule in units of gram protein per 1 ml of added solvent.

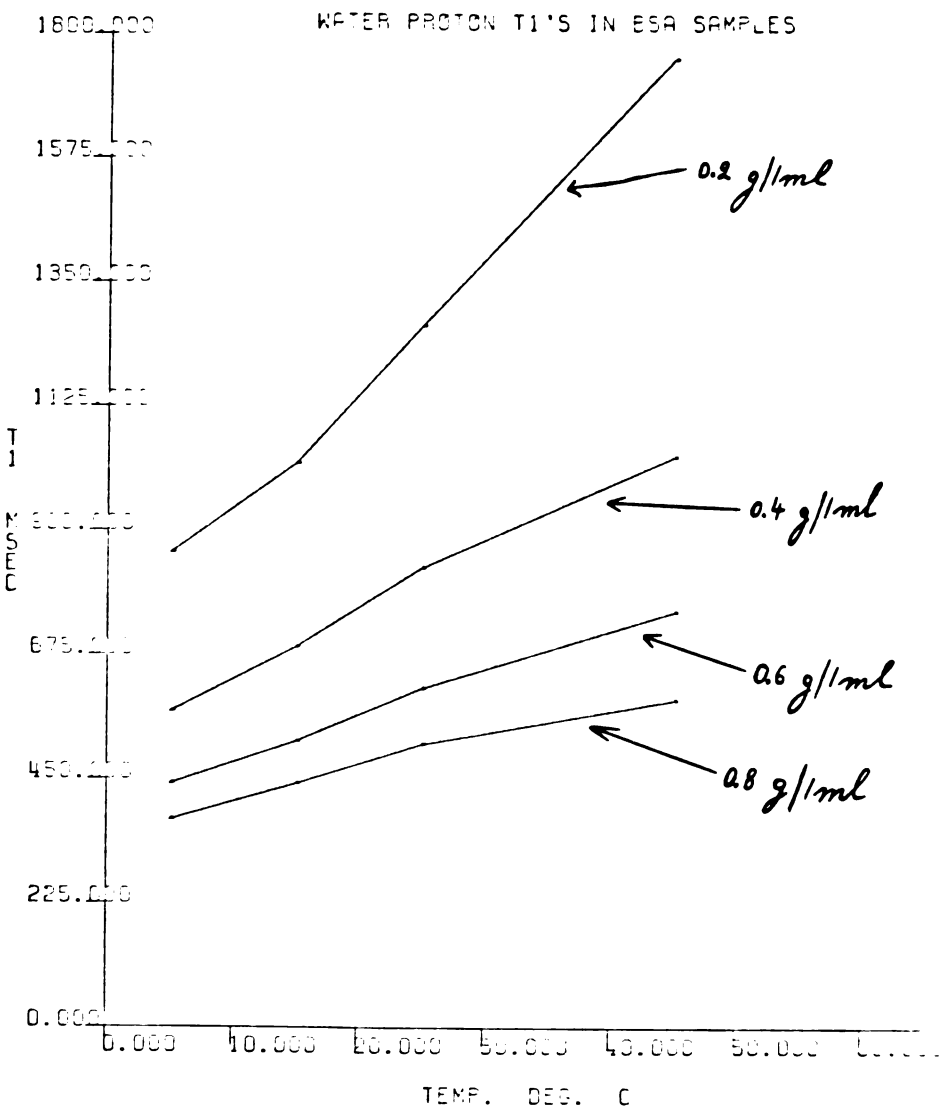

Fig. 6.27. Water proton T_1 relaxation times at 150 MHz in BSA samples. The high temperature region is shown. The arrows with the numbers indicate the concentration of the macromolecule in units of gram protein per 1 ml of added solvent.

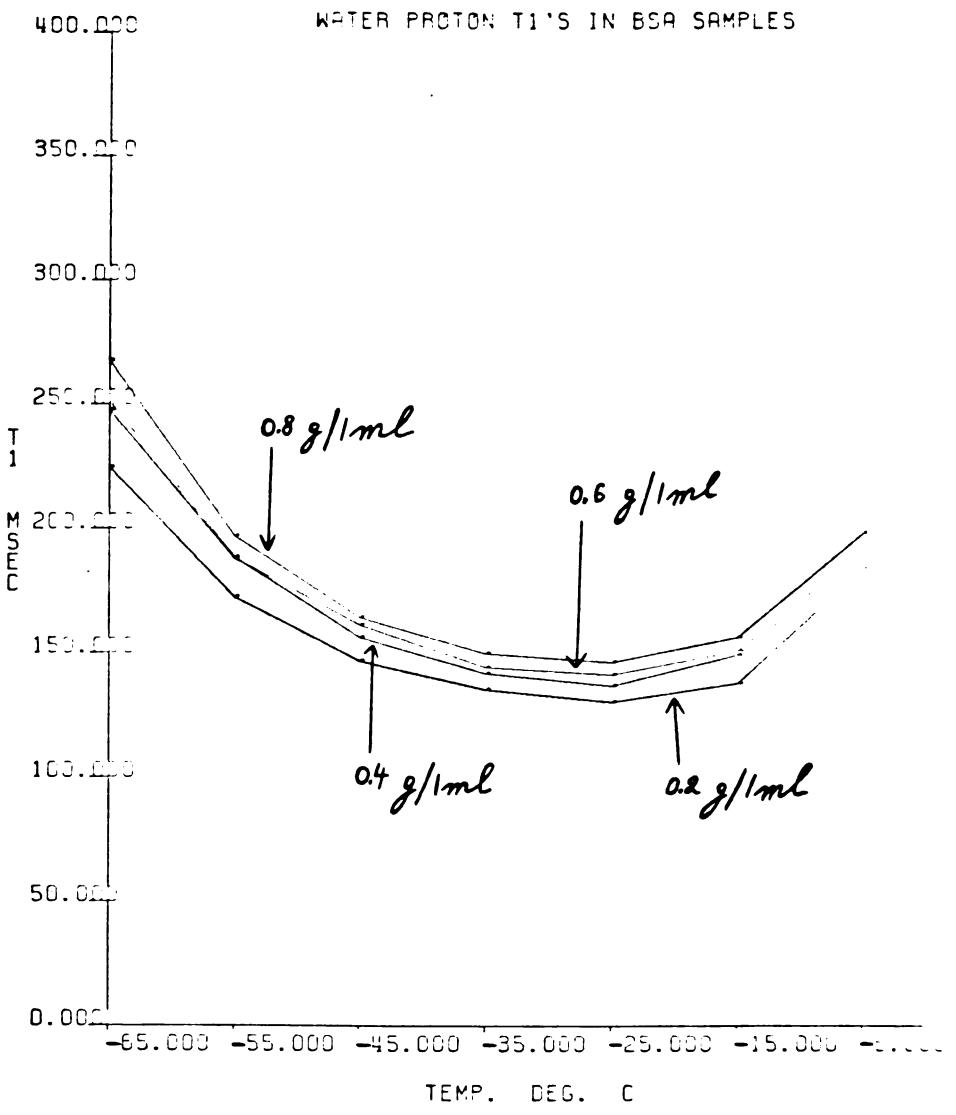

Fig. 6.28. Water proton T_1 relaxation times at 150 MHz in BSA samples. The low temperature region is shown. The arrows with the numbers indicate the concentration of the macromolecule in units of gram protein per 1 ml added solvent.

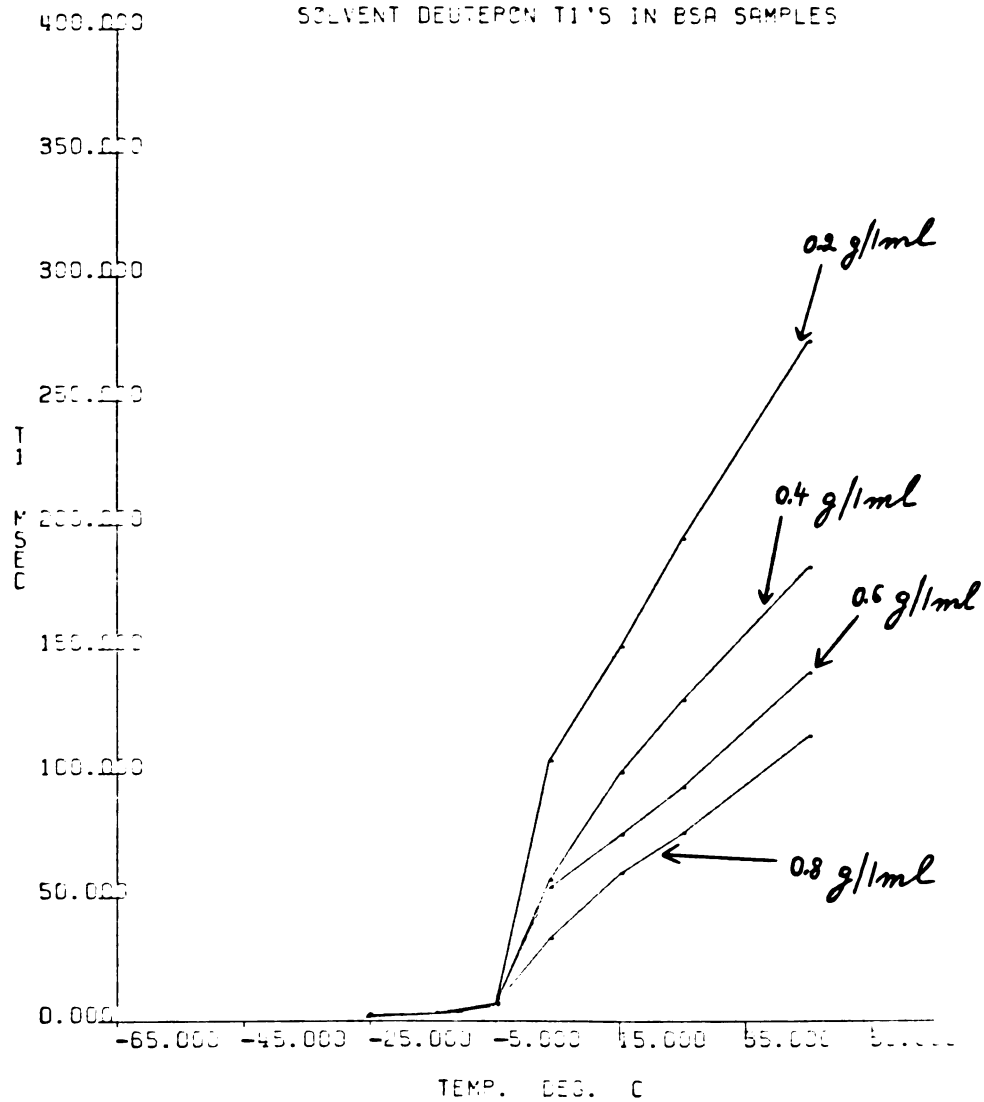

Fig. 6.29. Solvent deuteron T_1 relaxation times at 15.4 MHz in BSA samples. The high and the low temperature regions are shown. The arrows with the numbers indicate the concentration of the macromolecule in units of gram protein per 1 ml of added solvent.

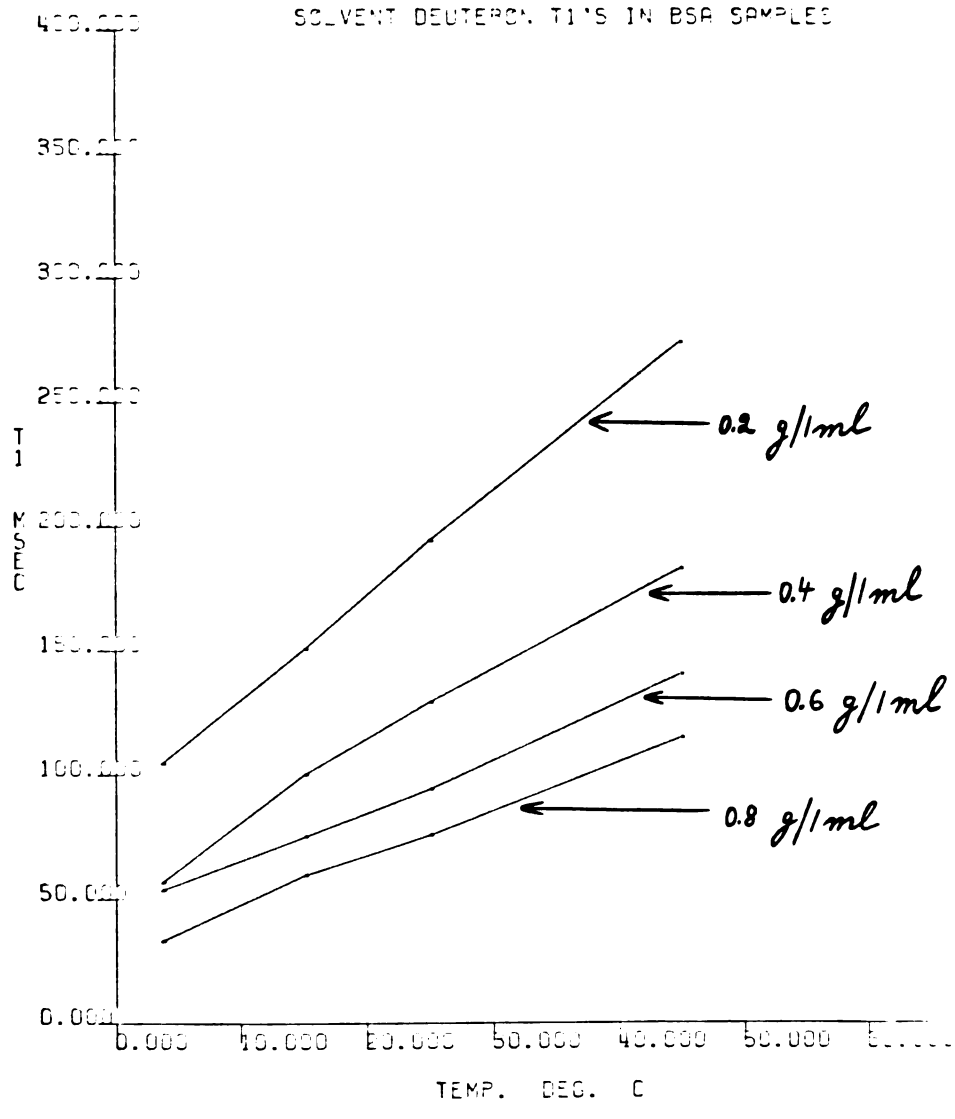

Fig. 6.30. Solvent deuteron T_1 relaxation times at 15.4 MHz in BSA samples. The high temperature region is shown. The arrows with the numbers indicate the concentration of the macromolecule in units of gram protein per 1 ml of added solvent.

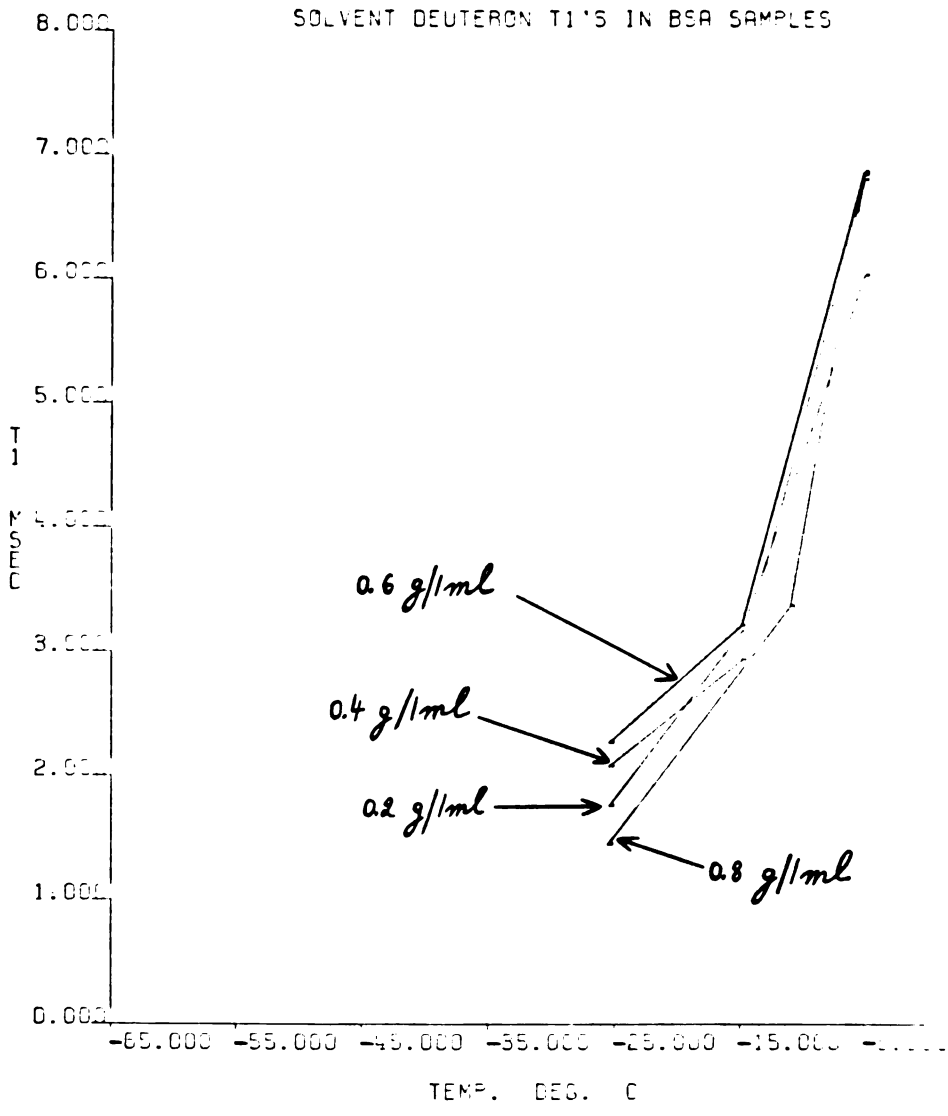

Fig. 6.31. Solvent deuteron T_1 relaxation times at 15.4 MHz in BSA samples. The low temperature region is shown. The arrows with the numbers indicate the concentration of the macromolecule in units of gram protein per 1 ml added solvent.

are equal at subzero temperatures. The deuterium T_1 values become shorter down to -25°C, but since data below this temperature could not be obtained it is not known whether the minimum has been reached. On the "high" temperature side of the T_1 plot in both the proton and the deuterium data the T_1 values are a linear function of the temperature. This is consistent with a simple two-site fast exchange model (14).

An interesting feature of the proton T_1 data at subzero temperatures (Figure 6.28) is that the T_1 curves are parallel and are spaced above each other; at any given temperature the sample of the higher protein concentration has a longer T_1 relaxation time. It should be noted that the spacings between the curves are very small. However, the fact that no deviations from this pattern are observed and the fact that the data were taken at a relatively high field (150 MHz), on an instrument with a high sensitivity (see Chapter 5, Section 5.2), and the fact that all the relaxation times had standard deviations <1% (Table 5.2), gives confidence that a true phenomenon was observed. Because of a lower signal/noise ratio, similar effects in the water-PLL system would not be detected, even if they were present.

At least six effects should be considered as possible explanations for the concentration dependence of the proton T_1 curves: (1) cross-relaxation, (2) distribution of correlation times, (3) paramagnetic impurities, (4) ice formation, (5) generation of metastable phases, and (6) experimental artifacts.

Cross-relaxation will be considered first. In solution the protein proton T_1 relaxation is dominated by the overall rotation of the protein molecule and its values are shorter than the T_1 values of the water protons. In frozen solutions protein rotation is practically absent (12, 53). In these systems the T_1 relaxation of the protein protons is dominated by the rotation of the methyl and the amino groups (43, 59); the energy of activation for the rotation of these groups is small and as a result the rotational correlation time for these groups is short, even at low temperatures. Because of cross-relaxation among the protein protons, the T_1 relaxation of the protein protons is dominated by the rotation of the methyl and amino groups and the T_1 minimum in dry protein powders occurs at very low temperatures, Temperature $\leqslant -70°C$ (59).

If cross-relaxation is present and special care is not taken, the short first component of the FID is usually lost and only the longer second component is

measured as an apparent T_1 relaxation time (5). In the presence of cross-relaxation the second component of the protein protons T_1 decay and the second component of the water protons T_1 decay become equal. The apparent T_1 relaxation time will have a value that is between the protein protons' T_1 and the water protons T_1. As a result, in solution the apparent T_1 relaxation times of the water protons will be shorter than their "true" T_1 values in the absence of cross-relaxation. In frozen systems the apparent T_1 values of the water protons will be longer than their "true" T_1 values, the apparent minimum will occur at lower temperatures than the "true" minimum and the apparent values of T_1 at the minimum will be longer than their "true" values. If one derives correlation times for the water protons in frozen systems based on the location of the apparent T_1 minimum, the derived correlation times will be shorter than the "true" correlation times in the absence of cross-relaxation.

The discrepancy between the apparent and the "true" values will depend on the relative contribution of cross-relaxation. If the relative contribution of cross-relaxation increases with increasing protein concentration, the T_1 curves of the more concentrated samples will be expected to lie above the curves of

the less concentrated samples and the minima will be expected to be broader and to be shifted towards lower temperatures.

Inspection of Figure 6.28 shows that only one of these predictions is fulfilled. While the T_1 curves of the more concentrated samples lie above those of the less concentrated samples, all the minima occur in the range $\sim$-25°C to $\sim$-30°C, i.e., they are temperature independent, within the experimental error, and no broadening of the minima is observed. One must conclude that either the contribution of cross-relaxation is small and/or its effects are such that it affects mostly the values of T_1 but has a smaller effect on the location of the minima and their breadths.

Because deuterium has a smaller gyromagnetic ratio than protons, cross-relaxation does not affect the deuterium relaxation (see Chapter 2, Section 2.7). In principle, one can measure the deuterium T_1 relaxation times to separate the contribution of cross-relaxation from other effects. In practice this approach may fail, because the deuterium signal is broader and noisier than the proton signal and is usually taken at lower frequencies. In addition, intermolecular relaxation processes which contribute to proton relaxation only, complicate direct comparison of the deuterium and the proton data.

In our study the deuterium peaks were broad and noisy in the frozen samples. The experimental error is bigger than the separation between the proton T_1 curves (in Figure 6.28) and therefore it is not known whether the deuterium T_1 curves are spaced in a similar way to the proton T_1 curves.

The deuterium T_1 values decrease with decreasing temperature down to $\sim$-25°C (the lowest temperature where reliable data could be obtained). This means that the deuterium T_1 minimum is located either at $\sim$-25°C or at a lower temperature. If cross-relaxation is important, the deuterium T_1 minimum in the frozen samples would be expected to occur at a higher temperature than the proton T_1 minima in frozen samples, i.e., at Temperature > $\sim$-25°C.

Direct interpretation is impossible, however, since the deuterium data were taken at an observing frequency of 15 MHz while the proton data were taken at a frequency of 150 MHz. If T_1 is frequency dependent, lowering the observing frequency will move the T_1 minimum to a lower temperature. The amount of the movement will be a function of the temperature dependence of the motions which contribute to T_1 relaxation.

The available frequency dependence data of T_1 for both the protons and the deuterons at -25°C

is summarized in Table 6.7. Data are for BSA samples of 0.8 g/1 ml H_2O or D_2O, except for the proton data at 44.4 MHz which was obtained on a BSA sample of 0.154 g/1 ml and the proton data at 100 MHz which was obtained on a BSA sample of 0.5 g/1 ml. The results in Table 6.7 indicate that T_1 is frequency dependent in the region 15-150 MHz.

We next consider the effects of having a distribution of correlation times instead of a single correlation time. If the relaxation is dominated by a single isotropic rotational correlation time the T_1 value at the minimum will be given by Equation 2.3. If a distribution of correlation times exists, the T_1 value at the minimum will become longer and the minimum itself will become broader (13). Similar effects are expected if a distribution of interproton distances exists (9). This latter term will be important only if intermolecular relaxation is dominant.

Inspection of the data in Figure 6.28 shows that although the T_1 relaxation times become longer for the more concentrated samples, no broadening of the minima is observed with increase in concentration. If such broadening was present, the curves of the higher concentrations would be expected to cross the curves of the lower concentrations. A

Table 6.7. Frequency dependence of the solvent proton and deuteron T_1 relaxation in frozen BSA samples.

Nucleus	Frequency (MHz)	T_1 (msec)
Deuterium	15.4	1.5[1]
	23.	2.6[1]
Protons	44.4	45.[2]
	100.	111.2[3]
	150.	146.6[4]

[1]BSA sample of 0.8g/1ml D_2O.

[2]BSA sample of 0.154g/1ml H_2O.

[3]BSA sample of 0.5g/1ml H_2O.

[4]BSA sample of 0.8g/1ml H_2O.

distribution of correlation times may exist within each sample, but the experimental data indicate that the width of the distribution is concentration independent at subzero temperatures in the concentration range 0.2-0.8 g BSA/1 ml water.

Inspection of the PLL data in Figure 6.2 shows that the 70% PLL sample (2.3 g PLL/1 ml water) has a longer T_1 value at the minimum than the less concentrated PLL samples. In addition, the T_1 minimum of the 70% sample is broader than the T_1 minima of the less concentrated samples and its T_1 curve crosses the curves of the less concentrated samples. These results indicate that the width of the distribution of the correlation times may become concentration dependent at high enough macromolecule concentration. In the water-PLL system this dependence may become important at a concentration of $\sim$70% macromolecule. Similar effects are expected if cross-relaxation becomes important at high macromolecule concentrations.

Our third topic is paramagnetic impurities. Paramagnetics shorten relaxation times (26). If paramagnetic impurities were present in the BSA powder, the samples of the higher protein concentration would have a higher concentration of paramagnetics and therefore shorter relaxation times. This is opposite to the experimentally observed effects

(Figure 6.28). If paramagnetic impurities originated in the water, the samples of the higher protein concentration would be expected to have smaller effective concentration of paramagnetics upon freezing and therefore longer relaxation times. The effective concentration of the paramagnetics upon freezing is expected to decrease when the protein concentration increases, because the amount of the unfreezable water is directly proportional to the amount of protein (in the concentration range studied by us), while the total amount of the paramagnetics remains constant. If a large fraction of the paramagnetics is trapped in ice, smaller effective concentrations will result.

To avoid contamination with paramagnetics we used doubly distilled water and handled all BSA powders with teflon coated spatulas. We also checked directly the water, the BSA powder, and a 0.5 g/1 ml solution of BSA in water for the presence of Mn^{++} ions by ESR spectroscopy (see Chapter 4, Section 4.4). No Mn^{++} ions could be detected within the sensitivity limits of our spectrometer, which was $\sim$10 μM (see also Section 6.3.2). Mn^{++} is the most effective paramagnetic ion. Although we cannot rule out the presence of other paramagnetic ions, it is very unlikely that they were present in high enough concentrations to affect our results.

What is the role of ice formation? Glasel (58) showed that the water proton T_1/T_2 ratios become larger than 1 when glass spheres of small diameter ($\sim$15 μm) are added to the water. The effect was interpreted to arise from restricted translational mobility of water in the presence of small particles. If water mobility is restricted, the intermolecular relaxation term which is equal to the intramolecular relaxation term in pure water may dominate the T_1 and T_2 relaxation. This is not true for the deuterium relaxation, where the intermolecular term is negligible.

In the water-BSA system at concentrations studied here ice is formed at subzero temperatures when part of the "bulk" water freezes. If the size of the ice particles is small, it may shorten the measured T_1 and T_2 values. The smaller the particles' size, the bigger the effect. When the initial concentration of the macromolecule in solution is increased the total amount of ice formed upon freezing decreases. The ice particles' size may be dependent on the total amount of ice formed. If the particles' size is in the molecular size range, i.e., order magnitude of angstroms, change in its size will affect the measured relaxation times. If the ice particles' size increases when the total amount of ice decreases, it may give rise to the observed

concentration dependence of the T_1 curves. If the ice particles' size is in the molecular size range its surface/volume ratio is large. In this case the contact area with the unfrozen water is large and may give rise to cross-relaxation effects between the ice and the unfrozen water.

Luyet (60) reported ice formations in frozen gelatin gels and blood plasma that had diameters on the order of 500-1000 Å. Formations of smaller sizes might also have been present.

The fact that upon freezing we obtained systems that were opaque to visible light indicates that a large fraction of the ice particles had a diameter of at least ∿4000 Å. A 70% PLL sample, in which ice formation was not detected by NMR methods (see Section 6.1.1), remained clear and transparent at subzero temperatures. This also indicates that the opacity in the frozen systems is not caused by trapped air bubbles.

In frozen KCl solutions, Luyet reported ice particles which measured a few hundred angstroms. We have conducted preliminary experiments on solutions of LiCl above the eutectic point, which contained different amounts of ice (see Chapter 4, Section 4.2.1.1). Although the T_1's became shorter and the linewidths broader as the temperature was lowered,

the changes were within the limits expected for the temperature effect on the viscosity. No abrupt change in any of these parameters occurred when ice particles first formed.

In order for these observations to be consistent with the experimental results of Glasel, one must conclude that additional factors are important. One of these may be magnetic susceptibility. If the magnetic susceptibility of the glass spheres is much different from that of the water it may be responsible, at least in part, for the effects observed by Glasel. In addition, similar effects could arise if the glass spheres contained paramegnetic impurities on the surface. The difference in the magnetic susceptibilities between water and ice is likely to be very small and this effect is likely to be insignificant in our systems. We conclude that ice formation is not an important contributing factor to the measured relaxation times.

Our fifth topic is metastable "phases." It is not known whether the "phases" generated upon freezing are true equilibrium thermodynamic phases. Hilton et al. (9) suggested that metastable "phases" are formed upon freezing, because the rate of ice growth is much faster than the diffusion of the macromolecule during the freezing process. It may be that different

metastable "phases" are formed upon freezing, depending on the initial macromolecule concentration in solution. If this is so, the differences among such "phases" must be small in the investigated temperature and concentration range, because the observed concentration dependence of T_1 is small. This is also confirmed by the results of Kuntz et al. (4) and Kuntz (51), who observed that the amount of unfrozen water is independent of the initial macromolecule concentration in solution before freezing and our observation that the linewidths are concentration independent, within the experimental error, in the temperature range ∿-5°C to -65°C (see next section).

Lastly, the possibility of experimental artifacts will be considered. As discussed in Section 6.1.1, the FID's may contain some residual signal from the macromolecule. The relative contribution of this component will increase with increasing macromolecule concentration and its effect will be similar to that of cross-relaxation.

It is unlikely that this was significant for the water proton T_1 measurements in the water-BSA system. The instrumental dead time was set to ∿100 μsec. Although the protein protons may have relatively long T_1's, their T_2's are very short (43) and their FID's will be practically absent after ∿100 μsec.

The experiments were performed by measuring the heights of the absorption peaks. No broad component was detected on the base-line even at very large sweepwidths (±25,000 Hz). The situation might be different in the water-PLL system, where the experiments were performed by measuring directly the FID heights and the instrumental dead times were varied between ∿10 μsec and ∿100 μsec. In addition, the highest macromolecule concentration in the water-PLL system was 70% while it was 44.4% in the water-BSA system.

At 150 MHz the theoretical values of the relaxation times for protons at the minimum can be calculated to be $T_1 \sim 32.20$ msec and $T_2 \sim 19.25$ msec. The ratio $T_1/T_2 \sim 1.7$. Table 6.8 summarizes the experimental T_1 and T_2 values at the minima and gives their T_1/T_2 ratios. T_2 values were obtained from $LW_{1/2}$ measurements (see Section 6.2.2). As can be seen from Table 6.8, the T_1/T_2 ratios for all the samples are larger by a factor of ∿140 than the theoretical ratio. The experimental values of T_1 are larger than the theoretical T_1 value by a factor of ∿4. The experimental values of T_2 are shorter than the theoretical value by a factor of ∿40.

It is interesting to compare the T_1/T_2 ratios at the minima found in the water-BSA system to the

Table 6.8. Water proton T_1, T_2 and T_1/T_2 values at 150 MHz in frozen BSA samples. The values were obtained at the temperature of the T_1 minimum.

BSA Sample (g/ml)	T_1 (msec)	T_2 (msec)	$\frac{T_1}{T_2}$
0.2	130.64	0.61	214.
0.4	137.02	0.47	292.
0.6	141.46	0.49	289.
0.8	141.63	0.57	257.

T_1/T_2 ratios at the minima found in the water-PLL system (Table 6.1). The ratios in the water-BSA system are larger than the ratios in the water-PLL system by a factor of ∿1.4. In both systems the experimental T_1 values differ from the theoretical values by the same factor of ∿4. The experimental values of T_2 in the water-PLL system differ from the theoretical T_2 values by a factor of ∿16. This is smaller than the factor of ∿40 found in the water-BSA system. This indicates that more effective slow motions or processes may exist in the water-BSA system.

If only isotropic rotational motions are present, the T_1 relaxation times of the protons are expected to be 10 times longer than those of the deuterons (see Chapter 2, Sections 2.1.2 and 2.3). If other kinds of motions are present also, these will contribute mostly to the relaxation of the protons but not the deuterons and the T_1 relaxation ratio of protons to deuterons will be less than 10.

The proton/deuteron T_1 ratios are summarized in Table 6.9. Deuterium data in the +5°C row entry was taken at +3.6°C. Data were corrected to +5°C by plotting a straight line through the data points in Figure 6.30 and reading the relaxation values from the graph.

Table 6.9 Proton/deuteron T_1 ratios in BSA samples. Proton data obtained at 150 MHz. Deuteron data obtained at 15.4 MHz.

Temp. (°C)	BSA Sample (g/ml)	Proton T_1 / Deuterium T_1
+45	0.2	6.4
	0.4	5.7
	0.6	5.4
	0.8	5.2
+25	0.2	6.6
	0.4	6.5
	0.6	6.5
	0.8	6.8
+15	0.2	6.8
	0.4	6.9
	0.6	6.9
	0.8	7.4
+5	0.2	7.8[1]
	0.4	7.9[1]
	0.6	7.9[1]
	0.8	10.7[1]
−5	0.2	30.6
	0.4	28.0
	0.6	28.0
	0.8	28.9
−15	0.2	43.6
	0.4	51.0
	0.6	47.0
	0.8	46.4
−25	0.2	74.2
	0.4	65.9
	0.6	62.3
	0.8	101.1

[1]Deuterium data taken at +3.6°C. Values corrected to +5°C.

As can be seen from Table 6.9, the T_1 ratios of protons to deuterons are less than 10 in the liquid samples above 0°C. Above +5°C the ratios are temperature and concentration independent, within the experimental error and have a value of ∿6-7. At +5°C the ratios have a higher value of ∿8. At this temperature the ratios are also concentration independent, within the experimental error. Below 0°C all ratios are greater than 10. The ratios increase as the temperature is lowered, but at each temperature the ratios are concentration independent.

Cross-relaxation can account for T_1 proton/deuteron ratios that are larger than 10, since only cross-relaxation will tend to make the proton T_1 values longer without affecting the deuterium T_1 values. All other processes and motions will reduce both the proton and the deuterium relaxation or that of the protons only. Since T_1 is frequency dependent in the 15-150 MHz region (Table 6.7), normalizing the proton/deuteron ratios to one frequency will reduce the ratios. The fact that below 0°C the ratios increase when the temperature is lowered indicates that the contribution of cross-relaxation may increase at the lower temperatures. No concentration dependence is seen at any given temperature, except perhaps at -25°C where the signal/noise ratio is the poorest.

It may be a true phenomenon, or the concentration dependence of cross-relaxation may be too small to be detected. It is also possible that the contribution of cross-relaxation increases with increasing concentration, but other motions, the contribution of which increases as well, mask the contribution of the cross-relaxation.

If the protein protons contribute to the water signal, the net effect will be similar to that of cross-relaxation. As discussed earlier, this effect is likely to be very small in the water-BSA system.

An additional experimental artifact should be considered. The deuterium spectra were taken on the XL-100 spectrometer, which has a relatively long dead time of ∿180-200 μsec. The deuterium absorption peaks had apparent linewidths on the order of KHz. Some of the broad components could have been lost due to the long dead time of the instrument. Since the broad components may be associated with long T_1 values, the apparent deuteron T_1 values may be shorter than their "true" T_1 values. This could have caused the T_1 ratios to appear greater than 10. If this effect is important, it may explain the increase in the T_1 ratios at +5°C, which cross-relaxation cannot. If at this temperature a broad component appears and is not detected the ratios will appear to increase.

Since at +5°C the system exists as a solution, cross-relaxation effects will tend to make the proton T_1's shorter and decrease the ratios.

6.2.2 $LW_{1/2}$ Data At Subzero Temperatures

Water proton $LW_{1/2}$ data at subzero temperatures were taken on the same samples and at the same temperatures as the T_1 data. The linewidths were measured at 150 MHz while the T_1 experiments were performed.

In frozen solutions the contribution of inhomogeneities was small compared to the linewidths and the T_2 values were calculated using Equation 2.6.

In solutions the contribution of inhomogeneities could not be ignored and the T_2's were measured by the Hahn spin-echo method. See Section 6.2.4 for a discussion of T_2 data in BSA solutions.

Plots of $\ln(1/T_2)$ as a function of the inverse temperature are illustrated in Figure 6.32. A change of slope occurs in the freezing region between +5°C and -15°C ($3.6 \times 10^{-3} - 3.8 \times 10^{-3}$ $^0K^{-1}$). When frozen, all samples have equal linewidths, within the experimental error.

Table 6.10 summarizes the T_1/T_2 ratios at subzero temperatures. If $\tau_r \leqslant \frac{1}{\omega_0}$ the theoretical T_1/T_2 ratio is close to 1. At the T_1 minimum the theoretical ratio is $\sim$1.7 (see previous section). All ratios

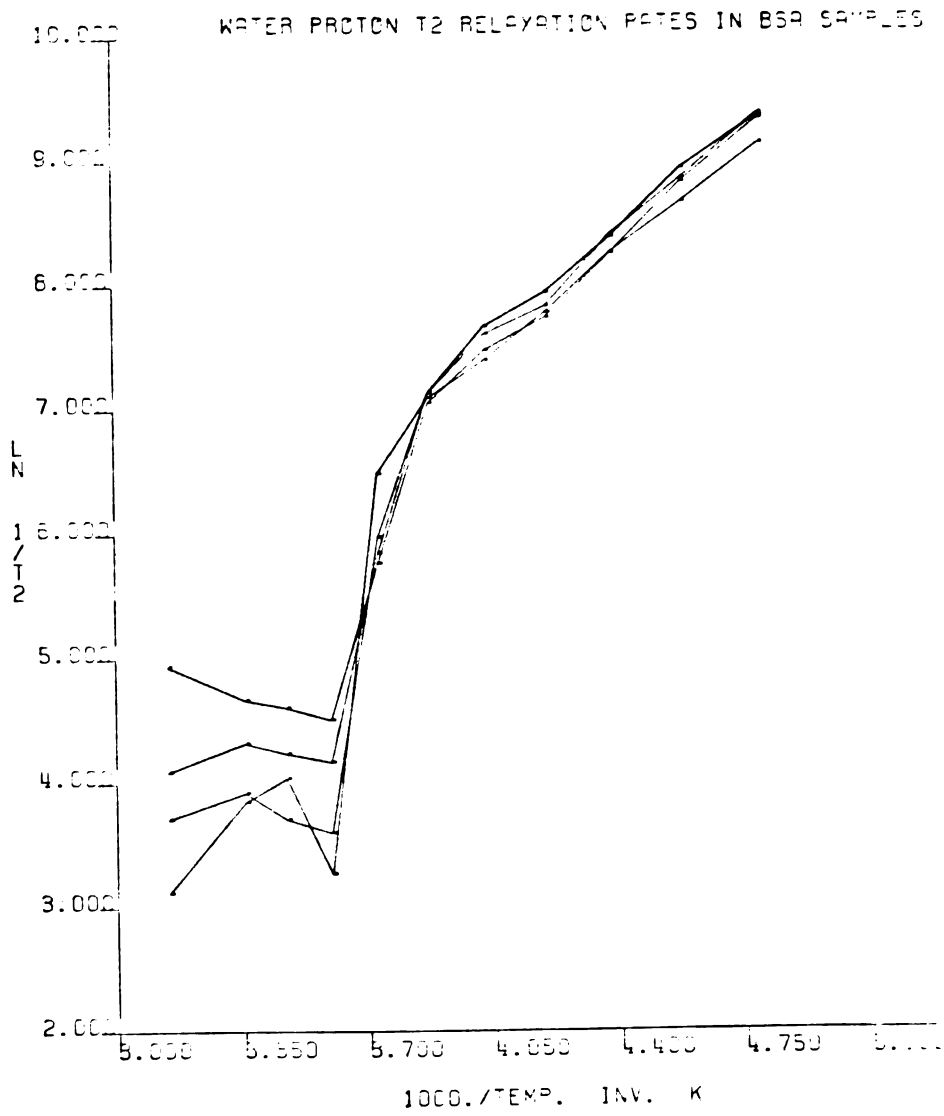

Fig. 6.32. Plots of ln ($1/T_2$) vs. the inverse (absolute) temperature for the water protons in BSA samples. The high and the low temperature regions are shown.

Table 6.10. Water proton T_1/T_2 ratios at 150 MHz in frozen BSA samples.

TEMP. (°C)	T_1/T_2 Ratios At 150 MHz			
	BSA 0.2g/ml	BSA 0.4g/ml	BSA 0.6g/ml	BSA 0.8g/ml
−5	121.	76.	66.	64.
−15	167.	188.	191.	183.
−25	213.	293.	286.	259.
−35	323.	397.	363.	347.
−45	568.	683.	720.	630.
−55	991.	1430.	1320.	1330.
−65	2080.	2880.	2900.	3030.

listed in Table 6.10 are much larger than the theoretical value. The experimental ratios increase as the temperature is lowered, but at each temperature they are concentration independent, within the experimental error. Comparison of the theoretical T_1 and T_2 values to their experimental values at the T_1 minimum shows that most of the effect is caused by the small values of T_2's (see previous section and Section 6.1.1). This result indicates that slow motions are present in the water-BSA system. The contribution of the slow motions increases as the temperature is lowered, but it is concentration independent in the range 0.2-0.8 g protein/1 ml water.

Large T_1/T_2 ratios may also arise if the motions are fast but anisotropic. Anisotropy may be approximately regarded as a slow motion about one axis superimposed on a fast motion along a second axis (8). If the slow component contributes more effectively to T_2 than to T_1 relaxation, a large T_1/T_2 ratio will result.

As discussed in Section 6.2.1, ice formation is not expected to contribute to the measured relaxation times. The macromolecule itself is a "particle" of molecular dimensions and may restrict water mobility. A large difference in magnetic susceptibilities may exist between the macromolecule "particles" and the water. These two effects will affect the relaxation

times and will increase the T_1/T_2 ratios (see also Section 6.2.3).

All the T_2's are concentration independent, within the experimental error, in the temperature range -5°C to -65°C. The experimental noise in the linewidth measurements is larger than the concentration dependence effects observed for the T_1's and, therefore, if similar effects exist in T_2's they will not be detected.

To derive the apparent energies of activation the plots of $\ln(1/T_2)$ versus the inverse temperature were fitted to straight lines. Data points in the temperature region -15°C to -65°C were used. A fit for a representative (0.6 g/1 ml) sample is illustrated in Figure 6.33.

Table 6.11 summarizes the slopes and the derived energies of activation. The experimental error in the linewidths measurements is estimated to be ∿25%. An additional error of ∿10% is estimated to contribute to the calculations of E_a's. The average value for the energies of activation listed in Table 6.11 is ∿4.7 ± 1.6 Kcal/mole, i.e., about the energy of activation needed to break one hydrogen bond. The E_a values for the water-BSA system at subzero temperatures are close to the values of E_a found for the 70% PLL sample (Table 6.2).

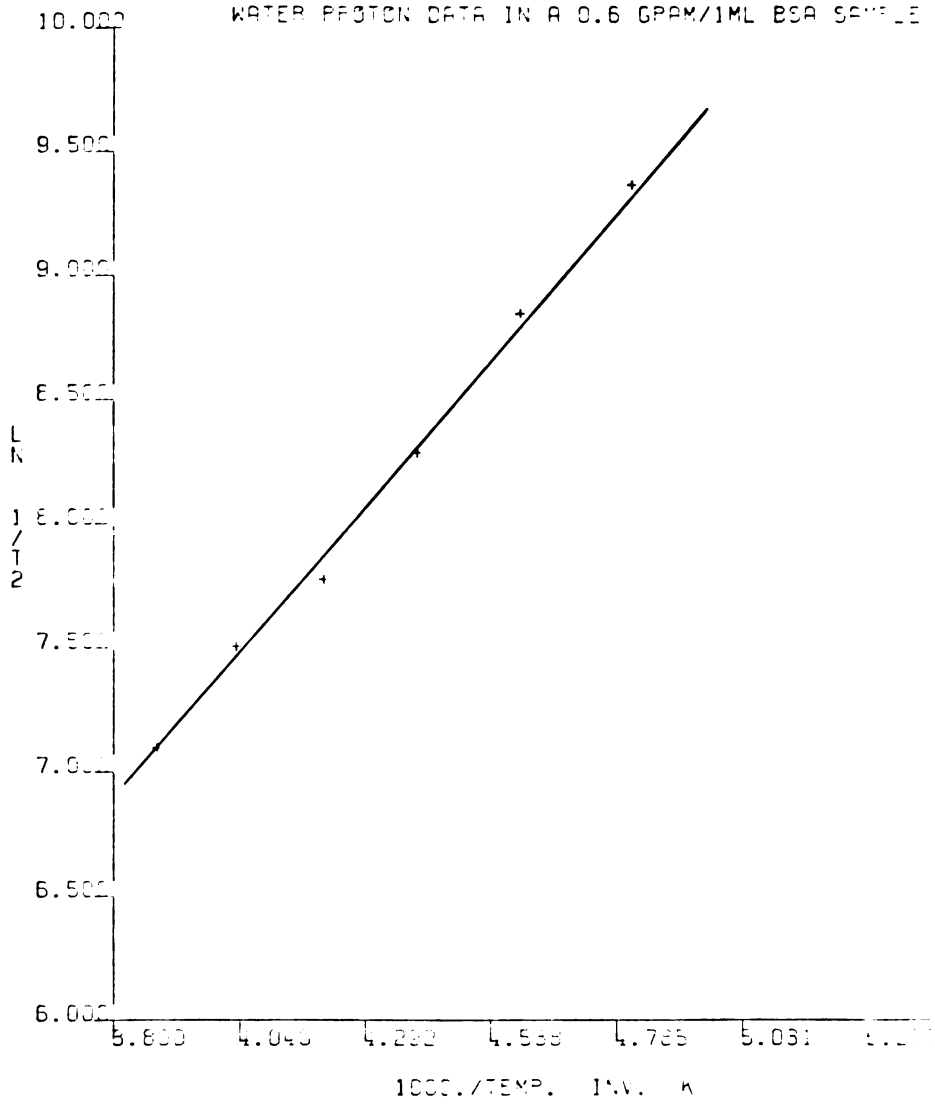

Fig. 6.33. An Arrhenius plot for the water protons at sub-zero temperatures in a 0.6 g/1ml BSA sample.

Table 6.11. Energies of activation for the water proton in frozen BSA samples.

BSA Sample (g/ml)	Slope[1] (°K)	E_a[2] (Kcal/mole)
0.2	2220 ± 555	4.4 ± 1.5
0.4	2350 ± 560	4.7 ± 1.6
0.6	2370 ± 560	4.7 ± 1.6
0.8	2450 ± 600	4.9 ± 1.7

[1]Slopes calculated by the Nicolet program.

[2]Reported errors are estimates (see text).

6.2.3 $T_{1\rho}^{on}$ Data At Subzero Temperatures

$T_{1\rho}^{on}$ dispersion data were obtained for a sample of 0.154 g BSA/1 ml water (13.3% wt/wt protein) at ν_0 = 44.4 MHz. Data were obtained at -15°C, -24.5°C, and -33.2°C and they are illustrated in Figure 6.34.

Approximate values of $1/T_2$ were obtained by extrapolating the $T_{1\rho}^{on}$ relaxation rates to $H_1 \approx 0$. In Table 6.12 the extrapolated $1/T_2$ values are compared to the $1/T_2$ values derived from the $LW_{1/2}$ measurements (see previous section) for a 0.2 g/1 ml BSA sample. The percentage deviation of the extrapolated $1/T_2$ values from the $1/T_2$ values derived from the $LW_{1/2}$ measurements are also given.

At -15.0°C the deviation is within the experimental error. At -25.4°C and at -33.2°C the deviations are large and exceed the experimental error. It has been previously reported that $1/T_2$ values derived by extrapolating $1/T_{1\rho}^{on}$ to $H_1 \approx 0$ may have higher values than $1/T_2$ values obtained by other methods. It was suggested that contributions from static nonzero dipolar interactions may be responsible for this effect (13, 61, 62). If this is true, it implies the existence of a partially oriented water fraction.

Oscillatory behavior was observed at the two lowest temperatures at the low H_1 fields (see Chapter 2,

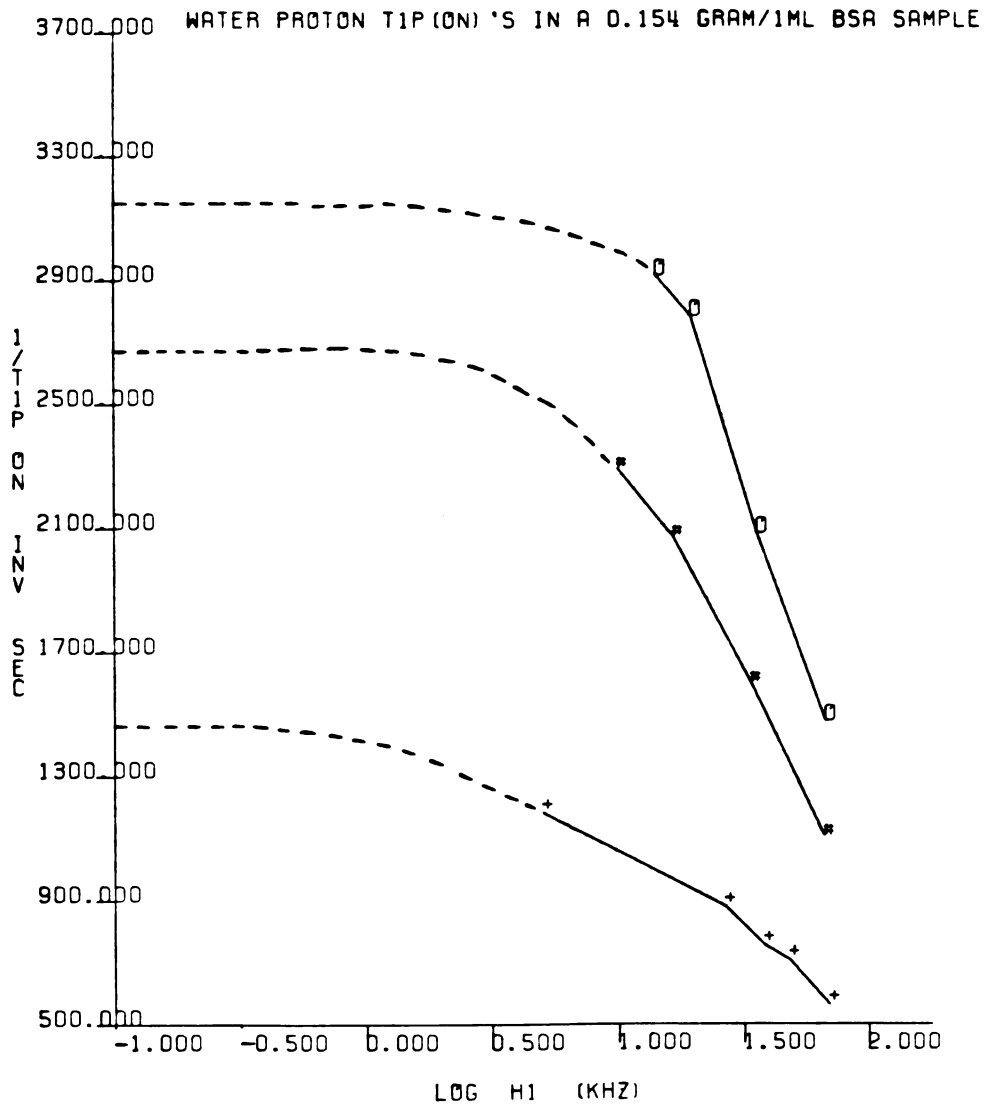

Fig. 6.34. Water proton $T_{1\rho}^{m}$ relaxation times at ν_0 = 44.4 MHz in a 0.154 g/1ml BSA sample. (+) −15.0°C; (#) −25.4°C; (0) −33.2°C. The dashed lines show extrapolation to $H_1 \approx 0$.

Table 6.12. Percentage deviation of the extrapolated $1/T_2$ values from the $1/T_2$ values derived from $LW_{1/2}$ measurements.

Temp. (°C)	$1/T_2$ Extrapolated $(sec)^{-1}$	$1/T_2$[1] From $LW_{1/2}$ $(sec)^{-1}$	Deviation (%)
−15.0	1370.	1210 ± 300	13.
−25.4	2640.	1630 ± 410	62.
−33.2	3160.	2200 ± 550	44.

[1]Reported errors are estimates (see Section 6.2.2).

Section 2.5.1). This may be responsible, in part, for the observed discrepancies between the extrapolated and measured $1/T_2$ values. If the amplitude and/or frequency of the oscillations is low, they may modify the experimentally measured $T_{1\rho}^{on}$ values, but remain undetected.

Figure 6.35 illustrates an Arrhenius plot using the extrapolated $1/T_{1\rho}^{on}$ values. The derived energy of activation is $\sim$5.8 $\pm$ 1.7 Kcal/mole. This is higher than the energy of activation obtained using $1/T_2$ values derived from the $LW_{1/2}$ measurements (Table 6.11). A similar observation was reported by Zipp et al. (13) in a water-erythrocyte system at subzero temperatures.

Plots of $1/T^{on}$ versus $\omega_1^{1/2}$ are shown in Figure 6.36. At each temperature the data points fall on a straight line. The slopes of the fitted straight lines and the derived diffusion-coefficients are summarized in Table 6.13. The total experimental error in calculating the values of the D's is estimated to be $\sim$35% (see Section 6.1.2).

The spin density (N) was estimated assuming an equal contribution from all the protons and a density of 1 g/ml. $N \sim 6.29 \times 10^{22}$ spins/cm^3 in good agreement with the value of 6.75×10^{22} spins/cm^3 used to calculate the diffusion coefficient of water

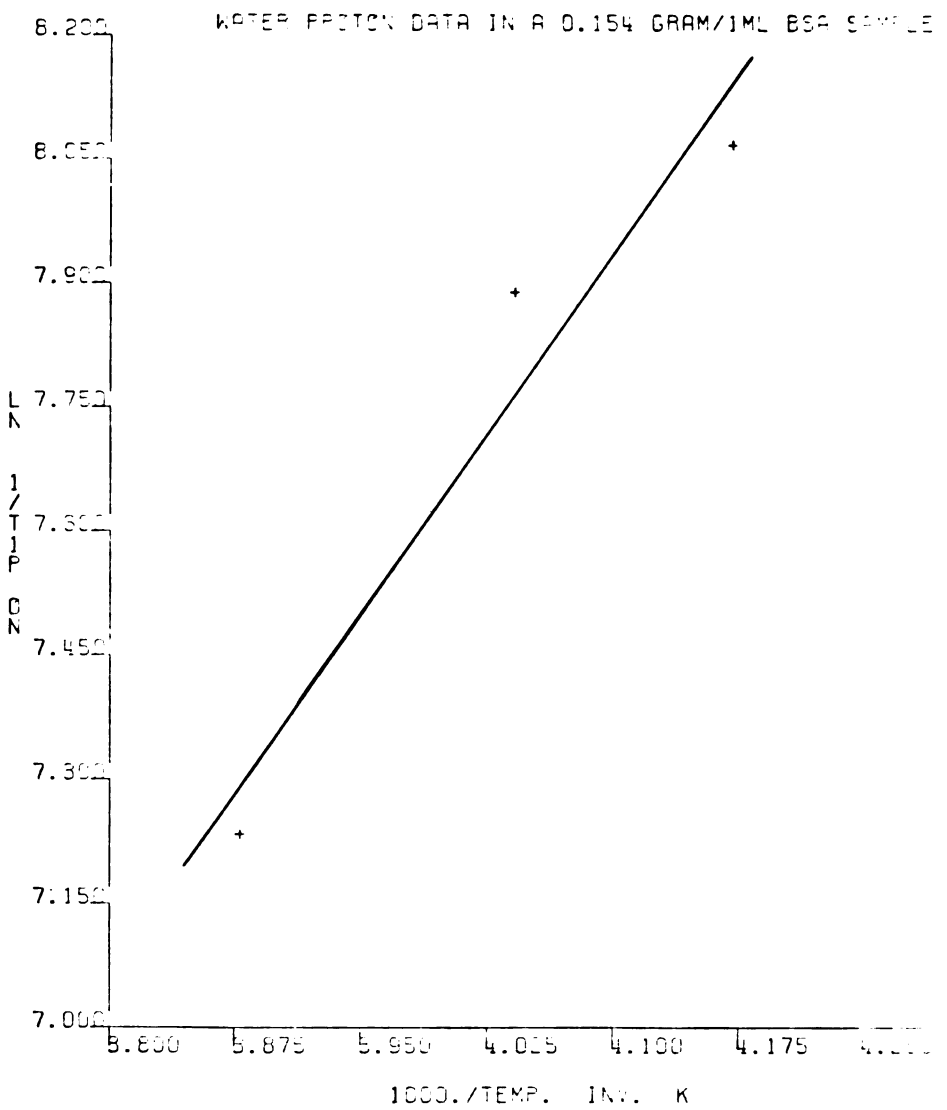

Fig. 6.35. A plot of ln $(1/T_{1\rho}^{m})$ at $H_1 \approx 0$ vs. the inverse (absolute) temperature. Data are for the water protons in a frozen 0.154 g/1ml BSA sample.

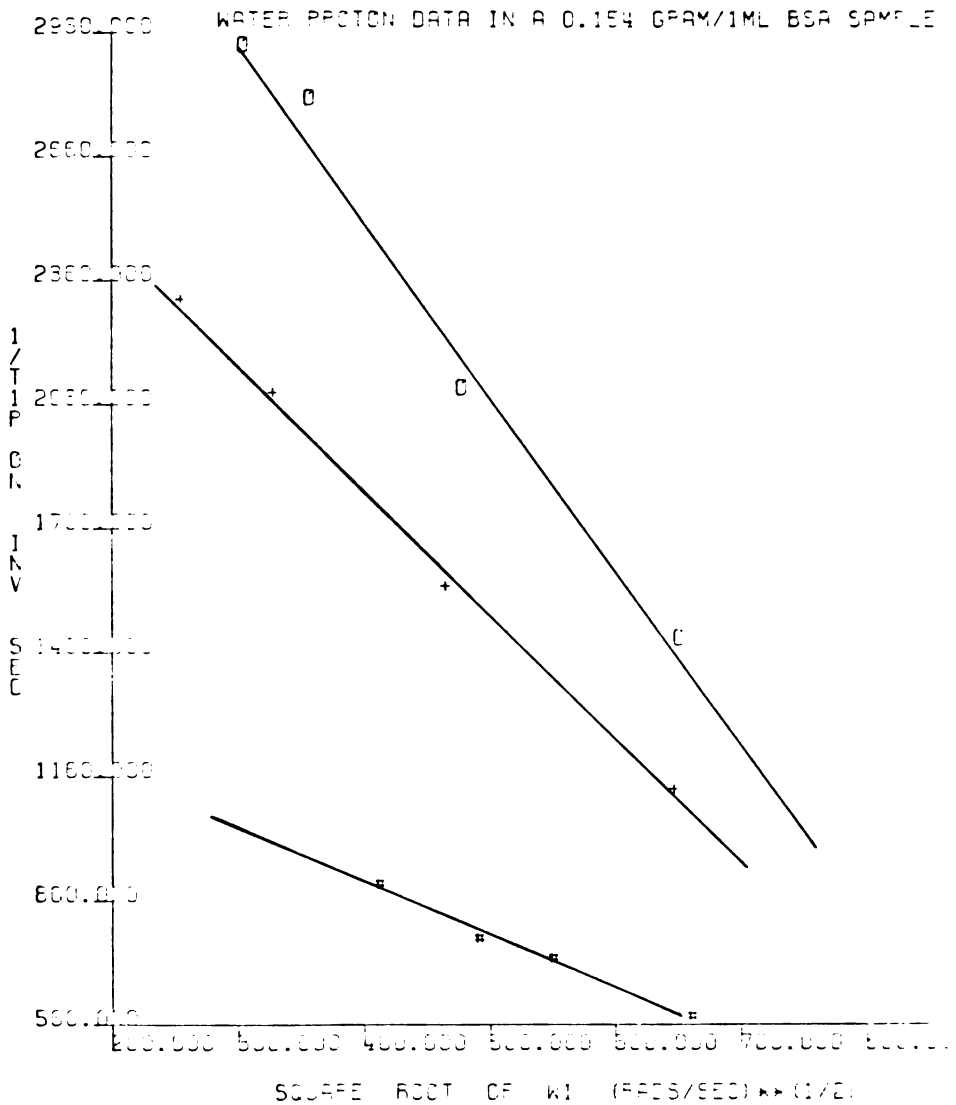

Fig. 6.36. Plots of $1/T_{1\rho}^{on}$ vs. $\omega_1^{1/2}$. Data are for the water protons in a 0.154 g/1ml BSA sample. (#) –15.0°C; (+) –25.4°C; (0) –33.2°C.

Table 6.13. Diffusion-coefficients of the water proton in a frozen 0.154g/1ml BSA sample.

Temp. (°C)	Slope[1] $(sec \times rads)^{-1/2}$	Diffusion-Coefficient (D)[2] (cm^2/sec) $\times 10^{10}$
−15.0	−1.27 ± 0.02	3.4 ± 1.2
−25.4	−3.05 ± 0.04	1.9 ± 0.7
−33.2	−4.29 ± 0.11	1.5 ± 0.5

[1]Slopes and standard deviations calculated by the Nicolet program.

[2]Reported errors are estimates (see text).

bound to red cell membrane (56) and of water in water-erythrocyte system at a subzero temperature (13). Since all protons were assumed to contribute equally and since no corrections were applied (see Section 6.1.2), the values reported in Table 6.13 (and Table 6.3) should be regarded as the high value limits for the water diffusion-coefficients.

Although the values of D found for water in the water-BSA system are the same, within the experimental error, as the values of D obtained for water in the water-PLL system (Table 6.3), the values in the water-BSA system are consistently somewhat higher than the values in the water-PLL system. The relatively big change in the D values in going from -15.0°C to -25.4°C corresponds to the big change in D values in the 40% PLL sample over a similar temperature range. The explanation in both systems may be similar: data were taken in, or close to, the temperature region where the freezing event takes place. The value of 1.51×10^{-10} cm^2/sec at -33.2°C in the water-BSA system is in good agreement with the value of 8.5×10^{-11} cm^2/sec in the water-erythrocyte system at -55°C reported by Zipp et al. (13).

Figure 6.37 illustrates a plot of ln(1/D) versus the inverse temperature. The total experimental error in calculating the values of E_a's is estimated

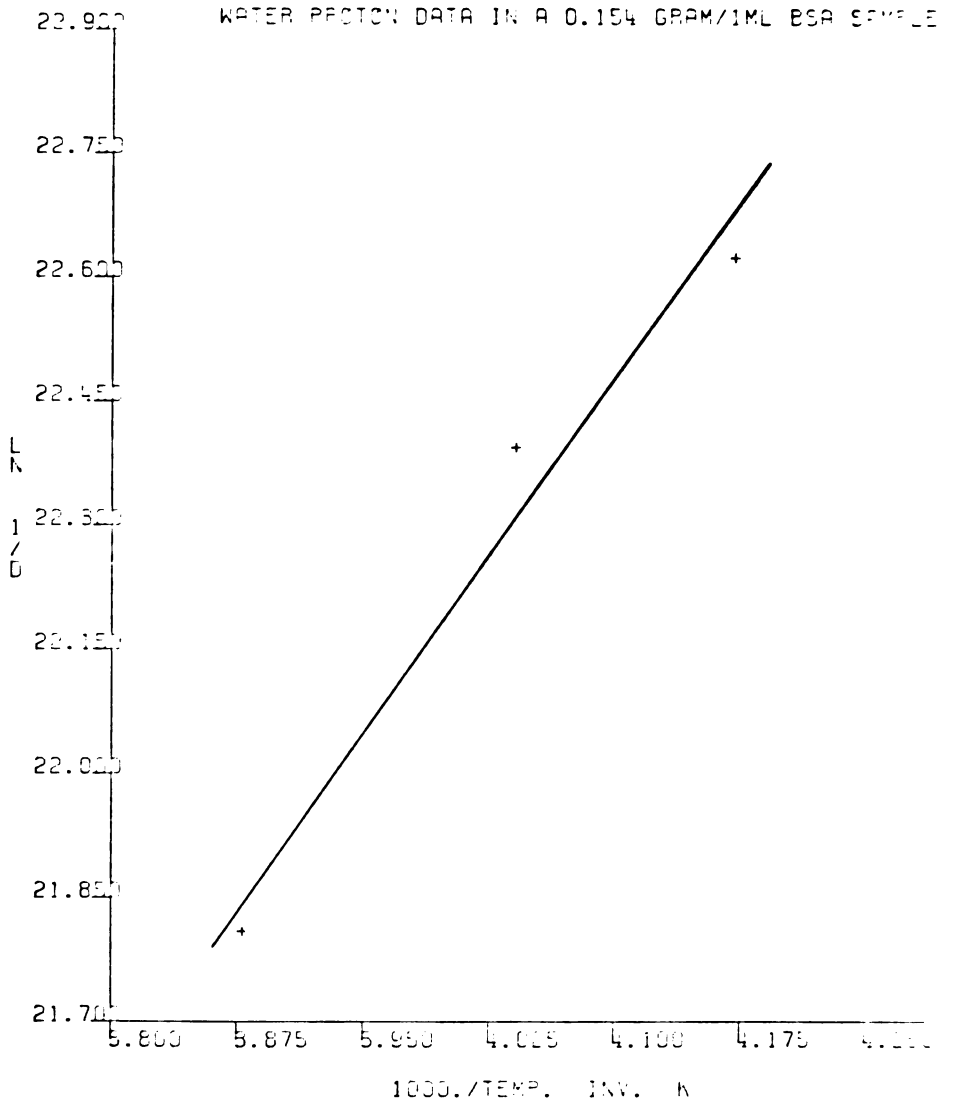

Fig. 6.37. A plot of ln (1/D) vs. the inverse (absolute) temperature. Data are for the water protons in a frozen 0.154 g/1ml BSA sample.

to be ∿40% (see Section 6.1.2). The derived energy of activation for the diffusion process is ∿5.6 ± 2.2 Kcal/mole. This value is the same, within the experimental error, as the values of E_a for the diffusion process found in the water-PLL system (Table 6.5).

Table 6.14 lists the fitted intercepts of the $1/T_{1\rho}^{on}$ versus $\omega_1^{1/2}$ plots, the $1/T_2$ values obtained by extrapolating $1/T_{1\rho}^{on}$ to $H_1 \simeq 0$ and gives the percentage deviation of the fitted intercepts from the extrapolated $1/T_2$ values. At -15.0°C the deviation is very small but it increases as the temperature is lowered. The deviations are not caused by the previously discussed difference between the extrapolated and measured T_2 values, because below ∿-20°C the fitted intercepts are bigger than the extrapolated $1/T_2$ values. The available data indicate that at least in the temperature region from ∿-25°C to ∿-35°C the frequency dependence of the relaxation processes does not arise from translational motions only (36). Other frequency dependent relaxation processes are present. This result is in contrast with the observations in the water-PLL system where the deviations decrease as the temperature is lowered (Table 6.4).

In pure water the rotational and translational motions are coupled and the intramolecular and intermolecular relaxation terms have about equal

Table 6.14. Percentage deviation of the fitted intercept from the extrapolated $1/T_2$ values in a frozen 0.154g/1ml BSA sample.

Temp. (°C)	Intercept[1] (sec)$^{-1}$	$1/T_2$ Extrapolated (sec)$^{-1}$	Deviation (%)
−15.0	1390 ± 280	1370.	1.
−25.4	3050 ± 610	2640.	16.
−33.2	4220 ± 850	3160.	34.

[1]Intercepts calculated by the Nicolet program.

contribution (see Chapter 2, Section 2.1.1). The fact that in both the water-PLL and the water-BSA systems at subzero temperatures straight lines are obtained when $1/T_{1\rho}^{on}$ are plotted versus $\omega_1^{1/2}$ indicates that in these systems decoupling takes place and the intermolecular relaxation term becomes important (see Chapter 2, Section 2.5).

The main reason for such a decoupling is probably the heterogeneous nature of the water-macromolecule systems. Ice formation was discussed in Section 6.2.1 and was ruled out as an important factor. The macromolecule itself is a "particle" of molecular dimensions and it may restrict water mobility. Translational motions are detected in the 70% PLL sample, where it is likely than no, or only very little, ice is formed at subzero temperatures.

Bryant (63) suggested that "channels" may exist on the surface of proteins. Water in such "channels" will be restricted in its mobility and may exchange slowly with the water on the surface. Scanlon and Eisenberg (64) presented experimental evidence that channels filled with solvent water may exist between the macromolecules in crystals of type A whale metmyoglobin. Similar channels may exist between macromolecules in frozen solutions.

Globular proteins have more complicated tertiary structures than PLL. They may have crevices and interior cavities which can trap water and modify its motions. The fact that the frequency dependence of the relaxation processes in the water-BSA system is more complicated than that in the water-PLL system may reflect the higher complexity of the tertiary structure of the protein.

6.2.4 T_2 and $T_{1\rho}^{on}$ Data of Solution

When water proton $T_{1\rho}^{off}$ data were taken as a function of temperature at 100 MHz it was noticed that the linewidths did not change in a monotonic way with temperature as would be expected from a single two-site fast exchange model. Since such a behavior may indicate the presence of a slow exchange process, a systematic study of T_2 in BSA solutions at different pH's and temperatures was undertaken.

Figure 6.38 shows the water proton T_2 relaxation times of four 0.4 g/1 ml BSA samples as a function of temperature. The T_2 relaxation times were measured by the Hahn spin-echo method at 150 MHz. Data were taken at four different pH's: 2.0, 4.45, 7.0, and 12.0. For a discussion of the problems associated with the pH measurements in these samples see Chapter 3. The same data are plotted as a function of pH at

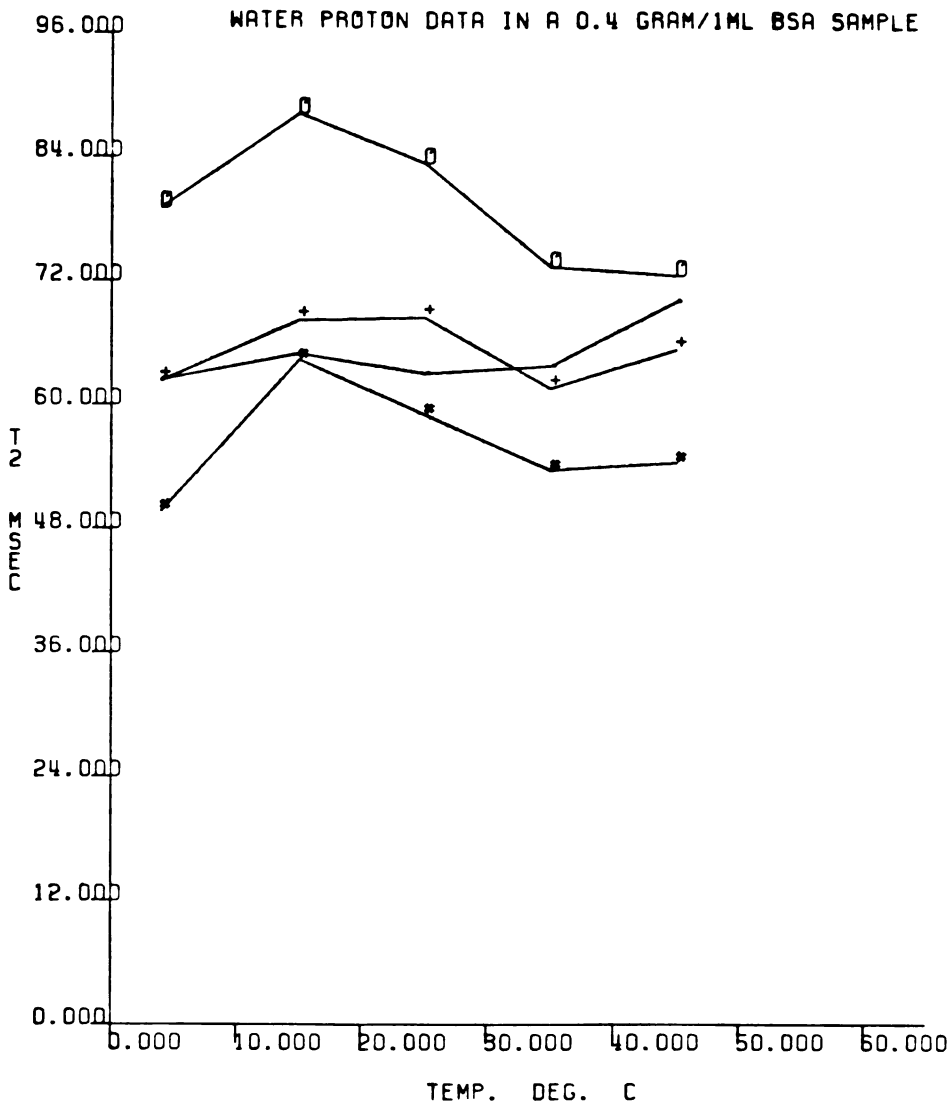

Fig. 6.38. Water proton T_2 relaxation times at 150 MHz vs. the temperature in a 0.4 g/1ml BSA sample at several pH's. (0) pH = 2.0; (+) pH = 4.45; (#) pH = 7.0; (•) pH = 12.0.

different temperatures in Figure 6.39. T_1 relaxation times were measured simultaneously and the results are illustrated in Figure 6.40.

In general, three regions can be distinguished when the experimental T_2 relaxation times are plotted as a function of temperature:

1. From +5°C to +15°C the T_2 values increase as the temperature is raised.
2. From +15°C to +35°C the T_2 values decrease as the temperature is raised.
3. From +35°C to +45°C the T_2 values increase again as the temperature is raised.

Data above +45°C were not taken because irreversible denaturation occurred.

It should be noted that within each sample the differences among the T_2 values are small and are close to being within the experimental error. However, the fact that a similar behavior was observed at 100 MHz and that all four samples exhibit the same general features, gives confidence that a real phenomenon was observed. A similar behavior was also observed in a 0.8 g/1 ml BSA sample at neutral pH, data taken at 55 MHz (Figure 6.41), and in a 0.8 g/1 ml BSA sample in D_2O, the deuterium data taken at 23 MHz (Figure 6.42).

Only the first two regions are seen in the 0.8 g/1 ml BSA samples and even at +45°C the T_2 values

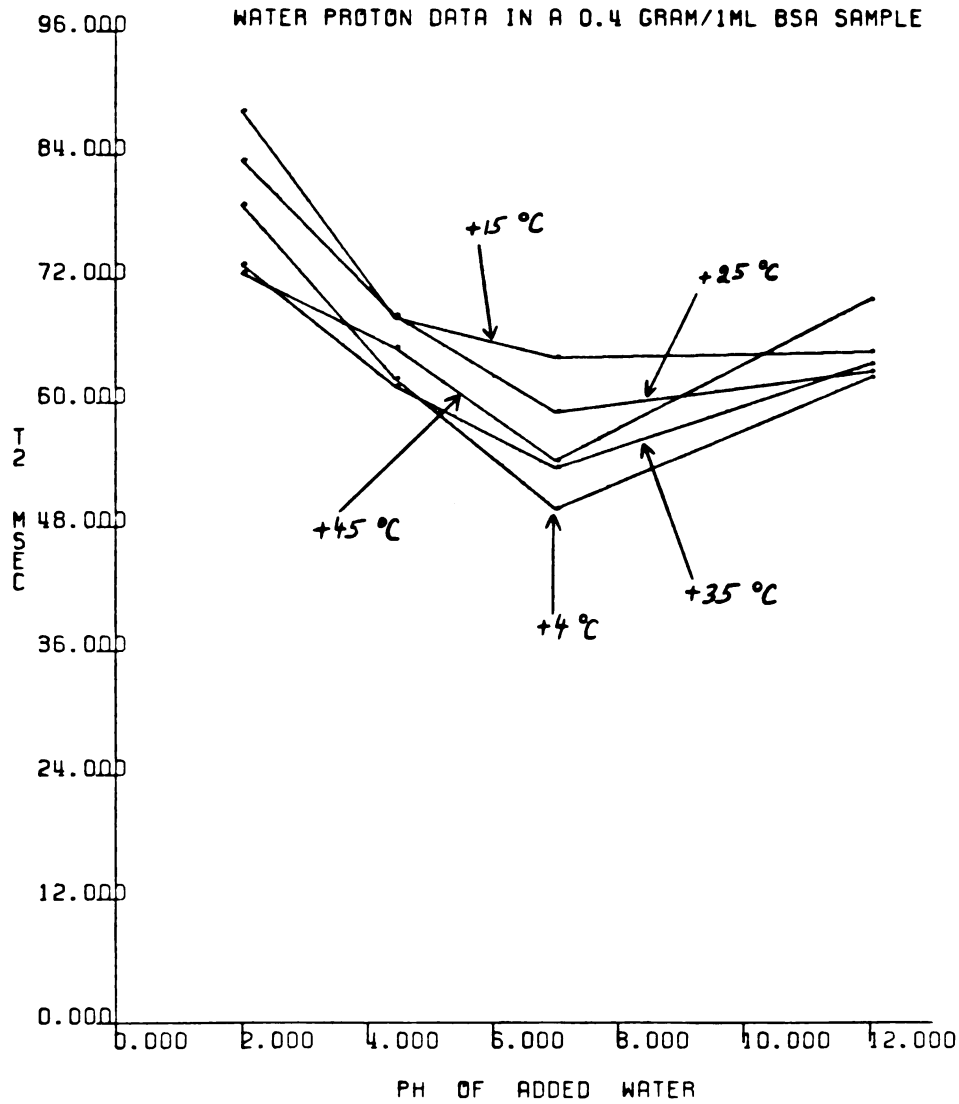

Fig. 6.39. Water proton T_2 relaxation times at 150 MHz vs. the pH in a 0.4 g/1ml BSA sample at several temperatures. The arrows with the numbers indicate the temperatures at which data were taken.

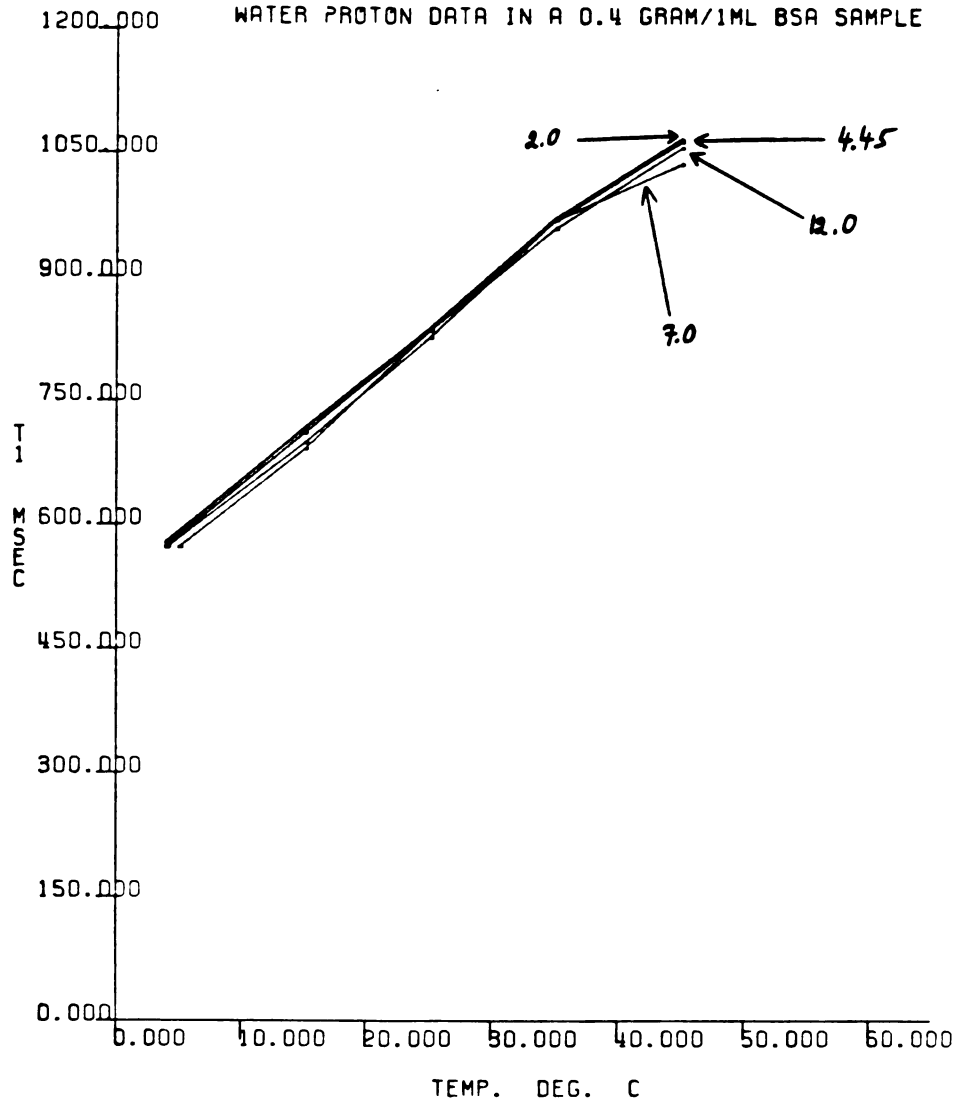

Fig. 6.40. Water proton T_1 relaxation times at 150 MHz vs. the temperature in a 0.4 g/1ml BSA sample at several pH's. The arrows with the numbers indicate the pH's at which data were taken.

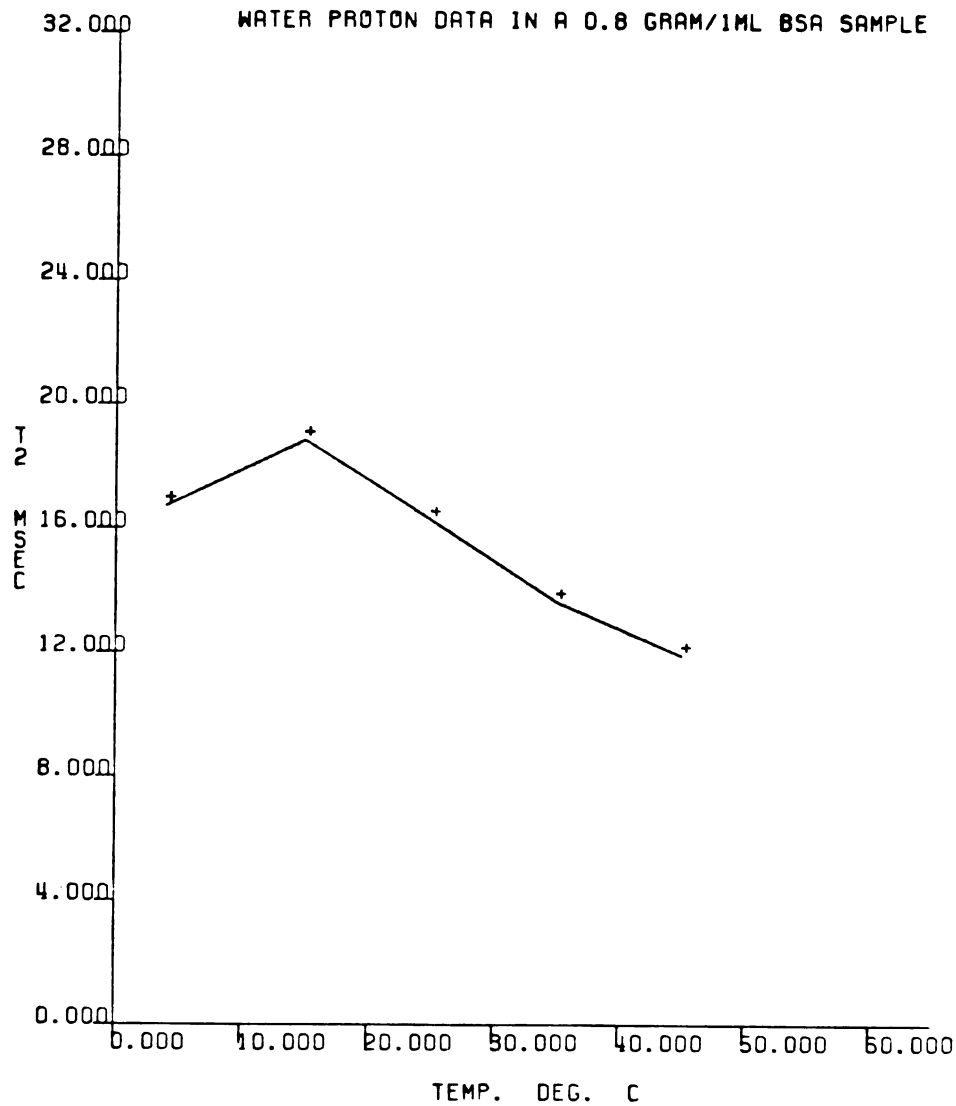

Fig. 6.41. Water proton T_2 relaxation times at 55 MHz vs. the temperature in a 0.8 g/1ml BSA sample.

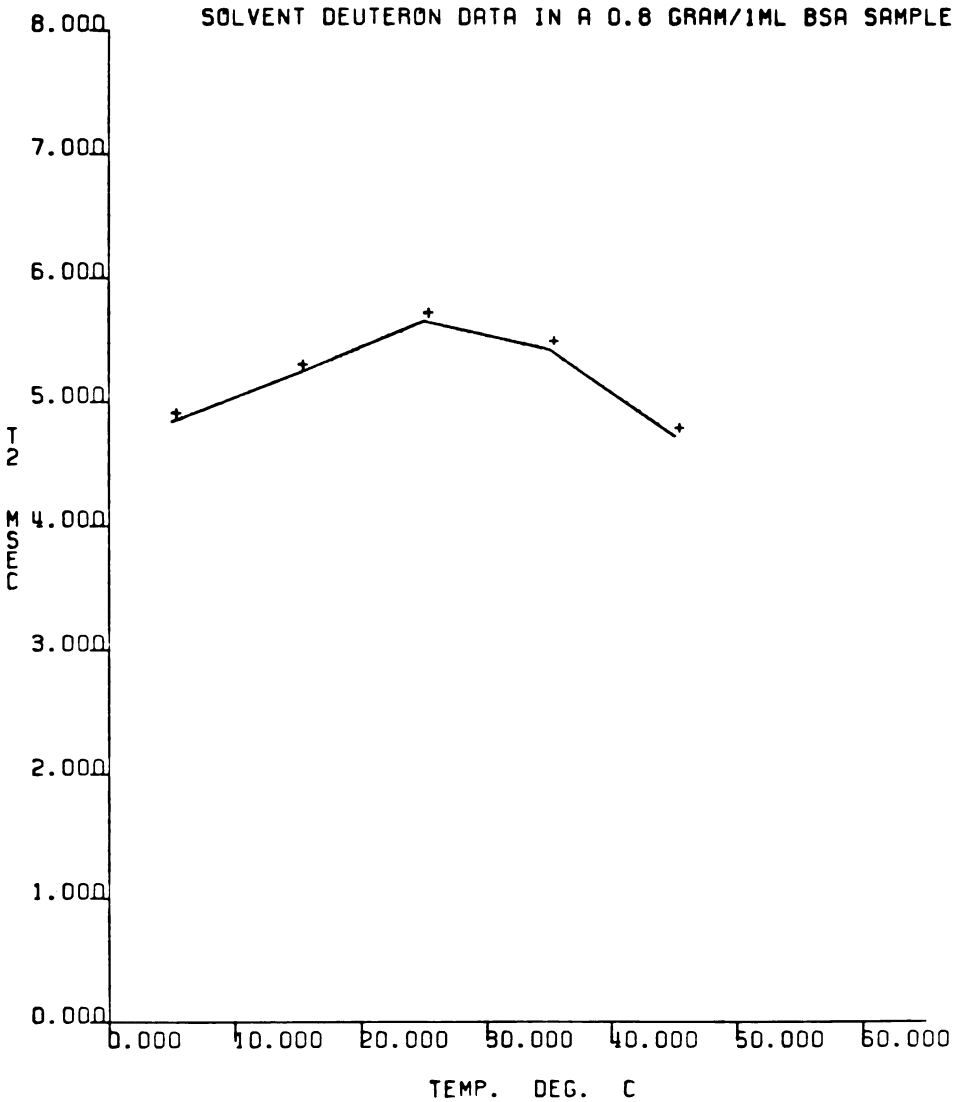

Fig. 6.42. Solvent deuteron T_2 relaxation times at 23 MHz vs. the temperature in a 0.8 g/1ml BSA sample.

still decrease as the temperature is raised. This behavior is expected. The frequency of exchange in the more concentrated sample is lower. Therefore, the T_2 minimum will be shifted to a higher temperature, as compared to the less concentrated samples. Because of denaturation above +45°C the T_2 minimum in the 0.8 g/1 ml samples could not be detected experimentally.

The deuterium T_2 values change over a smaller range as compared to the proton values. This is so because of the smaller gyromagnetic ratio of deuterium, which causes smaller chemical shift effects. In addition, the deuterium relaxation rates are larger because of its quadrupole moment.

If an exchange process is present two cases are possible:

1. The protons exchange between two sites which have the same or very similar chemical shifts.

In this case the exchange process does not contribute to T_2 relaxation, unless the T_2's of each site are quite different.

2. The protons exchange between two sites with different chemical shifts.

In this case the maximum contribution to T_2 relaxation will occur at the coalescence point. The residence time, τ_{res}, value at this point is given by (26)

$$\tau_{res} = \frac{\sqrt{2}}{(\omega_A - \omega_B)}$$

where $(\omega_A - \omega_B)$ is the difference in the chemical shifts between the two sites in the absence of exchange. If $\tau_{res} \ll \frac{1}{(\omega_A - \omega_B)}$ conditions of fast exchange prevail and only one peak is seen. If $\tau_{res} \gg \frac{1}{(\omega_A - \omega_B)}$ conditions of slow exchange prevail and two peaks may be seen.

The ability to resolve two peaks depends at least on three factors:

1. The relative linewidths of the two peaks.
2. The relative intensities of the two peaks.

If one of the peaks is very wide and/or its intensity is very weak, it will be lost in the noise. Lowering the temperature will increase the separation between the peaks. However, at the same time the linewidths will increase and this may offset the effect of lowering the temperature.

3. Resolution factors of the instrument such as homogeneity, dead time, and H_0 field strength.

In principle, if two peaks are present they can always be resolved by applying strong enough H_0 field and/or using very short dead times.

Because of the smaller gyromagnetic ratio of deuterium, if protons are substituted for deuterons and the deuterium spectrum is then observed, the two peaks will be more difficult to separate as compared to the respective proton spectrum.

In all albumin solutions at all temperatures only one water peak was detected. No attempts were made to establish whether at temperatures below ∿+35°C (the temperature where the T_2 minimum occurs), two unresolved peaks are present. However, even at very large sweepwidths (±25 KHz), at the lowest temperatures only one water peak was seen.

The occurrence of a minimum when T_2 values are plotted as a function of temperature in Figure 6.38 indicates that a proton fraction exists in albumin solutions that can exchange with water (65, 66).

As the pH is raised from 2.0 to neutral the T_2 values become shorter. As the pH is raised to 12.0 the T_2 values become longer and are close to the values at pH = 4.45. The minimum at pH = 12.0 is shifted to a somewhat lower temperature than at pH = 4.45. It has been previously suggested that the albumin molecule expands and undergoes conformational changes when the pH of its solution is changed from neutral (67, 68). These conformational changes may

expose additional residues to the solvent and thus modify the relaxation times.

The pH dependence of the T_2 relaxation times illustrated in Figure 6.39 provides additional evidence that an exchanging water fraction exists in albumin solutions. At all temperatures the T_2 values change with pH. At all temperatures the T_2 values go through a minimum at a neutral pH. The curve at +45°C behaves in a different way in that it crosses the curves of the lower temperatures. This may be caused by conformational changes because of partial denaturation at this temperature. James et al. (69) presented experimental evidence that proteins undergo conformational changes before complete denaturation takes place.

When T_2 values are measured as a function of pH the maximum contribution to T_2 relaxation will be observed at the pH where the exchange is the slowest. This is expected to occur when the degree of ionization is the highest. The isoelectric point of BSA occurs at pH $\sim$ 5. Kuntz (51) showed that in frozen systems anionic residues have hydration numbers bigger by about a factor of 2 as compared to cationic residues. If this observation is assumed to hold in solutions, then the T_2 minimum is expected to occur at pH > 5. The precise location of the minimum will be determined by other slow motions present and by conformational

changes that may occur as the pH is changed. Halle et al. (16) measured the excess T_2 relaxation rates of ^{17}O at 13.56 MHz in a solution of Human Plasma Albumin (HPA) in $D_2{}^{17}O$ as a function of pD. HPA should have properties similar to those of BSA and as expected, in both cases T_2 goes through a minimum at a similar (neutral) pH. The T_2 value at the minimum will depend on the exchange rate and other slow motions present, such as protein tumbling, internal motion of protein segments, and translational motion of water molecules along the protein surface (16).

An exchange process that contributes to T_2 values will have a frequency of exchange which is too low to contribute to T_1 values at 150 MHz. Figure 6.40 shows the temperature dependence of the T_1 relaxation times at 150 MHz at different pH's. Within experimental error the T_1 values are pH independent.

The T_1's are a linear function of the temperature. A similar result at pH = 5.6 has been reported by Oakes (14). Our results in Figure 6.40 show that the linear dependence of T_1 on temperature holds in acidic and basic solutions as well. Halle et al. (16) obtained similar results for the ^{17}O T_1 relaxation in HPA solutions.

The exchange process is expected to cause a dispersion of T_1 values in the region from a few MHz down to the KHz region. Grösch et al. (15) have observed such a dispersion in albumin solutions and Koenig et al. (17, 18, 22, 70) have observed similar dispersions in other protein solutions. Because of lack of direct evidence, slow exchange was not considered in the interpretation of the dispersion data. Grösch et al. (15) have failed to fit their dispersion data to a simple two-state model and had to invoke a three-state model to get a better fit. It is likely that slow exchange is responsible for the T_1 dispersion observed in the KHz region. This has also been proposed by Halle (71), based on his ^{17}O T_1 dispersion data.

In our study T_1 dispersion data could not be obtained because the instrumentation needed for this experiment was not available. However, a slow exchnage process is expected to cause a dispersion in the $T_{1\rho}^{on}$ relaxation times values. $T_{1\rho}^{on}$ dispersion data at ν_0 = 55 MHz were obtained for a 0.8 g/1 ml BSA sample at neutral pH at four temperatures. These data are shown in Figure 6.43.

When a slow exchange process dominates the dispersion of $T_{1\rho}^{on}$ values and data are taken at a few temperatures, some of the curves may intercept. In

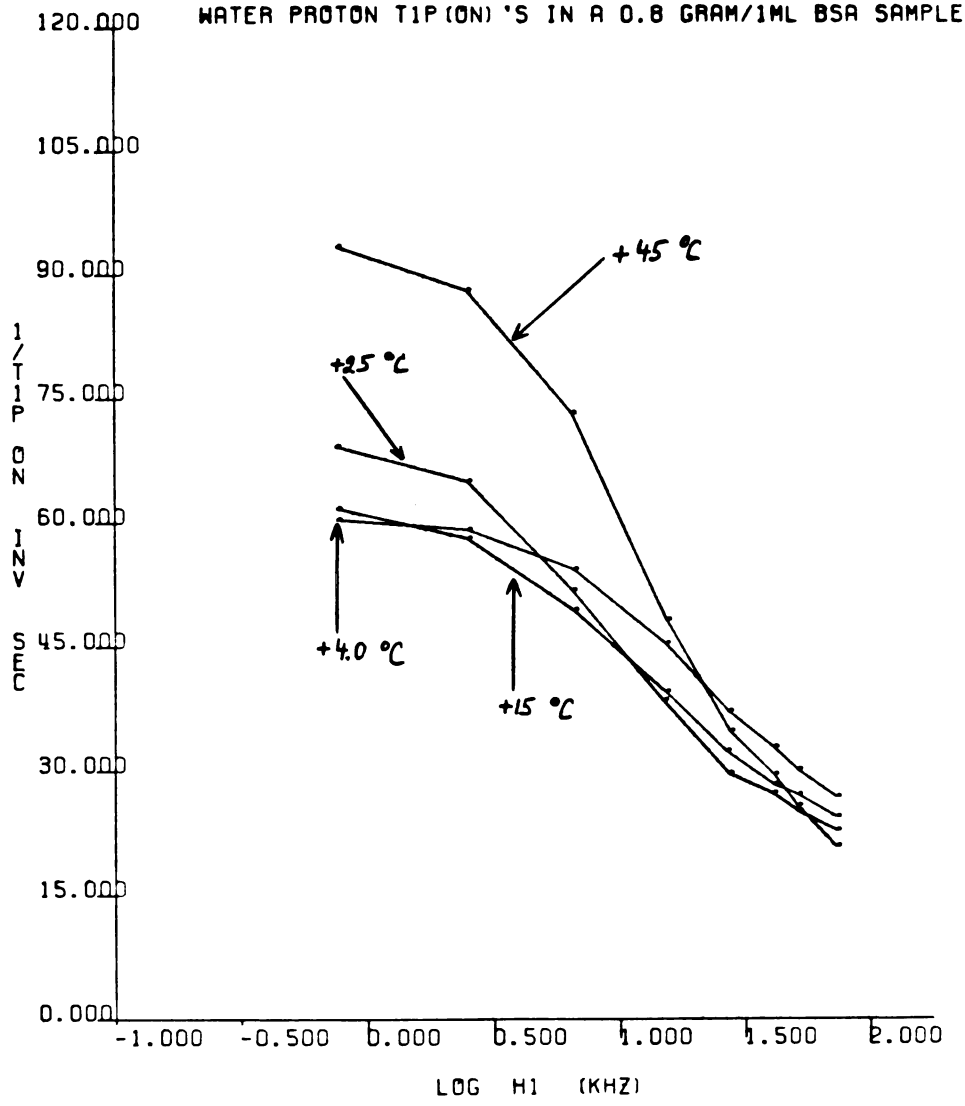

Fig. 6.43. Water proton $T_{1\rho}^{on}$ relaxation times at ν_0 = 55 MHz in a 0.8 g/1ml BSA sample. The arrows with the numbers indicate the temperatures at which data were taken.

the low H_1 field region the curves will be spaced in such a way that when extrapolated to zero H_1 field the $T_{1\rho}^{on}$ value of each curve will be approximately equal to the T_2 value at the temperature of the curve. In the high H_1 field limit the curves will be spaced in such a way that the $T_{1\rho}^{on}$ value of each curve will be approximately equal to $\frac{2}{5}T_1$ at the temperature of the curve (see Chapter 2, Section 2.5). Since, in the low field region curves at higher temperatures may lie above curves at lower temperatures, while in the high field region curves at the higher temperatures will always lie below curves at the lower temperatures, cross-over points may occur in the dispersion region. The number of cross-over points and the temperatures where they occur depends on the T_2 versus temperature profile of the sample.

For the 0.8 g/1 ml BSA sample the T_2 versus temperature profile is illustrated in Figure 6.41. The behavior of the dispersion curves in Figure 6.43 is as expected from this profile. At the highest field the curves of the higher temperatures lie below those of the lower temperatures. At the low fields the +15°C curve lies below the +4°C curve, and the +25°C and the +45°C curves lie above the +4°C curve. An unexpected crossing point occurs just before the lowest field is reached, between the +4°C and the

+15°C curves. This is most likely caused by experimental error, as the accuracy of the measurements decreases at low fields (see Chapter 2, Section 2.5, and Chapter 5, Section 5.3). The +25°C curve crosses the +4°C and the +15°C curves at lower fields and it crosses the +45°C curve at a higher field. The +45°C curve crosses the other three curves within a small H_1 field range.

If slow enough motions are present a dispersion of $T_{1\rho}^{on}$ values will be observed. The fact that the dispersion curves in Figure 6.43 have cross-over points and behave in a manner consistent with the T_2 versus temperature profile of the sample is a strong evidence that the dominant slow motion is the same one affecting T_2, that is, a slow exchange process.

An interesting feature of the dispersion curves is that the inflection points at all temperatures occur at $H_1 \sim 20$ KHz (log 20 $\sim$ 1.3). Within the experimental error the inflection points are temperature independent. Since the frequency of exchange increases with temperature, one would expect that at higher temperatures the inflection points would be shifted to higher H_1 values.

The inflection points will show only little temperature dependence if the activation energy (E_a) for the exchange process is small. If the Arrhenius equation is assumed to hold and both E_a and the

activation factor are assumed to be temperature independent, the ratio of the rate constants at two temperatures is given by (54)

$$\ln\frac{k_1}{k_2} = \frac{E_a}{R}\left(\frac{1}{T_2} - \frac{1}{T_1}\right),$$

where k_1 and k_2 are the two rate constants at their respective temperatures T_1 and T_2, R is the ideal gas constant, and ln stands for the natural logarithm. If the whole water molecule is assumed to participate in the exchange and the two hydrogen bonds are broken in the process ($E_a \sim 10$ Kcal/mole), the ratio of the rate constants at the two extreme temperatures (+4°C and +45°C) can be calculated to be $\ln\frac{k_1}{k_2} \sim 2.3$. Such a difference in the rate constants is more than the experimental error and would be detected. If only one hydrogen bond needs to be broken as the exchange takes place, the ratio is $\ln\frac{k_1}{k_2} \sim 1.15$. This difference lies within the experimental error and would not be easily detected. Therefore, it is likely that the slow exchange observed in the BSA solutions involves a hydrogen exchange rather than the exchange of a whole water molecule.

The residence time of the exchanging proton can be estimated from the dispersion curves in Figure 6.43 to be ~50 μsec. This value should be viewed only

as a rough estimate, since averaging over all the motions that contribute to $T_{1\rho}^{on}$ relaxation takes place.

One can only speculate as to the actual sites between which the proton exchange takes place. In principle, at least three cases are possible:

1. The proton exchanges between some site on the protein and the water. The water may include the "bulk" water or some "water of hydration."
2. The proton exchanges between sites on the same protein molecule. Such sites should be located closely in space.
3. The proton exchanges between sites on adjacent protein molecules. Such an exchange may occur in very concentrated protein solutions and/or if aggregates are formed.

No good methods exist to distinguish between the different possibilities. If case 2. holds, conformational changes that will cause the two sites to move far apart will eliminate this kind of exchange. If case 3. holds, the elimination of aggregates or dilution of the solution will eliminate this exchange.

6.3 $T_{1\rho}^{off}$ Experiments

6.3.1 Introduction

$T_{1\rho}^{off}$ experiments were performed in order to examine their use in the investigation of molecular motions. For a discussion of the relevant theory, see Chapter 2, Section 2.6. For the experimental details, see Chapter 4, Section 4.2.1.1.

All the proton data were obtained at ν_0 = 100 MHz and all the deuterium data were taken at ν_0 = 15.4 MHz. Data for the theoretical plots were calculated using the NMRRB program. For a listing of this program, see Appendix B.

The total delay time between the switching off of the H_1 field and the acquisition of the FID was 2.2 msec. This consisted of a 2 msec homospoil pulse and a 0.2 msec computer delay time. No corrections were applied to account for the T_1 relaxation during this interval. The T_1's were much longer than 2.2 msec and the correction was negligible. The deuterium FID's at subzero temperatures were very short and no homospoil pulse was applied. Preliminary experiments showed that no residual signal, which may arise in the x'-y' plane from the rapid switching off of the H_1 field, could be detected after 0.2 msec. The deuterium T_1's were much longer than 0.2 msec and no correction for T_1 decay was needed.

We estimate an error of up to ±15% in measuring the H_1 field strengths and an error of ±10% in measuring the peak heights.

The original data representation of James et al. (10) was modified and the ratios (R) of the peak intensities were plotted as a function of $\sin^2\theta$. When data are represented in this way, the presence of slow motions can be detected by simply inspecting the data plots. When 10^{-7} sec $> \tau_r > 10^{-9}$ sec the values of R (for protons) are dependent on the values of $\sin^2\theta$. When $\tau_r > 10^{-7}$ sec the R's also become dependent on the off-resonance H_1 field. When $\tau_r < 10^{-9}$ sec the R's are independent of both $\sin^2\theta$ and H_1. As the correlation time (τ_r) becomes longer the ratio decreases, for a given value of H_1 and $\sin^2\theta$, and the curves shift to the left side of the graph. When $\tau_r > 10^{-7}$ sec the curves of the lower H_1's lie below the curves of the higher H_1's, for a given correlation time. A few theoretical plots (for protons) are illustrated in Figure 6.44. The arrows with the numbers indicate the H_1 field strength in units of Gauss (g).

Figure 6.45 shows R as a function of τ_r for $\sin^2\theta = 9.977 \times 10^{-4}$ ($\log 9.977 \times 10^{-4} \sim -3.001$) and $H_1 = 1.00$ g. As can be seen from the plot, the values of R become sensitive to the correlation time when τ_r

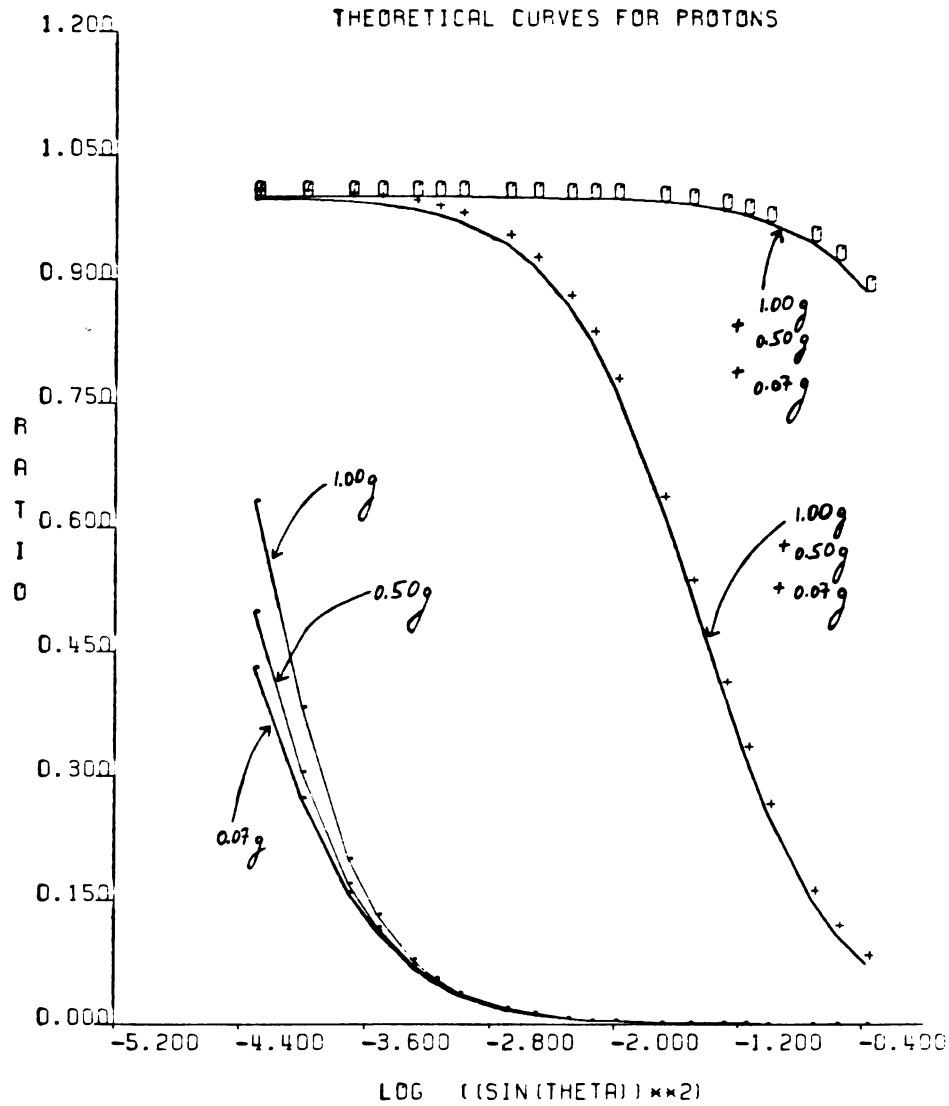

Fig. 6.44. Theoretical dependence of the ratio (R) on the logarithm of $\sin^2\vartheta$. (0) Correlation time 0.1 nanoseconds; (+) Correlation time 10 nanoseconds; (•) Correlation time 0.3 microseconds. The arrows with the numbers indicate the H_1 field strength in units of Gauss (g).

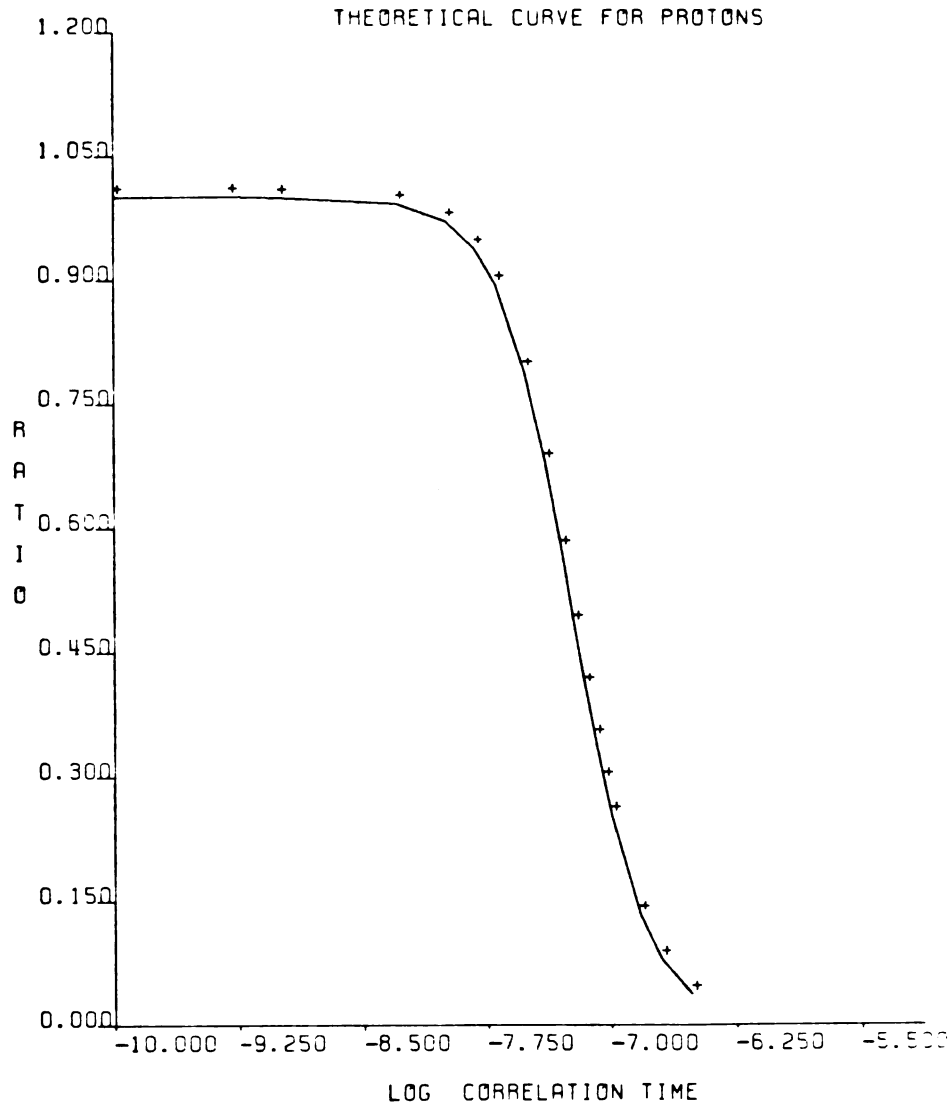

Fig. 6.45 Theoretical dependence of the ratio (R) on the logarithm of the correlation time. Values calculated for H_1 = 1.00g and $\sin^2\vartheta = 9.977 \times 10^{-4}$ ($\log(\sin^2\vartheta) \approx -3.001$).

is longer than $\sim$ 1.0 x 10^{-8} sec. As the correlation times become longer the values of R decrease.

The gyromagnetic ratio of deuterons is smaller by a factor of $\sim$7 than that of protons. To achieve a field for deuterons which is of the same magnitude like that of protons requires an amplifier with a power output higher by a factor of $\sim$7 for deuterons than for protons. The precise value of the H_1 field at the sample will depend on the details of the experimental set-up such as probe's coil geometry, sample tube geometry, tuning of the probe, the quality of the connections between the wires, etc. To obtain deuterium data we used the powerful Nicolet amplifier and the MONA probe and obtained H_1 fields of the same order of magnitude or higher than for protons.

6.3.2 Frozen BSA Solutions

Figure 6.46 shows plots of R versus $\sin^2\theta$ for the water protons in a sample of 0.5 g/1 ml BSA at -26.3°C. Data were taken on the XL-100-15 spectrometer at ν_0 = 100 MHz. Figure 6.47 shows similar plots for a sample of 0.5 g/1 ml BSA in D_2O at -25.1°C. Data shown are for the D_2O peaks at ν_0 = 15.4 MHz.

The proton data in Figure 6.46 have a few interesting features: (1) the values of R are highly dependent on the H_1 field strength; (2) the curves

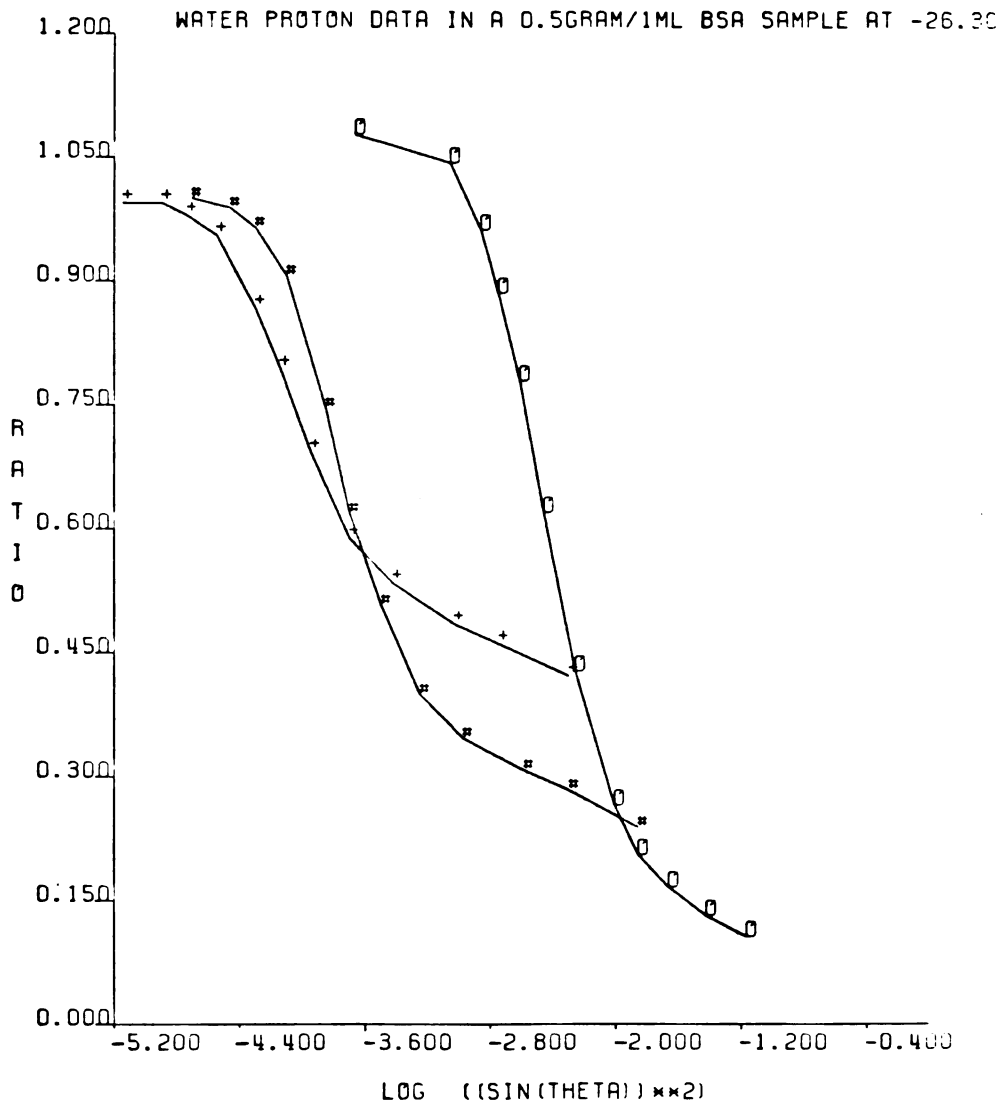

Fig. 6.46. Water proton off-resonance data in a 0.5 g/1ml BSA sample at −26.3°C. (+) H_1 field of 0.05 g; (#) H_1 field of 0.08 g; (0) H_1 field of 0.70 g.

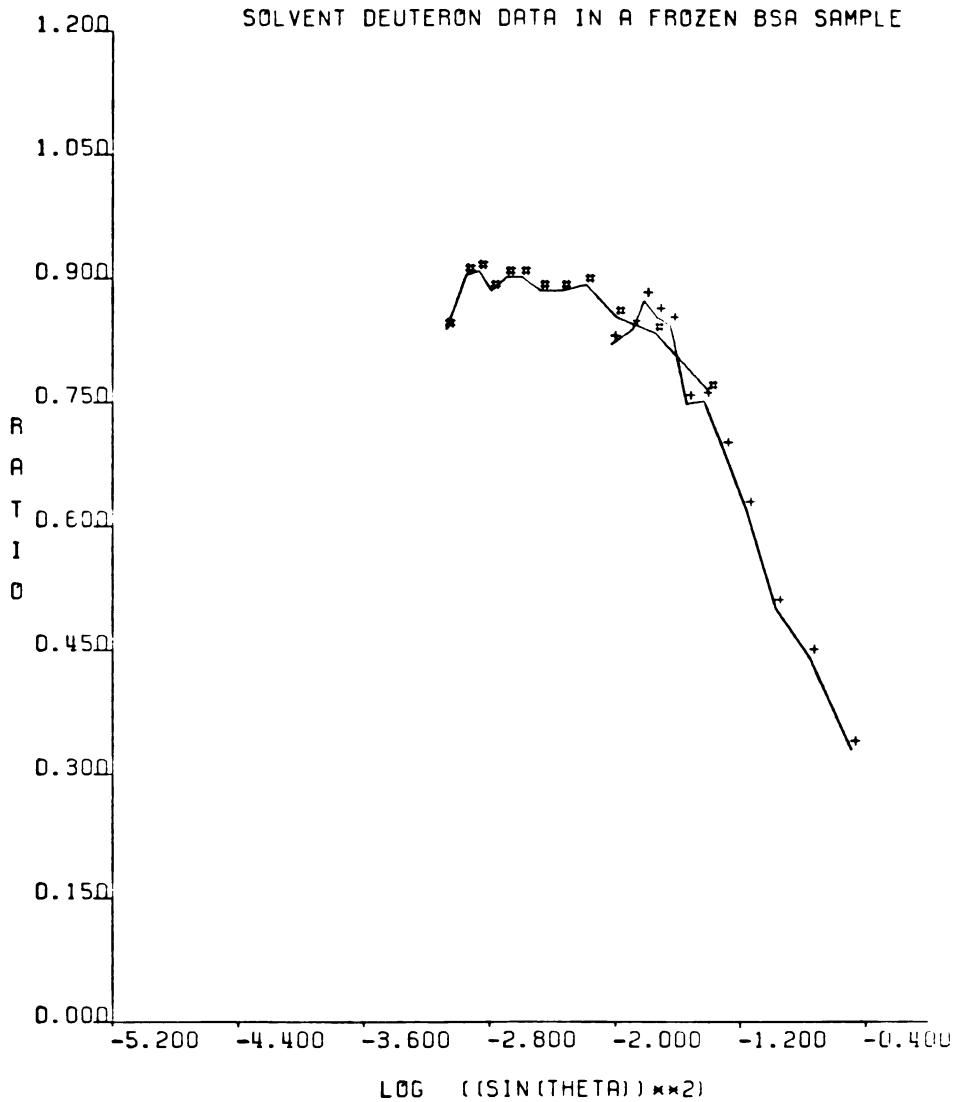

Fig. 6.47. Solvent deuteron off-resonance data in a 0.5 g/1ml BSA in D_2O sample at −25.1°C. (#) H_1 field of 0.62 g; (+) H_1 field of 2.10 g.

are not located on the extreme left side of the graph; (3) cross-over points are present. As the H_1 field is lowered, the cross-over occurs at smaller values of $\sin^2\theta$.

Theory predicts that in the presence of very slow motions the R versus $\sin^2\theta$ curves will be shifted to the extreme left side of the graph (see Figure 6.44). This, however, is not observed. Although the low H_1's' curves lie on the left side of the graph, the shift is not as big as would be expected for motions slow enough to cause as big an H_1 dependence as is observed experimentally. The high H_1 curve lies in the middle of the graph. The simple theory presented above assuming a single isotropic correlation time does not predict any cross-over points.

Inspection of the deuterium data in Figure 6.47 shows that none of the three effects is observed for deuterons. The curves are H_1 independent, within the experimental error. They are located on the right side of the graph and no cross-over points are seen, within the experimental error.

It is unlikely that the large H_1 field dependence is caused by errors in measuring the field strengths. We measured the H_1 fields at the beginning of each experimental set-up. The highest field used was measured on a sample of LiCl in water at the

temperature of the actual experiment. This sample had a strong signal and a narrow linewidth. The tube and its position in the probe were similar to those of the sample. If the sample was in a teflon tube, the H_1 field was also measured in a teflon tube. The lower H_1 fields could not be accurately measured directly. Therefore, we measured the voltage introduced into the probe at all the fields used. The strengths of the lower H_1 fields were calculated from the directly measured high field strength and the measured values of the voltages introduced into the probe. We measured the voltage at a point between the probe and the pulse-divider, after the cross-diodes (see Chapter 4, Section 4.2.1.1). Therefore, the H_1 field strength at the sample should be proportional to the voltage. If errors in measuring the H_1 fields were the source of the large field dependence, one would expect them to be distributed randomly among the samples. However, the large field dependence is present in frozen and concentrated solutions of macromolecules, but is absent in dilute solutions of BSA and lysozyme. Only a small field dependence is observed for glycerine at subzero temperatures.

To check whether the large H_1 field dependence (for protons) could arise from heating effects, we performed a preliminary experiment on a sample of

4.5 M LiCl in water at +25°C (see Chapter 4, Section 4.2.1.1). Heating of a sample will increase as the H_1 field increases. If this effect is significant, it may cause an apparent H_1 field dependence, because the R values at the higher fields will be sampled at a higher temperature. Our preliminary experiment showed that the temperature in this sample, at the highest H_1 field used in actual experiments, did not raise by more than ∿4°C. We did not add any salts to our samples. Therefore, the temperature raise in our samples should have been even less than ∿4°C. To average heating effects we applied all the off-resonance frequencies in a random fashion, i.e., never in an ascending or a descending order. We are confident that the heating effects were small and did not affect our results.

We conducted experiments to establish that contribution from paramagnetic impurities was negligible. ESR spectra of Mn^{++} ions at 9.525 GHz were obtained on a sample of water and on a portion of the 0.5 g/1 ml BSA solution. No Mn^{++} ions could be detected within the sensitivity limits of the ESR spectrometer, which was ∿10 μM. It is possible that the Mn^{++} ions bind strongly to the protein and give spectra which is too broad to be detected. To rule out this possibility we added $MnCl_2$ to a sample of 0.5 g/1 ml BSA solution to give a final concentration

of ∿0.2 mM Mn^{++}. ESR spectra of this sample were taken immediately and after a few hours. No line broadening or reduction in intensity could be detected in the later spectra. A portion of the dry BSA powder was completely decomposed by boiling it in concentrated hydrochloric acid and ESR spectra was then taken. No Mn^{++} ions could be detected.

Mn^{++} ions are the most efficient paramagnetics. It is very unlikely that other paramagnetics could be present in a high enough concentration to affect our results. Since Fe^{++} may be present in compounds of biological origin, such as BSA, we conducted an off-resonance experiment, at a few representative off-resonance frequencies, on a water sample containing ∿10 mM $FeSO_4$. The results are shown in Figure 6.48. Within the experimental error limits, Fe^{++} did not affect the water data. We conclude that paramagnetic impurities are not responsible for the effects observed in the water proton data in our samples.

It is very unlikely that the observed effects were caused by a contribution from the protein protons. The spectrometer dead time was relatively long, 180-200 μsec. Even at a sweepwidth of ±25,000 Hz no broad component could be detected on the baseline (see also the discussion in Section 6.2.1).

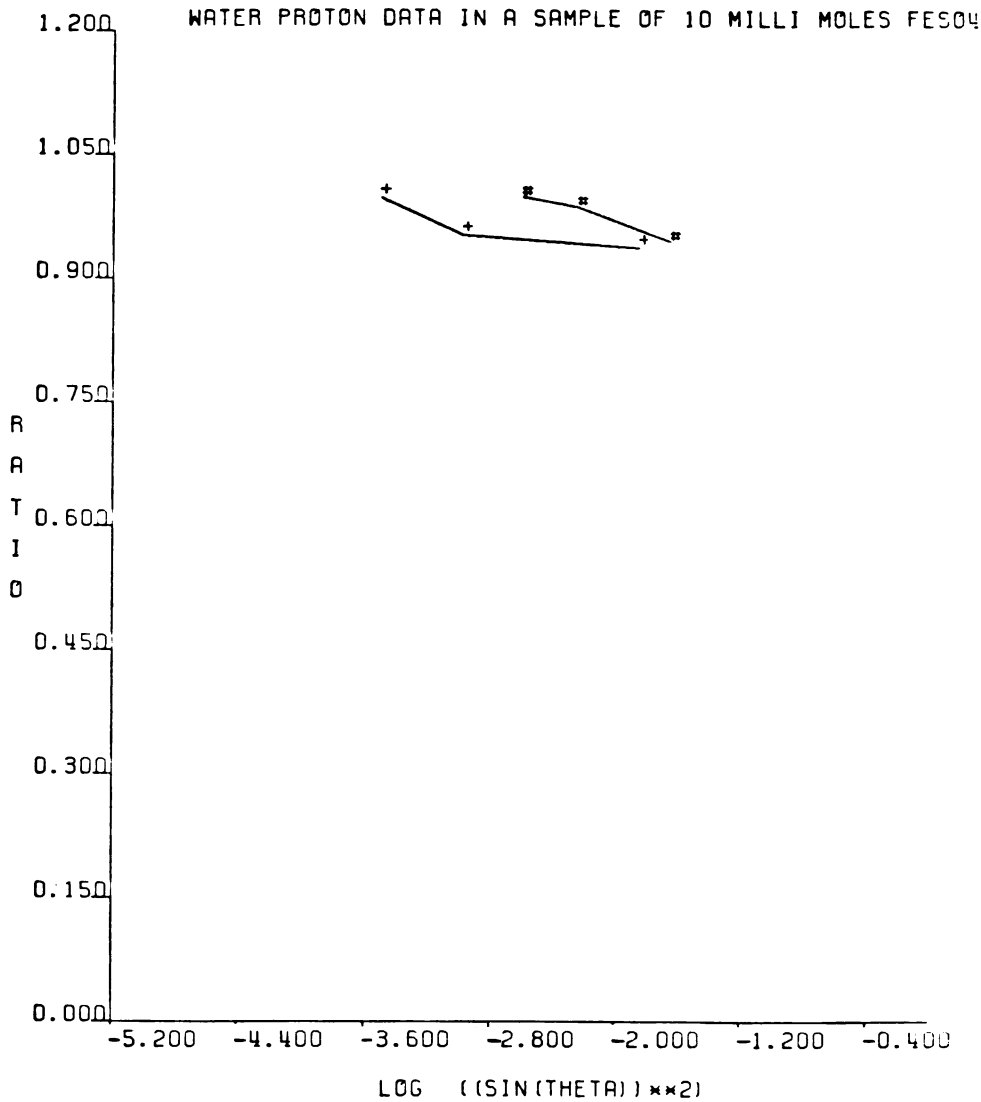

Fig. 6.48. Water proton off-resonance data in a 10 mM $FeSO_4$ sample at room temperature. (+) H_1 field of 0.09 g; (#) H_1 field of 0.72 g.

The deuterium linewidths were broader by a factor of $\sim$2 than those of the protons. Because the instrumental dead time was long relative to the inverse of the linewidth, some broad component could have been lost in the deuterium spectra. If a broad component is responsible for some of the effects observed in the proton data, then the absence of these effects in the deuterium data may be only apparent.

To check whether the effects are present in other types of systems, we obtained proton data for glycerine at -25.8°C, -15.4°C, and -5.4°C. The results are illustrated in Figure 6.49. The values of R are H_1 field dependent, but the field dependence is smaller than that in the frozen BSA sample. As the temperature is raised, the lines move to the right side of the graph and the field dependence decreases, as expected. Some field dependence remains at -5.4°C. No cross-over points are observed. Glycerine is a highly associated liquid that relaxes, at low temperatures, by slow translational motions (36, 41). These motions may cause some of the H_1 field dependence of R observed in glycerine.

Figure 6.50 illustrates deuterium data at -16.0°C of a perdeuterated glycerine sample. Data below -16°C could not be obtained because the deuterium

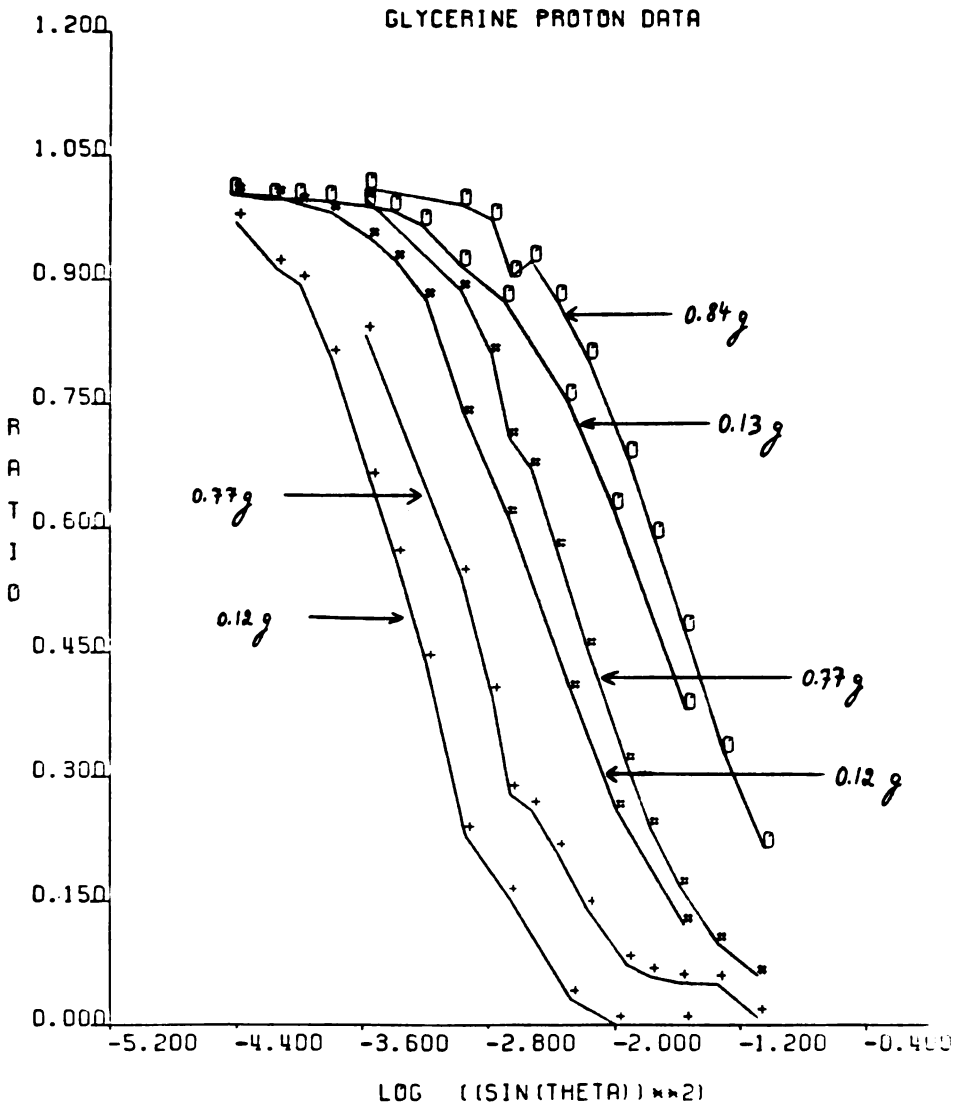

Fig. 6.49. Glycerine proton off-resonance data at three temperatures. (+) −25.8°C; (#) −15.4°C; (O) −5.4°C. The arrows with the numbers indicate the H_1 field strengths in units of Gauss (g).

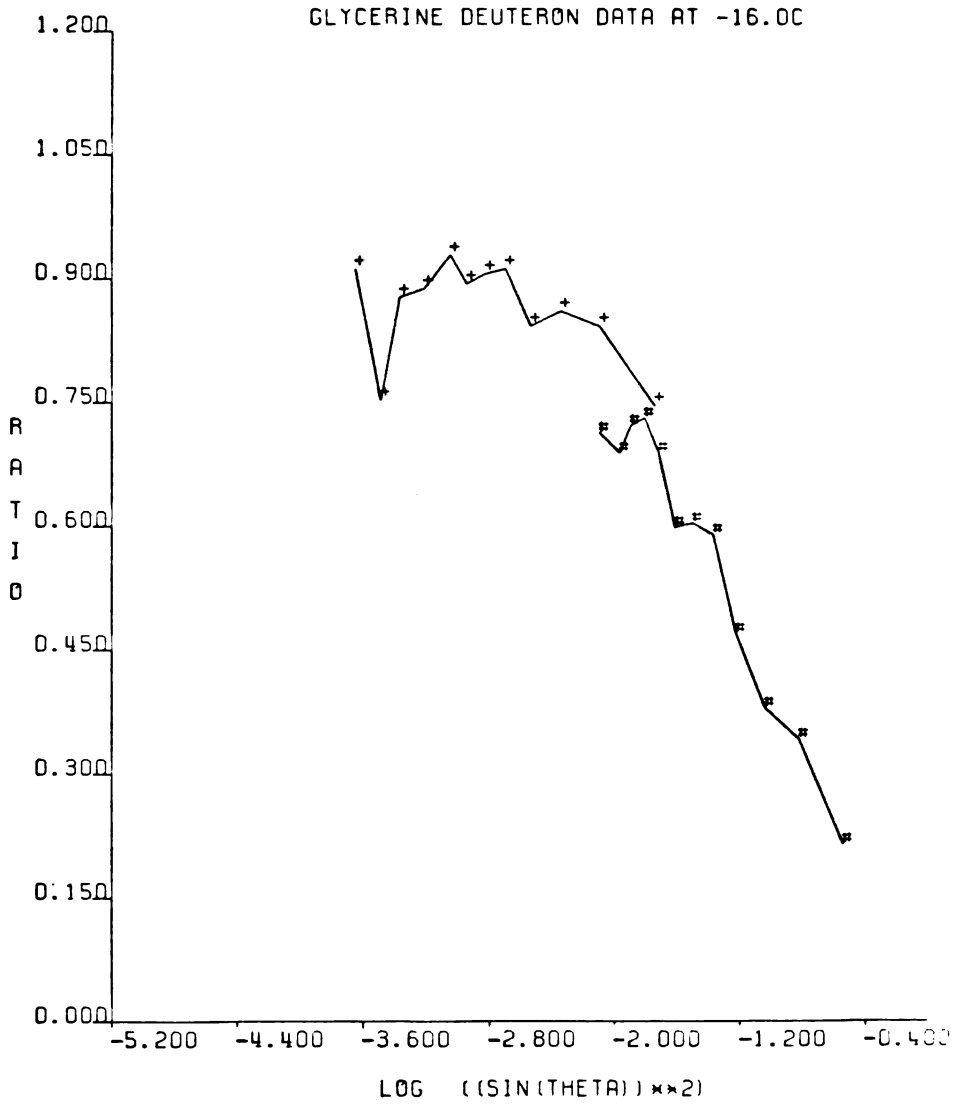

Fig. 6.50. Glycerine deuteron off-resonance data in a perdeuterated glycerine sample at −16.0°C. (+) H_1 field of 0.42 g; (#) H_1 field of 1.94 g.

lines became too broad. This data is similar to the deuterium data of the 0.5 g/1 ml frozen BSA solution in D_2O (Figure 6.47). The values of R are H_1 field independent, within the experimental error, the curves lie on the right side of the graph and no cross-over points are seen.

The ratio of the glycerin proton/deuteron T_1 relaxation times at $\sim$-15°C is $\sim$300(msec)/3(msec) $\approx$ 100, whereas the maximum theoretical ratio is expected to be 10. In frozen BSA samples we obtained proton/deuteron T_1 ratios that are higher than 10 (see Section 6.2.1 and Table 6.9). We pointed out that this result may be caused by the presence of cross-relaxation or may be due to a loss of a broad component in the deuterium signal. Since cross-relaxation is not a factor in the glycerine sample, it strongly indicates that a loss of a broad component in the deuterium spectra is responsible, at least in part, for the experimental T_1 proton/deuteron ratios which are larger than 10, both in the glycerine sample and in the frozen BSA solutions. These results also indicate that the absence of H_1 field dependence and the shift of the deuterium curves to the right side of the graph, in both the glycerine and the BSA frozen samples, may be only apparent. If we could avoid losing the broad component, the deuterium curves

may have been shifted towards the left side of the graph and some H_1 field dependence may have been present.

To check whether the effects could arise from a cross-relaxation process, we obtained proton data at +24.2°C for ∿20% wt/wt water adsorbed on an SiO_2 powder. The results are shown in Figure 6.51.

We have chosen SiO_2 powder because it has no protons. Upon hydration, SiO_2 forms silicic acid and -OH groups are present. Under our conditions the hydroxyl protons are in a fast exchange with the water and only one peak is observed. The hydroxyl protons are likely to have some contribution to the relaxation times, but they are located on the surface and their density is low. Cross-relaxation effects similar to those that may take place between the macromolecule and the water are not likely to be present in the water-SiO_2 powder system. The water-powder system resembles the water-macromolecule system in that they both are heterogeneous. Translational motions, anisotropy, and an exchanging proton fraction may be present in the two systems.

Data for the adsorbed water at +24.2°C were similar to the data of the frozen BSA sample (Figure 6.46). The values of R are H_1 field dependent, at least one cross-over point is present, and the curves

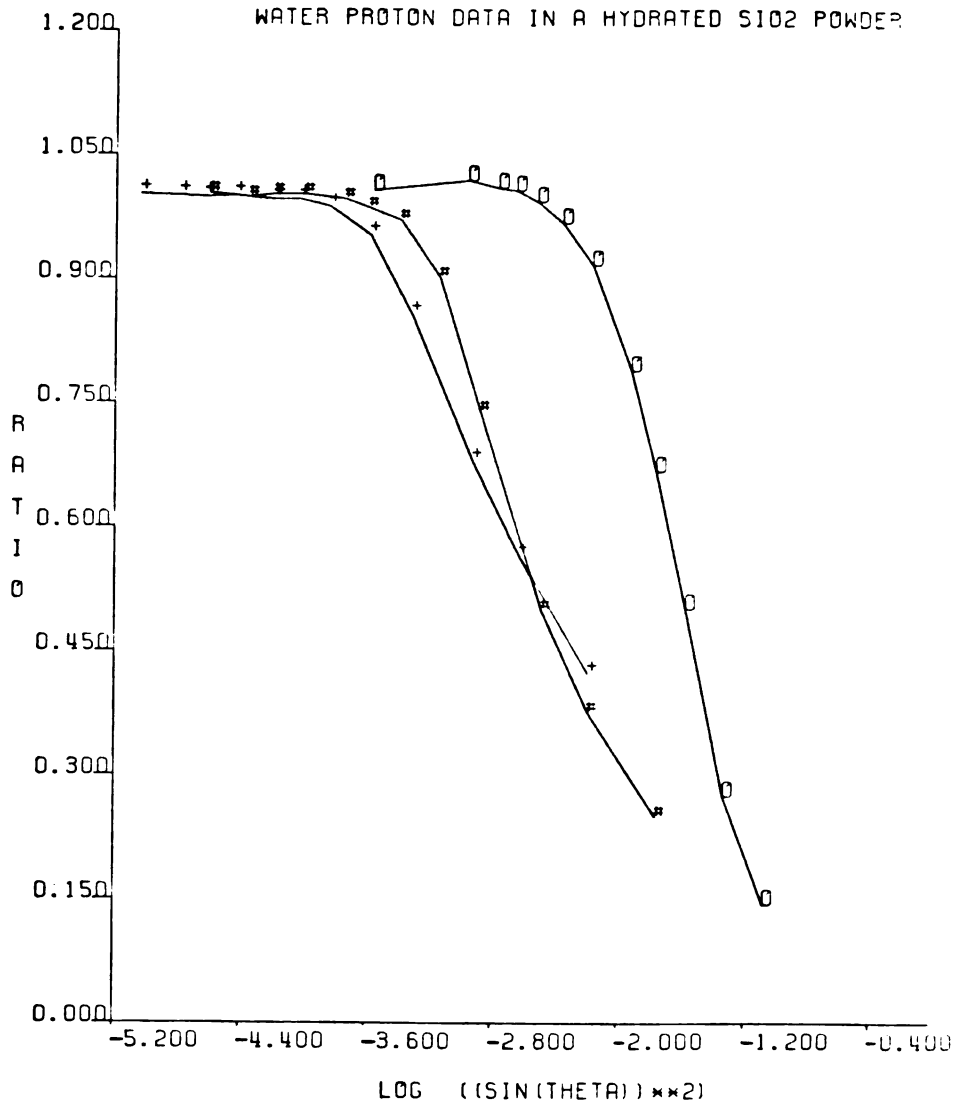

Fig. 6.51. Water proton off-resonance data in a SiO_2 powder hydrated with ~20% wt/wt water. Data obtained at +24.2°C. (+) H_1 field of 0.06 g; (#) H_1 field of 0.09 g; (0) H_1 field of 0.78 g.

are located at the center of the graph. These results indicate that the high H_1 field dependence and the cross-over of curves observed for the protons are not likely to be caused by cross-relaxation.

It is difficult to obtain direct evidence for the presence of anisotropy. No dipolar splittings were observed in the proton spectra. The deuterium spectra, which are expected to be more sensitive to a net anisotropy of the water motions (72), showed no quadrupolar splittings, within the experimental error. No splittings were seen by Borah and Bryant (72) in a similar experiment.

If anisotropy is present it must be small. A net anisotropic component, even if it is small, may still contribute significantly to relaxation times that are sensitive to slow motions, such as T_2 and $T_{1\rho}^{off}$ (72). We obtained experimental T_1/T_2 ratios at subzero temperatures that are larger by a factor of $\sim$100 or more than the theoretical ratios (see Tables 6.1 and 6.8). We showed that most of the effect is caused by the small values of T_2's (see Section 6.2.1). Translational motions and restricted water mobility (see Section 6.2.3) will cause large T_1/T_2 ratios. It is very likely that part of the effect is caused by a residual net anisotropy, which is too small to be detected by observation of the

deuterium quadrupolar splitting. An additional indirect evidence for the presence of anisotropy is provided by our observation that the values of $1/T_2$, for protons in the frozen BSA systems, obtained by extrapolating $1/T_{1\rho}^{on}$ relaxation rates to $H_1 \approx 0$, are bigger than $1/T_2$ values obtained from the linewidth measurements (see Table 6.12). This is usually interpreted as an evidence for the presence of static non-zero dipolar interactions (see Section 6.2.3).

Figures 6.52-6.53 show water proton data for the 70% PLL sample at +15°C and -25.3°C, respectively. The general shapes of the curves are very similar to those obtained for the BSA sample at -26.3°C and similar effects are present. Decreasing the temperature has mostly the effect of increasing the H_1 field dependence of the R's. Comparing the data of the PLL and the BSA samples to the glycerine data indicates that the presence of the cross-over points and part of the large H_1 field dependence is associated with the presence of the macromolecule. Both the BSA and the PLL samples have cross-over points and they both show large field dependence. The glycerine curves have no cross-over points, the field dependence is small, and the curves move to the right side of the graph when the temperature is raised.

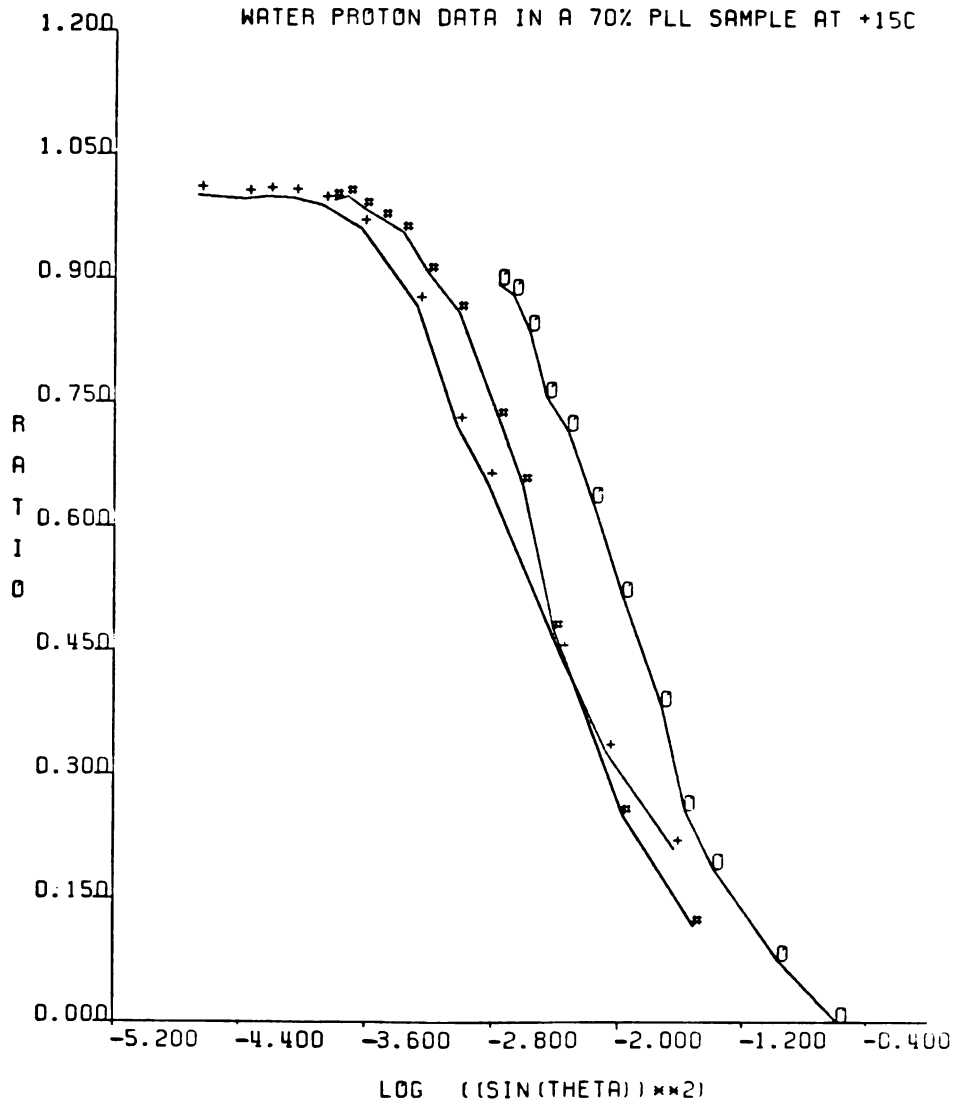

Fig. 6.52. Water proton off-resonance data in a 70% PLL sample at +15°C. (+) H_1 field of 0.11 g; (#) H_1 field of 0.29 g; (0) H_1 field of 0.98 g.

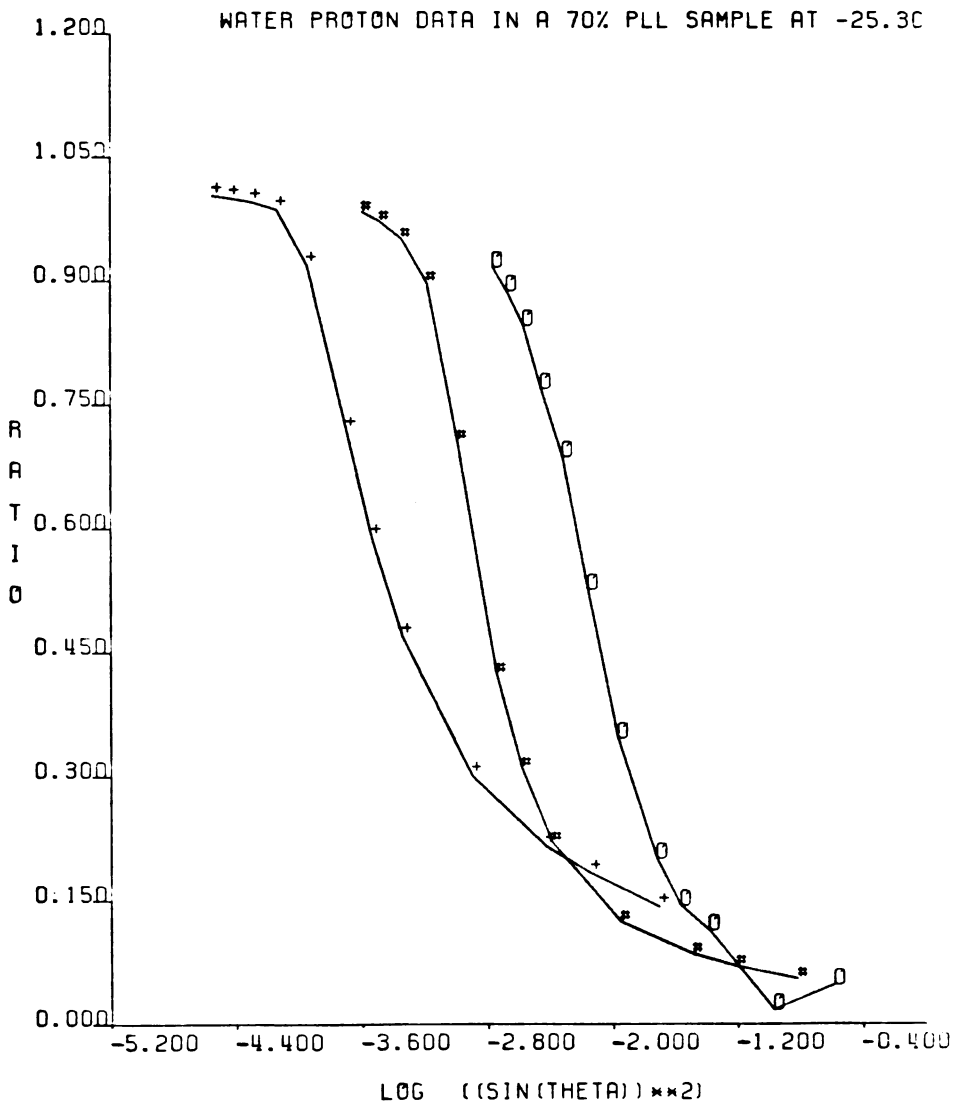

Fig. 6.53. Water proton off-resonance data in a 70% PLL sample at −25.3°C. (+) H_1 field of 0.10 g; (#) H_1 field of 0.30 g; (0) H_1 field of 0.98 g.

We attempted to derive explicit values for the water correlation times from the experimental data. We assumed that the data can be described by the simultaneous presence of three different correlation times. Our results indicate (see Section 6.2.1) that a fraction of the water has an effective correlation time in the nanosecond region. A slower water fraction is needed to account for the large H_1 field dependence of R and the $T_{1\rho}^{on}$ dispersion (see Section 6.2.3). In addition, a "bulk" water fraction is present. At room temperature the water molecule is reported to have an NMR correlation time of $\sim$3 picoseconds (see later discussion). We estimate that the correlation time is reduced by a factor of $\sim$3 at $\sim$-25°C and fixed this fraction at $\tau_r = 1.0 \times 10^{-11}$ sec. The precise value of this component does not affect the results of our fits and our conclusions.

A four parameter search (two independent correlation times and two independent fractions) requires hours of computer time and gives a large amount of possible combinations of parameters. To overcome this problem, the slowest fraction was fixed first by a two correlation time search of $T_{1\rho}^{on}$ values. Three experimental $T_{1\rho}^{on}$ values were used: values at a high H_1, at an intermediate H_1, and at a low H_1. $T_{1\rho}^{on}$ values for the frozen BSA sample were obtained

from the dispersion plots in Figure 6.34. Whenever the calculated values of $T_{1\rho}^{on}$ were within ±25% of the experimental values, the corresponding slow correlation time and its fraction were held constant. Only the intermediate correlation time and its fraction were then changed, until the calculated T_1 and T_2 values were within ±25% of their experimental values. The self-written NMRKS4 Fortran program, which was used to do the search, is listed in Appendix C.

Since R is the ratio of two relaxation times (see Chapter 2, Section 2.6), the rigid-lattice second moment cancels out, and its value does not affect R. To calculate explicit values for the relaxation times, the value of the rigid-lattice second moment must be known. Since the reported values of the rigid-lattice second moment vary, we used the value of 6.3×10^{10} rad^2/sec^2 which gives $T_1 \approx 3.5$ sec when $\tau_r \approx 3.0 \times 10^{-12}$ sec. These are the NMR parameters reported for water at room temperature (23, 75). For deuterons we used the value of 6.0×10^{11} rad^2/sec^2 for the rigid-lattice second moment, which gives $T_1 \approx 370$ msec when $\tau_r \approx 3.0 \times 10^{-12}$ sec. These are the NMR parameters reported for D_2O at room temperature (76).

The "best" theoretical fit to the BSA proton data at -26.3°C is shown in Figure 6.54. Even when the slow component is fixed by the experimental values

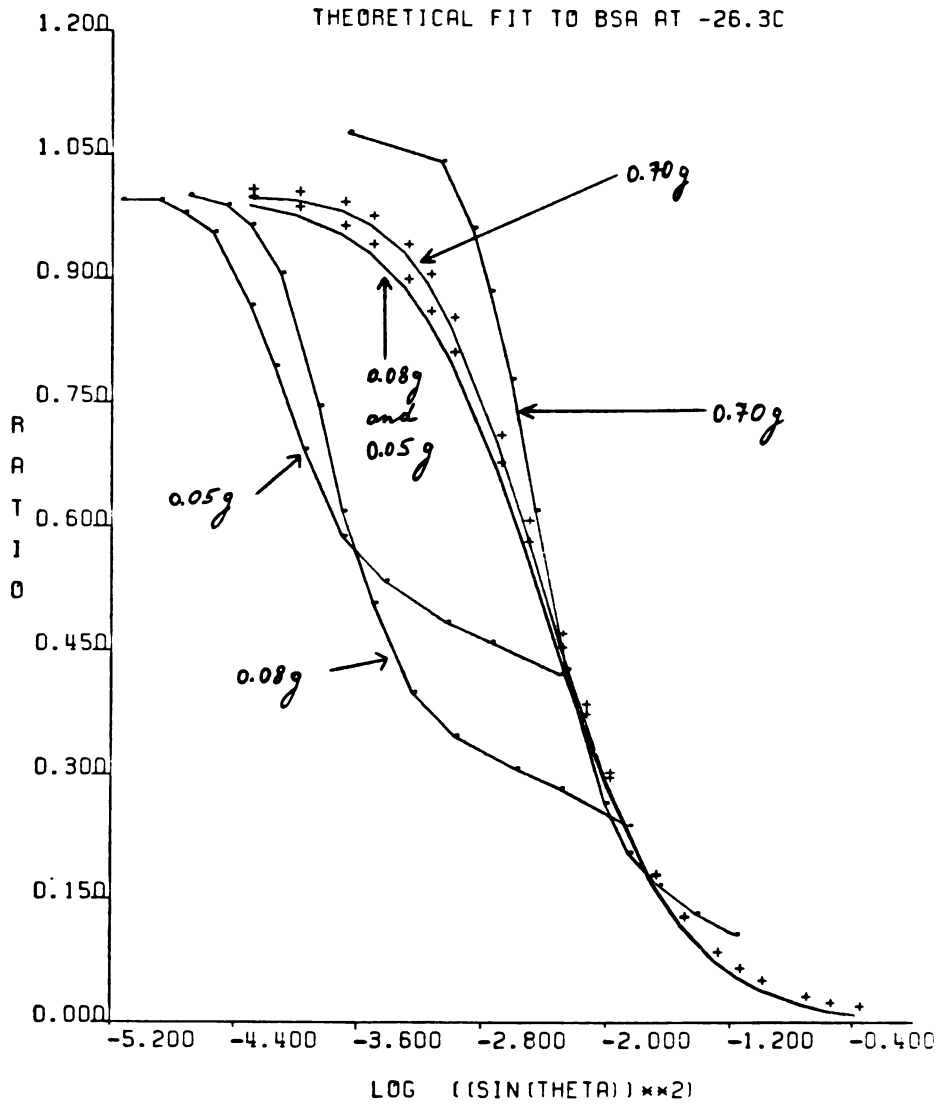

Fig. 6.54. Three correlation times off-resonance theoretical fit to water proton data in a 0.5 g/1ml BSA sample at −26.3C. (•) Experimental data; (+) theoretical fit. The fitted parameters are $\tau_a = 1.0\times10^{-11}$ sec, $P_a = 0.694$; $\tau_b = 2.5\times10^{-9}$ sec, $P_b = 0.236$; $\tau_c = 1.0\times10^{-6}$ sec, $P_c = 0.070$. The arrows with the numbers indicate the H_1 field strengths in units of Gauss (g).

of $T_{1\rho}^{on}$, a large number of possible combinations of the parameters is obtained. The "best" fit illustrated in Figure 6.54 was chosen because it provides the largest H_1 field dependence of the R values. This corresponds to the combination of parameters which includes the largest fraction of the slowest component that is still compatible with the experimental values of T_1 and T_2. The following parameter values were obtained: $\tau_a = 1.0 \times 10^{-11}$ sec, $P_a = 0.694$; $\tau_b = 2.5 \times 10^{-9}$ sec, $P_b = 0.236$; $\tau_c = 1.0 \times 10^{-6}$ sec, $P_c = 0.070$.

The intermediate correlation time has a value of 2.5 nanoseconds. This is a good agreement with our experimental findings that the T_1 values of the water protons at 150 MHz go through a minimum at $\sim$-25°C (see Section 6.2.1). Using Equation 2.2 the effective correlation time at this frequency is calculated to be $\sim$1.1 nanoseconds.

Inspection of Figure 6.54 shows that the "best" fit for protons is not satisfactory. The theoretical fit cannot account for the large experimental H_1 field dependence of the values of R. An apparent slow component much longer than a microsecond is needed. When one replaces the microsecond correlation time with a correlation time on the order of hundreds of microseconds, a large field dependence can be achieved.

However, in the presence of such a long correlation time the calculated values of T_2 are much shorter than their experimental values. It is unreasonable to assume that a very slow motion and/or process exist which contributes to $T_{1\rho}^{off}$ but not to T_2 relaxation times. The most likely explanation for our inability to obtain a good theoretical fit for the proton data is that we are observing behavior which cannot be described adequately by the simple off-resonance equations. See the discussion later in this section as to why such a behavior may be observed.

The parameters of the "best" fit for protons were used to calculate theoretical plots of R versus $\sin^2\theta$ for deuterons. This is illustrated in Figure 6.55. The theoretical curves are shifted to the left of the experimental curves. This indicates that if a slow component is present, it contributes mostly to the proton relaxation, but not to the deuterium relaxation.

We tried to obtain a three correlation times fit to the deuterium data by first fixing the slow component using the proton $T_{1\rho}^{on}$ dispersion data. Then the intermediate component was changed until the calculated T_1 and T_2 values for deuterons were within ±25% of the experimental deuteron T_1 and T_2 values. No possible combinations could be found. The proton $T_{1\rho}^{on}$ data

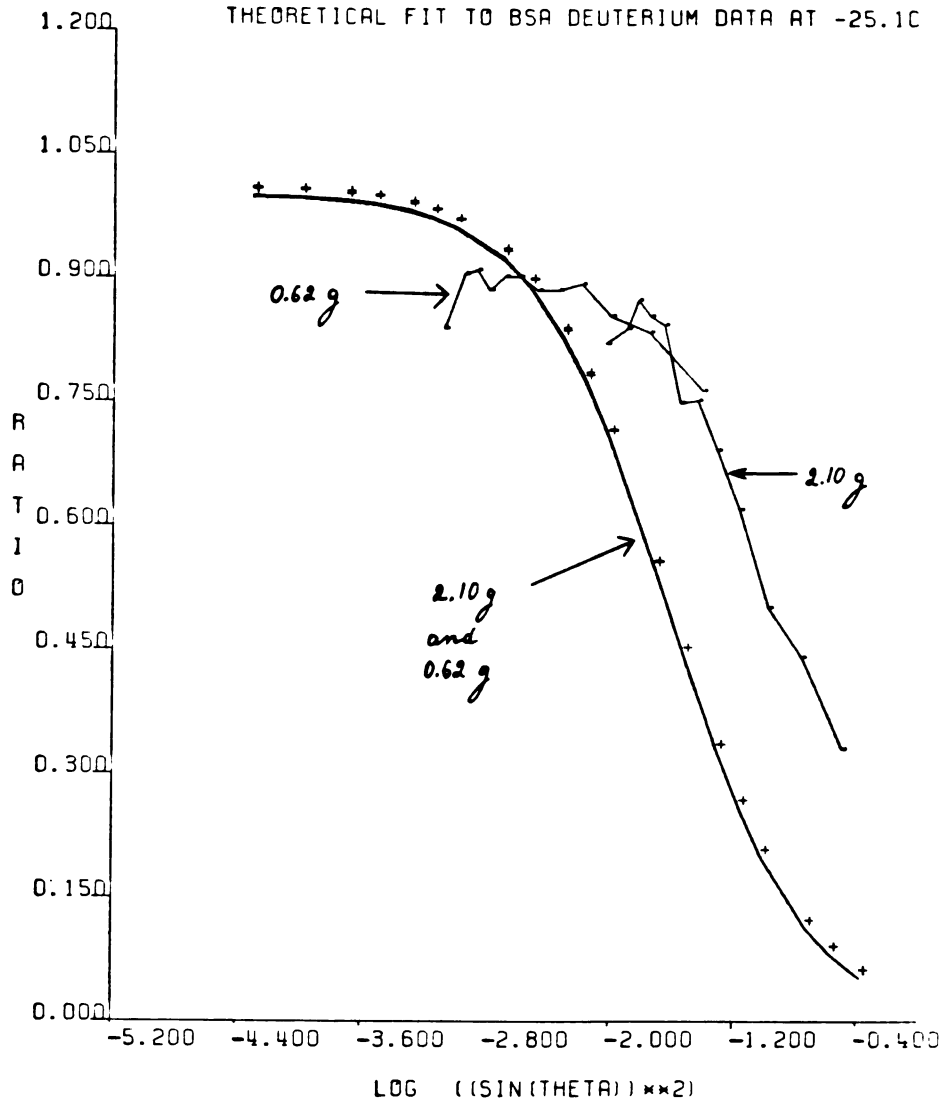

Fig. 6.55. Three correlation times off-resonance theoretical fit to solvent deuteron data in a 0.5 g/1ml BSA in D_2O sample at −25.1°C. (•) Experimental data; (+) theoretical fit. The parameters used are identical to those used in the three correlation times fit for protons in Fig. 6.54. The arrows with the numbers indicate the H_1 field strengths in units of Gauss (g).

requires the presence of a correlation time which is "too slow" to be consistent with the deuterium data. The calculated values of T_2 for deuterium using this slow component give T_2 values which are much shorter than the experimentally measured values.

We obtained a two correlation times fit for the deuterium data. The fast correlation time was fixed at $\tau_r = 1.0 \times 10^{-11}$ sec. The second correlation time and the corresponding fraction(s) were changed. The "best" fit is illustrated in Figure 6.56. The following parameter values were obtained: $\tau_a = 1.0 \times 10^{-11}$ sec, $P_a = 0.454$; $\tau_b = 3.5 \times 10^{-8}$ sec, $P_b = 0.546$.

The slower correlation time is 35 nanoseconds, i.e., it is a factor of $\sim$10 longer than the intermediate correlation time in the proton three correlation times fit. The relative contribution of the two fractions, in the two correlation times fit for deuterons, is about equal, i.e., the nanosecond fraction contributes more by a factor of $\sim$2 as compared to its contribution in the proton three correlation times fit.

If the slow component that contributes to the proton data did not contribute to the deuterium data, or if it was lost in the deuterium data because of the long instrumental dead time, we would expect the two correlation times fit for deuterium to have the same

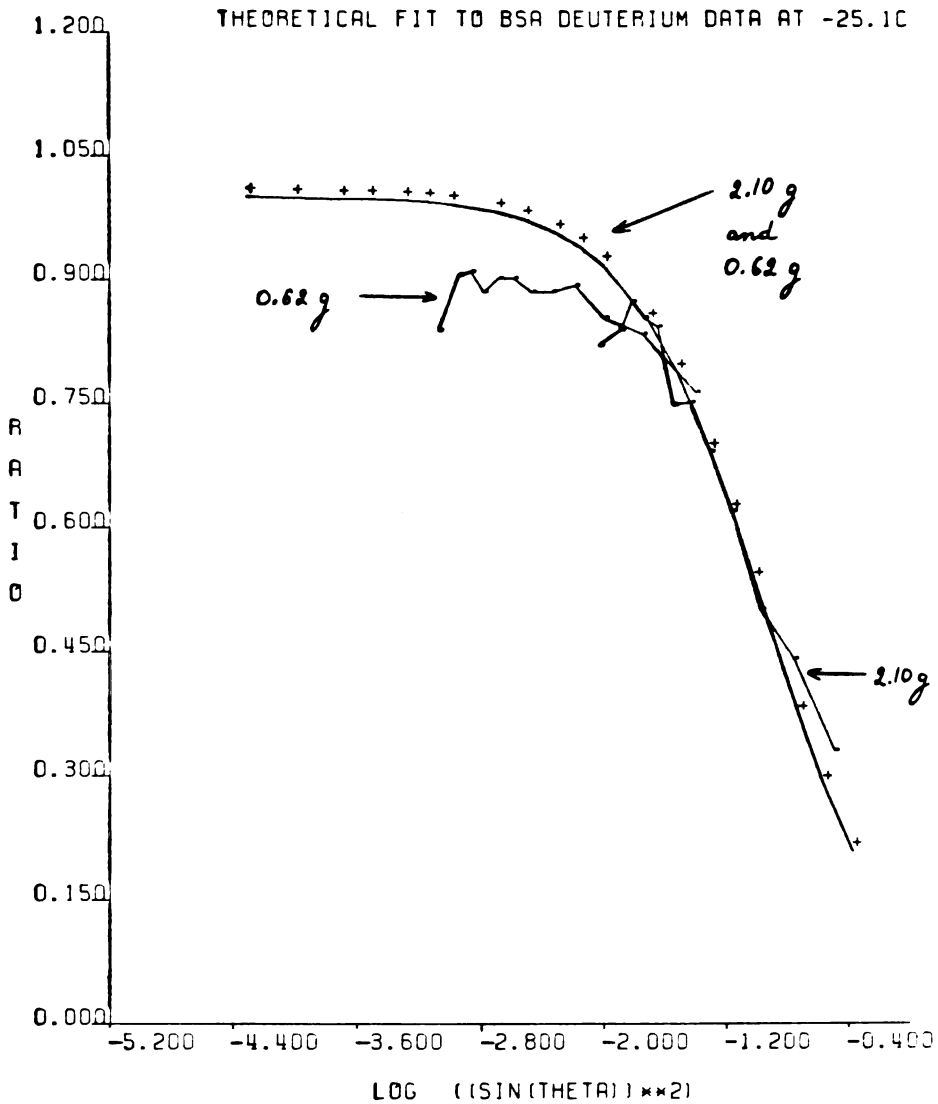

Fig. 6.56. Two correlation times off-resonance theoretical fit to solvent deuteron data in a 0.5 g/1ml BSA in D_2O sample at −25.1°C. (•) Experimental data; (+) theoretical fit. The fitted parameters are $\tau_a = 1.0 \times 10^{-11}$ sec, $P_a = 0.454$; $\tau_b = 3.5 \times 10^{-8}$ sec, $P_b = 0.546$. The arrows with the numbers indicate the H_1 field strengths in units of Gauss (g).

correlation times and the same relative contributions as the two fastest fractions in the proton three correlation times fit. The fact that the slower correlation time in the deuterium two correlation times fit is longer and its fraction larger than the intermediate correlation time in the proton three correlation times fit indicates that a slow component does contribute to the deuterium data. The effective correlation time for this component is, however, much shorter than the slowest correlation time for protons.

Figure 6.57 shows a two correlation times theoretical fit for protons using the same parameters used in the two correlation times fit for deuterons. The two and the three correlation times fits for protons are shown together in Figure 6.58. The two correlation times curve is shifted somewhat to the left as compared to the three correlation times curve. This is because the second component in the two correlation times fit is longer and has a larger fraction than the intermediate component in the three correlation times fit. The two correlation times fit shows no H_1 field dependence. Addition of a slow component is necessary to obtain at least some field dependence.

Bendel and James (77) plotted 1 - R as a function of the off-resonance frequency. If only one isotropic rotational motion is present, such a plot

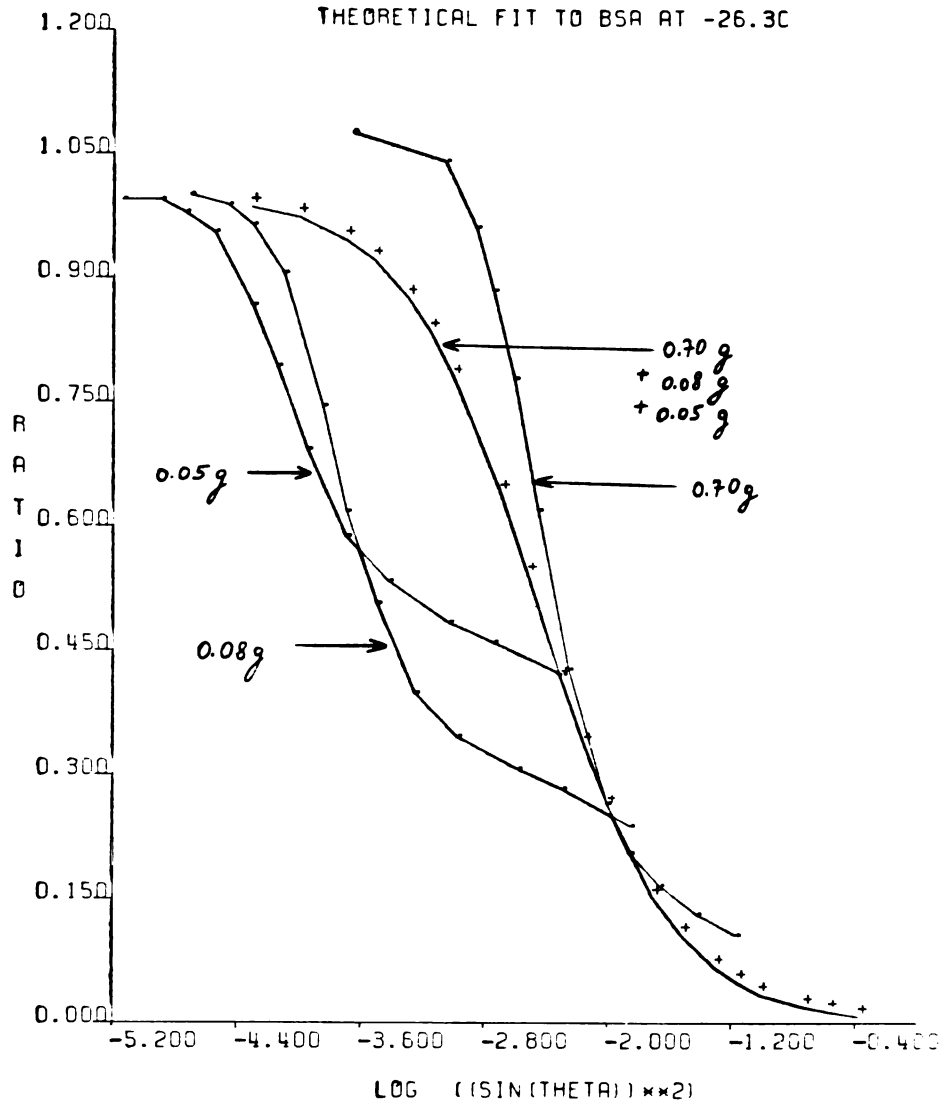

Fig. 6.57. Two correlation times off-resonance theoretical fit to water proton data in a 0.5 g/1ml BSA sample at −26.3C. (•) Experimental data; (+) theoretical fit. The parameters used are identical to those used in the two correlation times fit for deuterons in Fig. 6.56. The arrows with the numbers indicate the H_1 field strengths in units of Gauss (g).

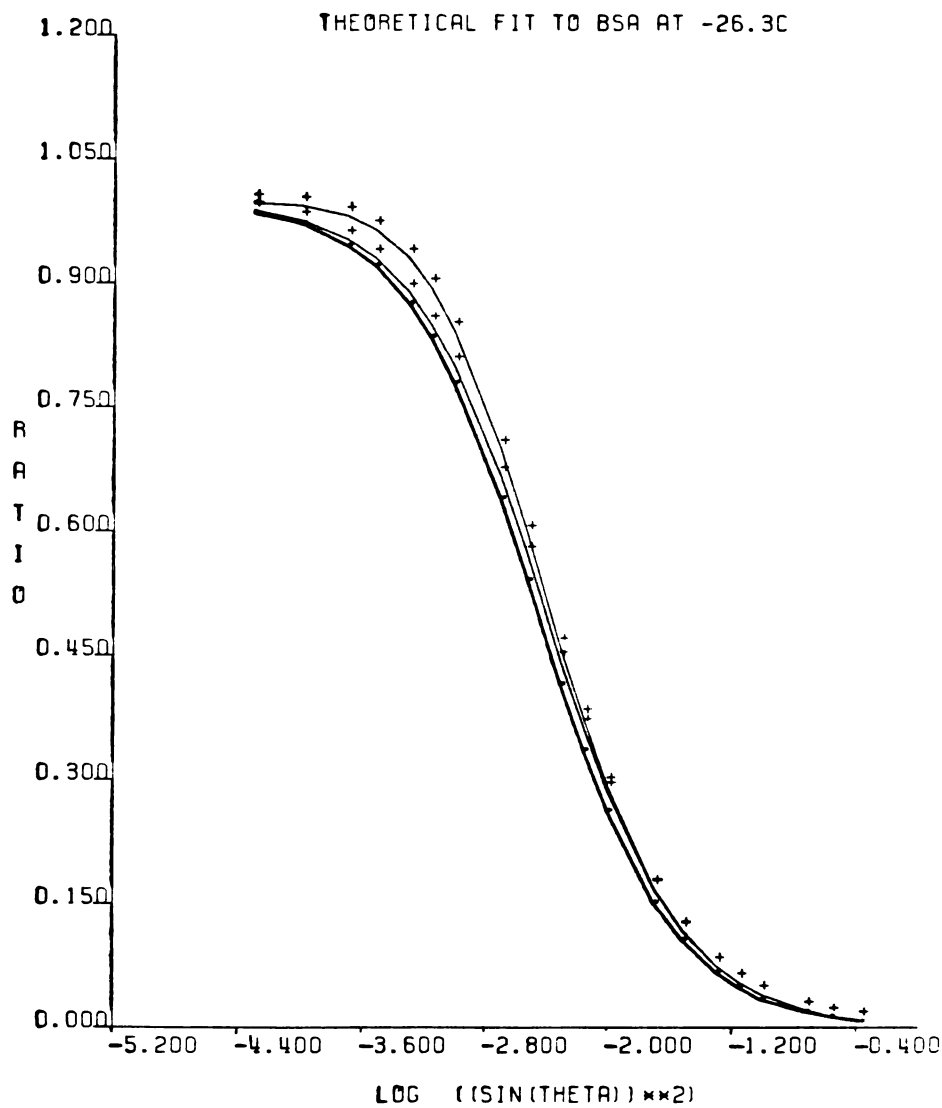

Fig 6.58. Two and three correlation times off-resonance theoretical fits to water proton data in a 0.5 g/1ml BSA sample at −26.3°C. (•) Two correlation times fit; (+) three correlation times fit. Plots are identical with the theoretical plots for protons in Fig. 6.54 and Fig 6.57 and they are shown together for clarity.

is expected to give a Lorentzian lineshape with the linewidth at half the amplitude (in units of Hz) given by (77)

$$(1/2)\nu_{1/2} = \frac{\gamma H_1}{2\pi}(T_1/T_2')^{1/2} \qquad [6.1]$$

where T_2' is equal to $T_{1\rho}^{on}$.

We subjected our 1 - R versus off-resonance frequency data to a Lorentzian fit (see Chapter 5, Section 5.5). The results for the frozen BSA sample at -26.3°C and at H_1 = 0.70 g, 0.08 g, and 0.05 g are illustrated in Figures 6.59-6.61, respectively. Figure 6.62 illustrates the results for the BSA in D_2O sample at -25.1°C. Data are for the deuterium signal at H_1 = 2.10 g. Deuterium data at the lower H_1 field were very noisy and were not used. We had data only on the positive side of the Lorentzian curve. In order to perform the fit, we entered also negative frequencies for every value of 1-R. The negative side of the data is thus a mirror image of the positive side.

Inspection of the data shows that for protons the points at the low values of 1-R deviate from the best fitted Lorentzian lineshape. The experimental points approach zero at a faster rate than the fitted line. Such a behavior may be observed

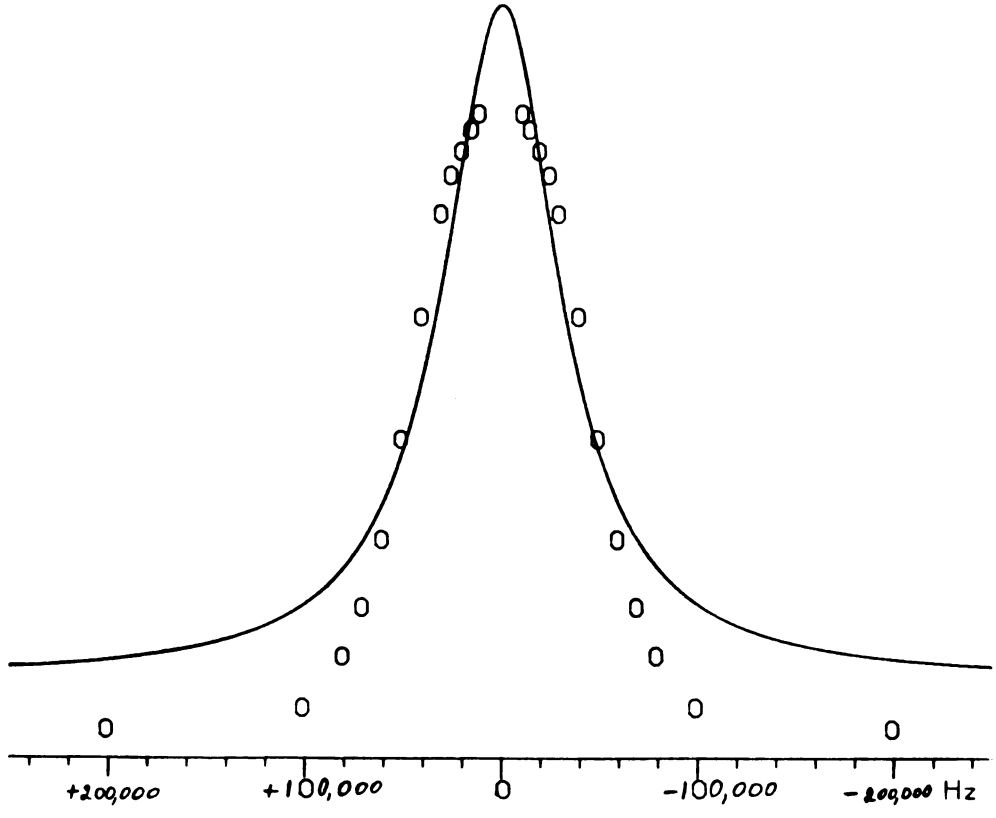

Fig 6.59. A plot of 1-R vs. the off-resonance frequency at H_1 = 0.70 g. Data is for the water protons in a 0.5 g/1ml BSA sample at −26.3°C. The circles represent the experimental points and the solid line represents a Lorentzian fit. Vertical scale is not shown.

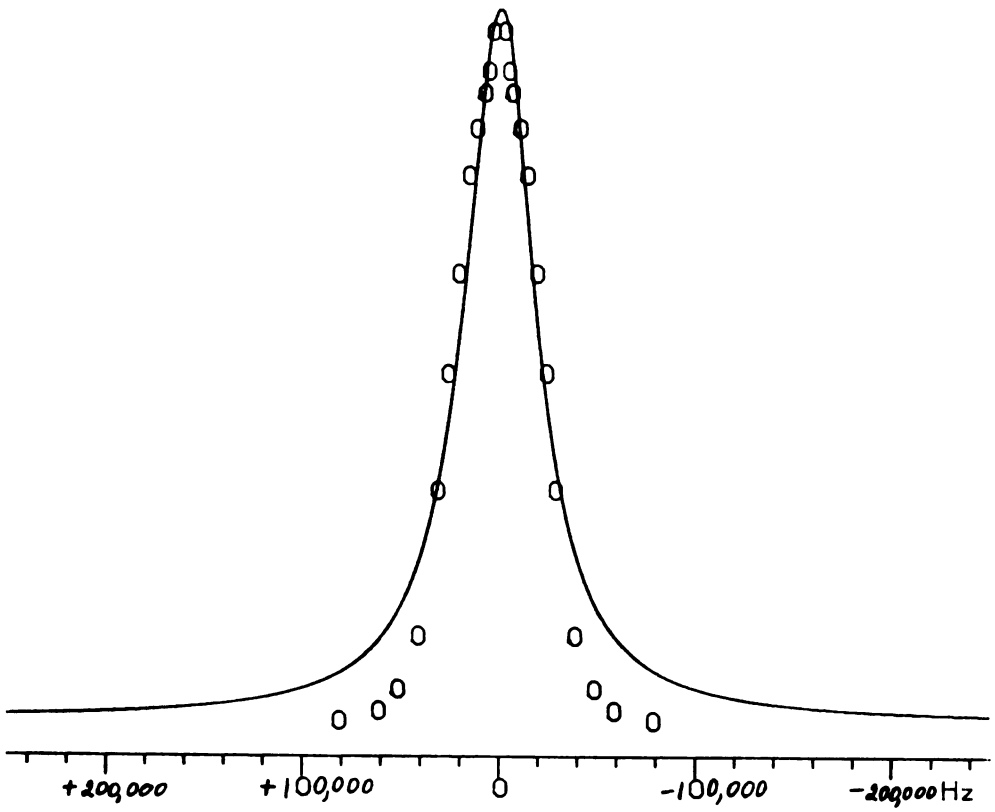

Fig 6.60. A plot of 1-R vs. the off-resonance frequency at H_1 = 0.08 g. Data is for the water protons in a 0.5 g/1ml BSA sample at −26.3°C. The circles represent the experimental points and the solid line represents a Lorentzian fit. Vertical scale is not shown.

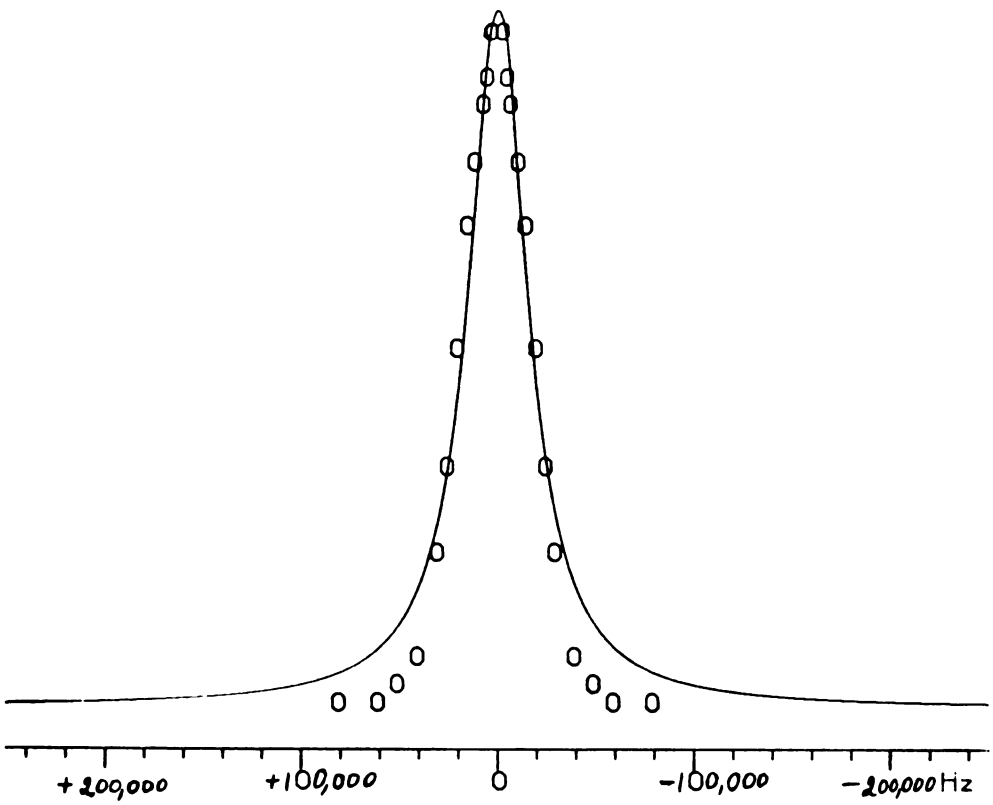

Fig 6.61. A plot of 1-R vs. the off-resonance frequency at H_1 = 0.05 g. Data is for the water protons in a 0.5 g/1ml BSA sample at −26.3°C. The circles represent the experimental points and the solid line represents a Lorentzian fit. Vertical scale is not shown.

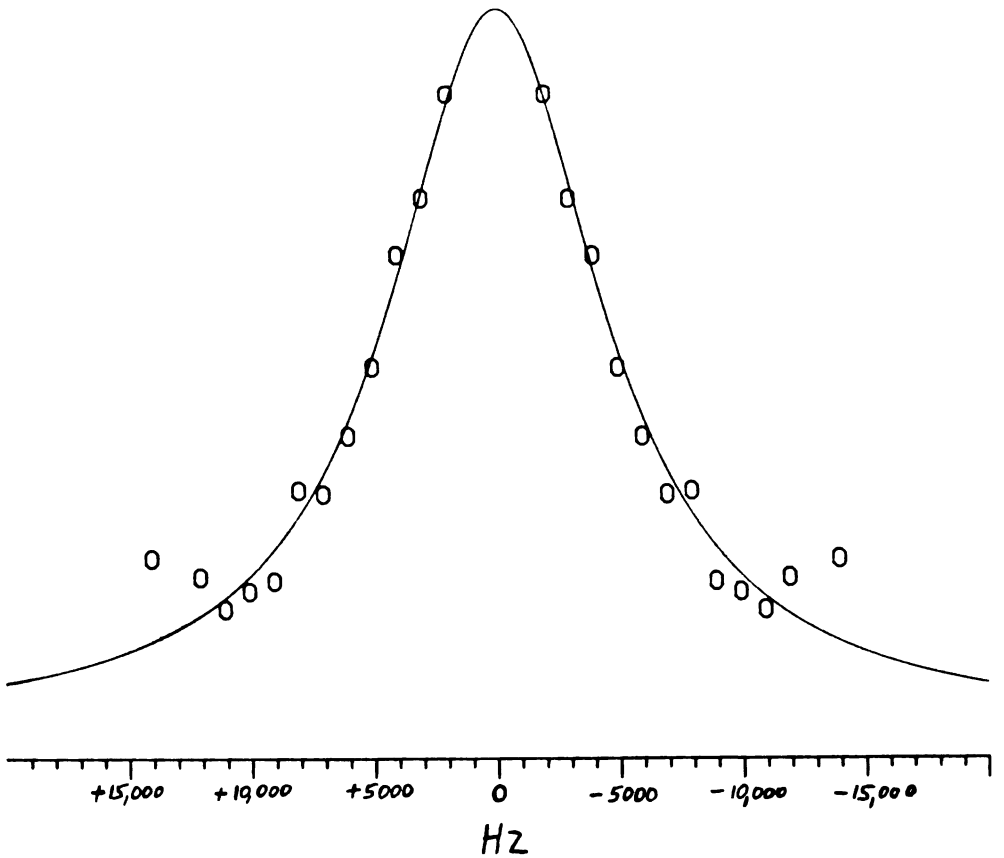

Fig 6.62. A plot of 1-R vs. the off-resonance frequency at H_1 = 2.10 g. Data is for the solvent deuterons in a 0.5 g/1ml BSA in D_2O sample at −25.1°C. The circles represent the experimental points and the solid line represents a Lorentzian fit. Vertical scale is not shown.

if the experimental data are described by a Gaussian lineshape. If the experimental lineshape is not Lorentzian it implies that the relaxation cannot be described by a single isotropic rotational motion.

A good Lorentzian fit is obtained for the deuterium data in Figure 6.62. This implies that the deuterium relaxation is governed by an isotropic rotational motion. If any anisotropy or additional motions contribute to the deuterium relaxation, their contribution must be small, so that within the experimental error they do not affect the Lorentzian lineshape.

The proton relaxation cannot be described by a simple isotropic rotation. Additional motions and/or processes contribute to the proton relaxation. Their contribution is significant, since the lineshape is not Lorentzian. These additional motions do not contribute, however, to the deuterium relaxation.

Table 6.15 summarizes the proton data for the frozen BSA sample. The fitted Lorentzian linewidths were calculated by the Nicolet 1180 computer and the associated program (Column 2). Equation 6.1 and the experimental values of T_1 = 111.2 msec, $T_2 \approx 0.66$ msec, and the corresponding experimental H_1 values were used to calculate the expected Lorentzian linewidths (Column 3). The linewidths of the fitted

Table 6.15. $\nu_{1/2}$ and T_2' values for the water proton at 100 MHz in a frozen 0.5g/1ml BSA sample.

Column 1	Column 2	Column 3	Column 4
H_1 (g)	$\nu_{1/2}$[1],[2] From Lorentzian Fit (KHz)	$\nu_{1/2}$[2] Calculated using Equation 6.1 (KHz)	T_2'[2] (msec)
0.70	71 ± 21	77 ± 23	0.78 ± 0.23
0.08	43 ± 13	9 ± 3	0.03 ± 0.009
0.05	36 ± 11	6 ± 2	0.02 ± 0.006

[1]Calculated using the Nicolet 1180 computer and the associated Nicolet program.

[2]Reported errors are estimates.

Lorentzian curves were used, together with the experimental value of T_1 = 111.2 msec and the corresponding experimental values of H_1, to calculate the values of T_2' (Column 4).

We used small enough H_1 fields so that $T_{1\rho}^{on} \approx T_2$ and $T_2' \approx T_2$. Therefore, the ratio T_1/T_2' is constant. Equation 6.1 predicts that if this ratio is constant, then the Lorentzian linewidth should be directly proportional to the H_1 field strength. Inspection of the data in Table 6.15 shows that the fitted linewidths (Column 2) decrease when the H_1's become smaller, but not by as much as is expected from the experimental T_1 and T_2 values (Column 3). This means that the T_2' values derived from the fitted linewidths at the smaller H_1 fields will be much shorter than the experimental value of $T_2 \approx 0.66$ msec. The calculated values of T_2' in column 4 show that this is indeed the case. At the highest H_1 field the derived and the experimental values of T_2 are the same, within the experimental error. At the lower fields a large discrepancy exists between these values.

Table 6.16 summarizes the proton data for the 70% PLL sample. The Lorentzian fits were performed using the Nicolet TT-100 data processor. The values of T_2 were calculated from the linewidths of the experimental absorption peaks. The values of T_1

Table 6.16. $\nu_{1/2}$, T_2 and T_2' values at 100 MHz for the water proton in a 70% PLL sample.

Temp. (°C)	H_1 (g)	$\nu_{1/2}$[1],[2] (KHz)	T_1[3] (msec)	T_2[2] (msec)	T_2'[2] (msec)
−25.3	0.978	85 ± 26	90	0.53 ± 0.16	0.86 ± 0.26
	0.100	40 ± 12			0.04 ± 0.01
+15.0	0.978	74 ± 22	120	1.2 ± 0.4	1.52 ± 0.46
	0.108	19 ± 6			0.29 ± 0.09

[1]Calculated using the Nicolet TT-100 data processor.

[2]Reported errors are estimates.

[3]Estimated from the T_1 values at 44.4 MHz assuming a linear dependence on the frequency between 44.4 and 100 MHz.

were estimated from the values at 44.4 MHz, assuming a linear dependence on the observing frequency between 44.4 and 100 MHz. The values of T_2' were calculated using Equation 6.1.

Inspection of Table 6.16 shows that, at the high H_1 fields ($H_1 \approx 1$ g) the experimental and the calculated values of T_2 for PLL are equal, within the experimental error. At the low H_1 fields ($H_1 \approx 0.1$ g) the calculated values of T_2' are much shorter than the experimentally measured values.

Table 6.17 summarizes the proton data for the glycerine sample at subzero temperatures. The Lorentzian fits were performed using the Nicolet TT-100 data processor. The values of T_2 were calculated from the linewidths of the experimental absorption peaks. The T_2 value at -5.4°C was estimated assuming that the T_2 values increase by the same factor between -15.4°C and -5.4°C as between -25.8°C and -15.4°C. The values of T_2' were calculated using Equation 6.1.

Inspection of the data in Table 6.17 shows that, at the high H_1 fields the calculated values of T_2' for glycerine are not equal to the experimentally measured T_2 values. The calculated T_2''s are longer than the experimental values. At the low fields the

Table 6.17. $\nu_{1/2}$, T_2 and T_2' values at 100 MHz for the glycerine protons.

Temp. (°C)	H_1 (g)	$\nu_{1/2}$[1],[2] (KHz)	T_1 (msec)	T_2[2] (msec)	T_2'[2] (msec)
−25.8	0.767	198 ± 59	500	0.18 ± 0.05	0.54 ± 0.16
	0.119	42 ± 13			0.29 ± 0.09
−15.4	0.767	84 ± 25	300	0.64 ± 0.19	1.8 ± 0.5
	0.119	17 ± 5			1.1 ± 0.3
−5.4	0.838	40 ± 12	160	2 ± 1[3]	5.1 ± 1.5
	0.125	9 ± 3			2.4 ± 0.7

[1]Calculated using the Nicolet TT-100 data processor.

[2]Reported errors are estimates.

[3]Estimated assuming that, the T_2 increases by the same factor between −15.4°C and −5.4°C as between −25.8°C and −15.4°C.

calculated and the experimental values of T_2 are equal, within the experimental error.

The calculated value of T_2' for deuterium at -25.1°C is 0.10 ± 0.04 msec. The value of T_2 from the experimental absorption line is 0.16 ± 0.06 msec. The two values are equal, within the experimental error.

Comparison of the data in Tables 6.15, 6.16, and 6.17 shows that, at the high H_1 fields, the calculated values of T_2' are consistently larger than the experimentally measured T_2 values. For the glycerine sample, the calculated values of T_2' are longer than the experimental values at the low fields also. For the water data in the water-macromolecule systems, all the calculated T_2' values at the low fields are much shorter than the experimental values.

It is reasonable to expect that the experimental T_2 values may be shorter than the T_2' values calculated from the Lorentzian fits of 1-R versus the off-resonance frequency plots. If very slow motions are present, they may contribute more to the T_2 relaxation time than to the $T_{1\rho}^{on}$ relaxation time. In such a case $T_2 < T_{1\rho}^{on}$. But $T_2' = T_{1\rho}^{on}$ and the T_2 values determined from the experimental absorption peaks contain all the contributions to the T_2 relaxation. Therefore, T_2' may

be longer than T_2 which was measured from the experimental absorption line.

It is unreasonable to expect that T_2' may be shorter than the experimental T_2. Yet, in the frozen water-macromolecule systems $T_2' < T_2$ at the low H_1 fields. This observation implies that we are observing an effect which cannot be described by the simple off-resonance theory and equations. One possible explanation for the frozen systems are local dipolar fields which do not average to zero. We have some evidence for the presence of such local fields, since we observed oscillations in the $T_{1\rho}^{on}$ experiments at low temperatures in a sample of 70% PLL and a BSA sample (see Sections 6.1.2 and 6.2.3). The oscillations occurred when $H_1 < 10$ KHz (2.3 g). The largest H_1 field used in the off-resonance experiments was only $\sim$1 g. It may be that the low H_1 fields are of the same order of magnitude as the local dipolar fields. If H_1 is not much larger than the local dipolar fields, we may be observing effects which are determined by the distribution of the local dipolar fields, rather than by "true" motions. It is possible that these effects cause the cross-over points and contribute to the large H_1 field dependence in the proton data.

Fisher and James (37) calculated the contribution of local (proton) dipolar fields in phospholipid

bilayers to the $T_{1\rho}^{on}$ relaxation. They found that the contribution was less than 10%. Although the contribution of local dipolar fields to the $T_{1\rho}^{on}$ relaxation rates may be small, local dipolar fields may cause large effects when the relaxation times are measured at low H_1 fields. Oscillatory behavior was observed by us and by others (39, 40) in the on-resonance experiments at low H_1 fields. Theoretical treatment (39, 40) shows that such oscillations are caused by the presence of local dipolar fields. No theory exists to describe the off-resonance experiment in the presence of local dipolar fields.

If the large H_1 field dependence of the proton data is not caused by "true" motions, it explains why we cannot obtain a good theoretical fit for the proton experimental data. If the experimental data is dominated by processes other than "true" motions, it cannot be adequately described by equations that assume a simple isotropic rotation. Therefore, one should be careful not to use low H_1 fields in the off-resonance experiments, unless care is taken to assure that no such effects are present.

No special effects are observed for the glycerine sample (Table 6.17) at the low H_1 fields. Comparison with the data in Tables 6.15 and 6.16 shows that the effects at the low H_1 fields are pronounced in the

systems which contain a macromolecule. We do not know why the effects are so pronounced for the water in the water-macromolecule systems. Very slow motions are expected to be present in the glycerine sample at -25°C. The glycerine and the water-macromolecule systems differ in that the glycerine is homogeneous, while the water-macromolecule systems are heterogeneous. In the glycerine sample only one type of molecule is present. In the water-macromolecule systems one measures the properties of a small molecule (the water) in the presence of a very big molecule (the macromolecule).

More experiments and theoretical work are needed to ascertain the mechanisms that cause the effects we see. More work is needed to establish the range of H_1 values, for different types of samples, that can be used in the off-resonance experiments without complicating the interpretation of results.

6.3.3 BSA Solutions

We performed off-resonance experiments on a series of BSA solutions. Data were obtained at ν_0 = 100 MHz at +25 ± 1°C. Data for the 0.05 g/1 ml (4.8% wt/wt), 0.1 g/1 ml (9.1% wt/wt), 0.3 g/1 ml (23.1% wt/wt), 0.4 g/1 ml (28.6% wt/wt), 0.5 g/1 ml (33.3% wt/wt), 0.6 g/1 ml (37.5% wt/wt), 0.7 g/1 ml (41.2%

wt/wt), and the 0.8 g/1 ml (44.4% wt/wt) samples are illustrated in Figures 6.63-6.70, respectively.

Inspection of the data shows that three regions can be identified:

1. Concentration range 0.05 g/1 ml to 0.4 g/1 ml. In this range the R's are H_1 field independent. The dependence of the R values on $\sin^2\theta$ is small at the low concentrations, but it increases progressively as the protein concentration increases. As the concentration increases, the curves shift to the left side of the graph.
2. Concentration range 0.5 g/1 ml to 0.6 g/1 ml. In this range the values of R are H_1 field dependent. The field dependence increases at the higher protein concentration. In this range the values of R are also $\sin^2\theta$ dependent and the curves shift to the left when the concentration is increased.
3. Concentration range 0.6 g/1 ml to 0.8 g/1 ml. In this range, increasing the protein concentration has mostly the effect of "spreading-out" the curves and increasing the H_1 field dependence of the R's. Throughout this range the R's are $\sin^2\theta$

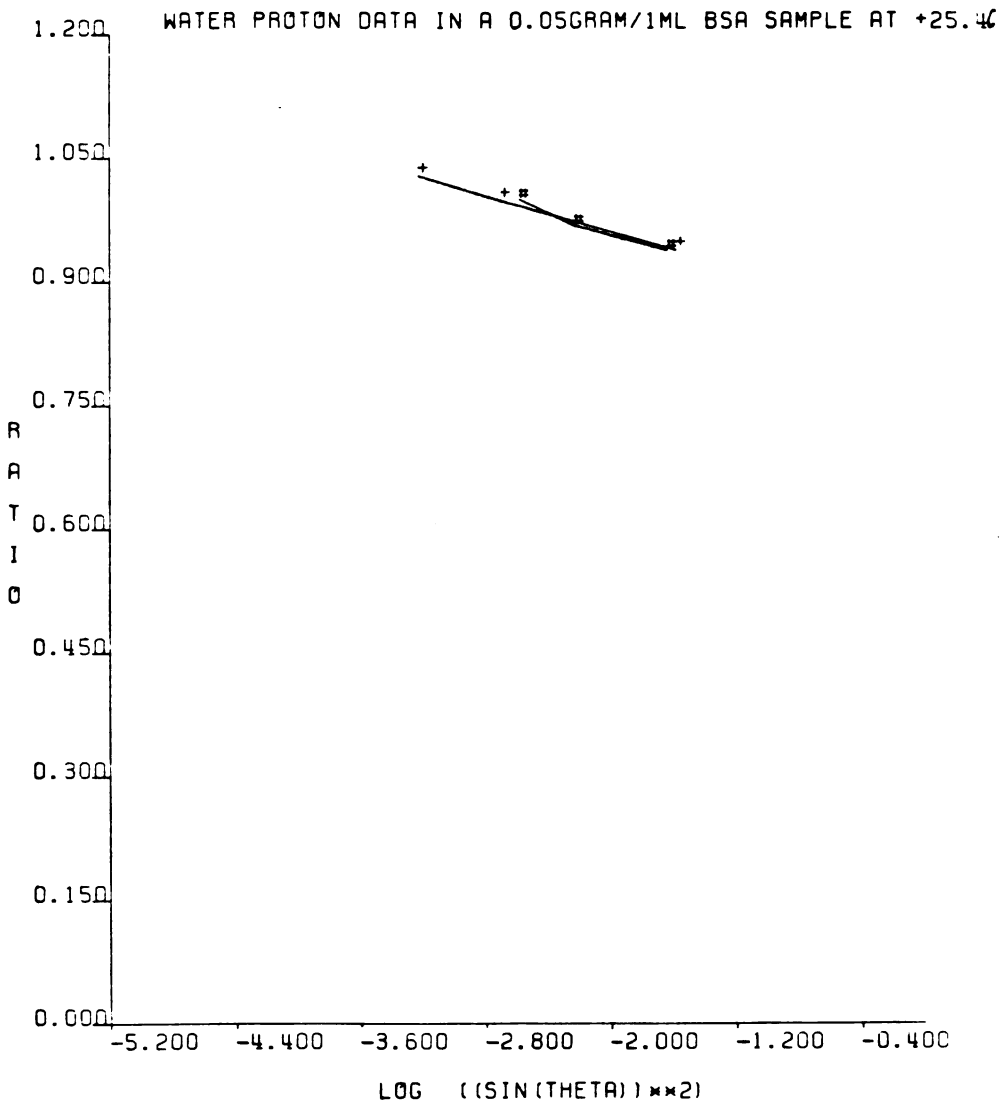

Fig. 6.63. Water proton off-resonance data in a 0.05 g/1ml BSA sample at +25.4°C. (+) H_1 field of 0.12 g; (#) H_1 field of 0.72 g.

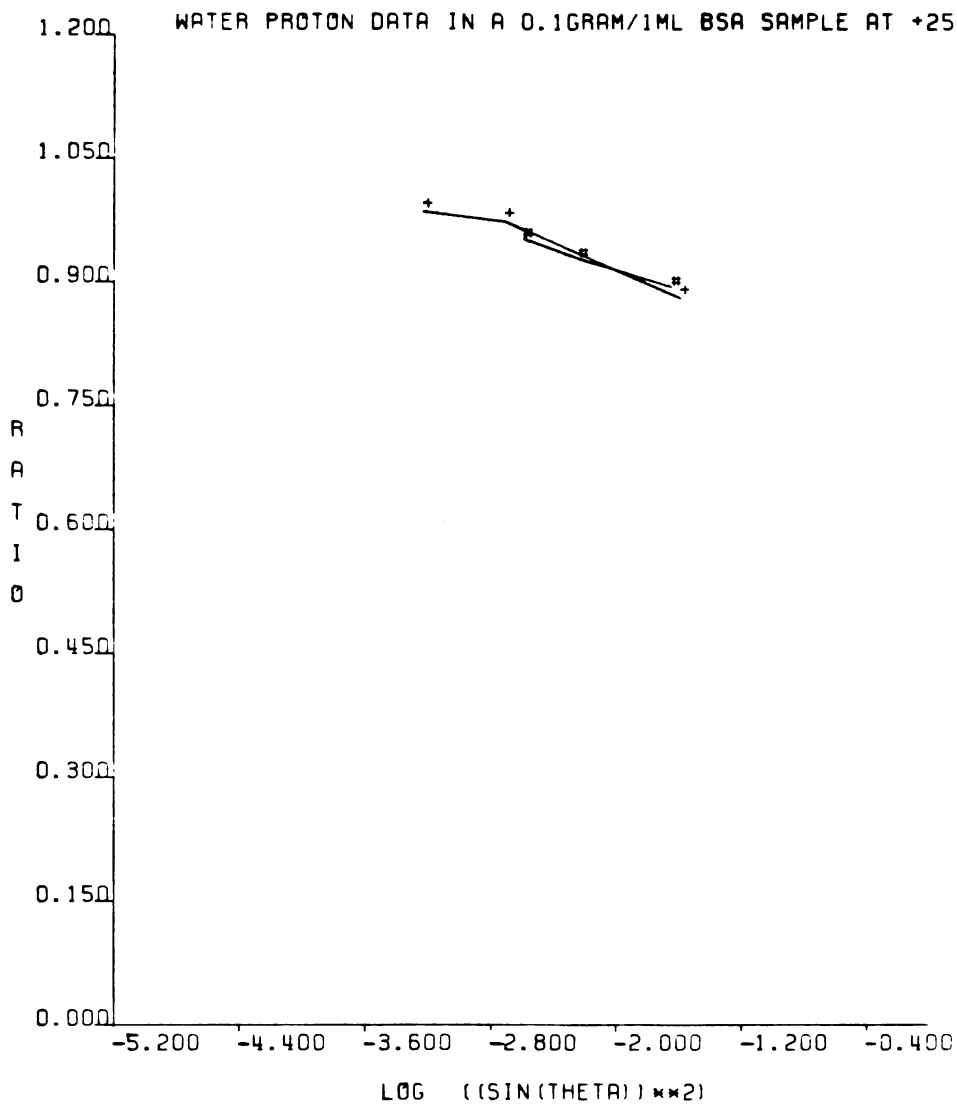

Fig. 6.64. Water proton off-resonance data in a 0.1 g/1ml BSA sample at +25.4°C. (+) H_1 field of 0.12 g; (#) H_1 field of 0.72 g.

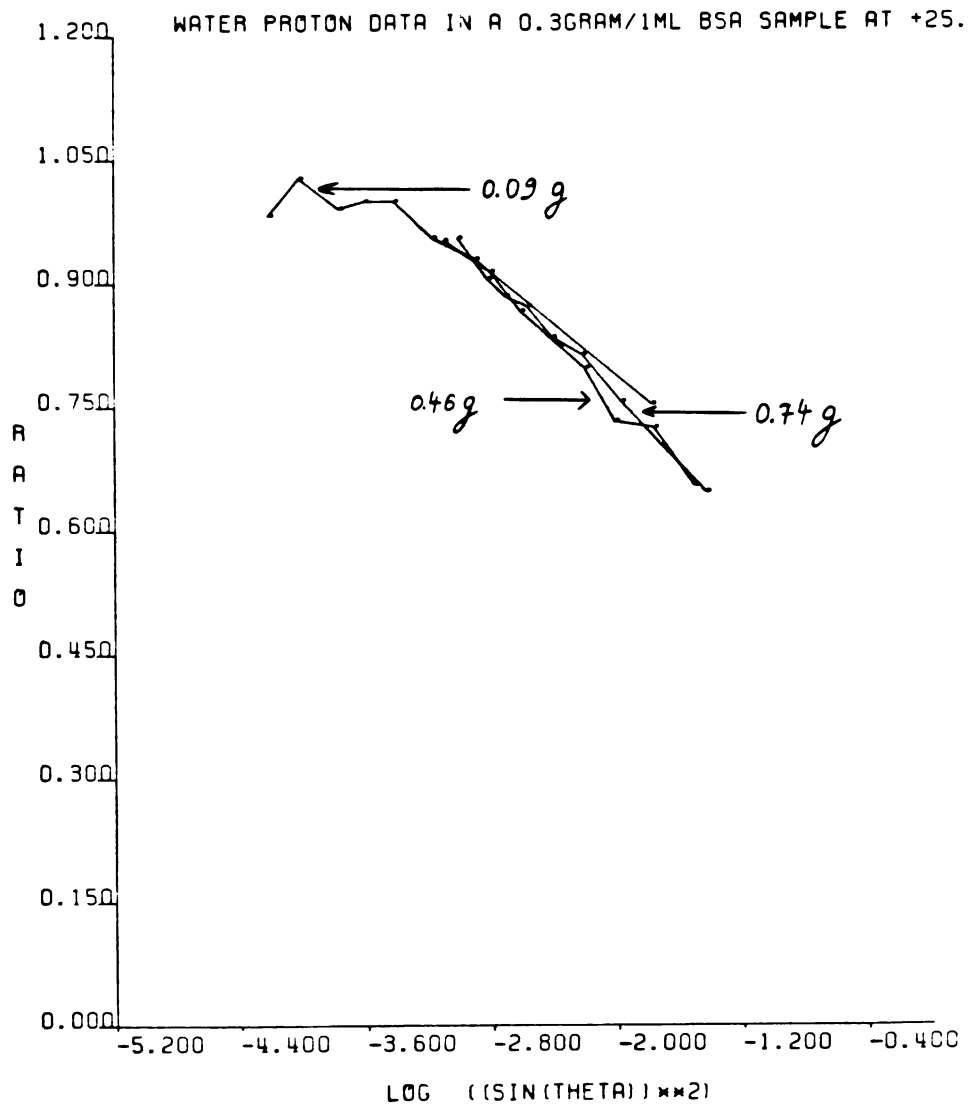

Fig. 6.65. Water proton off-resonance data in a 0.3 g/1ml BSA sample at +25.1°C. The arrows with the numbers indicate the H_1 field strengths in units of Gauss (g).

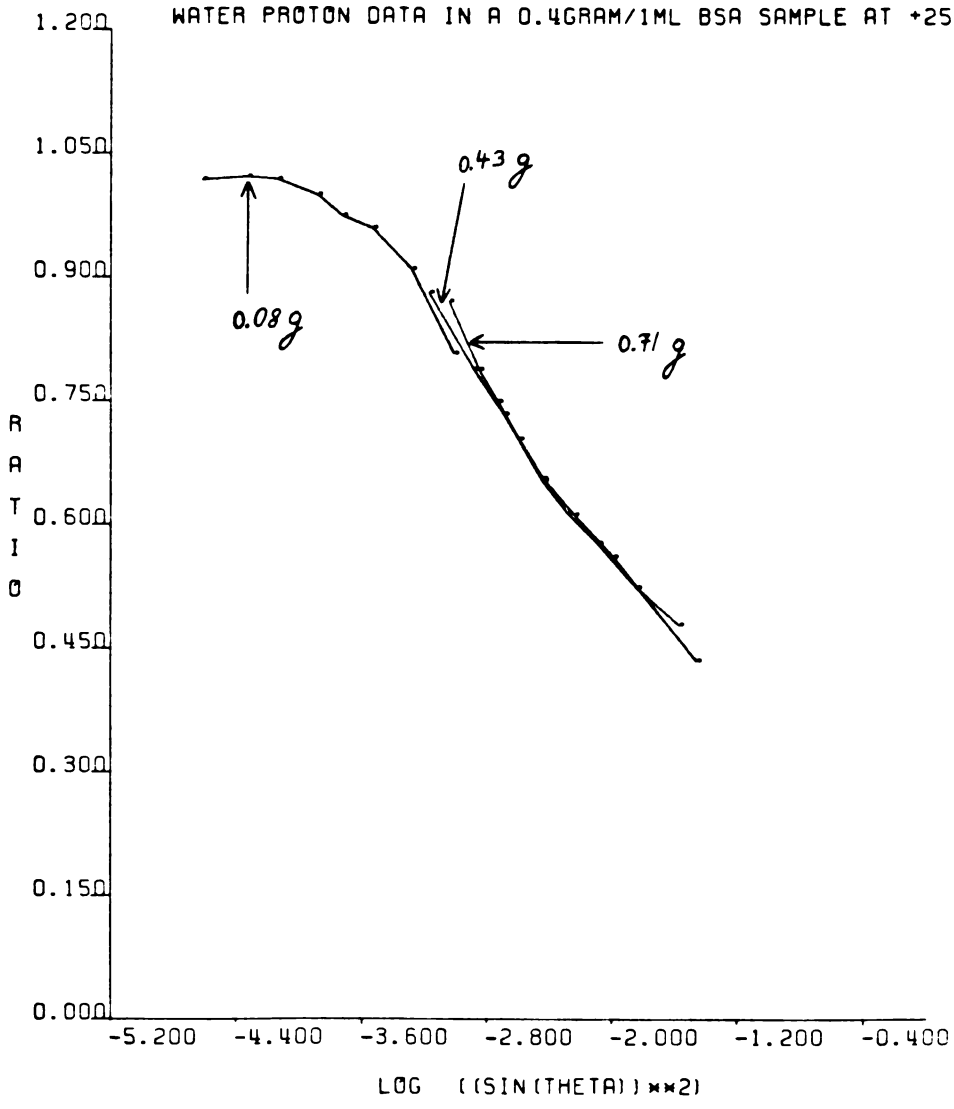

Fig. 6.66. Water proton off-resonance data in a 0.4 g/1ml BSA sample at +25.0°C. The arrows with the numbers indicate the H_1 field strengths in units of Gauss (g).

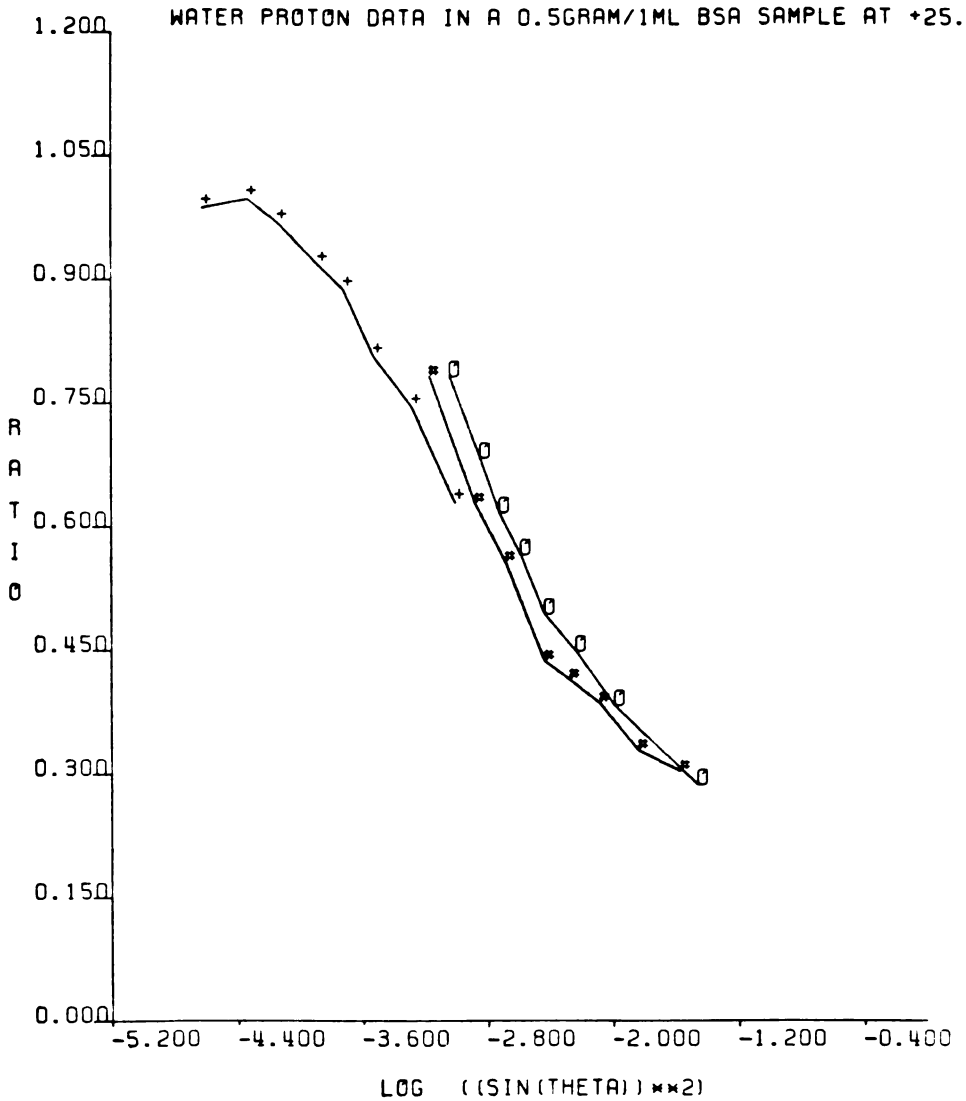

Fig. 6.67. Water proton off-resonance data in a 0.5 g/1ml BSA sample at +25.0°C. (+) H_1 field of 0.08 g; (#) H_1 field of 0.43 g; (0) H_1 field of 0.71 g.

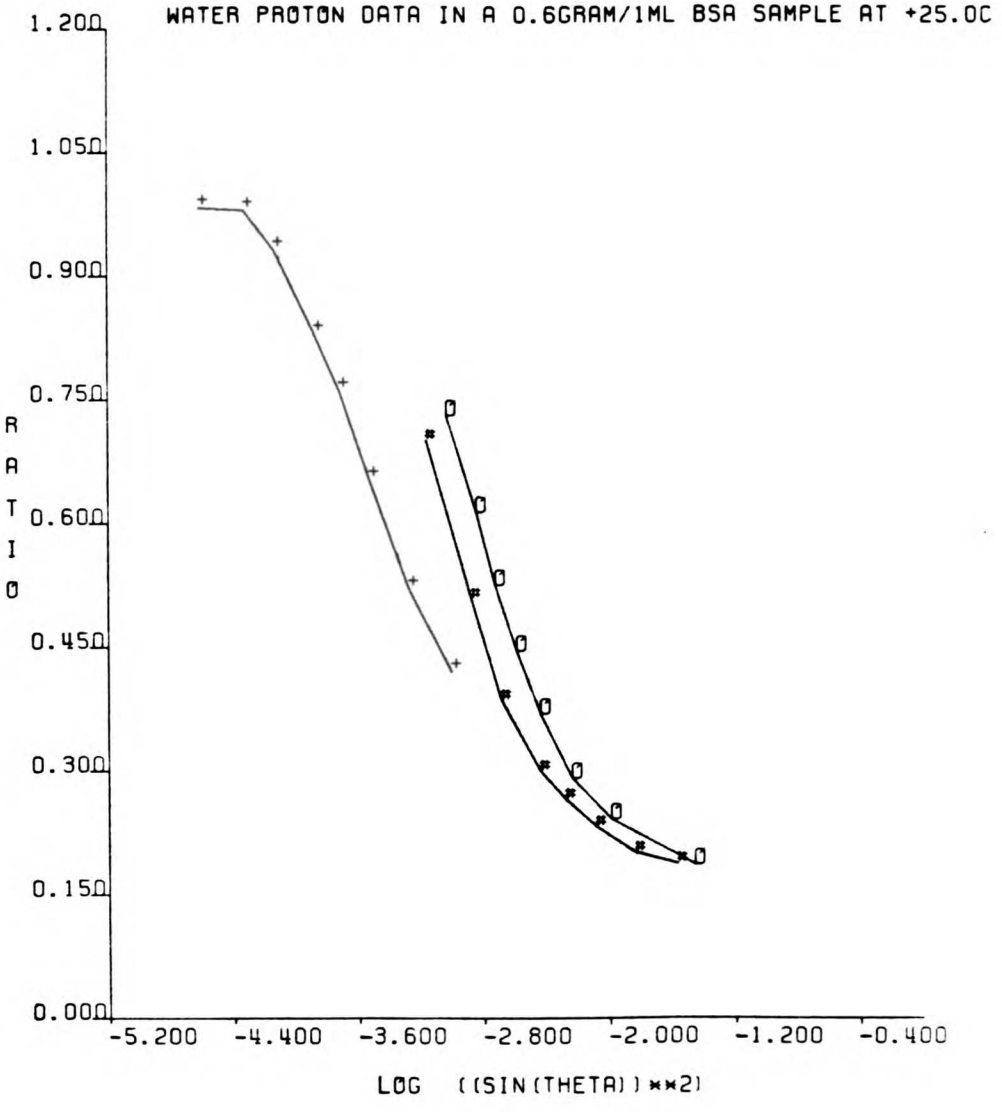

Fig. 6.68. Water proton off-resonance data in a 0.6 g/1ml BSA sample at +25.0°C. (+) H_1 field of 0.08 g; (#) H_1 field of 0.43 g; (0) H_1 field of 0.71 g.

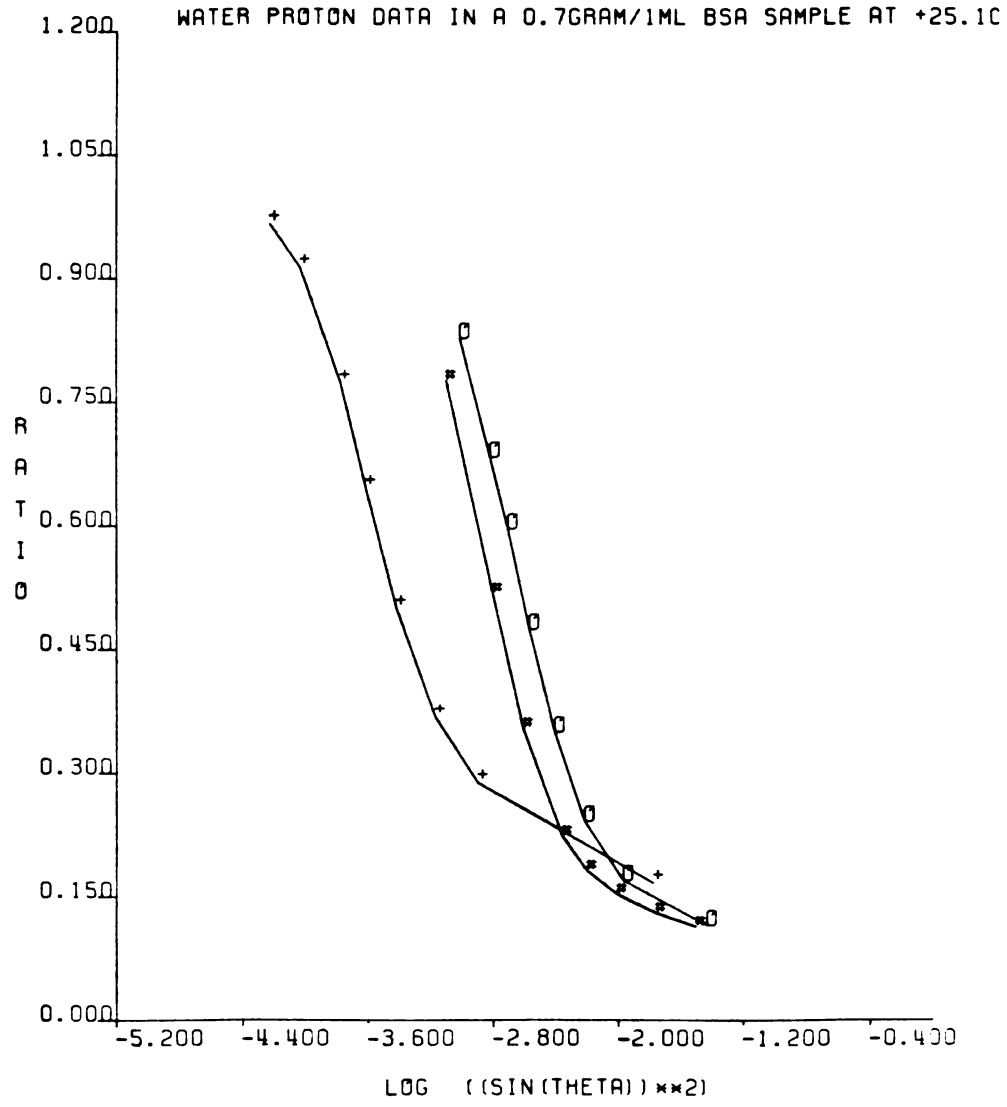

Fig. 6.69. Water proton off-resonance data in a 0.7 g/1ml BSA sample at +25.1°C. (+) H_1 field of 0.09 g; (#) H_1 field of 0.47 g; (0) H_1 field of 0.73 g.

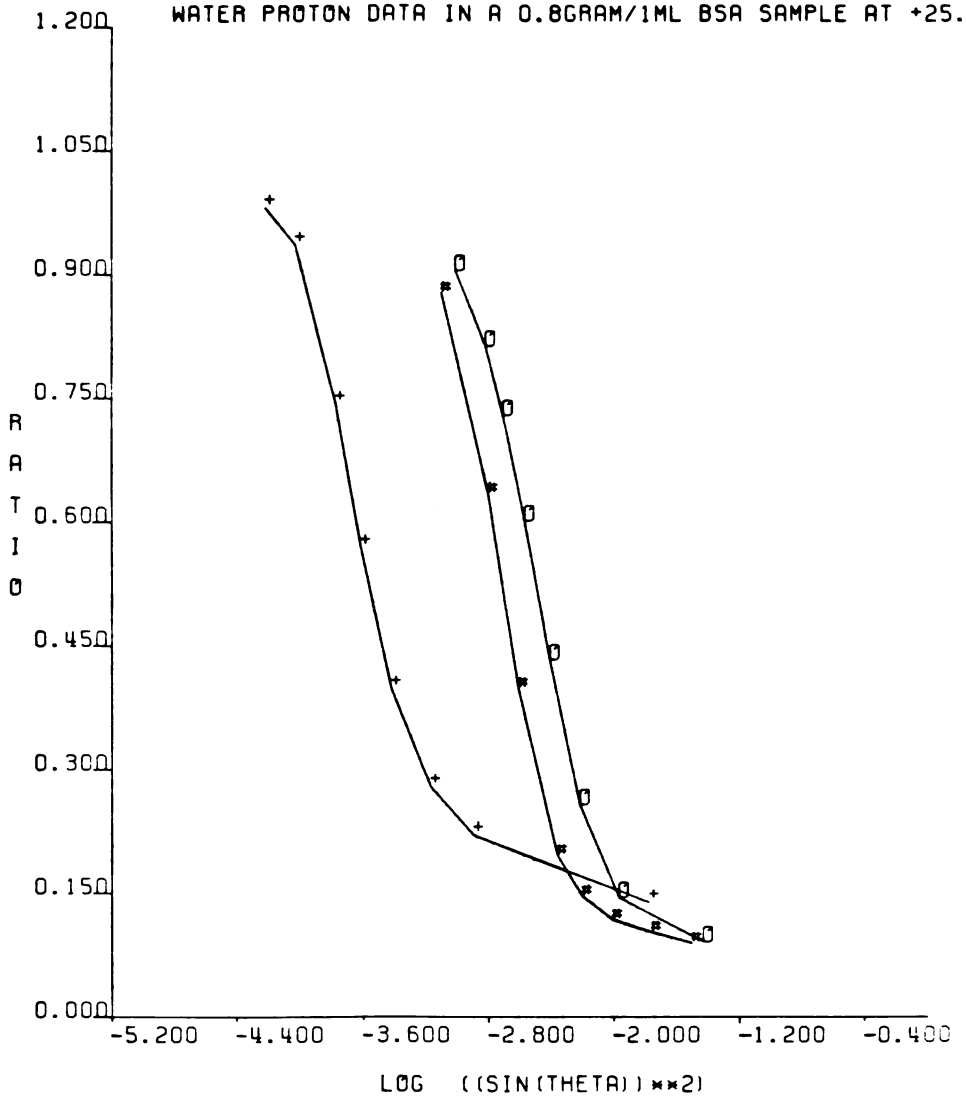

Fig. 6.70. Water proton off-resonance data in a 0.8 g/1ml BSA sample at +25.1°C. (+) H_1 field of 0.09 g; (#) H_1 field of 0.47 g; (0) H_1 field of 0.73 g.

dependent. At the two highest concentrations (0.7 g/1 ml and 0.8 g/1 ml) cross-over points are seen.

The results summarized in Figures 6.63-6.70 show that a slow motion and/or process is present in the BSA solutions. The relative contribution of the slow component is very small when the protein concentration is below ∿0.3 g/1 ml, but it increases progressively as the protein concentration is increased above ∿0.3 g/1 ml.

Two mechanisms, which may be important in solution, should be considered:

1. rotation of the protein, and
2. protein aggregation.

Experimental results show that, at least qualitatively, the water molecules reflect the rotational correlation time (τ_r) of the macromolecules in solution (70). Slowing down of the protein rotation as the macromolecule concentration increases may explain, qualitatively, the observations in the first concentration range (0.05 g/1 ml to 0.4 g/1 ml). Protein rotation may slow down as its concentration increases, because viscosity increases and/or aggregation takes place. If water molecules reflect protein rotation and if this rotation slows down with increasing protein concentration, the dependence of the values of R on $\sin^2\theta$ is

expected to increase and the curves are expected to shift to the left, as the protein concentration increases. These are the observed effects, up to a concentration of 0.4 g/1 ml.

We conducted experiments on lysozyme solutions of 0.3 g/1 ml at +20° ± 1°C at pH = 2.9 and pH = 5.4. The data are shown in Figure 6.71. The degree of aggregation of lysozyme in this pH range is known to increase as the pH is raised. If the water reflects the effective molecular weight of the macromolecule, increasing aggregation at pH = 5.4 is expected to show as an increase in the effective correlation time of the water. The $\sin^2\theta$ dependence is expected to increase and the curves are expected to move to the left side of the graph. As can be seen from Figure 6.71, at pH = 5.4 the R's become $\sin^2\theta$ dependent and the curves move to the left. No H_1 field dependence is seen. These results show that aggregation effects may contribute to off-resonance data.

Oakes (14) measured the water proton T_1 and T_2 relaxation times of BSA solutions at several temperatures and concentrations. Oakes suggested that the protein molecules associate at concentrations above 10%.

James et al. (78) performed off-resonance experiments on a series of BSA solutions at different concentrations. The R values of the ^{13}C carbonyl peak were monitored. The results indicated that the effective

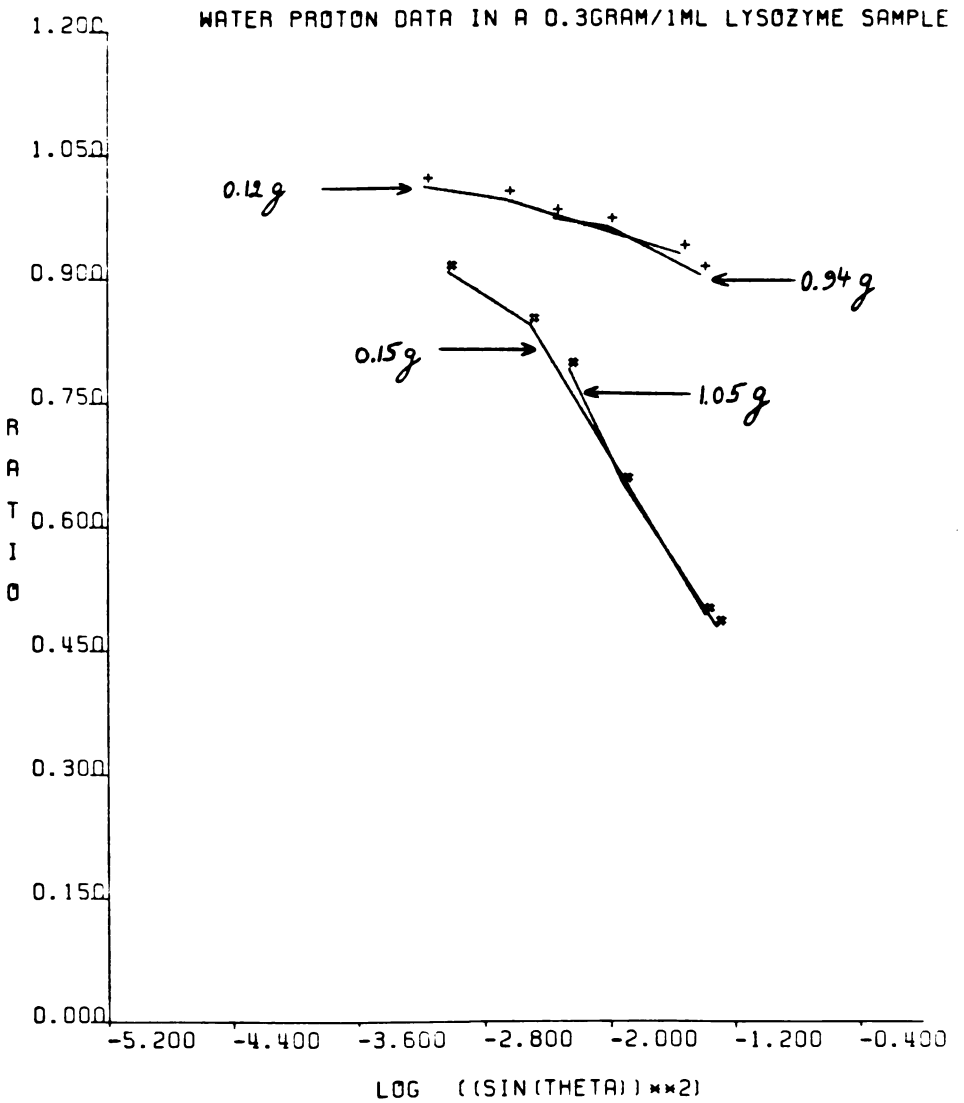

Fig. 6.71. Water proton off-resonance data in a 0.3 g/1ml lysozyme sample at +20°C at two pH's. (+) pH = 2.9; (#) pH = 5.4. The arrows with the numbers indicate the H_1 field strengths in units of Gauss (g).

rotational correlation times become longer with increasing BSA concentration.

BSA aggregation is likely to be affecting our results throughout the investigated concentration range (except possibly in the two least concentrated samples), but we cannot separate this effect from other effects.

At a concentration of 0.5 g/1 ml an H_1 field dependence appears. The field dependence increases at the higher concentrations. We showed in the previous section that if one tries to obtain theoretical fits using equations that assume a simple isotropic rotation, a correlation time is required with an apparent value longer than microseconds. It is unreasonable that such slow rotational motion exists in solution. In the 0.8 g/1 ml sample, where the field dependence is the highest, $T_2 \approx 13$ msec. This value is much longer than we would expect if correlation times longer than microseconds were present, even if only a small fraction of the protons were involved at any one instant.

In Section 6.2.4 we provided direct evidence, based on T_2 versus temperature profiles and $T_{1\rho}^{on}$ dispersion curves, that an exchange process is present in BSA solutions at temperatures above 0°C. An exchange process may also contribute to the off-resonance data in solutions.

Figure 6.72 shows plots of T_1 and T_2 relaxation times versus the protein concentration. T_1's were measured by the zero-point method and T_2's were calculated from the experimental absorption linewidths. The T_1 and T_2 data were taken from Table 6.18.

Straight lines are obtained for both T_1 and T_2. When extrapolated to zero protein concentration, both relaxation times give values shorter than the values of $\sim$3.5 sec for pure water. This most likely is caused by dissolved oxygen. The fact that the data points fall on a straight line down to a concentration of $\sim$0.1 g/1 ml indicates that, in the investigated concentration range, the relaxation is dominated by the presence of the macromolecule, rather than by the dissolved oxygen.

Off-resonance data were obtained for the 0.8 g/1 ml BSA sample at four different temperatures: +5.0°C, +15.2°C, +25.1°C, and +45.0°C. The results are illustrated in Figures 6.73-6.76. The data in the figures show that the curves at all temperatures are similar and the temperature dependence is very small.

Since R is proportional to $T_{1\rho}^{off}/T_1$, the values of R will remain constant, or change only little, if the two relaxation times change in the same direction and by a similar factor (see Chapter 2, Section 2.6). It is possible that changing the temperature, in the range $\sim$+5°C to $\sim$+45°C, affects the BSA solutions in

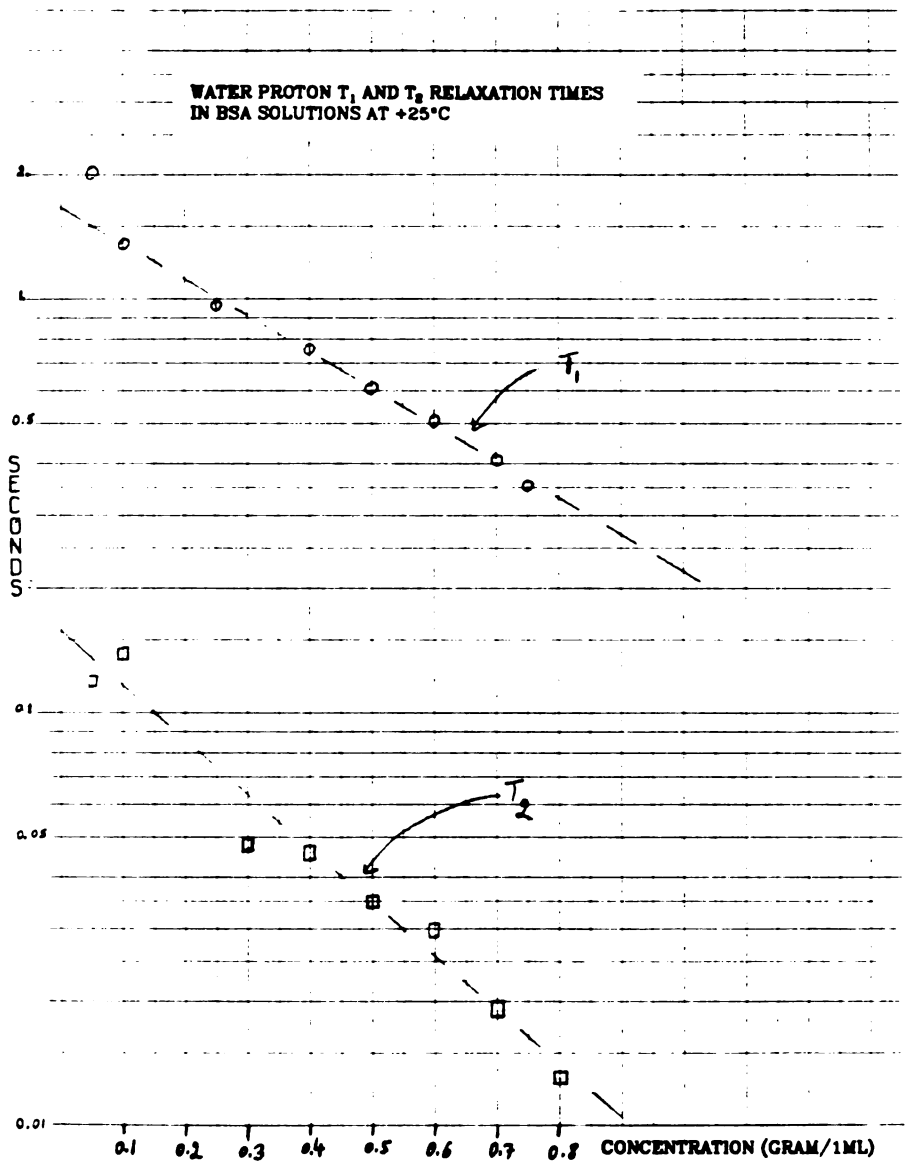

Fig. 6.72. Water proton T_1 and T_2 relaxation times at 100 MHz vs. the concentration of the protein in BSA solutions at +25 ± 1°C. Data taken from Table 6.18.

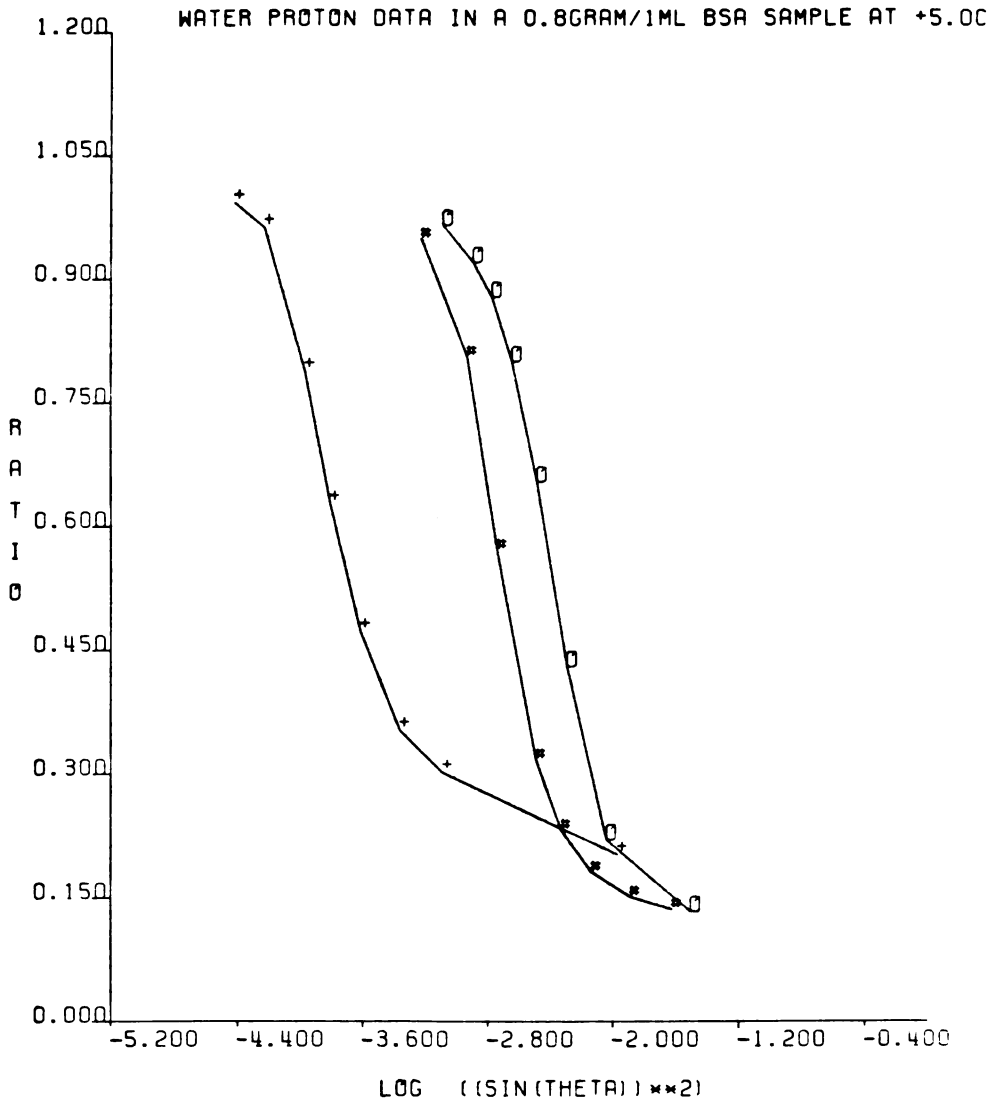

Fig. 6.73. Water proton off-resonance data in a 0.8 g/1ml BSA sample at +5.0°C. (+) H_1 field of 0.07 g; (#) H_1 field of 0.40 g; (0) H_1 field of 0.68 g.

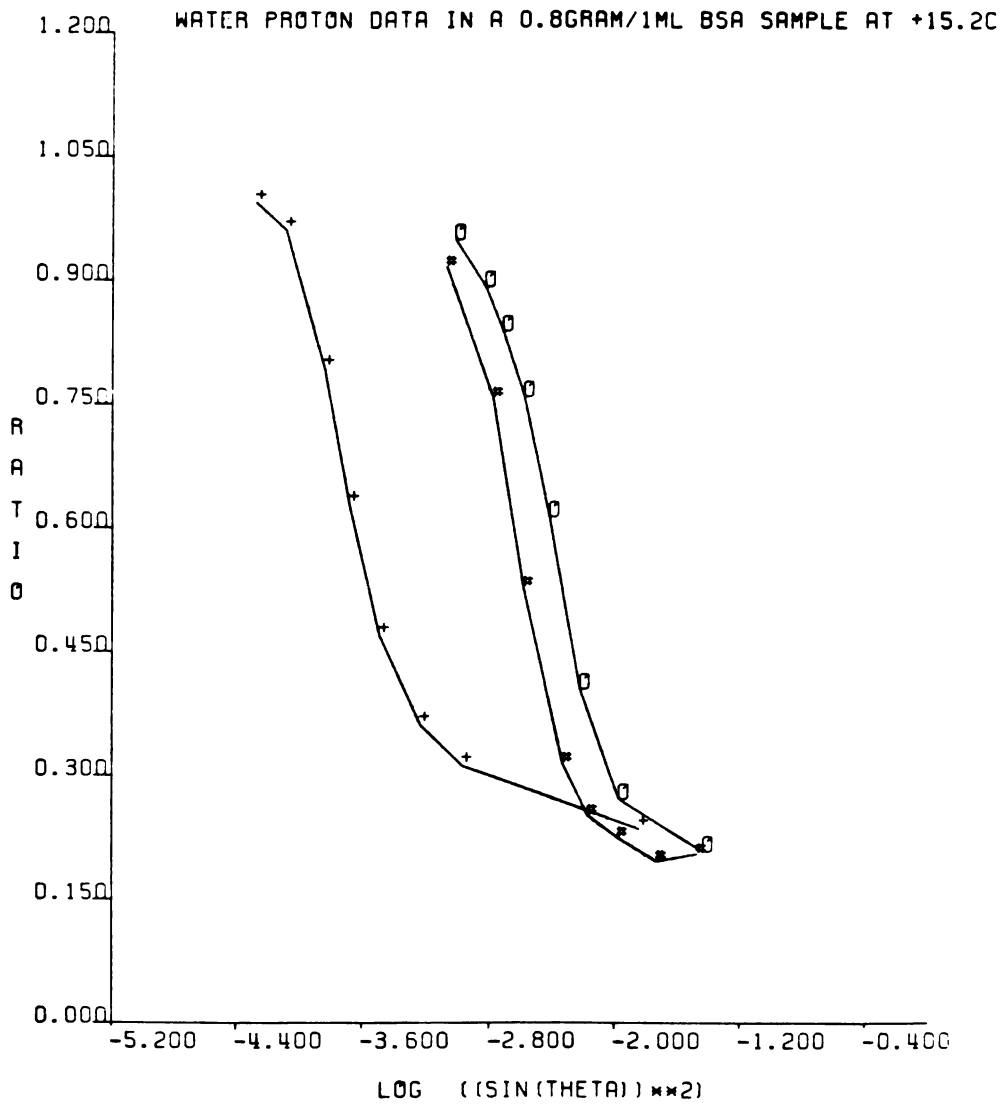

Fig. 6.74. Water proton off-resonance data in a 0.8 g/1ml BSA sample at +15.2°C. (+) H_1 field of 0.09 g; (#) H_1 field of 0.49 g; (0) H_1 field of 0.73 g.

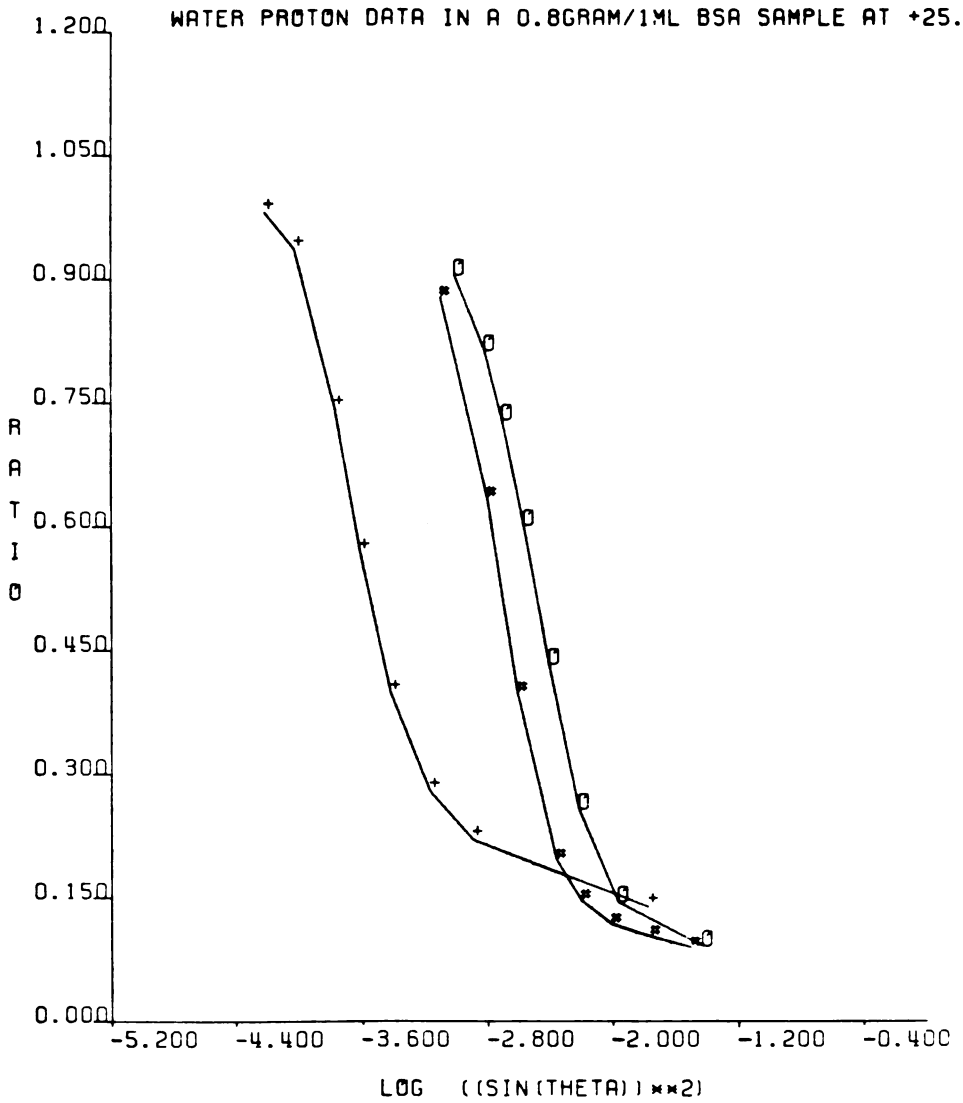

Fig. 6.75. Water proton off-resonance data in a 0.8 g/1ml BSA sample at +25.1°C. (+) H_1 field of 0.09 g; (#) H_1 field of 0.47 g; (O) H_1 field of 0.73 g.

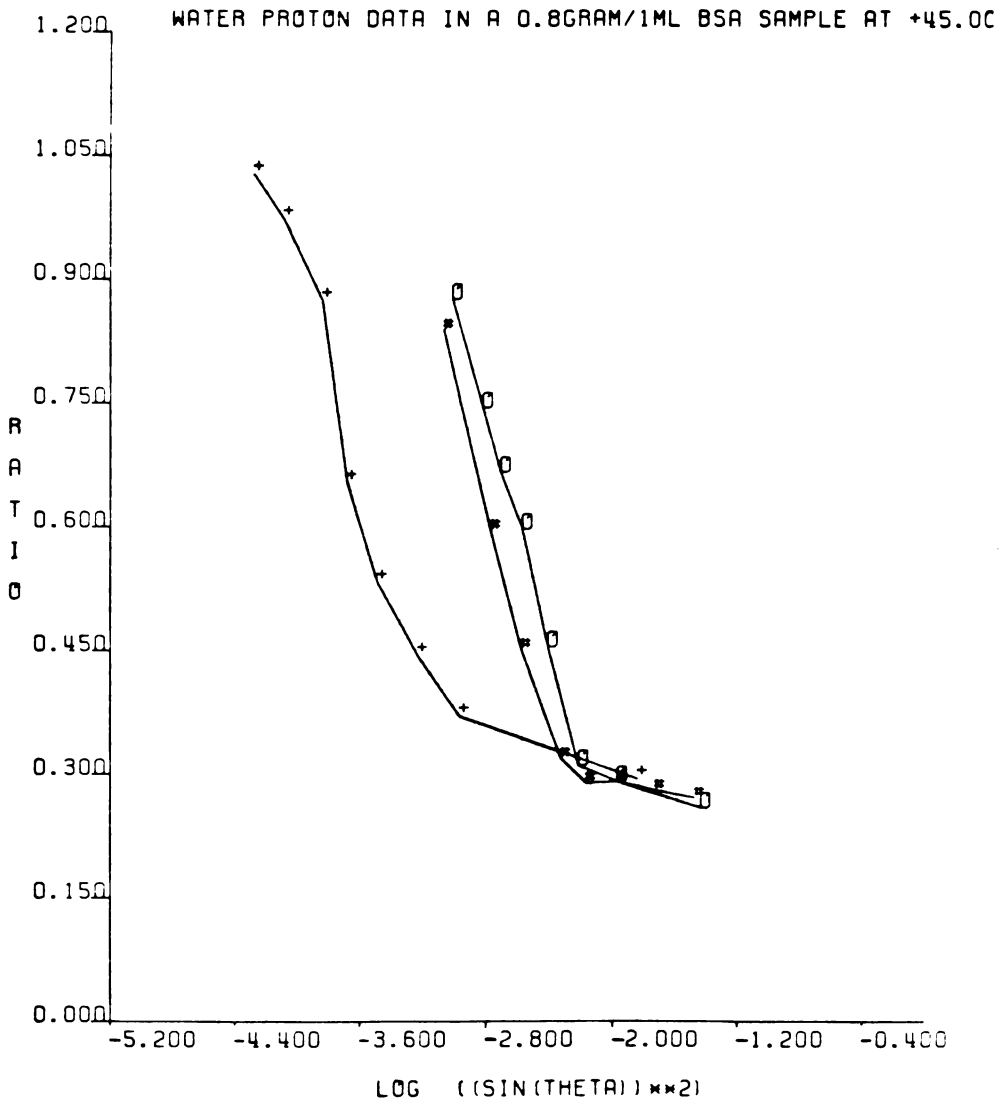

Fig. 6.76. Water proton off-resonance data in a 0.8 g/1ml BSA sample at +45.0°C. (+) H_1 field of 0.09 g; (#) H_1 field of 0.49 g; (O) H_1 field of 0.73 g.

such a way that the effective $T_{1\rho}^{off}$ and T_1 relaxation times change in the same direction and by a similar factor. In such a case the R versus $\sin^2\theta$ plots are expected to be temperature independent, or their temperature dependence may be very small.

The off-resonance data of the BSA solutions at room temperature were subjected to Lorentzian fits (see previous section), using the Nicolet TT-100 data processor. The resulting linewidths and the calculated values of T_2' are reported in Table 6.18. The table also lists the experimental T_1 and T_2 values. The T_2 values were calculated from the linewidths of the experimental absorption peaks. For samples that showed H_1 field dependence, T_2' values were calculated at the highest and at the lowest fields used, for each sample. The last entry lists data for a BSA solution at +5.0°C.

At all H_1 fields, the calculated values of T_2' are much shorter than the experimental T_2 values. In samples that show H_1 field dependence, the values of T_2' at the lower fields are always much shorter than their values at the higher fields.

In the frozen BSA sample, a good agreement between the values of T_2' and T_2 was obtained at $H_1 \approx 0.7$ g (see Table 6.15). In the BSA solutions, the highest H_1 fields were of a similar strength. It appears that in solutions H_1 fields stronger than

Table 6.18. $\nu_{1/2}$, T_2 and T_2' values at 100 MHz for the water proton in BSA solutions.

BSA (g/1ml)	H_1 (g)	$\nu_{1/2}$[2],[3] (KHz)	T_1 (msec)	T_2[3] (msec)	T_2'[3] (msec)
0.05	0.72	41 ± 12	2000	118 ± 35	45.4 ± 13.6
0.1	0.72	93 ± 28	1360	138 ± 41	5.9 ± 1.8
0.3	0.74	82 ± 25	964	48 ± 14	5.7 ± 1.7
0.4	0.71	116 ± 35	757	46 ± 14	2.1 ± 0.6
0.5	0.71	139 ± 42	607	35 ± 11	1.2 ± 0.4
	0.08	21 ± 6			0.64 ± 0.19
0.6	0.71	148 ± 44	507	29 ± 9	0.84 ± 0.25
	0.08	28 ± 8			0.30 ± 0.09
0.7	0.73	119 ± 36	414	18 ± 5	1.1 ± 0.3
	0.09	40 ± 12			0.16 ± 0.05
0.8	0.73	92 ± 28	357	13 ± 4	1.7 ± 0.5
	0.09	42 ± 13			0.12 ± 0.04
0.8[1]	0.68	67 ± 20	286	9 ± 3	2.2 ± 0.7
	0.07	40 ± 12			0.07 ± 0.02

[1]Data obtained at +5.0°C.

[2]Calculated using the Nicolet TT-100 data processor.

[3]Reported errors are estimates.

$\sim$0.7 g are needed to achieve agreement between the T_2' and the T_2 values.

The 0.8 g/1 ml BSA solution at room temperature (Figure 6.75) and the frozen 0.5 g/1 ml BSA sample (Figure 6.46) show similar effects. The curves are located in similar positions on the graph, the values of R are H_1 field (and $\sin^2\theta$) dependent, and cross-over points are present. The H_1 field dependence of the two samples differs only little.

In the previous section we suggested that local dipolar fields which do not average out to zero may be responsible for some of the observed effects. We do not know if such local dipolar fields are also present in the macromolecule solutions. More experimental and theoretical work is needed to find out the precise causes of the observed effects and to establish whether the apparently similar effects in the concentrated and the frozen macromolecule solutions are caused by similar mechanisms.

6.3.4 BSA in Mixed Aqueous and Organic Solvents

The off-resonance experiments may be applied to systems where several peaks have to be monitored simultaneously (10). Such systems are, for example, macromolecule solutions with a mixed aqueous and organic solvent. Addition of the third component may be required

to investigate the role of the water in "guiding" the protein in its folding path and in stabilizing the protein in its native conformation (2).

We obtained off-resonance data at ν_0 = 100 MHz on a series of BSA solutions containing different organic solvents as the third component. Our main objective was to show that large enough NMR effects may be present to allow the detection of a preferential interaction of one of the components with the macromolecule.

Preliminary experiments showed that the amount of the protein that could be incorporated into the water plus organic solvents without visual precipitation was roughly proportional to the polarity of the organic component. The higher the polarity of the organic component, the higher the concentration of the protein that could be used.

For these experiments the off-resonance frequency was centered between the peaks. The error introduced by this procedure in the actual off-resonance frequency of each peak was negligible and no corrections were applied.

Figures 6.77-6.83 illustrate off-resonance data for BSA in mixtures of water and organic solvents. Concentration of the organic solvents is reported in units of percentage volume/volume. The concentration of BSA is reported in units of grams BSA per 1 milliliter of

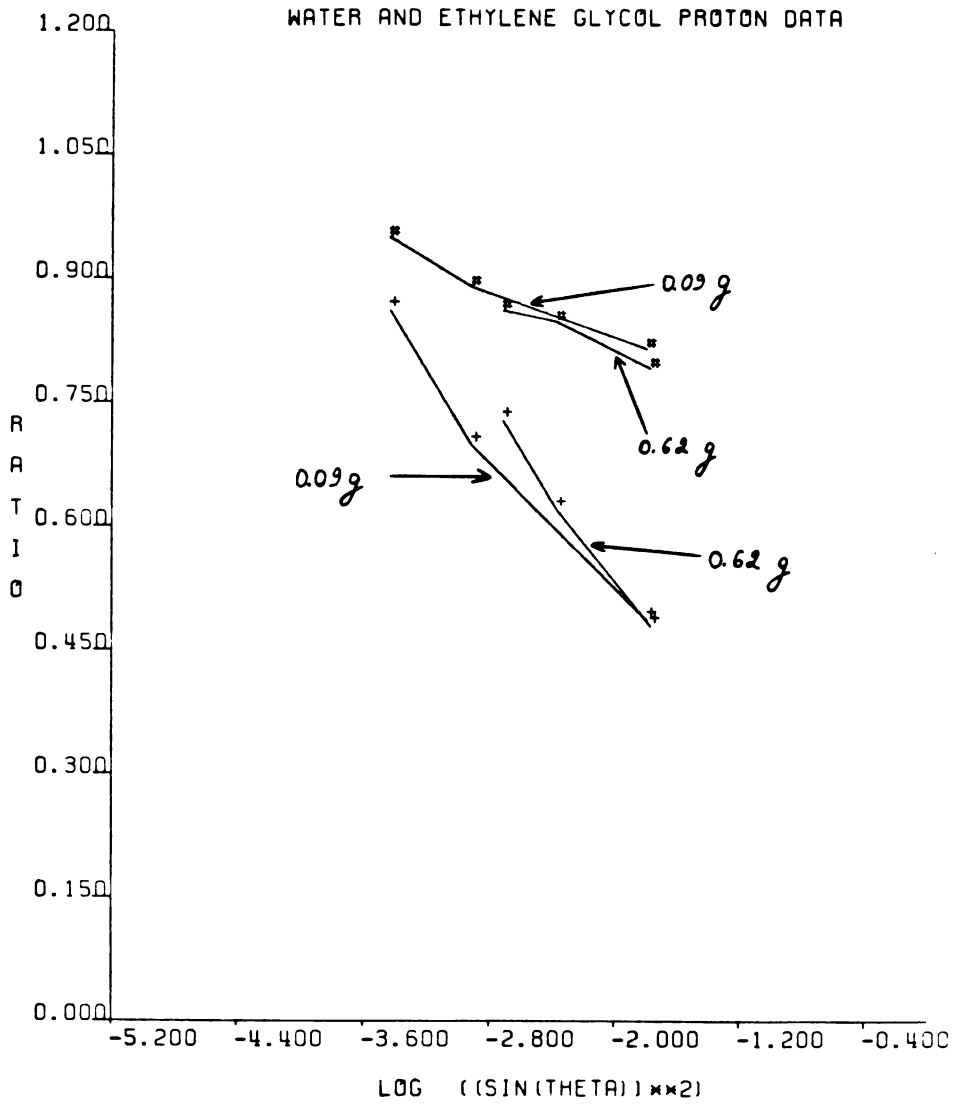

Fig. 6.77. Water (+) and ethylene glycol (#) off-resonance proton data in a three component system at +24.8°C. The sample contained 0.3 g/1ml BSA in a mixture of 50% water and 50% ethylene glycol. The arrows with the numbers indicate the H_1 field strengths in units of Gauss (g).

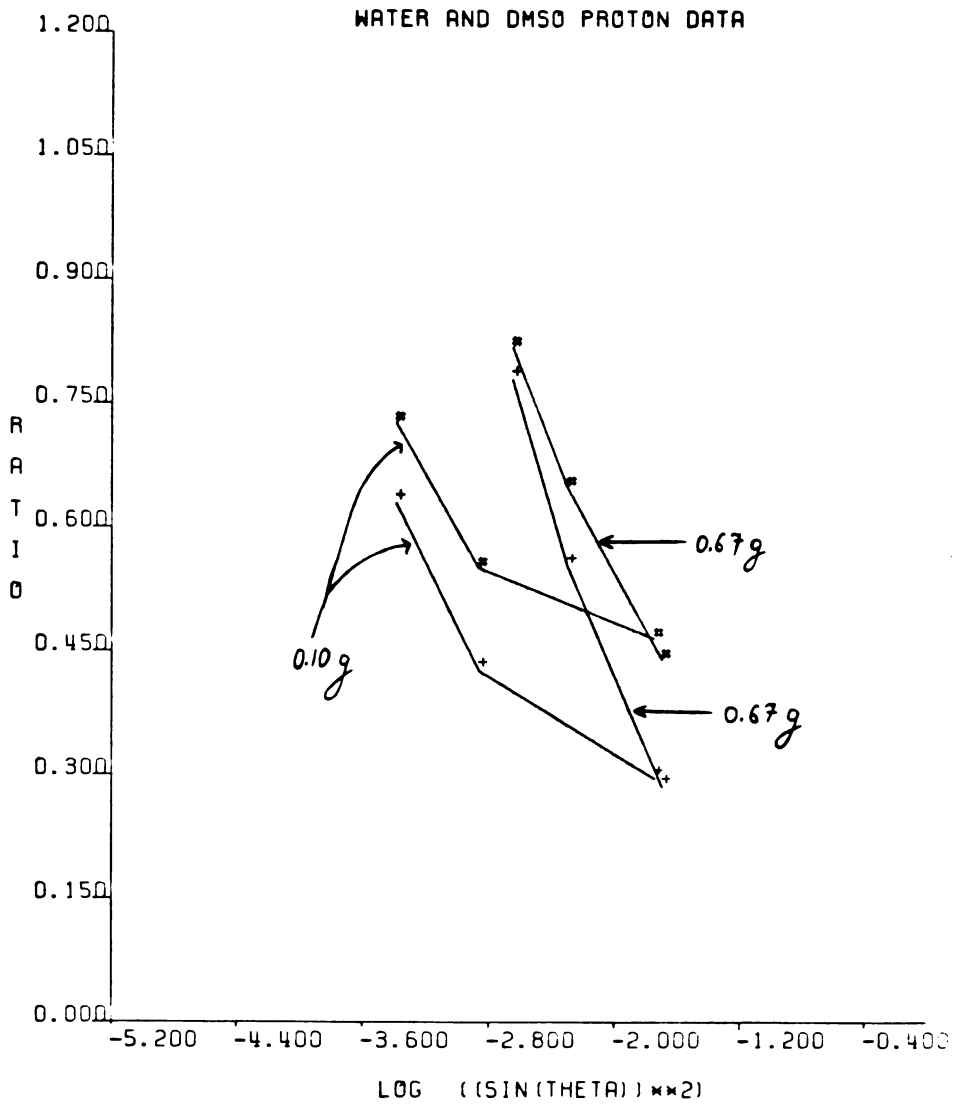

Fig. 6.78. Water (+) and DMSO (#) off-resonance proton data in a three component system at +22.0°C. The sample contained 0.3 g/1ml BSA in a mixture of 60% water and 40% DMSO. The arrows with the numbers indicate the H_1 field strengths in units of Gauss (g).

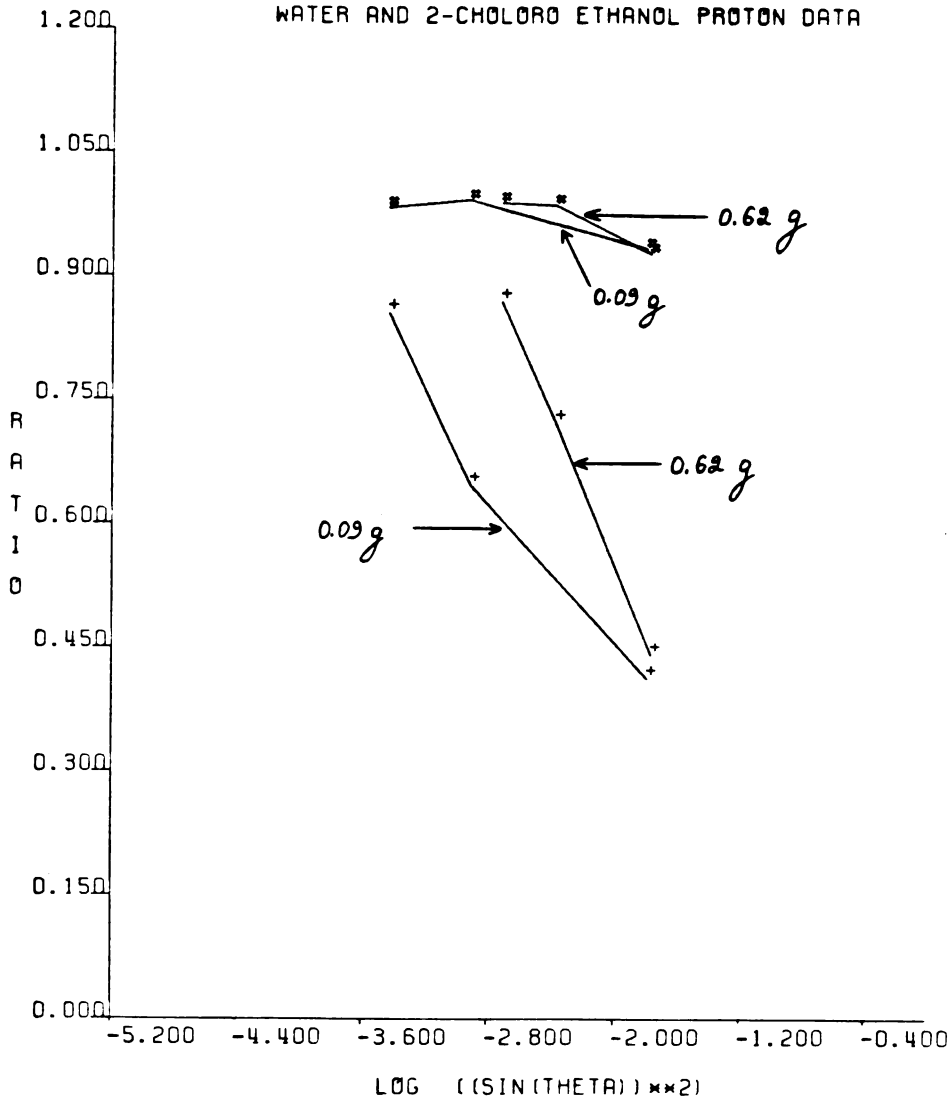

Fig. 6.79. Water (+) and 2-chloro ethanol (#) off-resonance proton data in a three component system at +24.8°C. The sample contained 0.3 g/1ml BSA in a mixture of 70% water and 30% 2-chloro ethanol. The arrows with the numbers indicate the H_1 field strengths in units of Gauss (g).

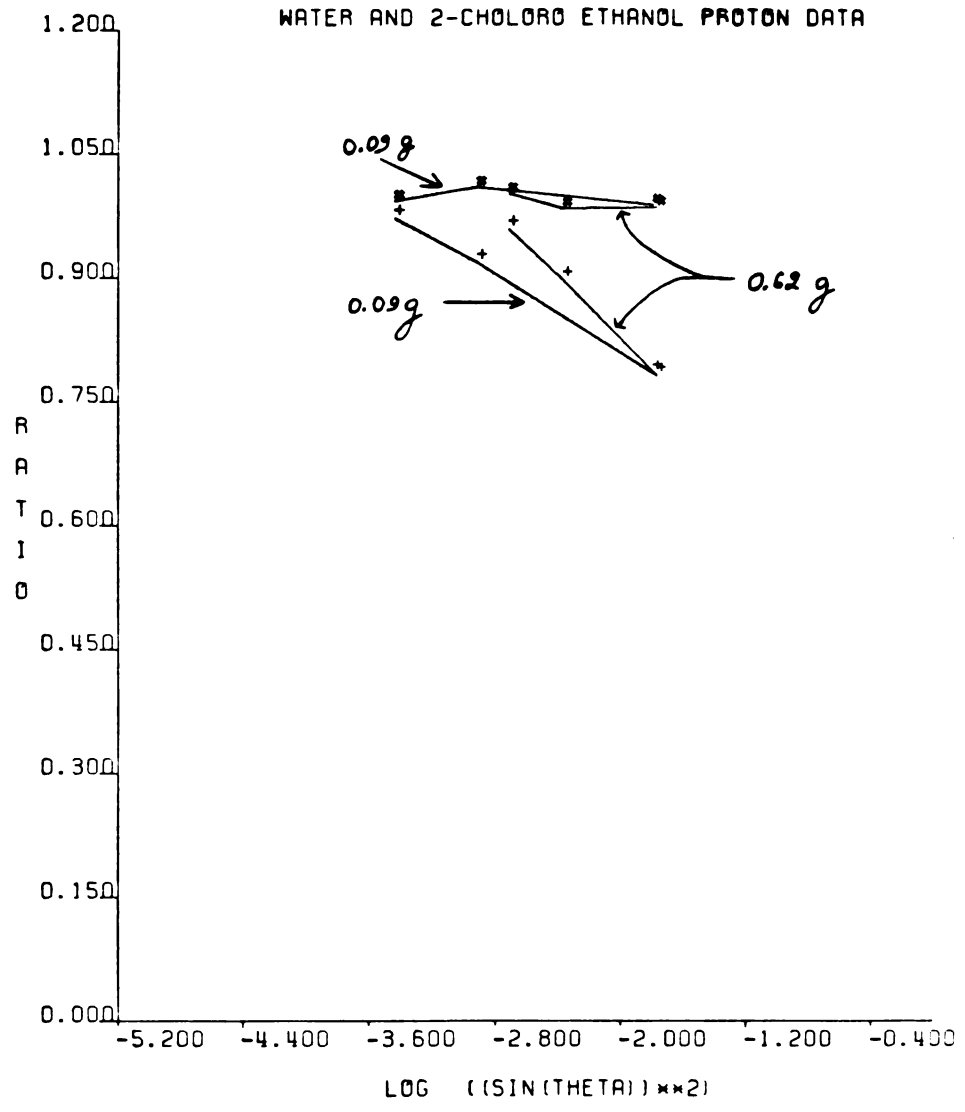

Fig. 6.80. Water (+) and 2-chloro ethanol (#) off-resonance proton data in a three component system at +24.8°C. The sample contained 0.3 g/1ml BSA in a mixture of 50% water and 50% 2-chloro ethanol. The arrows with the numbers indicate the H_1 field strengths in units of Gauss (g).

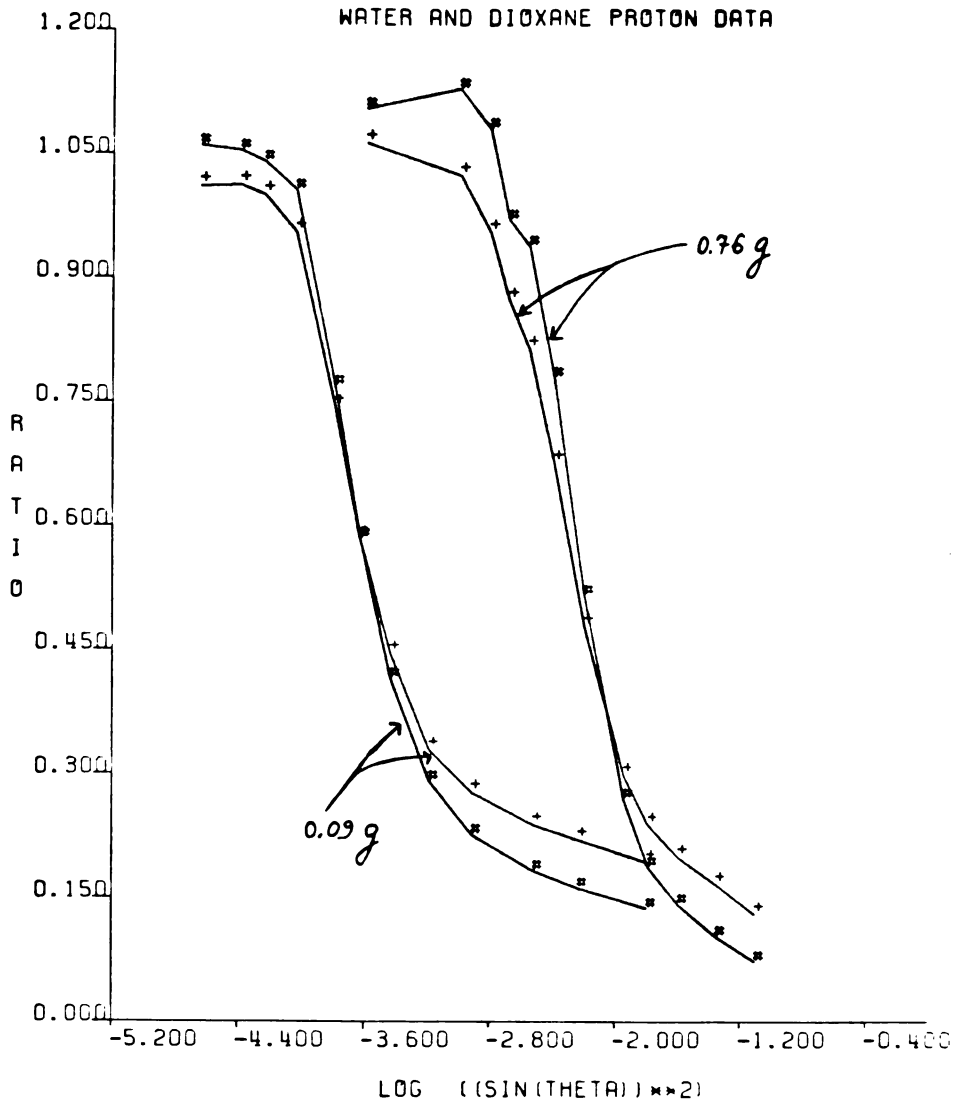

Fig. 6.81. Water (+) and dioxane (#) off-resonance proton data in a three component system at −14.0°C. The sample contained 0.25 g/1ml BSA in a mixture of 50% water and 50% dioxane. The arrows with the numbers indicate the H_1 field strengths in units of Gauss (g).

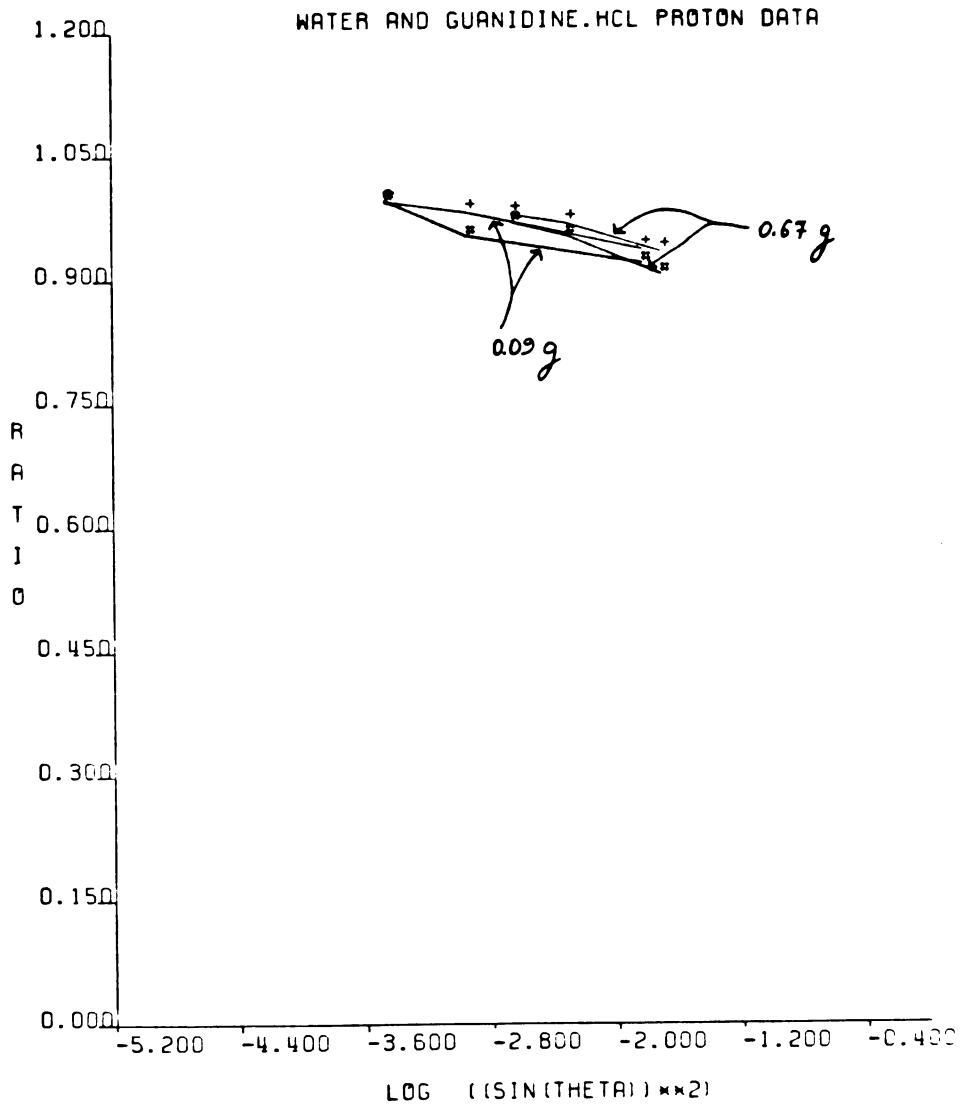

Fig. 6.82. Water (+) and guanidine·HCL (#) off-resonance proton data in a three component system at +21.2°C. The sample contained 0.3 g/1ml BSA in a mixture of water and ~10M guanidine·HCL. The sample also contained ~0.2 moles of dithiothreitol to prevent gelling. The arrows with the numbers indicate the H_1 field strengths in units of Gauss (g).

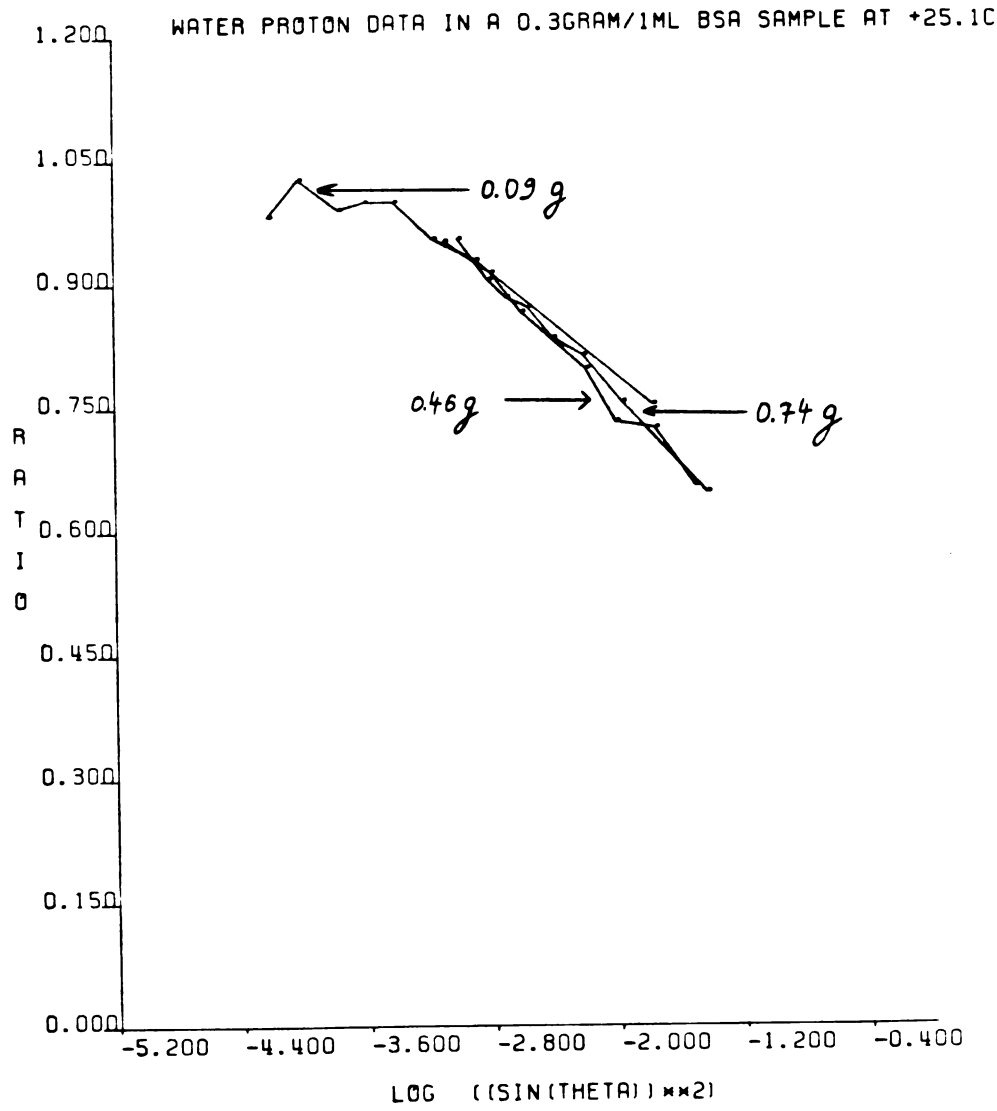

Fig. 6.83. Water proton off-resonance data in a 0.3 g/1ml BSA sample at +25.1°C. The arrows with the numbers indicate the H_1 field strengths in units of Gauss (g).

the water plus organic mixture. Figure 6.77 shows data for a sample of 0.3 g/1 ml BSA in 50% ethylene glycol at +24.8°C. Figure 6.78 shows data for a sample of 0.3 g/1 ml BSA in 40% dimethyl sulfoxide (DMSO) at +22.0°C. Figure 6.79 shows data for a sample of 0.3 g/1 ml BSA in 30% 2-chloro ethanol (2-ClEt) at +24.8°C. Figure 6.80 shows data for a sample of 0.3 g/1 ml BSA in 50% 2-ClEt at +24.8°C. The 2-ClEt peaks apepared as a multiplet. Within the experimental error, the components of the multiplet had identical R versus $\sin^2\theta$ plots and identical T_1 values. Figure 6.81 shows data for a sample of 0.25 g/1 ml BSA in ∿50% dioxane at -14.0°C. The concentration of dioxane was estimated from the number of drops added to a 0.5 g/1 ml BSA solution in water. Figure 6.82 shows data for a sample of 0.3 g/1 ml BSA to which ∿10 M guanidine-HCl was added. The sample also contained 33 mg (∿0.2 moles) of dithiothreitol (DTT). DTT reduces -SH bonds (79) and it prevented gelling of the sample for a few days. Data were taken before gelling occurred. For comparison, the off-resonance data of a 0.3 g/1 ml BSA in water sample is shown in Figure 6.83.

Table 6.19 summarizes the T_1 values of the water and the organic peaks in the three component systems and lists the ratios organic peak T_1/water

Table 6.19. Water proton T_1, organic proton T_1 and organic T_1/water T_1 values at 100 MHz.

Sample	Water T_1[1] (sec)	Organic T_1[1] (sec)	$\frac{\text{Organic } T_1}{\text{Water } T_1}$
0.3g/1ml BSA In 50% Ethylene Glycol	0.32	0.49	1.5
0.3g/1ml BSA In 40% DMSO	0.30	0.57	1.9
0.3g/1ml BSA In 30% 2-ClEt	0.37	0.54[2]	1.5
0.3g/1ml BSA In 50% 2-ClEt	0.24	0.53[2]	2.2
0.3g/1ml In 10M Guanidine·HCl + DTT	0.93	0.93	1.0
0.25g/1ml BSA In ~50% Dioxane	----------[3]		

[1]Estimated by the zero-point method.
[2]Data for the multiplet components were identical.
[3]Data not available.

peak T_1. T_1's were estimated by the zero-point method. For pure water at +25.0°C and 150 MHz T_1 ≈ 3.2 sec.

Inspection of the figures shows that, except for the systems containing dioxane and guanidine, different plots are obtained for the water and the organic component, in each system. In these plots, the R versus $\sin^2\theta$ curves of the water are located below the curves of the organic component, for a given value of H_1 and $\sin^2\theta$. None of the organic peaks, except for DMSO and dioxane, show H_1 field dependence, within the experimental error. These results indicate that the effective correlation time of the water in the presence of a macromolecule and an organic solvent is longer than the effective correlation time of the organic solvent in the same systems. We do not have R versus $\sin^2\theta$ plots for solutions containing water and organic solvents only. Such plots are expected to have no $\sin^2\theta$ and H_1 field dependence, the values of R are expected to be close to unity and the water and the organic components in such plots are expected to be indistinguishable. The differential effects observed in our systems are, therefore, likely to be related to the presence of the macromolecule.

In the system containing 50% ethylene glycol, the water peak's ratios are highly $\sin^2\theta$ dependent, but show only a small H_1 field dependence. The values of R

for ethylene glycol are only moderately $\sin^2\theta$ dependent and no H_1 field dependence is seen.

In the system containing DMSO, a large H_1 field dependence is observed for both the water and the DMSO. The values of R for both components are highly $\sin^2\theta$ dependent and the plots are very similar.

A large field dependence is seen in the water peak in the system containing 30% 2-ClEt. The field dependence becomes small when the concentration of the organic is increased to 50%. Increasing the concentration of the 2-ClEt also has the effect of shifting the water curves to the top of the graph. This means that the values of R for water, for a given value of H_1 and $\sin^2\theta$, become closer to unity at the higher concentration of 2-ClEt. Increasing the concentration of the organic solvent has no effect on the shape and the location of the organic peaks' curves.

The only system for which data were obtained at a subzero temperature (-14.0°C) was the system containing dioxane. Within the experimental error, the plots for the water and the organic component are the same. A large H_1 field and $\sin^2\theta$ dependence are present. We do not know if such similarity is common to other frozen three component systems, or whether this effect is specific to dioxane.

In the system containing guanidine, the plots for the water and the organic are the same and no H_1 field dependence is present, within the experimental error. The plots are located at the top of the graph. The T_1's of the two signals are relatively long and equal (see Table 6.19).

The guanidine protons exchange with the water protons. The fact that we observed a separate peak for guanidine indicates that under our conditions the system is not in the fast exchange limit. Significant averaging still may take place and this may be responsible, in part, for the relatively long values and the equality of T_1's. To study the interactions of guanidine with the macromolecule a ^{13}C study may be more appropriate.

The fact that in systems containing ethylene glycol, DMSO, and 2-ClEt the water curves lie below the organic curves in each system indicates that in these systems the water is affected preferentially by the macromolecule. The details of the water-macromolecule interaction are different for each system and depend on the concentration of the organic solvent. Comparison with the water curves for the 0.3 g/1 ml BSA sample in Figure 6.83 (a two component system which has the same concentration of protein but no organic solvent) shows that the water plots

in the three component systems are located below the water plots in the two component system. No H_1 field dependence is seen in the two component system, while large H_1 field dependence is seen in the three component systems containing DMSO and 30% 2-ClEt and a small field dependence is seen in the system containing ethylene glycol. The comparison indicates that in the presence of these organic solvents the motions of the water molecule are affected to a higher degree by the protein than the motions of the water in protein solutions that contain no organic solvents.

An interesting concentration effect is seen in the system that contains 2-ClEt. As the concentration of the organic solvent is increased from 30% to 50%, the water curves move to the top of the graph (the values of R become closer to unity) and the H_1 field dependence becomes small. No change is seen in the shape and position of the organic peaks' curves. Since R is proportional to $T_{1\rho}^{off}/T_1$ (see also the previous section), an increase in the values of R means that either $T_{1\rho}^{off}$ becomes longer or T_1 becomes shorter, or both effects take place simultaneously. The data in Table 6.19 shows that the T_1 ratio increases from 1.5 to 2.2. The effect arises because the T_1's of the water become shorter. The T_1's of the organic are unaffected.

Timasheff and Inoue (80) used optical methods to study solutions of BSA that contained different amounts of 2-ClEt (as well as other proteins and solvents). A model was presented in which the organic component binds to the nonpolar regions of the protein and gradually disrupts the native conformation. The amount of the bound organic solvent increases as its concentration in the solution increases and at high enough organic concentration the protein unfolds. Because in globular proteins the polar residues tend to be located on the surface, these residues are already hydrated in the native form. Unfolding exposes a few new polar residues to the solvent, but the change in the amount of the bound water is very small.

Our results are consistent with this model. If the amount of the bound water remains unchanged, increasing the concentration of the organic solvent will increase the fraction of the bound water. Since the bound fraction has a shorter T_1 relaxation time, this will result in a decrease in the experimentally measured T_1. This is the observed effect. Increasing the organic solvent concentration increases the bound amount of this component. The change in the bound fraction of the organic component will depend on the change in the bound amount relative to the change in

the total concentration of the organic component. No change is observed experimentally in the organic T_1's.

When a globular protein unfolds, the backbone and the side chains may gain more flexibility. This may introduce faster motions. If the solvent molecules bind to the protein and reflect its motions, unfolding of a globular protein may cause the effective correlation time of the solvent to become shorter. In such a case, the T_1 values for the solvent may become longer, the $\sin^2\theta$ dependence of R may become smaller, and the R versus $\sin^2\theta$ plots may be shifted to the top of the graph.

In the system containing 2-ClEt, the water T_1 becomes shorter and the R versus $\sin^2\theta$ plots move to the top of the graph, when the concentration of the organic component increases from 30% to 50%. These results indicate that unfolding of the protein may take place between 30% and 50% 2-ClEt.

In the system containing guanidine, plots for both the water and the organic component (Figure 6.82) are located at the top of the graph and the R's show very little $\sin^2\theta$ dependence. As discussed earlier, part of the effect may arise because of exchange between the guanidine and the water protons. At $\sim$10 M guanidine the protein is likely to be unfolded. The similarity of the plots for the water and the guanidine and their

location at the top of the graph indicate that both components may be bound to the protein and may reflect the faster motions in the unfolded state.

If the organic component causes the protein to unfold, one would like to know whether this effect is a consequence of the direct binding of the organic component to the macromolecule, whether the effect arises from changes in the solvent structure or whether both effects take place simultaneously. The data in Figures 6.79 and 6.80 show that the 2-ClEt remains unaffected when its concentration is increased from 30% to 50%. At the same time, the effective correlation time of the water becomes shorter. We interpreted the decrease in the water correlation time as arising from protein unfolding. If the unfolding is caused by direct binding of 2-ClEt to the protein, we would expect the 2-ClEt to have values of R smaller than unity, at least in the sample that contains 30% of the organic. Since the values of R for the water are less than unity in the 30% 2-ClEt mixture, it is not likely that the protein is unfolded to a high degree at this concentration of 2-ClEt. Because the 2-ClEt appears to cause unfolding of the protein while its own spectra is unaffected it is likely that this organic solvent affects the conformation of the macromolecule mostly by changing the

structure of the solvent, rather than by binding directly to the protein.

If changes in the solvent structure are involved, we would expect the T_1's of both the water and the organic solvent to change when the concentration of 2-ClEt changes. The data in Table 6.19 show that the T_1 of water decreases but that of 2-ClEt remains constant when the concentration of the 2-ClEt is increased from 30% to 50%. Direct interpretation of T_1 data is difficult because the experimental values reflect the average of several effects that may take place simultaneously. As discussed earlier, changes in the concentration of the organic solvent may change the fraction of each component. This may mask the contribution of other effects. T_1 data also contains structural information about the probe molecule through the rigid lattice second moment. Changes in the values of T_1 may contain contributions from changes in the values of the rigid lattice second moment. In the off-resonance experiment, one measures the ratio of two relaxation times and the rigid lattice second moment cancels out.

In the solvent mixtures that contain ethylene glycol and DMSO (Figures 6.77 and 6.78), the values of R are less than unity for the organic components. We interpret these results to mean that a fraction of the organic solvents binds to the protein. We do not know

the effect of these organic components on the solvent structure.

We showed that off-resonance experiments can be applied to the study of multicomponent systems. Large enough NMR effects are present, in most of the systems that we investigated, to allow the detection of a differential interaction of the solvent components with the macromolecule.

6.4 Fluoride Binding to BSA

We performed T_1, T_2, $T_{1\rho}^{on}$, $T_{1\rho}^{off}$, and saturation experiments on the $^{19}F^-$ ion in order to study its binding to BSA in solution. T_1 and T_2 relaxation times were measured at 141 MHz. $T_{1\rho}^{on}$ experiments were performed at ν_0 = 52 MHz. The off-resonance and the saturation experiments were performed at ν_0 = 94 MHz and the protons were saturated with a broadband frequency at 100 MHz. See Chapter 4, Section 4.2.3.1, for experimental details, and Chapter 2, Section 2.1.3, for fluorine relaxation theory.

Samples were prepared by allowing ∿1 M of NaF in a 0.5 g/1 ml BSA solutions to equilibrate. Then the samples were centrifuged and only the clear supernatant solutions used for the experiments. Two samples were prepared: in water and in D_2O.

Figure 6.84 shows the R versus $\sin^2\theta$ plots at +21.6°C. Identical plots, within the experimental error, were obtained in water and in D_2O solutions. Figures 6.85-6.86 illustrate, respectively, the T_1 and T_2 data in the D_2O solution. Data were obtained at +4.0°C, +15.0°C, +25.0°C, +35.0°C, and +45°C. Data were obtained during the same experimental set-up.

The fluoride in a saturated solution of KF, in a mixture of 30% D_2O plus 70% water, had $T_1 \approx 0.94$ sec and $LW_{1/2} \approx 3$ Hz. In a solution containing BSA in water $T_1 \approx 64.3$ msec and in a solution containing BSA in D_2O $T_1 \approx 57.2$ msec. The three T_1 values were estimated at 94 MHz by the zero-point method at +21°C ± 1°C.

The values of T_1 at 94 MHz are somewhat shorter than the value of T_1 = 89.4 msec at 141 MHz and the value of T_1 = 73.6 msec at 62 MHz, which were determined by the inversion-recovery method and a three parameter fit. The difference is probably caused by the experimental error associated with the zero-point technique. Our preliminary experiments showed that this method may introduce large errors if the 180° pulse is misadjusted. Accurate T_1 values could be obtained if the inversion-recovery technique and a three parameter fit were used (see Chapter 5, Section 5.2). The "true" values of T_1 at 94 MHz are probably ∿75-85 msec. Since the T_1's in water and in D_2O were measured with the same experimental

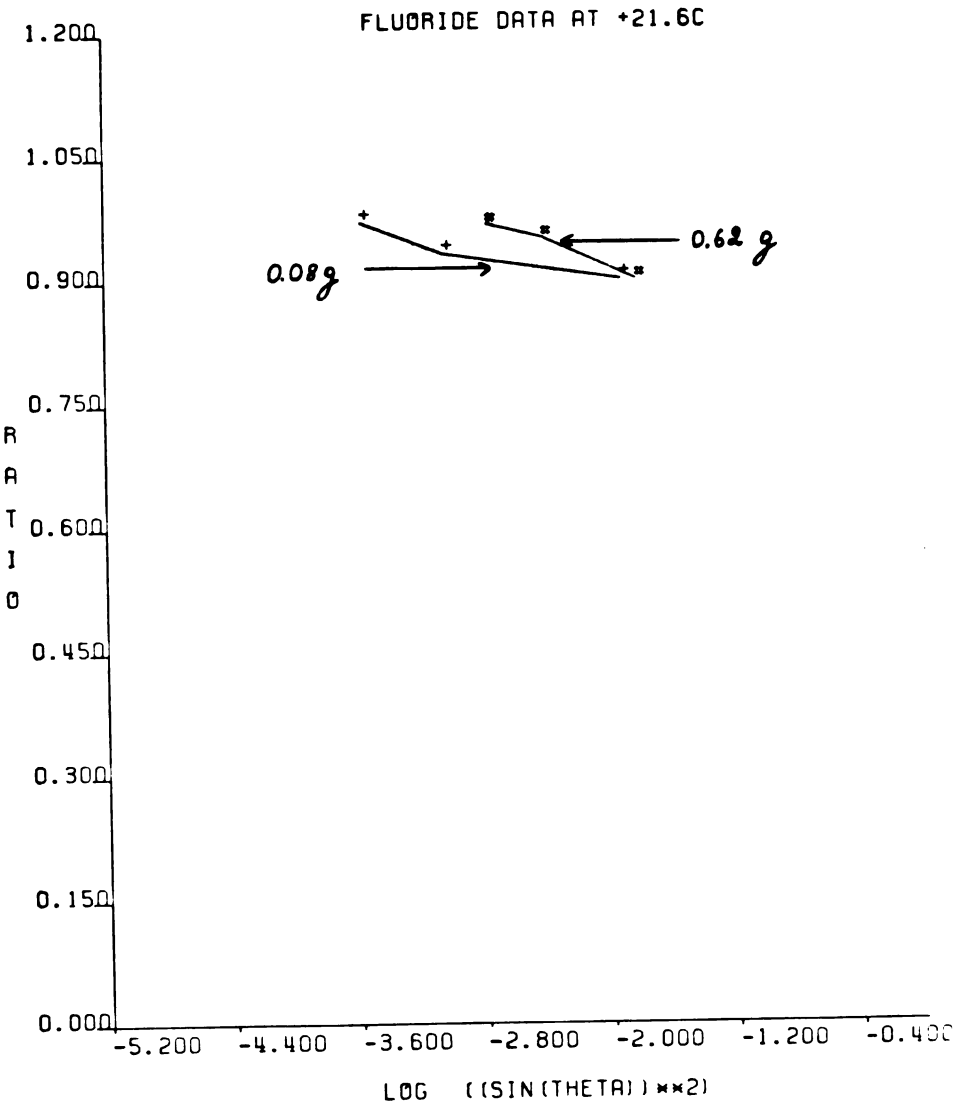

Fig. 6.84. Fluoride off-resonance data at ν_0 = 94 MHz at +21.6°C. The sample contained NaF in a 0.5 g/1ml solution of BSA in D_2O. The arrows with the numbers indicate the H_1 field strengths in units of Gauss (g).

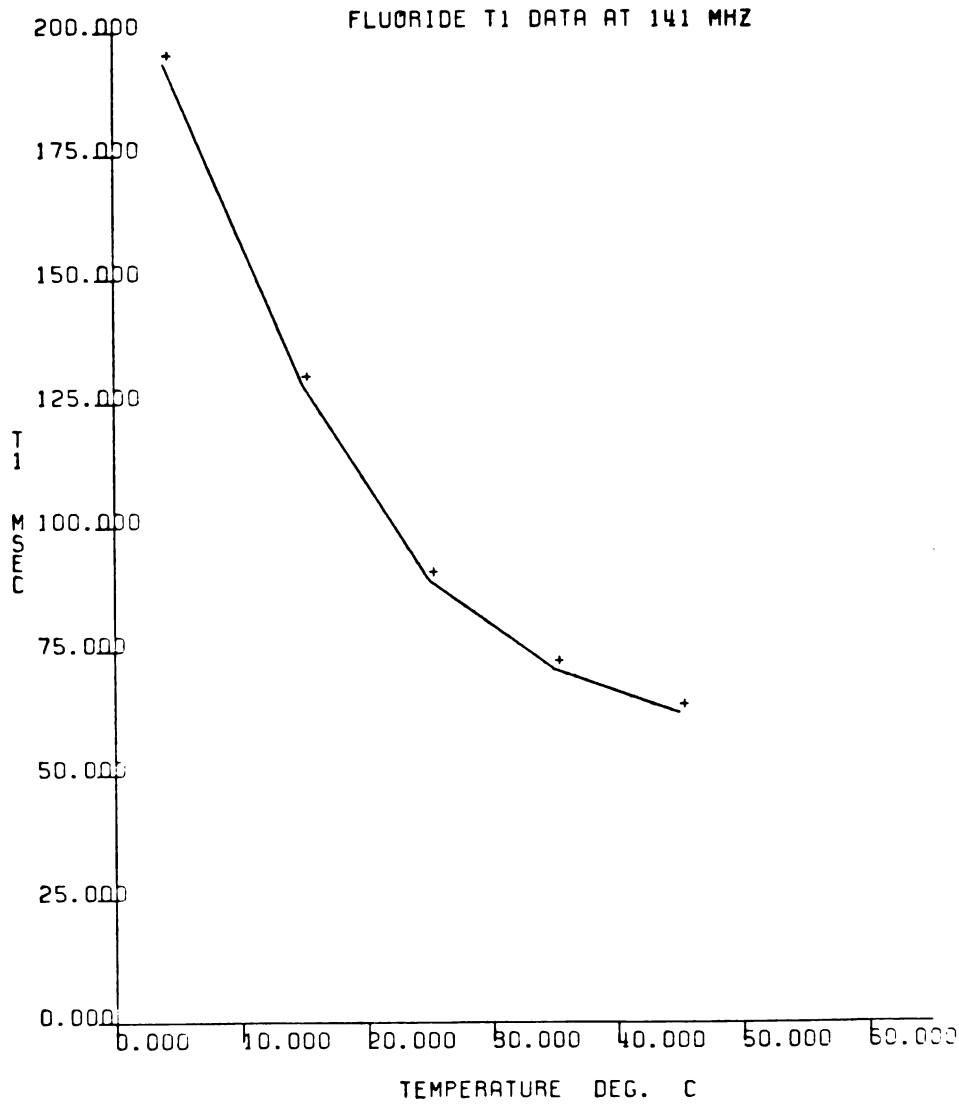

Fig. 6.85. Fluoride T_1 relaxation times at ν_0 = 141 MHz as a function of temperature. The sample contained NaF in a 0.5 g/1ml solution of BSA in D_2O.

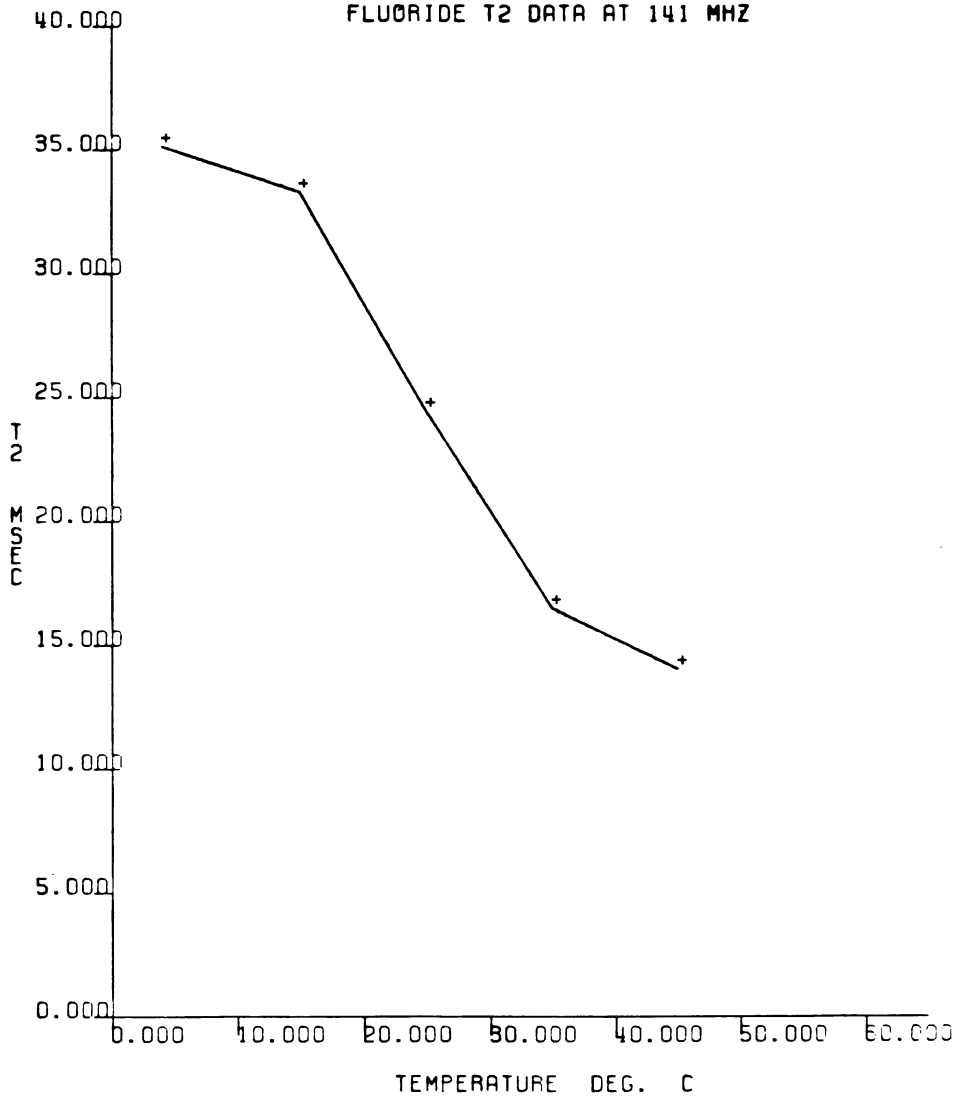

Fig. 6.86. Fluoride T_2 relaxation times at ν_0 = 141 MHz as a function of temperature. The sample contained NaF in a 0.5 g/1ml solution of BSA in D_2O.

set-up, the similarity of the two values should still hold for their "true" values. The precise values of T_1 at 94 MHz cannot, however, change our main observation: addition of the protein reduces sharply (by a factor of $\sim$11) the fluoride T_1 relaxation time. The similarity of the T_1 relaxation times in H_2O and in D_2O indicates that fluoride does not relax by a dipolar interaction with the water protons.

From the linewidth we can calculate $T_2^* \approx 100$ msec. Upon addition of the protein $T_2^* \approx 20$ msec (see later discussion). A reduction by a factor of $\sim$5 in the fluoride T_2 values takes place upon addition of the protein. This is only a lower limit estimate since T_2^* includes contributions from inhomogeneities.

The R versus $\sin^2\theta$ plots (in Figure 6.84) show that although small H_1 field dependence may be present, the plots are located at the top of the graph and the values of R are close to unity. This later fact indicates that in our system $T_{1\rho}^{off} \approx T_1$. Motions and/or processes with an effective correlation time in the nanosecond region may be present. Motions and/or processes with an effective correlation time in the microsecond region are not likely to be present.

If motions and/or processes with an effective correlation time in the nanosecond region are present, a T_1 dispersion in the MHz region is expected. A small

frequency dependence (change by a factor of ∿1.2) was observed experimentally in the frequency range 62-141 MHz.

We measured the fluoride $T_{1\rho}^{on}$ relaxation times at +24.0°C and ν_0 = 52 MHz at three H_1 field strengths: 14.7 g (58.8 KHz), 6.6 g (26.6 KHz), and 1.7 g (6.9 KHz) (for fluorine γ = 4.01 KHz/Gauss). No H_1 field dependence could be detected, within the experimental error, and all the $T_{1\rho}^{on}$ relaxation times had a value of ∿20 msec. The absence of a $T_{1\rho}^{on}$ dispersion confirms that no slow motions, with an effective correlation time in the microsecond region, are present.

The T_2 value at 141 MHz is 24.4 msec. This is very close to the value of $T_{1\rho}^{on} \approx$ 20 msec at ν_0 = 52 MHz. The absence of $T_{1\rho}^{on}$ dispersion implies that $T_{1\rho}^{on} \approx T_2$. This means that T_2 is not (or is only slightly) frequency dependent in the range 52-141 MHz.

Relaxation by the chemical shift anisotropy mechanism is not expected to be important for a spherical hydrated ion, such as the fluoride ion. However, if binding to a macromolecule occurs, distortion of the electronic shell around the ion may take place. In such a case, the chemical shift anisotropy relaxation mechanism may become important.

Relaxation by the anisotropic chemical shift mechanism is proportional to the square of the external

field H_0 (see the theoretical chapter). A factor of $\sim$5 reduction in T_1 and T_2 values would be expected in changing the frequency from 141 MHz to 62 MHz. The observed reduction in the values of T_1 in this region is much too small to be caused by this mechanism. It is not matched by a reduction in the T_2 values. We conclude, therefore, that fluoride relaxation by the chemical shift anisotropy mechanism does not play a role in our systems.

We performed a saturation (INDOR) experiment. A sample containing D_2O at +20°C was used. The protons were irradiated with a broadband amplifier, whose frequency was centered at 100 MHz. The fluoride peak intensity was monitored at 94 MHz (see the experimental chapter). No changes in the fluoride peak intensity could be detected, within the experimental error, even with a very high ($\sim$20 watts) rf output from the broadband amplifier.

A preliminary experiment showed that (see the experimental chapter) when a fluoride signal was irradiated directly at 94 MHz with a power much smaller ($\sim$5 watts) than the saturating power at 100 MHz, the fluoride peak disappeared completely. The preliminary experiment was performed using the same set-up like the actual experiment. It indicates that the absence

of any effects in the INDOR experiment is not likely to be an experimental artifact.

The absence of any effects in the INDOR experiment indicates that no significant dipolar interactions take place between the fluoride ion and the protein protons.

The effects in the INDOR experiments are frequency dependent (26). The effects may be zero at a certain set of frequencies. Since we performed our experiment only at one set of frequencies, we cannot rule out the possibility that the absence of any effects was due to the frequency dependence factor.

The data in Figures 6.85-6.86 show that both the T_1 and the T_2 values decrease, as the temperature is raised from +4.0°C to +45.0°C.

It is very unlikely that we are observing the descending part of a T_2 versus temperature profile in the presence of a slow exchange. Our $T_{1\rho}^{on}$ and $T_{1\rho}^{off}$ data indicate that no slow enough processes to give rise to such an effect are present.

An exchange process with a frequency of ∿100 MHz may contribute to T_1 values at 141 MHz. We cannot rule out the presence of such an exchange process since T_1 is slightly frequency dependent in the range 62-141 MHz. However, even if such a process is present, it is too fast to account for the temperature dependence of T_2.

A more likely explanation is that, rather than interacting with a few fluoride ions in well defined binding sites, the protein interacts weakly with a large number of fluoride ions. The effect of this interaction is mostly to impart a small anisotropic component to the fluoride ions. This anisotropic component is responsible for the sharp decrease in the T_1 and T_2 values of the fluoride ions upon addition of the protein. In solution, fluoride ions relax by the spin rotation mechanism (26). This mechanism becomes important at the higher temperatures and therefore T_1 and T_2 may decrease as the temperature is raised (26). Because of fast exchange among the fluoride ions, the T_1 and T_2 values are short and decrease as the temperature is raised.

Koenig et al. (17, 18) studied the proton, deuteron, and ^{17}O T_1 dispersion of water in protein solutions. They suggested a similar mechanism for the water relaxation in protein solutions. It appears that the fluoride ion can be used as a probe to investigate this mechanism. Complicating factors, such as slow exchange and cross-relaxation, are absent.

6.5 Summary

When the water proton T_1's are measured as a function of the temperature, a freezing event is observed when the concentration of the macromolecule is below $\sim$1.5

g/1 ml. Above ∿1.5 g/1 ml no freezing event can be detected. In both the water-PLL and the water-BSA systems, the T_1's go through a minimum between ∿-20°C and ∿-25°C. In each system, the temperature at which the minimum occurs, the T_1 values at the minimum and the T_1 values below the temperature of the minimum are concentration independent, within the experimental error. In both systems, the $T_{1\rho}^{on}$ relaxation rates at subzero temperatures are H_1 field dependent. The T_1 and $T_{1\rho}^{on}$ data combined indicate that at least two classes of interactions for water exist in frozen solutions: one with an apparent correlation time in the nanosecond region and the other with an apparent correlation time in the microsecond region.

When the water proton $T_{1\rho}^{on}$ relaxation rates are plotted versus $\omega_1^{1/2}$ straight lines are obtained at subzero temperatures. This indicates that translational motions may be important in the frozen solutions. At ∿-20°C the diffusion-coefficients (D) are the same, within the experimental error, in the PLL and the BSA samples and $D \approx (1.7 \pm 0.6) \times 10^{-10}$ cm^2/sec.

Study of the solvent proton and deuteron T_2 relaxation rates as a function of the temperature in BSA solutions above 0°C shows that the T_2 relaxation rates do not change in a monotonic way. This indicates

that a fraction of the protons/deuterons exchanges slowly with the water.

In BSA solutions that contain an organic solvent the water is affected to a larger degree by the macromolecule than the organic solvent. The water in the three component systems is affected more by the macromolecule than is water in the two component water-macromolecule system.

When BSA is added to a solution of sodium fluoride, the fluorine spin-lattice relaxation time decreases from ∿940 msec to ∿60 msec and the spin-spin relaxation time decreases from ∿100 msec (lower limit) to ∿20 msec. A saturation experiment shows that no dipolar interactions between the macromolecule and the fluoride ions take place. If any fluoride ions bind to the macromolecule, the frequency of such an exchange process is not less than ∿100 MHz. In the presence of a macromolecule in solution, the fluoride ions relax by the spin rotation mechanism.

In an off-resonance experiment the water protons in frozen and concentrated solutions show a large dependence on the off-resonance field strength. No field dependence is seen in dilute solutions and in solvent deuterons in frozen solutions. The field dependence is not caused by "true" molecular motions,

but may arise from the presence of local dipolar fields which do not average out to zero.

APPENDIX

A. VOFFH Program

The VOFFH Fortran program was used to prepare the proton off-resonance experimental data for plotting by the VERSATEC plotter. The deuterium off-resonance experimental data were prepared for plotting using the VOFFD Fortran program. This program was similar to the VOFFH program, except that for deuterium "v1=0.654*h0."

```
      dimension amp(31), voff(31)
      character*(72) row1, row2, row3
      character*(60)fname, fplot
      integer voff, corr1, corr2
      real h0
      write(6,26)
26    format(/'THIS PROGRAM CALCULATES VOFF PARAMETERS'
     &'FOR PROTONS')
      write(6,28)
28    format(/'GYROMAGNETIC RATIO=2.6752E4 1/GAUSSxSEC.)'
     &'=4.26 KHZ/GAUSS')
c     input section
      write(6,48)
48    format(/'file name ?')
56    read(5,'(a)')fname
      write(6,1)
1     format(/'comments: (3 rows maximum)')
      read(5,3)row1
      read(5,3)row2
      read(5,3)row3
3     format(a72)
      write(6,31)
31    format('H1(gauss)?')
      read (5,33)h0
33    format(f7.5)
      v1=4.26*h0
59    write(6,5)
5     format(/'type in voff(khz), type 1 for inf.
         values:'/)
```

```
      do 10 j=1, 30
      write(6,7)
7     format('voff(khz) ?')
      read(5,9,err=57) voff(j)
9     format(i5)
      if (voff(j) .eq. 0) goto 2
10    continue
      goto 2
57    write(6,58)
58    format(/'TYPING ERROR!!! PLEASE, TYPE VALUES'
     &//' OF VOFF(KHZ) AGAIN USING THE RIGHT FORMAT: i5'/)
      read(5,'()')
      goto 59
2     write(6,11)
11    format(/'type in corresponding amplitudes:'/)
      do 20 j=1,30
      write(6,13)
13    format('corresponding amplitude ?')
      read(5,15,err=62) amp(j)
15    format(f9.4)
      if (amp(j) .eq. 0) goto 4
20    continue
      goto 4
62    write(6,63)
63    format(/'TYPING ERROR!!! PLEASE, TYPE VALUES OF'
     &//' AMPLITUDES AGAIN USING THE RIGHT FORMAT: f9.4'/)
      read(5,'()')
      goto 2
c     this section sorts
4     do 40 i=1,29
      j=30-i
      n=31-i
      do 50 m=1,j
      if (voff(m) .gt. voff(n)) goto 6
      goto 50
6     voff(31)=voff(m)
      voff(m)=voff(n)
      voff(n)=voff(31)
      amp(31)=amp(m)
      amp(m)=amp(n)
      amp(n)=amp(31)
50    continue
40    continue
c     this section counts inf. points
      do 90 j=1,30
      if (voff(j) .eq. 0) goto 90
      if (voff(j) .eq. 1) goto 16
90    continue
16    n0=j
      do 100 j=1,30
      if (voff(j) .eq. 0) goto 100
      if (voff(j) .eq. 1) goto 100
```

```
      if (voff(j) .gt. 1) goto 18
100   continue
18    n1=j
      n=n1-n0
c     this section calculates average inf.
      s=0.
      do 60 j=1,30
      if (voff(j) .eq. 0) goto 60
      if (voff(j) .eq. 1) goto 8
      if (voff(j) .gt. 1) goto 12
8     s=s+amp(j)
60    continue
12    av=s/n
c     this section prints out results
      open (1,file=fname, status='unknown')
      rewind(1)
      write(6,17)row1
      write(1,17)row1
      write(6,29)row2
      write(1,29)row2
      write(6,29)row3
      write(1,29)row3
17    format(////,9x,a72)
29    format(9x,a72)
      write(6,19)
      write(1,19)
19    format(///3x,'#',3x,'VOFF(KHZ)',6x,'AMPLITUDE',8x,
     &'RATIO',7x,'(SIN(THETA))**2',4x,'LOG(SINT)')
      do 70 j=1,30
      if (voff(j) .eq. 0) goto 70
      if (voff(j) .eq. 1) goto 70
      r=amp(j)/av
      th=atan(v1/voff(j))
      r1=(sin(th))**2
      r2=log10(r1)
      n2=j-n1+1
      write(6,21)n2, voff(j), amp(j), r, r1, r2
      write(1,21)n2, voff(j), amp(j), r, r1, r2
21    format(1x,i3,4x,i4,9x,f9.3,5x,f9.3,5x,e13.3,5x,f10.3)
70    continue
      write(6,23)
      write(1,23)
23    format(//,9x,'infinity amplitudes')
      do 80 j=30, 1, -1
      if (voff(j) .gt. 1) goto 80
      if (voff(j) .eq. 0) goto 14
      n3=n2+n1-j
      write(6,27)n3, amp(j)
      write(1,27)n3, amp(j)
27    format(1x,i3,4x,f9.4)
80    continue
```

```
14  write(6,25)av
    write(1,25)av
25  format(//9x,'average infinity value=',2x,f9.4)
    write(6,24)h0, v1
    write(1,24)h0, v1
24  format(//9x,'H1=',1x,f5.3,'gauss=',1x,f5.3,1x,'khz')
    close(1,status='keep')
c   this section for corrections
    write(6,45)
45  format(///4x,'corrections in data input? if yes type
       1')
    read(5,9)m1
    if (m1 .eq. 0) goto 32
    goto 22
46  write(6,47)
47  format(4x,'more corrections in data input? if yes
       type 1')
    read(5,9)m1
    if (m1 .eq. 0) goto 42
22  write(6,35)
35  format(4x,'type in line #, voff(khz), amplitude:')
    read(5,37)corr1, corr2, corr3
37  format(2i5,f9.4)
    if (corr2 .eq. 1) goto 52
    do 110 j=1,30
    if (voff(j) .eq. 0) goto 110
    if (voff(j) .eq. 1) goto 110
    n4=j-n1+1
    if (corr1 .eq. n4) goto 51
    goto 110
51  voff(j)=corr2
    amp(j)=corr3
    goto 46
110 continue
52  do 120 j=30, 1, -1
    if (voff(j) .gt. 1) goto 120
    n5=n2+n1-j
    if (corr1 .eq. n5) goto 53
    goto 120
53  voff(j)=corr2
    amp(j)=corr3
    goto 46
120 continue
32  write(6,39)
39  format('  changes in comments? if yes type 1')
    read(5,9)m1
    if (m1 .eq. 0) goto 44
    if (m1 .eq. 1) goto 34
42  write(6,39)
    read(5,9)m1
    if (m1 .eq. 0) goto 4
34  write(6,41)
```

```
41  format('   what row ?')
    read(5,9)m1
    if (m1 .eq. 0) goto 4
    if (m1 .eq. 2) goto 36
    if (m1 .eq. 3) goto 38
    write(6,43)
43  format('   corrected row:')
    read(5,3)row1
    goto 34
36  write(6,43)
    read(5,3)row2
    goto 34
38  write(6,43)
    read(5,3)row3
    goto 34
44  write(6,61)
61  format(/,3x,'make a file for plotting ? yes=1,
       no=0')
    read(5,9)m1
    if (m1 .eq. 0) goto 55
    write(6,64)fname
64  format(//,3x,'REMINDER, CURRENT FILE NAME IS:',a,)
    write(6,65)
65  format(/,3x,'file name for plotting ?')
    read(5,'(a)')fplot
    open(2,file=fplot, status='unknown')
    rewind(2)
    write(2,66)
    write(6,66)
66  format('#',10x,'RATIO',10x,'LOG(SINT)'/
   &'#',10x,'-----',10x,'---------')
    do 130 j=1,30
    if (voff(j) .eq. 0) goto 130
    if (voff(j) .eq. 1) goto 130
    r=amp(j)/av
    th=atan(v1/voff(j))
    r1=(sin(th))**2
    r2=log10(r1)
    write(2,67)r, r2
    write(6,67)r, r2
67  format(7x,f9.3,6x,f10.3)
130 continue
    close(2,status='keep')
    write(6,49)
49  format(//'another set of data ? yes=1, no=0')
    read(5,9)m1
    if (m1 .eq. 0) goto 55
    do 30 j=1,30
    voff(j)=0
    amp(j)=0.
30  continue
```

```
    write(6,54)
54  format(/'new file name ?')
    goto 56
55  end
```

B. NMRRB Program

The NMRRB Fortran program was used to calculate the theoretical values of R as a function of $\sin^2\theta$ for protons. The same program also calculated the theoretical values of T_1 and T_2. Theoretical values for deuterium were calculated using the NMRRBD Fortran program. This program was similar to the NMRRB program, except that for deuterons "gam=654.0, k=6.0*1.e11, w0=pi*1.54e07 and r11=3.e06."

```
    dimension th(20),h1(3),r(3)
    real h1,lw,k,k1,k2,lgsin
    data th/.707,.548,.447,.316,.265,.224,.174,.141,
       .100,
   &.0837,.0707,.0548,.0447,.0316,.0265,.0224,.0173,
   &.0141,.01,.00707/
    nv=20
    write(0,6)
6   format(' # of h1"s?upto3; values,i1,3f5.3')
    read(5,7)nh1,h1(1),h1(2),h1(3)
7   format(i1,3f5.3)
20  write(0,1)
1   format(' Ta,Tb,Tc,Pa,Pb')
    read(5,2,3nd=40) ta,tb,tc,pa,pb
2   format(3e15.5,4f9.3)
    pc=1.00-pa-pb
    if (pc .gt. 0. .and. pc .le. 1.00) goto 30
    write(0,21)pc
21  format(' pc incorrect',f9.3)
    goto 20
30  write(6,8)ta,tb,tc,pa,pb,pc
8   format('#',3e15.5,4f9.3)
    write(0,2)ta,tb,tc,pa,pb,pc
ccc protons only from here on. k's used to calc. t1,t2
    gam=4260.
    k=6.3*1.e10
```

```
      k1=0.3*k
      k2=0.15*k
      pi=2.*3.14159
ccc   w0 calc. for 100mhz
      w0=pi*1.e08
ccc   calc. w*tc terms
      b0a=(w0*ta)**2
      b0b=(w0*tb)**2
      b0c=(w0*tc)**2
ccc   calc. each t1,t2
ccc   first calc. rates, then take recip.
      t1a=k1*ta*(1./(1.+b0a)+4./(1.+4.*b0a))
      t1b=k1*tb*(1./(1.+b0b)+4./(1.+4.*b0b))
      t1c=k1*tc*(1./(1.+b0c)+4./(1.+4.*b0c))
ccc   t1=total rate
      t1=pa*t1a+pb*t1b+pc*t1c
ccc   total t1
      t1=1000./t1
ccc   t2's calc. in conventional way
ccc   w1 effects not considered
      t2a=k2*ta*(3.+5./(1.+b0a)+2./(1.+4.*b0a))
      t2b=k2*tb*(3.+5./(1.+b0b)+2./(1.+4.*b0b))
      t2c=k2*tc*(3.+5./(1.+b0c)+2./(1.+4.*b0c))
ccc   check for rigid lattice limit
      r11=3.e05
      if (t2a .gt. r11)t2a=r11
      if (t2b .gt. r11)t2b=r11
      if (t2c .gt. r11)t2c=r11
ccc   t2=total rate
      t2=pa*t2a+pb*t2b+pc*t2c
      lw=t2/3.14159
ccc   t2=total t2
      t2=1000./t2
      write(6,9)t1,t2,lw
9     format('#',4x,'t1,t2,lw',3f10.3)
      write(0,4)t1,t2,lw
4     format(' t1,t2,lw',f10.1,f10.3,f10.1)
ccc   calc. t1p terms
ccc   sin theta, we*Tc
      write(6,11)(h1(k),k=1,3)
11    format('#',5x,'LOG(SIN)',8x,'RATIO FOR H1=',
     &f7.3,2x,f8.3,2x,f8.3)
      write(0,5)(h1(k),k=1,3)
5     format(/,6x,'LOG(SIN)',6x,(SIN(THETA))**2',5x,
         'RATIO FOR H1=',
     &f7.3,2x,f8.3,2x,f8.3)
      do 10 i=1,nv
      do 60 ih=1,nh1
      if(h1(ih).eq.0.) goto 60
      voff=h1(ih)*gam/tan(th(i))
      cth=cos(th(i))
```

```
ccc calc. theta
ccc (we*tc)**2 terms
    bea=(pi*voff*ta)/cth
    beb=(pi*voff*tb)/cth
    bec=(pi*voff*tc)/cth
    bea=bea*bea
    beb=beb*beb
    bec=bec*bec
ccc calc. sin(theta)
    snth=(sin(th(i)))**2
    lgsin=log10(snth)
    sth=1.5*snth*k1
ccc t1P rates
    t1pa=sth*ta/(1.+bea)+t1a
    t1pb=sth*tb/(1.+beb)+t1b
    t1pc=sth*tc/(1.+bec)+t1c
ccc totlp total rate
    t1p=pa*t1pa+pb*t1pb+pc*t1pc
ccc t1p
    t1p=1000./t1p
60  r(ih)=t1p/t1
    write(6,12) lgsin, (r(ih),ih=1,nh1)
12  format(3x,f10.3,7x,14x,3f10.3)
    write(0,3) lgsin, snth,(r(ih),ih=1,nh1)
3   format(3x,f10.3,4x,e13.3,7x,14x,3f10.3)
10  continue
40  write(0,41)
41  format(' file data exhausted, stop=0, more=1')
    read(5,42)icon
42  format(i1)
    if (icon .eq. 1) goto 20
    if (icon .eq. 0) goto 50
    goto 40
50  end
```

C. NMRKS4 Program

The NMRKS4 Fortran program was used to find the "best" three correlation times theoretical fits to the experimental data. The values of kp, v1, t1p1, v2, t1p2, v3, t1p3, t1, and t2 were adjusted for each experimental data. For deuterons, the values of w00d, kd, and r11 were changed as well, to correspond to their values for deuterium.

```
ccc THIS PROGRAM SEARCHES FOR VALUES OF
ccc THREE CORRELATION TIMES,
ccc FOR A GIVEN PAIR OF T1, T2.
ccc SLOW FRACTION AND POPULATION ARE FIXED FIRST,
ccc BY "HIGH" AND "LOW" FIELD T1'PS
ccc ONLY THE RANGE OF CORRELATION TIMES IS PRINTED
ccc "SUBMIT" VERSION
      dimension tb(7,18), tc(7,18)
      integer*4 na,nb
      real kp,kd,k1p,k2p,k1d,k2d
ccc THIS SECTION FILLS IN ARRAYS
ccc AND ASSIGNS CONSTANTS
      t0=1.0e-10
      na=1
      do 20 j=1, 7
      na=10*na
      nb=na/10
      sm=0.5
      do 30 i=1, 18
      sm=(sm+0.5)
      tb(j,i)=sm*t0*nb
      tc(j,i)=sm*t0*nb
30    continue
20    continue
      write(6,1)
1     format('THIS PROGRAM SEARCHES FOR VALUES OF THREE'/
     &/'CORRELATION TIMES FOR A GIVEN PAIR OF T1,T2'/
     &/'SLOW FRACTION IS FIXED FIRST BY'/
     &/'"HIGH," "INTERMEDIATE" AND "LOW" FIELDS T1P"S'/
     &/'ONLY THE RANGE OF CORRELATION TIMES IS PRINTED
         OUT'/
     &/'TAUB CHANGED FROM 1.0E-10 TO TAUC IN STEPS OF
         0.5'/
     &/'TAUC CHANGED FROM 1.0E-9 TO 9.5E-4 IN STEPS OF
         0.5'/
     &/'Pb AND Pc CHANGED IN STEPS OF 0.001'/)
ccc
ccc LINES 35 TO 42 TO BE ADJUSTED FOR
ccc THREE EXPERIMENTAL T1P DATA
      w00p=44.4e6
      kp=6.3e10
      v1=65.79
      t1p1=0.902
      v2=33.78
      t1p2=0.625
      v3=10.00
      t1p3=0.436
      tap=1.0e-10
ccc LINES 45 TO 50 TO BE ADJUSTED
ccc FOR EACH EXPERIMENTAL T1, T2 DATA
      w00d=100.e6
```

```
      kd=6.3e10
      t1=111.2
      t2=0.663
      tad=1.0e-11
      s=25.0
      step=0.0001
ccc
      pi=2.*3.14159
      w0p=pi*w00p
      w0d=pi*w00d
      r11=3.0e+05
      k1p=0.3*kp
      k2p=0.15*kp
      k1d=0.3*kd
      k2d=0.15*kd
      b0ap=(w0p*tap)**2
      b0ad=(w0d*tad)**2
      be1=1000.*pi*v1
      be2=1000.*pi*v2
      be3=1000.*pi*v3
      bea1=(be1*tap)**2
      bea2=(be2*tap)**2
      bea3=(be3*tap)**2
      r1a=k1d*tad*(1./(1.+b0ad)+4./(1.+4.*b0ad))
      r2a=k2d*tad*(3.+5./(1.+b0ad)+2./(1.+4.*b0ad))
      r1pa1=k1p*tap*((1.5/(1.+4.*bea1))+(2.5/(1.+b0ap))
         +(1./(1.+4.*b0ap)))
      r1pa2=k1p*tap*((1.5/(1.+4.*bea2))+(2.5/(1.+b0ap))
         +(1./(1.+4.*b0ap)))
      r1pa3=k1p*tap*((1.5/(1.+4.*bea3))+(2.5/(1.+b0ap))
         +(1./(1.+4.*b0ap)))
      ra=t1/t2
      s1=t1+(s*t1/100.)
      s2=t1-(s*t1/100.)
      s3=t2+(s*t2/100.)
      s4=t2-(s*t2/100.)
      s5=t1p1+(s*t1p1/100.)
      s6=t1p1-(s*t1p1/100.)
      s9=t1p3+(s*t1p3/100.)
      s10=t1p3-(s*t1p3/100.)
      nc=0
      tbw=0.
      tcw=0.
      paw=0.
      pbw=0.
      pcw=0.
      t1tw=0.
      t2tw=0.
      write(6,3)w00p
3     format(////'SPECTROMETER FREQUENCY FOR T1P"S (HZ)
         =',e11.4/)
```

```
      write(6,27)w00d
27    format(/'SPECTROMETER FREQUENCY FOR T1,T2 (HZ)
         =',e11.4/)
      write(6,4)kp
4     format(/'VALUE OF K FOR PROTONS =',e11.4/)
      write(6,28)kd
28    format(/'VALUE OF K FOR DEUTERONS =',e11.4/)
      write(6,9)v1,t1p1
9     format(/'H1(KHZ) =',f8.3,2x,';',2x,'T1P1 (MSEC.)
         =',f15.5/)
      write(6,11)v2,t1p2
11    format(/'H2(KHZ) =',f8.3,2x,';',2x,'T1P2 (MSEC.)
         =',f15.5/)
      write(6,12)v3,t1p3
12    format(/'H3(KHZ) =',f8.3,2x,';',2x,'T1P3 (MSEC.)
         =',f15.5/)
      write(6,33)t1
33    format(/'T1 (MSEC.) =',f15.5/)
      write(6,31)t2
31    format(/'T2 (MSEC.) =',f15.5/)
      write(6,32)s
32    format(/'LIMITS FOR T1, T2 AND T1P"S (+/- %)
         =',f7.2/)
      write(6,5) ra
5     format(/'RATIO T1/T2 =',f15.5/)
      write(6,7)tap
7     format(/'TAUA FOR PROTONS =',e11.4/)
      write(6,13)tad
13    format(/'TAUA FOR DEUTERONS =',e11.4/)
      write(6,6)
6     format(/4x,'Pa',9x,'Pb',9x,'Pc',11x,'TAUB',12x,
         'TAUC',
     &12x,'T1',13x,'T2'
     &/3x,'------',5x,'------',5x,'------',6x,
         '----------',
     &6x,'----------',6x,'--------',7x,'-------')
ccc THIS SECTION FIXES SLOW POPULATION, BY
ccc A TWO CORRELATION TIME SEARCH FOR T1P
      do 10 jc=5, 7
      do 50 ic=2, 18
      b0cp=(w0p*tc(jc,ic))**2
      bec1=(be1*tc(jc,ic))**2
      bec2=(be2*tc(jc,ic))**2
      bec3=(be3*tc(jc,ic))**2
      r1pc1=k1p*tc(jc,ic)*((1.5/(1.+4.*bec1))+
         (2.5/(1.+b0cp))+(1./(1.+4.*b0cp)))
      r1pc2=k1p*tc(jc,ic)*((1.5/(1.+4.*bec2))+
         (2.5/(1.+b0cp))+(1./(1.+4.*b0cp)))
      r1pc3=k1p*tc(jc,ic)*((1.5/(1.+4.*bec3))+
         (2.5/(1.+b0cp))+(1./(1.+4.*b0cp)))
      do 40 pc=step, 1.0-step,step
```

```
      write(6,27)w00d
27    format(/'SPECTROMETER FREQUENCY FOR T1,T2 (HZ)
         =',e11.4/)
      write(6,4)kp
4     format(/'VALUE OF K FOR PROTONS =',e11.4/)
      write(6,28)kd
28    format(/'VALUE OF K FOR DEUTERONS =',e11.4/)
      write(6,9)v1,t1p1
9     format(/'H1(KHZ) =',f8.3,2x,';',2x,'T1P1 (MSEC.)
         =',f15.5/)
      write(6,11)v2,t1p2
11    format(/'H2(KHZ) =',f8.3,2x,';',2x,'T1P2 (MSEC.)
         =',f15.5/)
      write(6,12)v3,t1p3
12    format(/'H3(KHZ) =',f8.3,2x,';',2x,'T1P3 (MSEC.)
         =',f15.5/)
      write(6,33)t1
33    format(/'T1 (MSEC.) =',f15.5/)
      write(6,31)t2
31    format(/'T2 (MSEC.) =',f15.5/)
      write(6,32)s
32    format(/'LIMITS FOR T1, T2 AND T1P"S (+/- %)
         =',f7.2/)
      write(6,5) ra
5     format(/'RATIO T1/T2 =',f15.5/)
      write(6,7)tap
7     format(/'TAUA FOR PROTONS =',e11.4/)
      write(6,13)tad
13    format(/'TAUA FOR DEUTERONS =',e11.4/)
      write(6,6)
6     format(/4x,'Pa',9x,'Pb',9x,'Pc',11x,'TAUB',12x,
         'TAUC',
     &12x,'T1',13x,'T2'
     &/3x,'------',5x,'------',5x,'------',6x,
         '----------',
     &6x,'----------',6x,'--------',7x,'-------')
ccc THIS    TION FIXES SLOW POPULATION, BY
c     A T    RELATION TIME SEARCH FOR T1P
      do      5, 7
      do      2, 18
      b0      *tc(jc,ic))**2
      b       *tc(jc,ic))**2
      h       *tc(jc,ic))**2
                c,ic))**2
                c,ic)*((1.5/(1.+4.*bec1))+
              cp))+(1./(1.+4.*b0cp)))
                c,ic)*((1.5/(1.+4.*bec2))+
              cp))+(1./(1.+4.*b0cp)))
                c,ic)*((1.5/(1.+4.*bec3))+
              cp))+(1./(1.+4.*b0cp)))
      4       , 1.0-step,step
```

```
      pa=1.0-pc
      r1p1t=pa*r1pa1+pc*r1pc1
      r1p2t=pa*r1pa2+pc*r1pc2
      r1p3t=pa*r1pa3+pc*r1pc3
      t1p1t=1000./r1p1t
      t1p2t=1000./r1p2t
      t1p3t=1000./r1p3t
      if (t1p1t .le. s5 .and. t1p1t .ge. s6
     &.and. t1p3t .le. s9 .and. t1p3t .ge. s10) goto 2
      goto 40
ccc THIS SECTION CALCULATES FOR
ccc THREE CORRELATION TIMES
2     write(6,57)t1p1t,t1p2t,t1p3t,pc,tc(jc,ic)
57    format('T1P1T,T1P2T,T1P3T,Pc,Tc',3(1x,f15.5),3x,
         f6.4,5x,e11.4)
      b0cd=(w0d*tc(jc,ic))**2
      r1c=k1d*tc(jc,ic)*(1./(1.+b0cd)+4./(1.+4.*b0cd))
      r2c=k2d*tc(jc,ic)*(3.+5./(1.+b0cd)+2./(1.+4.*b0cd))
      if (r2c .gt. r11)r2c=r11
      do 70 jb=1, 7
      do 80 ib=1, 18
      if (tc(jc,ic) .le. tb(jb,ib)) goto 80
      b0bd=(w0d*tb(jb,ib))**2
      r1b=k1d*tb(jb,ib)*(1./(1.+b0bd)+4./(1.+4.*b0bd))
      r2b=k2d*tb(jb,ib)*(3.+5./(1.+b0bd)+2./(1.+4.*b0bd))
      if (r2b .gt. r11)r2b=r11
      do 110 pb=step, 1.0, step
      pa=1.0-(pb+pc)
      if (pa .le. 0.0 .or. pa .gt. 0.0 .and. pa .lt. step)
         goto 110
      r1t=pa*r1a+pb*r1b+pc*r1c
      r2t=pa*r2a+pb*r2b+pc*r2c
      t1t=1000./r1t
      t2t=1000./r2t
      if (t1t .le. s1 .and. t1t .ge. s2 .and.
     &t2t .le. s3 .and. t2t .ge. s4 .and. nc .eq. 0)
         goto 49
      if (t1t .le. s1 .and. t1t .ge. s2 .and.
     &t2t .le. s3 .and. t2t .ge. s4) goto 39
      goto 110
39    if (tb(jb,ib) .eq. tbw .and. tc(jc,ic) .eq. tcw)
         goto 51
      goto 52
51    tbs=tb(jb,ib)
      tcs=tc(jc,ic)
      pas=pa
      pbs=pb
      pcs=pc
      t1ts=t1t
      t2ts=t2t
      goto 110
```

```
52  write(6,8)pas,pbs,pcs,tbs,tcs,
   &t1ts,t2ts
8   format(3x,f6.4,2(5x,f6.4),2(5x,e11.4),2(5x,f9.4))
    write(6,37)
37  format(//)
    write(6,8)pa,pb,pc,tb(jb,ib),tc(jc,ic),
   &t1t,t2t
53  tbw=tb(jb,ib)
    tcw=tc(jc,ic)
    paw=pa
    pbw=pb
    pcw=pc
    t1tw=t1t
    t2tw=t2t
    tbs=tb(jb,ib)
    tcs=tc(jc,ic)
    pas=pa
    pbs=pb
    pcs=pc
    t1ts=t1t
    t2ts=t2t
    goto 110
49  nc=1
    write(6,8)pa,pb,pc,tb(jb,ib),tc(jc,ic),
   &t1t,t2t
    goto 53
110 continue
80  continue
70  continue
40  continue
50  continue
10  continue
    if(nc .eq. 0) goto 55
    write(6,8)pas,pbs,pcs,tbs,tcs,
   &t1ts,t2ts
55  write(6,21)
21  format(//'THREE CORRELATION TIMES SEARCH
       COMPLETED.')
    if (nc .eq. 0) then
    write(6,56)
56  format(/'NO T1,T2 VALUES FOUND.')
    end if
    end
```

LIST OF ABBREVIATIONS

BSA	bovine serum albumin
D	diffusion-coefficient
DE	instrumental dead time
DMSO	dimethyl sulfoxide
DT	delay time between pulse cycles
d	distance of closest approach between two spins
ESR	electron spin resonance
E_a	energy of activation
FID	free induction decay
FT	Fourier transform
G	magnetic field gradient
g	Gauss
H_e	effective field
H_L	local dipolar field
H_0	stationary magnetic field strength (Gauss)
H_1	secondary magnetic field strength (Gauss)
h	Planck's constant
I	nuclear spin quantum number
INDOR	internuclear double resonance
IT	integration time
$\vec{i}$	unit vector along the x axis

$\vec{k}$	unit vector along the z axis
$LW_{1/2}$	linewidth at half maximum height
M.W.	molecular weight
M_e	steady state magnetization along the effective field
M_0	macroscopic magnetic moment for a system at thermal equilibrium
msec	milliseconds
m_I	magnetic quantum number
N	spin density (spins/cm^3)
NMR	nuclear magnetic resonance
PLL	poly-L-lysine
P_a, P_b, P_c	proton, or deuteron, fractions with a given correlation time
QCC	quadrupole coupling constant
QPD	quadrature detection mode
R	ratio of amplitudes in the off-resonance experiment
rf	radio-frequency
r_{ij}	internuclear distance
$\langle r^2 \rangle$	translational root mean squared jumping distance
SD	standard deviation
S/N	signal to noise ratio
sec	seconds
T_1	spin-lattice relaxation time
T_2	"true" spin-spin relaxation time
T_2^*	spin-spin relaxation time that contains contributions from inhomogeneities

$T_{1\rho}^{off}$	rotating frame spin-lattice relaxation time in the presence of an off-resonance rf field
$T_{1\rho}^{on}$	rotating frame spin-lattice relaxation
t_{π}	180° pulse
$t_{\pi/2}$	90° pulse
Δ	distance from resonance in the off-resonance experiment (rads/sec)
Ω	electrical resistance (ohms)
η	asymmetry parameter
γ	gyromagnetic ratio
μsec	microseconds
ν_{off}	distance from resonance in the off-resonance experiment (KHz)
ν_0	observing frequency (Hz)
ν_1	secondary magnetic field (KHz)
$(\omega_A - \omega_B)$	the difference in chemical shift between two exchanging sites
ω_e	effective field (rads/sec)
ω_0	Larmor precession frequency (rads/sec)
ω_1	rotating frame angular frequency (rads/sec)
σ_0^2	rigid lattice second moment
τ	waiting time between pulses, or the length of time a pulse is on
τ_a, τ_b, τ_c, τ_r	rotational correlation times
τ_{res}	the residence time of a nucleus in a given environment

θ	angle of nutation, or the angle between the stationary and the effective fields
2-ClEt	2-chloro ethanol

REFERENCES

1. W. A. P. Luck. Top. Curr. Chem., 64, 1976, 115.

2. S. N. Timasheff. Acc. Chem. Res., 3, 1970, 62.

3. M. J. Tait and F. Franks. Nature, 230(5289), 1971, 91.

4. I. D. Kuntz, T. S. Brassfield, G. D. Law, and G. V. Purcell. Science, 163, 1969, 1329.

5. H. T. Edzes and E. T. Samulski. J. Mag. Res., 31, 1978, 207.

6. M. Suwalsky and A. Llanos. Biopolymers, 16, 1977, 403.

7. A. Darke and E. G. Finer. Biopolymers, 14, 1975, 441.

8. D. R. Woodhouse and W. Derbyshire. J. Mag. Res., 19, 1975, 267.

9. B. D. Hilton, E. S. P. Hsi, and R. G. Bryant. Biophys. J., in press.

10. T. L. James, G. B. Matson, I. D. Kuntz, R. W. Fisher, and D. H. Butlaire. J. Mag. Res., 28, 1977, 417.

11. I. D. Kuntz and W. Kauzmann. Advan. Prot. Chem., 28, 1974, 239.

12. R. G. Bryant. Ann. Rev. Phys. Chem., 29, 1978, 167.

13. A. Zipp, I. D. Kuntz, and T. L. James. J. Mag. Res., 24, 1976, 411.

14. J. Oakes. J. Chem. Soc., Farad. Trans. I, 72(1), 1976, 216.

15. L. Grösch and F. Noack. Biochim. Biophys. Acta., 453, 1976, 218.

16. B. Halle, T. Andersson, S. Forsén, and B. Lindman. J. Am. Chem. Soc., 103(3), 1981, 500.

17. S. H. Koenig, K. Hallenga, and M. Shporer. Proc. Nat. Acad. Sci., 72(7), 1975, 2667.

18. K. Hallenga and S. H. Koenig. Biochemistry, 15(19), 1976, 4255.

19. B. D. Hilton, E. Hsi, and R. G. Bryant. J. Am. Chem. Soc., 99(26), 1977, 8483.

20. E. Hsi and R. G. Bryant. J. Phys. Chem., 81, 1977, 462.

21. M. Eisenstadt and M. E. Fabry. J. Mag. Res., 29, 1978, 591.

22. S. H. Koenig, R. G. Bryant, K. Hallenga, and G. S. Jacob. Biochemistry, 17(20), 1978, 4348.

23. D. Eisenberg and W. Kauzmann. The Structure and Properties of Water. Oxford: Clarendon Press, 1969.

24. P. Bendel. J. Mag. Res., 42, 1981, 364.

25. J. M. Jauch. Are Quanta Real? Bloomington: Indiana University Press, 1973, Third Day.

26. T. L. James. Nuclear Magnetic Resonance in Biochemistry. New York: Academic Press, 1975.

27. A. Abragam. The Principles of Nuclear Magnetism. Oxford: Oxford University Press, 1973.

28. N. Bloembergen, E. M. Purcell, and R. V. Pound. Phys. Rev., 73(7), 1948, 679.

29. H. A. Resing. J. Phys. Chem., 80(2), 1976, 186.

30. I. J. Lowe and R. E. Norberg. Phys. Rev., 107(1), 1957, 46.

31. R. L. Vold, J. S. Waugh, M. P. Klein, and D. E. Phelps. J. Chem. Phys., 48, 1968, 3831.

32. T. C. Farrar and E. D. Becker. Pulse and Fourier Transform NMR. New York: Academic Press, 1971.

33. E. L. Hahn. Phys. Rev., 80(4), 1950, 580.

34. G. P. Jones. Phys. Rev., 148(1), 1966, 332.

35. H. E. Bleich and J. A. Glasel. Biopolymers, 17, 1978, 2445.

36. L. J. Burnett and J. F. Harmon. J. Chem. Phys., 57(3), 1972, 1293.

37. R. W. Fisher and T. L. James. Biochemistry, 17(7), 1978, 1177.

38. I. Solomon. C. R. Acad. Sci. Paris, 248, 1959, 92.

39. J. Jeener, R. Du Bois, and P. Broekaert. Phys. Rev., 139(6A), 1965, A1959.

40. J. Charvolin and P. Rigny. J. Chem. Phys., 58(9), 1973, 3999.

41. P. Bendel. "Experimental and Theoretical Studies of ^{31}P NMR Imaging and Proton Off-Resonance Relaxation." Ph.D. Dissertation, State University of New York at Stony Brook, 1980.

42. H. T. Edzes and E. T. Samulski. Nature, 265, 1977, 521.

43. A. Kalk and H. J. C. Berendsen. J. Mag. Res., 24, 1976, 343.

44. International Critical Tables, Vol. 3, p. 77. New York: McGraw-Hill, 1926.

45. Nicolet Technology Corporation. NTCFT Manual. Mountain View, CA: NTC, 1975.

46. J. Kowalewski, G. C. Levy, L. F. Johnson, and L. Palmer. J. Mag. Res., 26, 1977, 533.

47. U. Shmueli and W. Traub. J. Mol. Biol., 12, 1965, 205.

48. K. Kakiuchi and H. Akutsu. Biopolymers, 20, 1981, 345.

49. M. E. Fuller and W. S. Brey. J. Biol. Chem., 243(2), 1968, 274.

50. A. Zipp, T. L. James, I. D. Kuntz, and S. B. Shohet. Biochim. Biophys. Acta, 428, 1976, 291.

51. I. D. Kuntz. J. Am. Chem. Soc., 93, 1971, 514.

52. H. S. Gutowsky and C. H. Holm. J. Chem. Phys., 25(6), 1956, 1228.

53. I. D. Kuntz and T. S. Brassfield. Arch. Biochem. Biophys., 142(2), 1971, 660.

54. D. Eisenberg and D. Crothers. Physical Chemistry with Applications to the Life Sciences. Menlo Park, CA: The Benjamin/Cummings Publishing Company, Inc., 1979.

55. F. Franks. Water, A Comprehensive Treatise. New York: Plenium Press, 1972.

56. E. D. Finch and A. S. Schneider. Biochim. Biophys. Acta, 406, 1975, 146.

57. B. Blicharska, Z. Florkowski, J. W. Hennel, G. Held, and F. Noack. Biochim. Biophys. Acta, 207, 1970, 381.

58. J. A. Glasel. Nature, 227, 1970, 704.

59. E. R. Andrew, T. J. Green, and M. J. R. Hoch. J. Mag. Res., 29, 1978, 331.

60. B. J. Luyet. Ann. N.Y. Acad. Sci., 125, 1965, 502.

61. B. M. Fung. Science, 190, 1975, 800.

62. B. M. Fung and T. W. McGaughy. Biochim. Biophys. Acta, 343, 1974, 663.

63. R. G. Bryant. Private Communications.

64. W. J. Scanlon and D. Eisenberg. J. Am. Chem. Soc., 85(2), 1981, 3251.

65. D. E. Woessner. J. Chem. Phys., 39(11), 1963, 2783.

66. J. W. Emsley, J. Feeney, and L. H. Sutcliffe. Progress in Nuclear Magnetic Resonance Spectroscopy, Vol. 3, Chapter 3. Oxford: Pergamon Press, 1967.

67. W. J. Leonard, K. K. Vijai, and J. F. Foster. J. Biol. Chem., 238(6), 1963, 1984.

68. M. Sogami and J. F. Foster. Biochemistry, 7(6), 1968, 2172.

69. T. L. James and S. P. Sawan. J. Am. Chem. Soc., 101(23), 1979, 7050.

70. S. H. Koenig and W. E. Schillinger. J. Biol. Chem., 244(12), 1969, 3283.

71. B. Halle. "Oxygen-17 Spin Relaxation and Molecular Dynamics in Aqueous Systems." Ph.D. Dissertation, Lund University, Lund, Sweden, 1981.

72. B. Borah and R. G. Bryant. Biophys. Chem., in press.

73. B. D. Hilton and C. K. Woodward. Biochemistry, 17(16), 1978, 3325.

74. M. Sheinblatt and H. S. Gutowsky. J. Am. Chem. Soc., 86, 1964, 4814.

75. A. Carrington and A. D. McLachlan. Introduction to Magnetic Resonance, with Applications to Chemistry and Chemical Physics. New York: Harper & Row, 1967.

76. J. C. Hindman, A. J. Zielen, A. Svirmickas, and M. Wood. J. Chem. Phys., 54(2), 1971, 621.

77. P. Bendel and T. L. James. J. Mag. Res., in press.

78. T. L. James, G. B. Matson, and I. D. Kuntz. J. Am. Chem. Soc., 100(11), 1978, 3590.

79. W. W. Cleland. Biochemistry, 3(4), 1964, 480.

80. S. N. Timasheff and H. Inoue. Biochemistry, 7(7), 1968, 2501.